Implementation of DeD AM in future manufacturing (IDiD)

Report

DED Experiments

Abstract

Technical report

Implementation of DeD AM in future manufacturing (IDiD)

Timetable: 1.1.2023– 31.12.2025

Reference number: 20358021

Partners: University of Oulu, Luleå tekniska universitet, UiT The Arctic University of Norway and LUT University

Program: Interreg Aurora

This report presents experimental research on wire-based additive manufacturing of steels within the project Implementation of DeD AM in Future Manufacturing (IDiD). The work focuses on evaluating the microstructure, mechanical properties, and fatigue performance of additively manufactured metallic materials, particularly those produced using Wire Arc Additive Manufacturing (WAAM) and laser wire Directed Energy Deposition (DED) processes.

Several materials were investigated, including WAAM-fabricated 316L stainless steel, carbon steel, and ultra-high-strength (UHS) steel, as well as laser wire DED 316L. The influence of different processing conditions and post-treatments—such as severe shot peening, surface condition, interpass temperature, shielding gas composition, and filler wire selection—was examined. Mechanical characterization included hardness measurements, tensile testing, surface roughness analysis, microstructural characterization, and fatigue testing under both bending and axial loading conditions.

The results demonstrate that WAAM-produced steels exhibit mechanical properties comparable to conventional materials, with significant ductility and competitive strength levels. Fatigue performance was found to be strongly influenced by surface condition, residual stresses, and manufacturing parameters. Surface treatments such as shot peening improved fatigue resistance, while as-built surface roughness reduced fatigue performance. Comparisons between different welding wires and shielding gases revealed measurable effects on both static strength and fatigue behavior.

Laser wire DED 316L showed a dense microstructure without detectable internal defects, with nearly isotropic tensile properties. Additional studies examined dissimilar material interfaces between WAAM deposits and wrought steels, demonstrating good metallurgical bonding and stable fatigue performance. Finally, WAAM steels were compared with cast steel G24Mn6+QT1, showing that additively manufactured materials can provide competitive or superior fatigue resistance, particularly in high-cycle fatigue conditions.

The results highlight the potential of DED technologies for structural components, repair applications, and replacement of conventionally manufactured steel parts.

Table of contents

1 Introduction

Additive manufacturing (AM) technologies for metals have gained increasing attention in recent years due to their ability to produce complex geometries, reduce material waste, and enable flexible manufacturing. Among the available AM techniques, Directed Energy Deposition (DED), is particularly attractive for manufacturing large-scale metallic components. This technology utilizes welding-based deposition of metal wire or powder feedstock layer by layer, enabling relatively high deposition rates and cost-efficient production compared with powder-based additive manufacturing processes.

Wire Arc Additive Manufacturing (WAAM) has been widely studied for structural steels and stainless steels because of its capability to produce components with good mechanical performance and relatively low material cost. However, the layer-by-layer deposition process introduces complex thermal cycles that influence the resulting microstructure, residual stresses, and mechanical properties of the deposited material. Consequently, understanding how process parameters, material selection, and post-processing treatments affect the final properties is essential for the reliable industrial application of WAAM-produced components.

In addition to WAAM, laser wire DED offers an alternative wire-based additive manufacturing approach with lower heat input and potentially improved dimensional accuracy. Comparing these two technologies provides valuable insight into how different heat sources and deposition conditions influence microstructure formation, mechanical performance, and fatigue resistance.

For structural applications, the fatigue performance of additively manufactured materials is of particular importance, since cyclic loading often governs the lifetime of engineering components. Surface quality, residual stresses, and microstructural features can strongly influence fatigue behavior in additively manufactured metals. Therefore, systematic experimental investigation is required to evaluate both static mechanical properties and fatigue performance under different manufacturing and post-processing conditions.

This report presents the results of experimental work carried out within the Implementation of DeD AM in Future Manufacturing (IDiD) project. The study focuses on the microstructure, mechanical properties, and fatigue behavior of steels produced using WAAM and laser wire DED processes. Several materials were investigated, including 316L stainless steel, carbon steel, and ultra-high-strength steel, along with comparisons to conventional materials such as wrought and cast steels.

The research includes investigations of process parameter effects, shielding gas composition, filler wire selection, surface condition, and post-processing treatments such as severe shot peening. Mechanical characterization was performed using hardness measurements, tensile testing, microstructural analysis, and fatigue testing under both bending and axial loading conditions.

The aim of this work is to evaluate the suitability of wire-based additive manufacturing for structural components and repair applications, and to provide a better understanding of how processing conditions influence the mechanical performance and fatigue resistance of additively manufactured steels.

2 WP4 WAAM experiments

2.1 Testing procedure for DED materials

This section outlines the experimental procedures used for mechanical testing and fatigue experiments. Unless otherwise stated in specific sections of the report, these methods were applied consistently throughout the study. The dimensions of the test specimens are also presented in this section.

2.1.1 WAAM printed part

The test samples were obtained from a WAAM-produced part featuring an oval shape. For each successive layer, the starting point alternated between opposite ends of the component, as shown in Fig. 1 and 2, and the deposition direction was reversed every other layer. The printed part measured 240 mm in length and 40 mm in width, with the curved sections having a radius of 20 mm. Fabrication was carried out on a 20 mm thick substrate plate. In this report, the terminology for printing directions shown in Fig. 1 has been used.

For the as-built specimens, the samples were first extracted from the WAAM part by laser cutting, after which they were machined to the required final dimensions.

For the machined-surface specimens, the WAAM component was first machined to the desired thickness. After this initial machining step, the specimens were laser cut from the part and subsequently machined to their final dimensions.

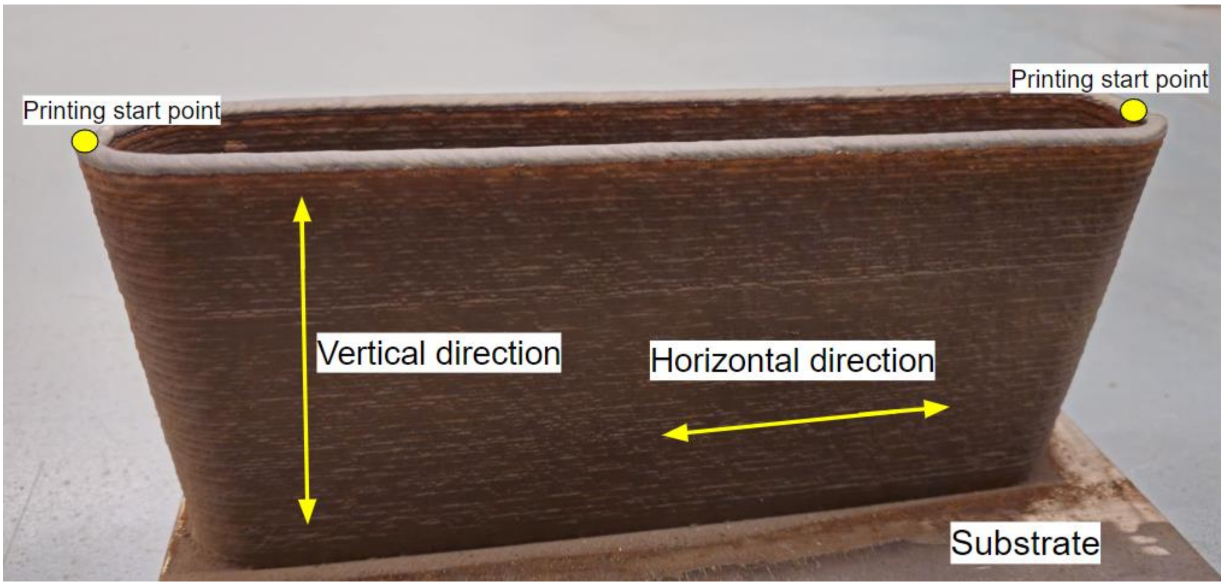

Fig. 1. The WAAM printed part.

2.1.2 Mechanical testing setup

Tensile properties were evaluated using an Instron 8802 universal testing machine in accordance with SFS-EN ISO 6892-1:2016. The tests were performed at a constant speed of 1.0 mm/min. The gauge length of the specimen was 15 mm, and the width of the gauge section was 6 mm. The gauge section was designed to provide a well-defined region of uniform stress distribution during testing, ensuring that deformation and failure occur within this area.

Microhardness measurements were performed using an Innovatest Falcon 500 Vickers hardness tester, applying a load of 0.2–0.3 kg (HV0.2–HV0.3). The indentations were placed at regular intervals of 0.1 or 0.2 mm, depending on the resolution required for the measurement.

2.1.3 Bending fatigue test setup

The bending fatigue strength of the specimens was evaluated using a custom-built reversed bending test apparatus based on the WEBI system originally developed by Carl Schenck. The fatigue tests were conducted under fully reversed loading conditions ($R = -1$), where the stress ratio represents the ratio of minimum to maximum stress within a loading cycle. A run-out limit of 2×10^6 cycles was applied.

Different stress amplitudes were applied to assess fatigue behavior across both low- and high-cycle regimes. Prior to testing, each specimen was individually calibrated using a force sensor to ensure accurate stress application and repeatability of the results. This calibration procedure minimized variability between specimens and improved the reliability of the fatigue data obtained.

2.1.3.1 Bending fatigue test specimen

Figure 1 presents the specimen geometry used in the bending fatigue tests. The main dimensions and key features of the specimen are illustrated in the figure. The samples were designed to ensure uniform stress distribution in the gauge section during cyclic loading, allowing reliable evaluation of fatigue performance.

The geometry includes a well-defined reduced cross-section in the central region, where fatigue crack initiation is expected to occur. This design minimizes the influence of gripping conditions and ensures that failure takes place within the intended test section. All specimens were machined to the same dimensions to ensure consistency and repeatability between tests.

The dimensions shown in Fig. 1 were selected in accordance with established fatigue testing practices, ensuring comparability of the results with existing literature. The controlled geometry also enables accurate calculation of stress amplitudes applied during the bending fatigue experiments.

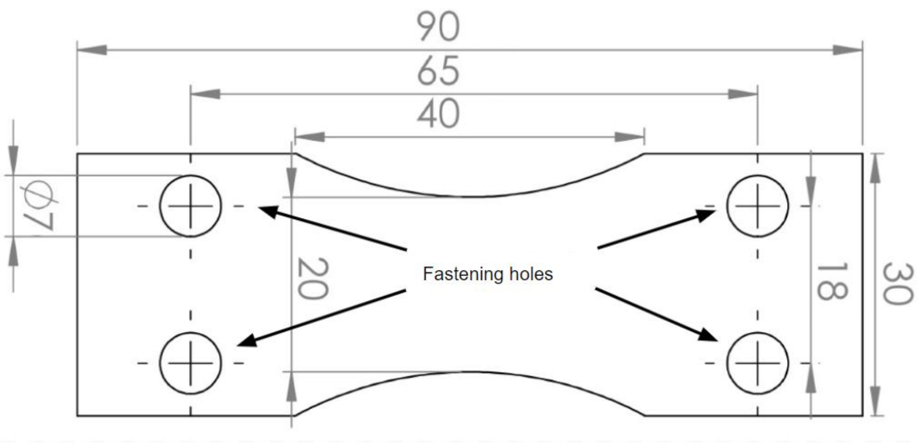

Fig. 1. Sample for bending fatigue tests.

2.1.4 Axial fatigue test setup

Axial fatigue tests were carried out using a StepLab UD020 testing machine. The experiments were conducted under a stress ratio of R = 0.

The tests were performed at loading frequencies ranging from 10 to 100 Hz, depending on the applied stress level and test duration. Lower frequencies were used for higher stress amplitudes to ensure stable loading conditions and avoid excessive heating of the specimens, while higher frequencies were applied at lower stress levels to reduce overall testing time. A run-out limit of 2×10^6 cycles was applied.

The selected testing conditions enabled efficient evaluation of fatigue behavior across a wide range of cycles, covering both low- and high-cycle fatigue regimes. All specimens were carefully aligned in the testing machine to ensure uniform loading and to minimize bending effects. The results obtained from these tests provide reliable information on the fatigue performance and fatigue limits of the materials investigated.

2.1.4.1 Sample for axial fatigue test

Figure 2 presents the specimen geometry used in the axial fatigue tests. The main dimensions and key features of the specimen are illustrated in the figure. The specimens were designed to ensure a uniform stress distribution within the gauge section during cyclic loading, enabling accurate evaluation of fatigue behavior.

The geometry includes a clearly defined gauge length with a reduced cross-sectional area, where fatigue crack initiation is expected to occur. This design minimizes the influence of stress concentrations at the gripping ends and ensures that failure occurs within the intended test region.

All specimens were machined to identical dimensions to ensure consistency and repeatability of the results. The selected geometry complies with standard fatigue testing practices, allowing reliable comparison with literature data. The defined dimensions also enable precise calculation of the applied stress amplitude during axial fatigue testing.

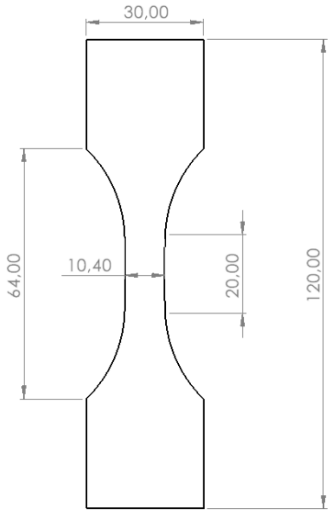

Fig. 2. Sample for axial fatigue tests.

2.2 Mechanical Properties and Fatigue Strength of WAAM 316L

2.2.1 WAAM equipment and welding wire

The WAAM parts were printed using Fronius TransPuls Synergic 2700 CMT welding equipment. The printing speed was 0.64 m/min, current 111 A, voltage 12.7 V, wire feed 3,2 m/min and lift between layers was 1.25 mm. An interpass temperature of 150 °C was controlled using an Optris CT infrared pyrometer. The flow rate of shielding gas was 12 l/min, and the composition of the gas was 98% Argon + 2% O_2.

The welding wire used in the WAAM experiments was Wurth AISI 316LSI. The thickness of the wire was 1.2 mm. The chemical composition of the 316L wire is presented in Table 1, and its mechanical characteristics, as specified by the manufacturer, are given in Table 2.

Table 1. Chemical composition (%) of the stainless steel 316L welding wire.

Cr	Ni	Mo	Mn	Si	C
18.0	12.0	3.0	1.70	0.80	<0.03

Table 2. Mechanical properties of the stainless steel 316L wire.

Yield strength MPa	Tensile strength MPa	Elongation %
>320	>510	>25

2.2.2 Hardness measurements

Hardness measurements were performed on WAAM-fabricated 316L stainless steel in the vertical build direction to evaluate the material's mechanical properties (Fig. 1). The results showed that the average hardness of the WAAM 316L material was approximately 195 HV. The relatively uniform hardness suggests that the deposition process produced a homogeneous austenitic microstructure with limited variation across the measured region.

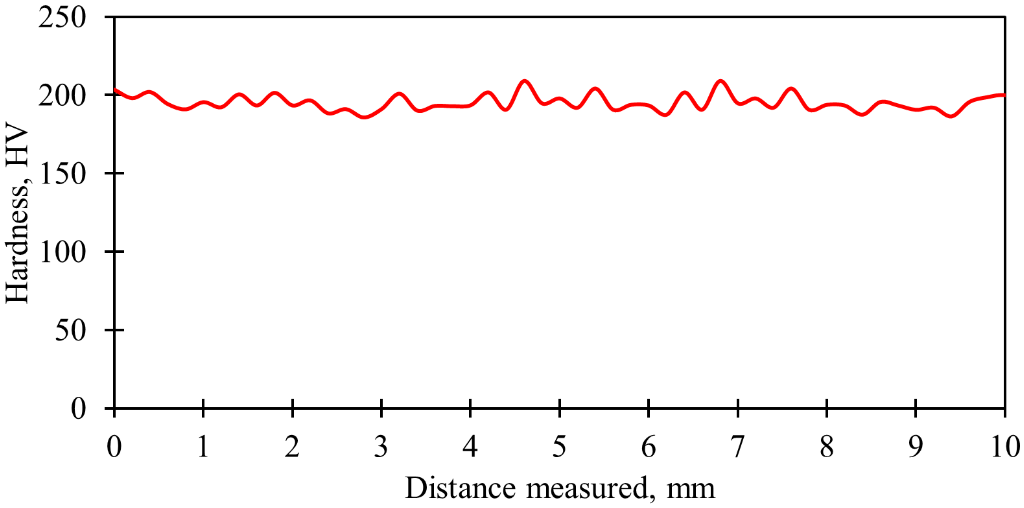

Fig. 1. Hardness profile of WAAM 316L.

2.2.3 Mechanical properties

The tensile test results show a clear dependence on build orientation (Table 1). In the vertical direction, the yield strength is 375 MPa, the ultimate tensile strength is 635 MPa, and the elongation at fracture is 37.2%. In the horizontal direction, the yield strength is 333 MPa, the ultimate tensile strength is 543 MPa, and the elongation reaches 44.8%. These results demonstrate moderate anisotropy in both strength and ductility.

The yield strength of the vertically printed specimens is approximately 13% higher than that of the horizontally printed specimens. This difference can be attributed primarily to the solidification behavior during WAAM processing. The process typically produces elongated, columnar austenitic grains that grow preferentially along the build direction due to steep thermal gradients and directional solidification. When tensile loading is applied parallel to the build direction, the load is transferred along these columnar grains and across successive deposited layers.

The ultimate tensile strength follows a similar trend. The vertically oriented specimens reach 635 MPa, whereas the horizontally oriented specimens reach 543 MPa, corresponding to a difference of approximately 17%. The higher tensile strength in the vertical direction suggests effective interlayer fusion and a relatively homogeneous load transfer along the build direction. In contrast, horizontally loaded specimens are more sensitive to the layered nature of the structure. When stress is applied perpendicular to the build direction, interlayer boundaries and potential microstructural heterogeneities play a more significant role in deformation and fracture.

In contrast to strength, ductility is higher in the horizontal direction. The elongation at fracture reaches 44.8% horizontally, compared to 37.2% vertically. This indicates that although the horizontal specimens are somewhat weaker, they are capable of accommodating more plastic deformation prior to fracture. The difference in ductility may be related to the interaction between the applied stress and the columnar grain structure. When loaded horizontally, deformation intersects grain boundaries and melt pool features in a manner that may promote more distributed plastic flow.

Table 1. Tensile strength of WAAM 316L.

	Yield strength [Mpa]	Tensile strength [Mpa]	Elongation [%]
Vertical	375	635	37.2
Horizontal	333	543	44.8

2.2.4 Bending fatigue strength

The bending fatigue performance of WAAM 316L stainless steel demonstrates a clear dependence on printing direction, reflecting the anisotropic microstructure inherent to the layer-by-layer deposition process. Figure 2 presents the S–N curves obtained from bending fatigue tests for specimens fabricated in vertical and horizontal orientations.

A distinct difference between the two build directions is observed throughout the entire fatigue life regime. Specimens loaded in the vertical direction consistently sustain higher stress amplitudes at equivalent cycle counts compared to horizontally printed specimens. The fatigue limit, defined as the stress amplitude corresponding to long-life performance was determined to be 317 MPa in the vertical direction and 246 MPa in the horizontal direction. This represents an increase of approximately 26% in fatigue limit for vertically built specimens.

The better fatigue resistance in the vertical direction can be attributed primarily to microstructural orientation and interlayer characteristics. In WAAM processing, solidification occurs under steep thermal gradients, producing elongated columnar austenitic grains that grow preferentially along the build direction. When cyclic bending stresses are applied in alignment with this direction, crack initiation and propagation may be hindered by the grain morphology and the relatively strong metallurgical bonding between successive layers. Furthermore, the repeated thermal cycles during deposition promote good interlayer fusion, which contributes to improved resistance against crack nucleation along layer interfaces.

In contrast, horizontally oriented specimens are more sensitive to the layered architecture of the material. Under bending loads applied perpendicular to the build direction, interlayer boundaries act as preferential sites for fatigue crack initiation. Even in well-optimized WAAM material, minor variations in melt pool geometry, residual stresses, or microstructural heterogeneities between layers can locally concentrate stress and accelerate crack formation. As a result, fatigue cracks propagate more readily across layer interfaces, leading to a lower fatigue limit of 246 MPa.

The observed anisotropy in fatigue performance is consistent with the tensile properties, where higher strength was also measured in the vertical direction.

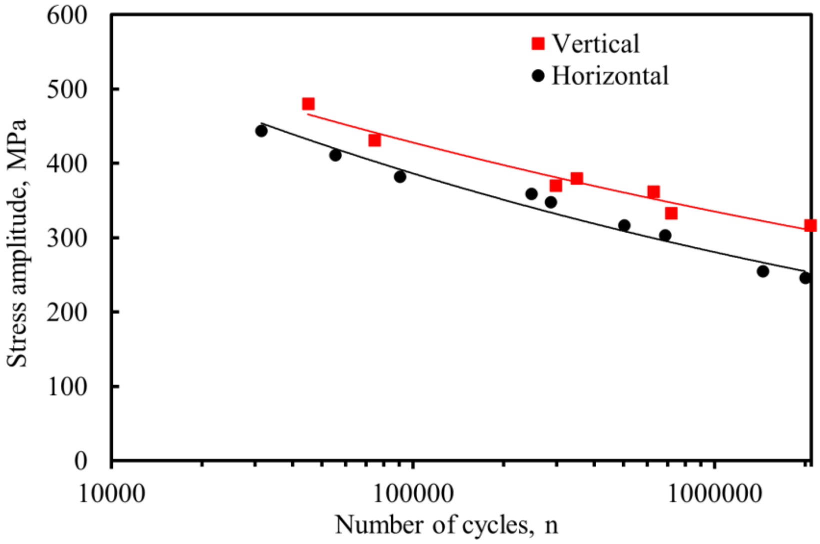

Fig. 2. Bending fatigue strength of WAAM 316L.

2.2.5 Axial fatigue strength

The axial fatigue behavior of WAAM 316L stainless steel further demonstrates the influence of build orientation on cyclic performance. Figure 3 presents the S–N curves obtained from axial fatigue testing for vertically and horizontally fabricated specimens.

A consistent difference between the two orientations is observed throughout the entire range of cycles. Specimens produced in the vertical direction exhibit slightly higher stress amplitudes at comparable fatigue lives than horizontally built specimens. The fatigue limit, defined at approximately

2*10⁶ cycles, was determined to be 280 MPa for the vertical direction and 255 MPa for the horizontal direction. This corresponds to an increase of roughly 10% in fatigue limit for vertically printed material.

The improved axial fatigue resistance in the vertical direction is closely related to the microstructural features generated during the WAAM process. Directional solidification under steep thermal gradients produces elongated columnar austenitic grains aligned predominantly with the build direction. When axial loading is applied parallel to this direction, the load transfer occurs along the grain growth direction and across well-fused interlayer regions. This alignment can delay crack initiation and reduce the effective driving force for crack propagation under cyclic tensile loading.

In contrast, horizontally oriented specimens experience axial stresses perpendicular to the build direction. Under these conditions, interlayer boundaries are oriented unfavorably with respect to the loading axis. Although metallurgical bonding between layers is generally strong in well-optimized WAAM processes, these interfaces may still act as preferential sites for fatigue crack initiation due to microstructural heterogeneity, residual stresses, or minor lack-of-fusion imperfections. Consequently, the fatigue limit in the horizontal direction is slightly lower.

Compared to the bending fatigue results, the anisotropy in axial fatigue strength is less pronounced. The difference between vertical and horizontal fatigue limits (25 MPa) is moderate, indicating relatively uniform material integrity and good interlayer bonding. This suggests that the WAAM process parameters used were effective in minimizing internal defects and producing a homogeneous microstructure.

Overall, WAAM 316L demonstrates good axial fatigue performance in both build orientations. Although some degree of anisotropy is present due to the inherent layer-wise deposition and columnar grain structure, the difference between orientations remains moderate. For fatigue-critical components subjected to axial cyclic loading, aligning the build direction with the principal stress axis may provide a measurable improvement in fatigue life. However, the relatively small difference between vertical and horizontal fatigue limits confirms that WAAM 316L possesses robust cyclic performance and is suitable for structural applications involving repeated tensile loading.

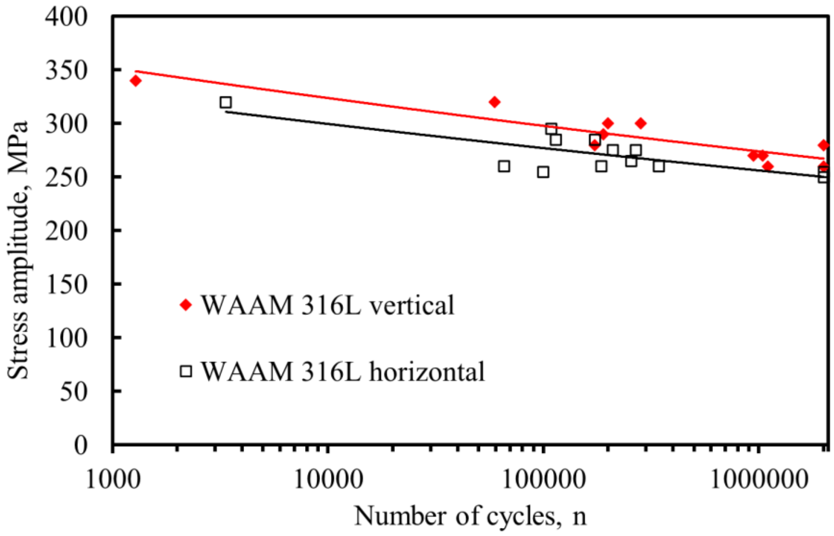

Fig. 3. Axial fatigue strength of WAAM 316L.

2.3 Influence of Severe Shot Peening on Mechanical Properties and Bending Fatigue Resistance of WAAM Printed 316L

2.3.1 WAAM equipment and welding wire

The WAAM experiments were carried out using a Fronius TransPuls Synergic 2700 CMT welding machine. In the deposition process, the wire was supplied at a rate of 3.2 m/min. The welding parameters were controlled at 107 A for current and 13.5 V for voltage. The printing speed was 0.64 m/min, and each new layer was deposited with a vertical step of 1.25 mm. An idle time of 90 seconds was introduced between successive layers to regulate heat accumulation. Shielding was provided by a protective gas mixture composed of 82% argon and 18% carbon dioxide.

A stainless steel wire of type INEFIL INOX AISI 316L with a diameter of 1.2 mm was employed as the consumable material in the WAAM process. The chemical composition of the 316L wire is presented in Table 1, and its mechanical characteristics, as specified by the manufacturer, are given in Table 2.

Table 1. Chemical composition (%) of the stainless steel 316L welding wire.

Cr	Ni	Mo	Mn	Si	C
18.5	12.2	2.50	1.70	0.80	0.02

Table 2. Mechanical properties of the stainless steel 316L wire.

Yield strength MPa	Tensile strength MPa	Elongation %
440	560	40

2.3.2 Test setup

The WAAM-fabricated component was post-processed by machining, during which approximately 1 mm of material was removed from each side of the deposited wall. This procedure was necessary to obtain a uniform plate with a final thickness of 2 mm and a smooth surface suitable for testing. Test specimens for tensile and fatigue characterization were prepared from this 2 mm thick plate. Initially, the blanks were cut by laser, followed by precision machining to achieve the required final dimensions.

Tensile properties were evaluated using an Instron 8802 universal testing machine in accordance with SFS-EN ISO 6892-1:2016. The tests were performed at a constant crosshead speed of 1.0 mm/min. Microhardness measurements were carried out with an Innovatest Falcon 500 hardness tester, applying a load of 0.05 kg. Indentations were placed at intervals of 0.1 mm.

The flexural fatigue performance of the WAAM specimens was assessed using a custom-built reversed bending apparatus derived from a WEBI system originally produced by Carl Schenck. Fatigue experiments were conducted under fully reversed loading conditions (R = −1), where the stress ratio represents the relationship between minimum and maximum stress within one loading cycle. Stress amplitudes ranging from 230 MPa to 470 MPa were applied. Each specimen was individually calibrated using a force sensor prior to testing.

Electron backscatter diffraction (EBSD) analysis was performed with a JEOL JSM-7900F scanning electron microscope equipped with an Oxford Instruments Symmetry EBSD detector. An accelerating voltage of 20 kV and a working distance of 17 mm were used for EBSD measurements. For energy-dispersive X-ray spectroscopy (EDS), the accelerating voltage was set to 10 kV with a working distance of 8 mm.

The severe shot peening (SSP) treatment was carried out inside an enclosed chamber using an ABB industrial robot. The nozzle remained stationary within the cabinet, while the specimen was manipulated by the robot. A dedicated fixture was designed to ensure consistent treatment of both sides of the samples. After each SSP pass, the specimen was rotated by 180° to promote uniform peening intensity on both surfaces. The procedure was repeated up to 22 passes per side.

SSP was performed using spherical martensitic chromium steel shots (STELUX C40). The shot diameter ranged from 0.30 to 0.85 mm, and their hardness was 36 HRC. Peening was conducted at an air pressure of 7.4 bar with a nozzle-to-sample distance of 70 mm. Almen intensity was determined using type A strips, reaching approximately 300 A after 22 passes.

2.3.3 Microstructure analysis

Figure 1 illustrates the microstructure of the WAAM-fabricated 316L stainless steel. EBSD characterization revealed partial remelting of previously deposited layers caused by the thermal input from subsequent passes. Pronounced epitaxial grain growth was observed, resulting in a coarse columnar grain morphology, as evident in the band contrast image presented in Fig. 1a. A higher magnification view taken from the central region of the specimen (Fig. 1b) highlights the dendritic solidification structure.

The phase distribution map shown in Fig. 1c, obtained from the SSP-treated surface, indicates the presence of a BCC phase (displayed in red) arranged in a network-like pattern within the FCC matrix. Considering the substantial heat input associated with the WAAM process, this BCC phase is most likely δ-ferrite, formed during solidification and retained during the relatively slow cooling of the deposited layer.

Detailed examination of the plastically deformed SSP surface layer suggests that the dominant deformation mechanisms are dislocation slip and possibly mechanical twinning, as indicated by the red boundaries in Fig. 1d and its magnified inset. No evidence of martensitic transformation was detected. This absence is likely related to the comparatively high stacking fault energy of the material, although this parameter was not quantitatively evaluated in the present study.

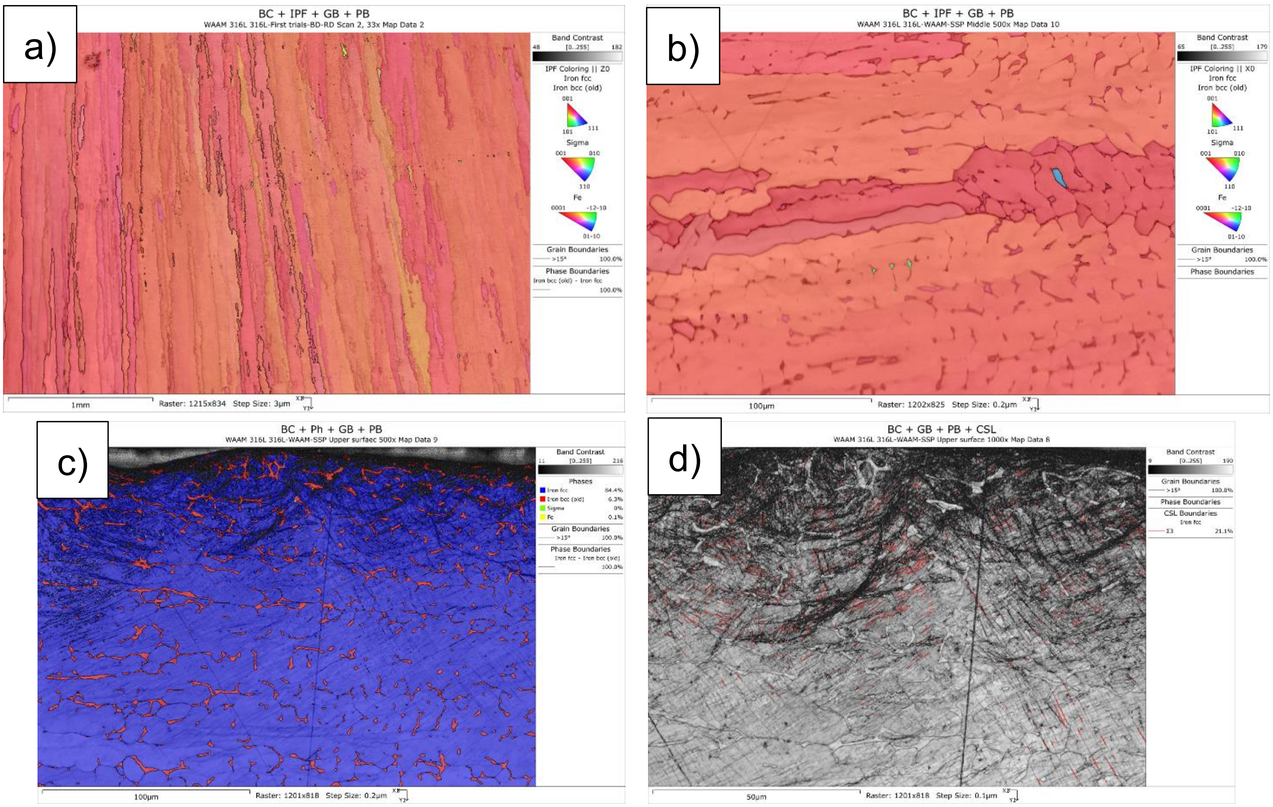

Fig. 1. (a) Band contrast image acquired from the central region of the deposited layer at low magnification, (b) Enlarged band contrast view highlighting the local microstructural features, (c) Phase distribution map obtained from the SSP surface of the fabricated structure, (d) Magnified region extracted from (c), illustrating twinning-induced deformation within the SSP-modified layer.

2.3.4 Hardness measurements

Figure 2 presents the cross-sectional hardness profile of the SSP-treated WAAM specimen. The measurements indicate that the influence of the SSP process extends to a depth of roughly 0.4 mm from the surface. The maximum hardness was recorded at the treated surface, reaching approximately 453 HV. In contrast, the hardness measured at the mid-thickness of the sample was about 201 HV. These findings demonstrate that SSP enhanced the surface hardness by approximately 225% compared to the base material.

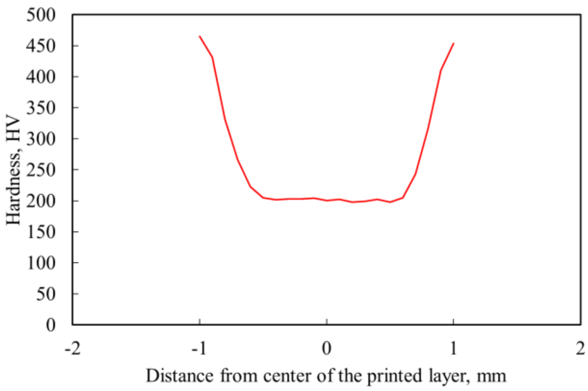

Fig. 2. Hardness profile for the SSP-treated WAAM specimen.

2.3.5 Mechanical properties

The tensile properties of the as-built WAAM 316L and SSP-treated WAAM 316L specimens are summarized in Table 3. All samples were manufactured and tested in the horizontal direction. The results show a clear increase in strength after the SSP treatment.

The yield strength of the untreated WAAM 316L was 345 MPa, while the SSP-treated material reached 462 MPa, corresponding to an increase of approximately 34%. The ultimate tensile strength also improved after SSP processing, increasing from 641 MPa to 688 MPa, which represents an increase of about 7%.

Although the SSP treatment significantly enhanced the strength of the material, it resulted in a reduction in ductility. The elongation at fracture decreased from 41.5% for the as-built WAAM 316L to 26% for the SSP-treated material. This reduction in elongation is typical for surface strengthening treatments, where increased strength is often accompanied by a decrease in plastic deformation capacity.

Table 3. Tensile strength of WAAM 316L and WAAM 316L SSP.

	Yield strength [Mpa]	Tensile strength [Mpa]	Elongation [%]
WAAM 316L	345	641	41.5
WAAM 316L SSP	462	688	26

2.3.6 Bending fatigue strength

Bending fatigue tests were performed on WAAM 316L and SSP-treated WAAM 316L specimens extracted in the build direction. The tests were conducted up to a run-out limit of 2×10^6 cycles, and the corresponding S–N curves are presented in Fig. 3.

The results indicate that SSP treatment significantly improved the fatigue performance of WAAM 316L across the entire fatigue life range. The fatigue limit of the as-built WAAM material was 211 MPa, whereas the SSP-treated specimens exhibited a fatigue limit of 360 MPa. This represents an increase of approximately 70% in fatigue limit after SSP treatment.

In addition to the higher fatigue limit, the SSP-treated specimens also showed improved fatigue strength in the low- and medium-cycle fatigue regimes. The observed improvement in fatigue behavior can be attributed to the surface strengthening effect introduced by SSP, which increases material strength and introduces beneficial compressive residual stresses near the surface. These effects delay fatigue crack initiation and slow down crack propagation, resulting in enhanced fatigue resistance of the treated WAAM 316L material.

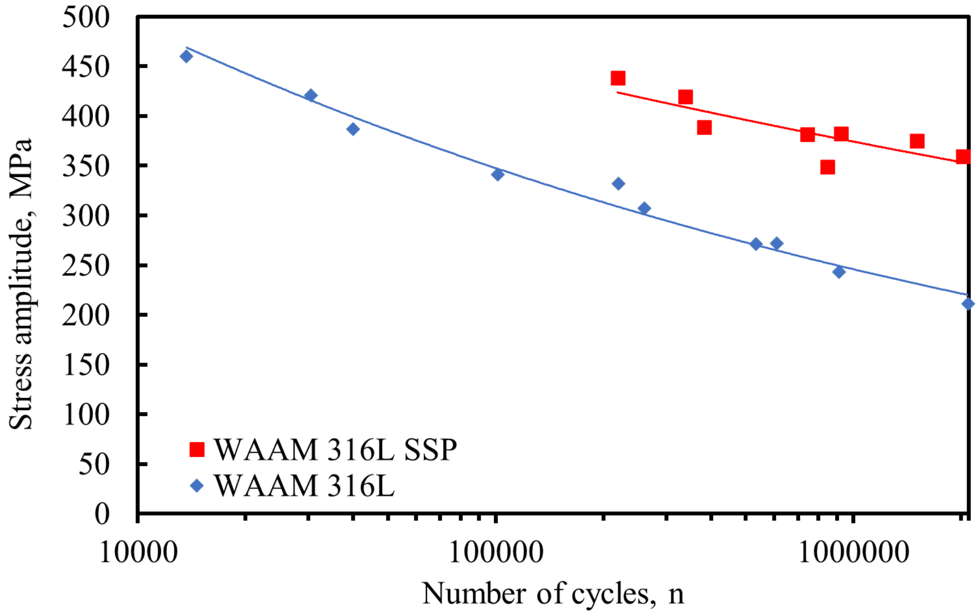

Fig. 3. Bending fatigue test results for the as-built WAAM and SSP-treated WAAM specimens.

2.4 Effect of Surface Condition on the Fatigue Performance of WAAM 316L Stainless Steel

2.4.1 WAAM printing setup

The WAAM components were fabricated using a Fronius TransPuls Synergic 2700 CMT welding system. The deposition was carried out at a travel speed of 0.64 m/min with a welding current of 107 A and an arc voltage of 13.5 V. The wire feed rate was set to 3.2 m/min, and a vertical increment of 1.25 mm was applied between successive layers. To ensure thermal stabilization and controlled heat accumulation, an idle time of 90 seconds was maintained after each deposited layer. Shielding gas was supplied at a flow rate of 12 l/min using a gas mixture composed of 82% argon and 18% carbon dioxide.

The filler material used in the experiments was INEFIL INOX AISI 316LSI stainless steel wire with a diameter of 1.2 mm. According to the manufacturer’s specifications, the wire provides a minimum yield strength of 440 MPa, an ultimate tensile strength of 560 MPa, and an elongation of 40%. The nominal chemical composition of the filler material is summarized in Table 1.

Table 1. Chemical composition of the stainless steel 316L welding wire.

Cr	Ni	Si	Mn	Mo	C
18.50	12.20	0.80	1.70	2.50	0.02

2.4.2 Mechanical testing

Standard tensile and bending fatigue specimens were machined from the WAAM-built component. Approximately 1.2 mm of material was milled from both sides of the deposited wall to remove the uneven as-built surface layer and ensure uniform thickness. The remaining material was machined into 2 mm thick plates, from which the tensile and fatigue specimens were subsequently cut and milled.

For comparison, as-built bending fatigue specimens were also prepared directly from the WAAM structure. In these samples, machining was performed on only one side, leaving the opposite surface in the as-deposited condition. Surface finishing of selected specimens was carried out using a DLyte HF100+ dry electropolishing system. The polishing process employed solid polymer media to improve surface quality without conventional liquid electrolytes.

Tensile testing was performed using an Instron 8802 servo-hydraulic universal testing machine in accordance with SFS-EN ISO 6892-1:2016. A constant crosshead speed of 1.0 mm/min was applied during testing. Vickers microhardness measurements were conducted on WAAM 316L cross-sections using an Innovatest Falcon 500 hardness tester with a load of 0.02 kg (HV0.02). Indentations were placed at 0.1 mm intervals to evaluate hardness distribution. Surface roughness was measured using a Keyence VK-X200 laser scanning microscope operating in non-contact mode, with a vertical resolution of 0.5 nm.

The bending fatigue performance of WAAM 316L specimens was evaluated using a custom-built bending fatigue testing machine developed by the FMT research group at the University of Oulu. Fatigue tests were carried out under fully reversed loading conditions (stress ratio R = –1), with stress amplitudes ranging from 125 MPa to 420 MPa. Prior to testing, each specimen was individually calibrated using a force sensor to ensure accurate stress application.

2.4.3 Geometry

A representative cross-section of the WAAM-fabricated wall structure is shown in Figure 1. The overall wall thickness was about 4.3 mm, while the average height of an individual deposited layer was approximately 1.22 mm. As observed in Figure 1, the WAAM 316L material exhibited a dense structure without visible porosity or other significant deposition-related defects.

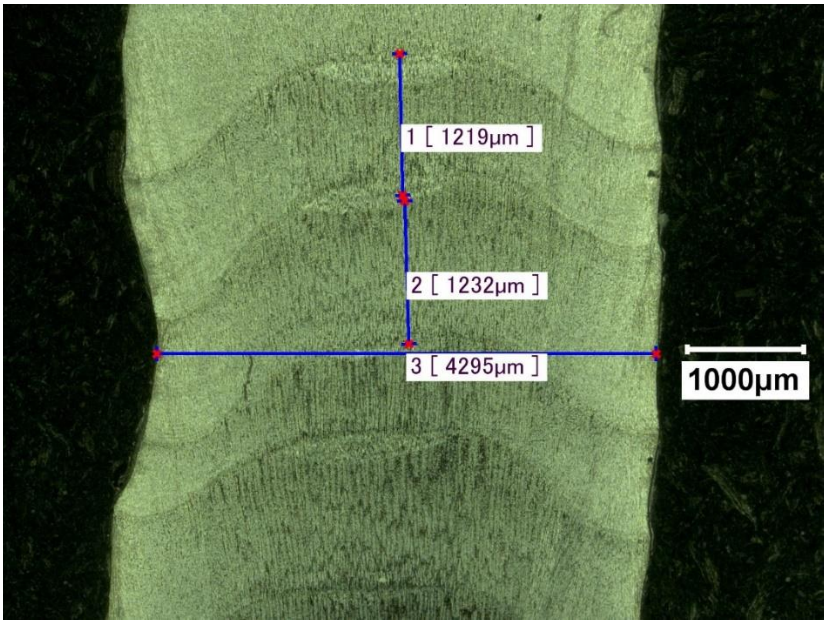

Fig. 1. Cross-section of the WAAM 316L wall.

2.4.4 Hardness measurements

Figure 2 presents the hardness profile measured from the as-built surface toward the machined surface of the WAAM 316L specimen. The average hardness of the material was approximately 211 HV. A slightly elevated hardness value of 224 HV was recorded at the as-built surface compared to the bulk material.

This localized increase in hardness is likely attributed to the higher cooling rate at the free surface during deposition. The accelerated solidification near the surface can promote subtle microstructural refinement, resulting in a modest increase in hardness in the outermost layer of the WAAM-fabricated component.

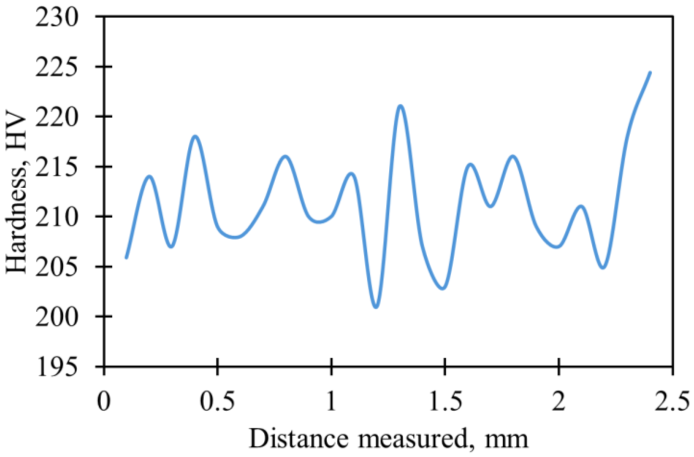

Fig. 2. Hardness profile from the cross-section of the WAAM 316L specimen.

2.4.5 Surface roughness measurement

Surface roughness was evaluated using non-contact laser scanning on three different surface conditions: milled, polished, and as-built. The average arithmetic roughness (Ra) and the average maximum peak-to-valley height (Rz) values are summarized in Table 2, while representative surface profiles are shown in Figure 3.

The polished specimen exhibited the highest surface quality, with an Ra value of 0.24 µm. The milled surface showed slightly greater roughness, with an Ra of 0.55 µm. In contrast, the as-built surface demonstrated significantly higher roughness, with an Ra value of 21.89 µm. The corresponding Rz values were 5.54 µm for the polished sample, 17.43 µm for the milled sample, and 150.45 µm for the as-built specimen.

Based on these measurements, it can be anticipated that the as-built condition will exhibit the lowest fatigue strength due to its substantially higher surface roughness, which may promote earlier crack initiation under cyclic loading.

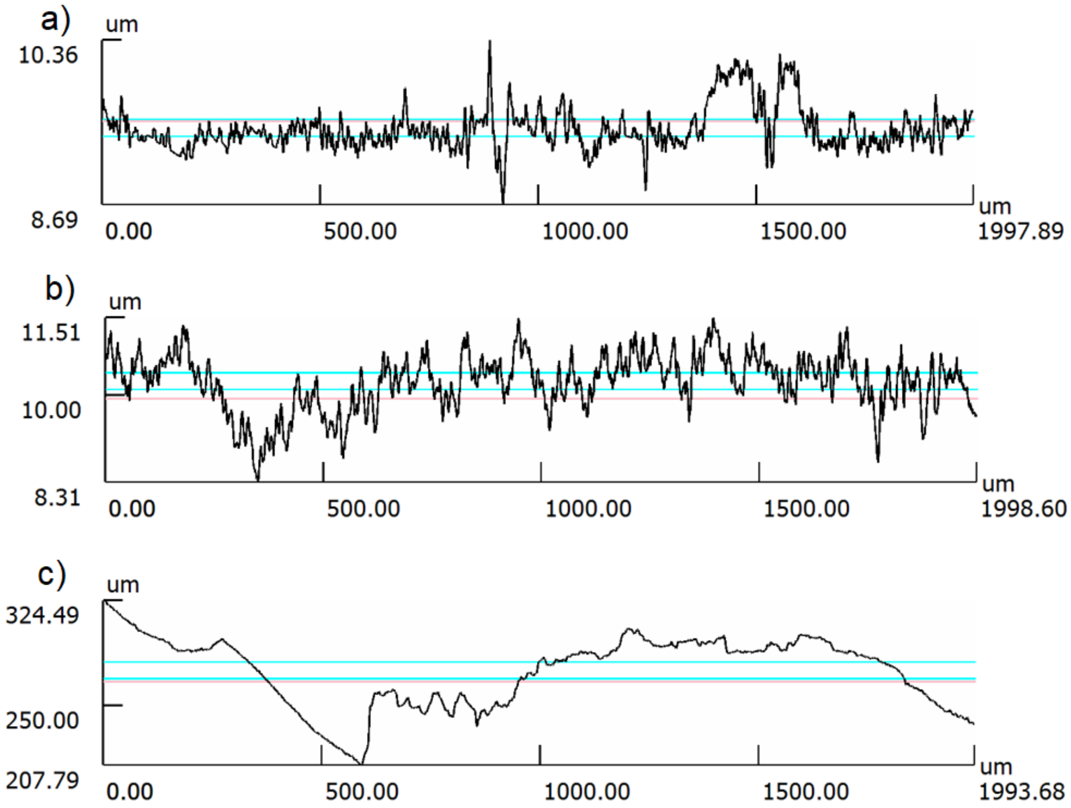

Fig. 3. Surface topography profiles of WAAM 316L in (a) polished, (b) milled, and (c) as-built conditions.

Table 2. Surface texture characteristics of the WAAM 316L.

	Ra [μm]	Rz [μm]
Polished	0.24	5.54
Milled	0.55	17.43
As-built	21.89	150.45

2.4.6 Mechanical properties

The mechanical properties of the WAAM-fabricated 316L stainless steel were evaluated through tensile testing, and the results are summarized in Table 3. The measured yield strength was 371 MPa in the vertical direction and 354 MPa in the horizontal direction, indicating that the vertical specimens exhibited approximately 4.8% higher yield strength.

A more noticeable difference was observed in the ultimate tensile strength (UTS). The vertical specimens demonstrated a value roughly 12% higher than that measured in the horizontal orientation. In addition, the elongation at fracture was slightly greater in the vertical direction, showing an increase of about 6.8% compared to the horizontal specimens.

Overall, these results suggest a moderate anisotropy in the static mechanical properties of the WAAM-produced 316L stainless steel. The vertical orientation consistently showed somewhat higher strength and ductility, which may be related to the microstructural characteristics and thermal history associated with the layer-by-layer deposition process.

Table 3. Mechanical properties of WAAM 316L.

	Yield strength [MPa]	Tensile strength [MPa]	Elongation [%]
Vertical	371	664	47
Horizontal	354	593	44

2.4.7 Bending fatigue strength

Bending fatigue tests were carried out on WAAM-fabricated 316L specimens with three different surface conditions: as-built, milled, and polished. All specimens were manufactured in the vertical build direction. The fatigue tests were conducted up to 2 × 10^6 cycles, which was defined as the fatigue limit.

The milled specimens exhibited the highest fatigue performance, reaching a fatigue limit of 223 MPa. The polished specimens showed slightly lower fatigue strength, with a fatigue limit of 207 MPa. Although polishing improved the surface finish, previous studies suggest that the dry electropolishing process used in this work can introduce tensile residual stresses at the surface. Such tensile stresses are detrimental to fatigue performance, as they promote earlier crack initiation and reduce resistance to cyclic loading.

The as-built specimens demonstrated the lowest fatigue resistance, with a fatigue limit of approximately 106 MPa. As shown earlier in Table 2, the as-built surface condition exhibited significantly higher surface roughness. Surface irregularities act as stress concentration sites, facilitating crack initiation under cyclic loading and thereby reducing fatigue strength. Consequently, the results clearly demonstrate the strong influence of surface condition and surface integrity on the fatigue behavior of WAAM-produced 316L stainless steel.

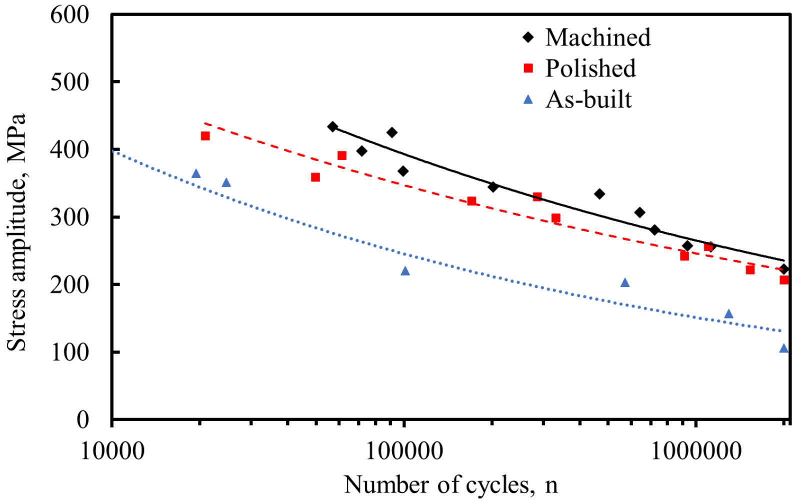

Fig. 4. Bending fatigue strength of WAAM 316L part with different surface qualities.

2.5 Influence of Process Parameters on Surface Finish and Mechanical Performance of WAAM Carbon Steel

2.5.1 WAAM equipment

A carbon steel (CS) filler wire designated (Esab OK Aristorod 12.50), compliant with EN ISO 14341-A: G 38 3 C1 3Si1, was utilized in the welding trials. The wire diameter was 1.2 mm. Its mechanical characteristics are summarized in Table 1, while the chemical composition is provided in Table 2.

The WAAM trials were carried out using a Fronius TransPuls Synergic 2700 system. A total of five distinct sets of processing parameters were applied, as listed in Table 3. Each parameter set was identified by a specific code (e.g., parameter 1 = P1). The shielding gas was supplied at a flow rate of 12 l/min, consisting of a mixture of 82% argon and 18% carbon dioxide.

Table 1. Properties of the carbon steel wire.

Yield strength [MPa]	Tensile strength [MPa]	Elongation [%]
470	560	26

Table 2. Chemical composition (%) of the carbon steel wire.

C	Mn	Cu	S	Si	P
0.1	1.11	0.07	0.012	0.72	0.013

Table 3. WAAM parameters.

Printing parameter	Printing speed [m/min]	Current [A]	Voltage [V]	Wire feeding speed [m/min]	Idle time [s]	Lift between layers [mm]
P1	0.64	163	11.6	3.5	60	1.5
P2	0.85	161	11.4	3.4	60	1.4
P3	0.55	156	11.1	3.4	60	1.4
P4	0.80	196	11.9	4.9	75	1.5
P5	0.30	135	11.0	2.8	60	1.5

2.5.2 Sample preparation and mechanical testing

The mechanical performance of the WAAM-fabricated components was evaluated through tensile testing. The tests were performed with an Instron 8802 hydraulic universal testing machine at a constant crosshead speed of 1.0 mm/min. For each set of printing parameters, five tensile specimens were examined.

Microhardness was assessed using an Innovatest Falcon 500 hardness tester. The measurements were carried out with a 0.1 kg load, and the spacing between successive indentations was 0.1 mm.

Surface topography was analyzed with a Keyence VK-X200 laser microscope employing non-contact laser scanning technology. The microscope provides a measurement resolution of 0.5 nm.

2.5.3 Hardness testing

Hardness testing was carried out on all specimens manufactured using the different parameter sets. The measurements were performed along the vertical direction of each component to evaluate potential variations through the deposited structure.

The results indicated that the base material hardness was nearly identical across all printing conditions, as illustrated in Fig. 1. The average hardness value of the printed carbon steel components was approximately 162 HV. The hardness distributions were consistent and exhibited minimal fluctuation along the measured paths. This uniformity suggests that the WAAM-produced carbon steel components possess homogeneous mechanical properties, with no significant strength variations attributable to the selected processing parameters.

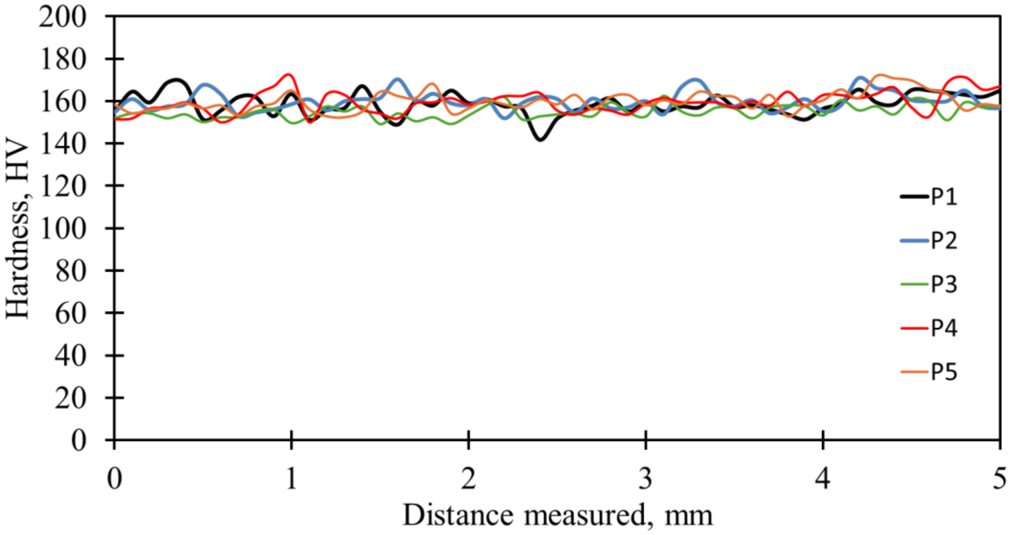

Fig. 1. Hardness curves of WAAM-fabricated carbon steel produced using various process parameter sets.

2.5.4 Geometry and surface profile of WAAM carbon steel

Figure 2 presents cross-sectional views of the components fabricated using the different parameter sets. The largest wall thickness was achieved with parameter set P5, measuring approximately 5.62 mm. In contrast, the smallest average wall thickness, 3.95 mm, was obtained with P3.

Based on Fig. 2, parameter sets P1 and P5 provided the most consistent geometrical quality. In these cases, adjacent layers overlapped effectively, resulting in relatively uniform wall thickness with minimal variation. Conversely, P2 (shown in Fig. 2b) demonstrated inferior geometrical accuracy, as indicated by noticeable fluctuations in wall thickness.

Importantly, none of the evaluated parameter combinations produced porosity or other major fabrication defects, indicating stable and defect-free WAAM processing across all tested conditions.

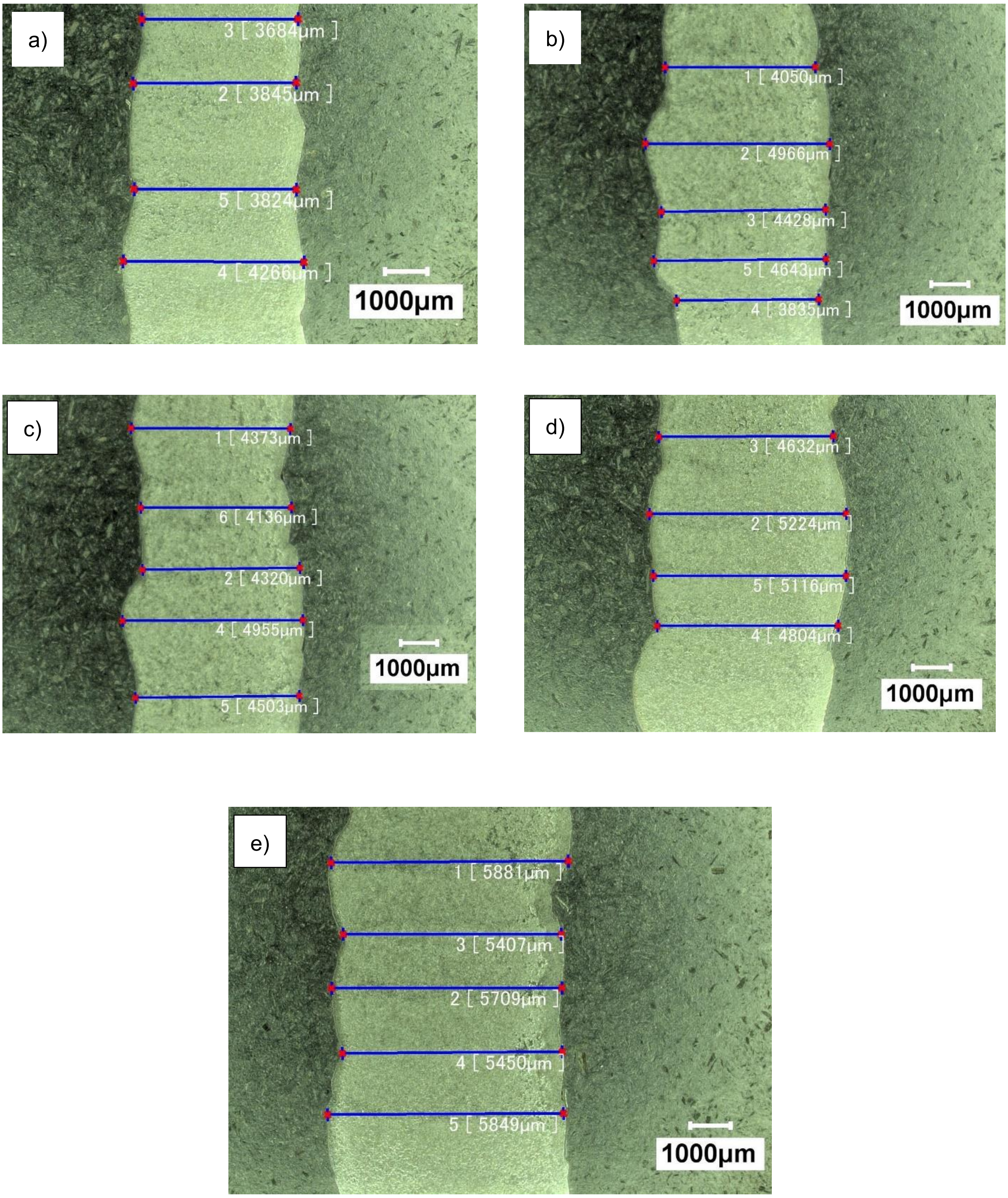

Fig. 2. The geometries of the WAAM carbon steel with a parameter (a) P1, (b) P2, (c) P3, (d) P4 and (e) P5.

Figure 3 illustrates the top surfaces of the fabricated walls, representing the final deposited layer. The images clearly indicate that the selected process parameters strongly influence the surface quality of this uppermost layer.

Parameter set P2 provides a clear example of inadequate print quality, as the top layer appears highly irregular and uneven. In contrast, the most uniform and visually consistent surfaces were achieved with parameter sets P5 and P1.

The condition of the top layer is particularly critical when the component is intended for use without subsequent finishing operations such as machining. Moreover, the appearance and uniformity of the final layer serve as practical indicators of whether the selected printing or welding parameters are well suited to the material and process conditions.

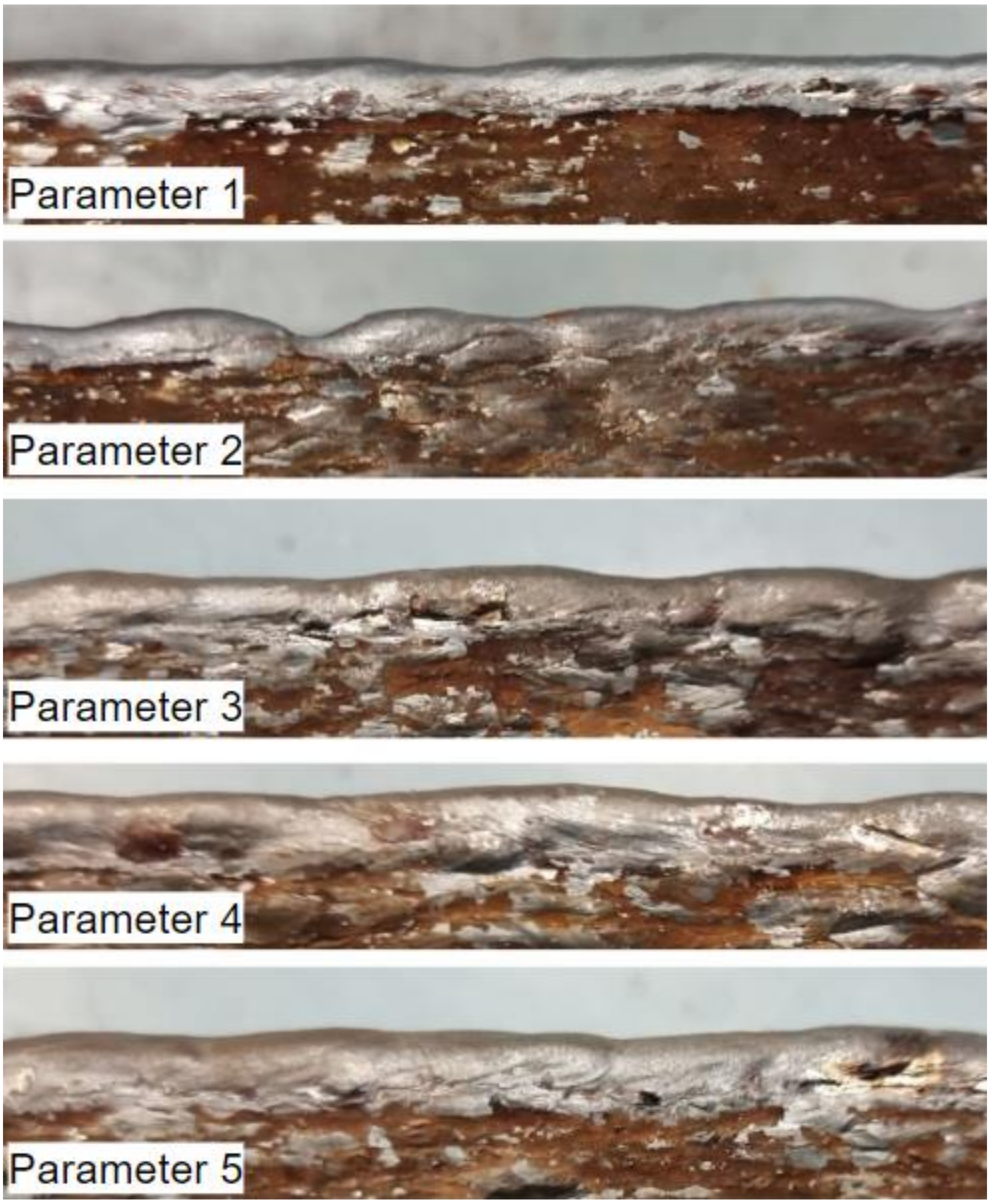

Fig. 3. The top layer with different parameters.

Figure 4 presents the surface roughness profiles of the printed walls produced using different parameter sets. Although the roughness profiles alone do not provide a direct assessment of overall build quality, surface roughness plays a critical role in fatigue performance and in the visual and functional surface appearance of the component.

According to the measurements summarized in Table 4, the smoothest surface was obtained with parameter set P2, which yielded an Ra value of 59 µm. In contrast, parameter set P4 resulted in the highest surface roughness and therefore the poorest surface finish.

The variation in surface roughness between the different parameter sets was considerable. Specifically, the highest Ra value measured with P4 was approximately 188% greater than the lowest Ra value recorded with P2, highlighting the strong influence of process parameters on surface characteristics.

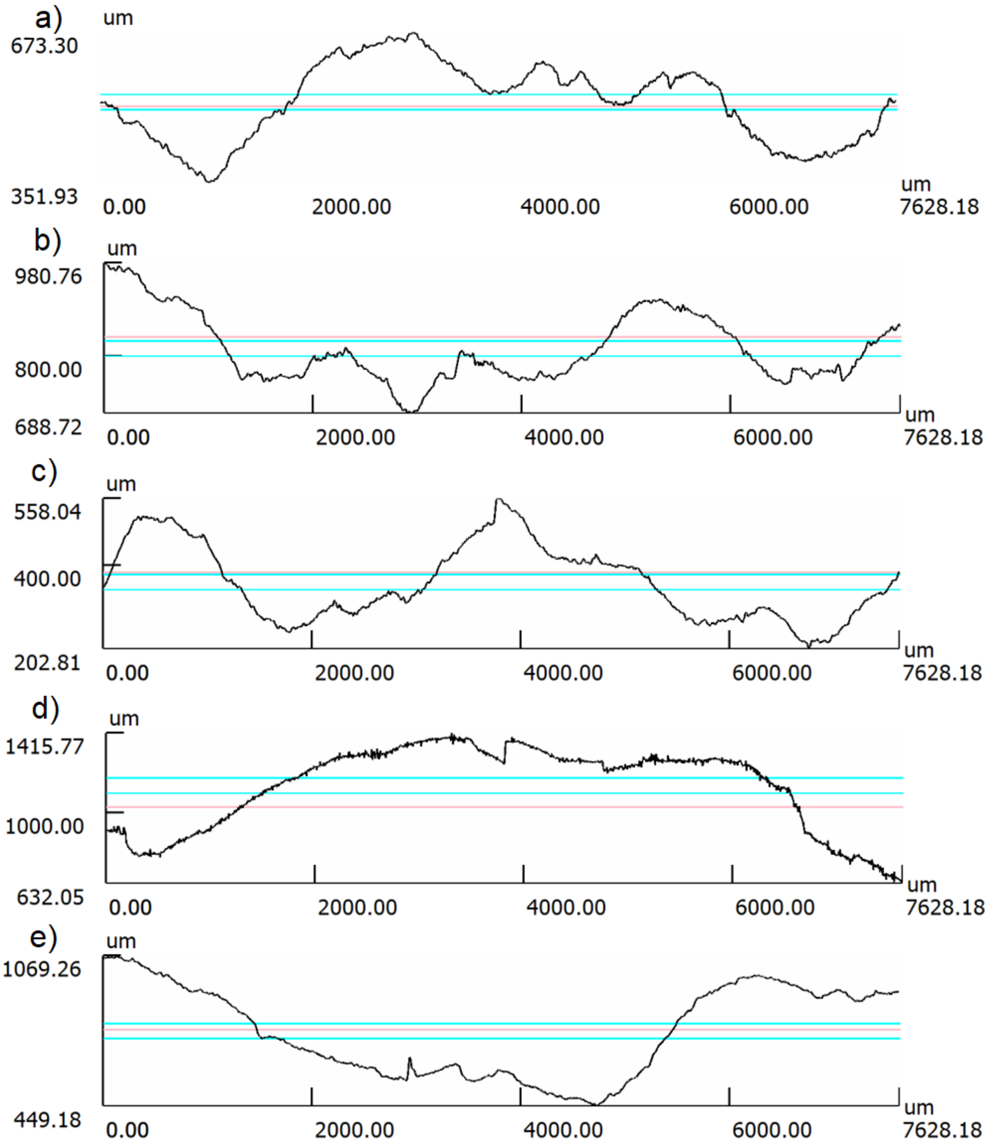

Fig. 4. Surface roughness of the WAAM carbon steel with different parameters. (a) P1, (b) P2, (c) P3, (d) P4 and (e) P5.

Table 4. Ra and Rz values of the WAAM carbon steel with different parameters.

	Rz µm	Ra µm
Parameter 1	468	83
Parameter 2	449	59
Parameter 3	487	75
Parameter 4	919	170
Parameter 5	733	152

2.5.5 Mechanical properties

The tensile properties of the WAAM-fabricated carbon steel components are summarized in Table 5. For all parameter sets, the yield strength was consistently higher in the build direction than in the deposition direction. The highest yield strength was obtained with parameter set P2. However, the variation in yield strength among the different parameter combinations was relatively small, with an approximate difference of 9% between the maximum and minimum values. This limited variation is consistent with the uniform hardness results observed earlier.

In contrast, the elongation values showed more pronounced differences. The gap between the lowest and highest elongation was approximately 26%, indicating a noticeable influence of process parameters on ductility.

The WAAM carbon steel exhibited lower ultimate tensile strength compared to the manufacturer's specified values (Table 1). Notably, parameter set P2 delivered the highest static strength, despite showing the least favorable wall geometry and weld bead appearance in the earlier geometrical assessment.

Table 5. Static properties of the WAAM carbon steel with different parameters.

Parameter	Printing direction	Yield strength [MPa]	Tensile strength [MPa]	Elongation [%]
P1	horizontal	379	499	44.9
P1	vertical	392	503	41
P2	horizontal	394	512	33.2
P2	vertical	400	504	38.2
P3	horizontal	364	484	40.4
P3	vertical	367	483	41
P4	horizontal	365	501	37
P4	vertical	373	497	37.3
P5	horizontal	367	477	42.8
P5	vertical	375	487	41.4

2.6 Bending Fatigue Strength of WAAM Carbon Steel Without Interpass Temperature Control

2.6.1 WAAM equipment

The WAAM trials were performed using a Fronius TransPuls Synergic 2700 system operating with Cold Metal Transfer (CMT) technology. The process parameters were defined as follows: wire feed speed of 3.5 m/min, welding current of 163 A, and arc voltage of 11.6 V. The deposition speed during printing was maintained at 0.64 m/min, and the vertical increment between successive layers was set to 1.6 mm. To promote thermal stability, a 90-second idle time was applied between each deposited layer. Shielding was provided by a gas mixture of 82% argon and 18% carbon dioxide at a flow rate of 12 l/min.

Carbon steel filler wire (Esab OK Aristorod 12.50), compliant with EN ISO 14341-A: G 38 3 C1 3Si1, was used in the experiments. The wire diameter was 1.2 mm, enabling controlled and stable material transfer during deposition. The mechanical properties of the filler material are summarized in Table 1, while its chemical composition is presented in Table 2.

Table 1. Static properties of the carbon steel wire.

Yield strength [MPa]	Tensile strength [MPa]	Elongation [%]
470	560	26

Table 2. Chemical composition (%) of the carbon steel wire.

C	Mn	Si	Cu	S	P
0.1	1.11	0.72	0.07	0.0012	0.013

2.6.2 Mechanical characterization

Tensile testing was carried out using an Instron 8802 universal testing machine in accordance with the SFS-EN ISO 68921:2016 standard. The experiments were performed at a constant crosshead speed of 1.0 mm/min to ensure repeatable and reliable measurements.

Microhardness was measured with an Innovatest Falcon 500 hardness tester using a load of 0.2 kg. Indentations were placed at 0.1 mm intervals to obtain detailed hardness profiles. Microstructural characterization was conducted using a Keyence VK-X200 laser microscope.

The bending fatigue performance of the WAAM-fabricated specimens was evaluated with a custom-built reversed bending fatigue apparatus based on the WEBI machine originally produced by Carl Schenck. The fatigue tests were performed under fully reversed loading conditions with a stress ratio $R = -1$, where R denotes the ratio of minimum to maximum stress within a loading cycle. Stress amplitudes between 230 MPa and 470 MPa were applied. Each specimen was individually calibrated using a force sensor prior to testing to ensure accurate load application and improve the reliability of the fatigue data.

2.6.3 Microstructure analysis

As illustrated in Fig. 1, the material is characterized by relatively coarse grains with a clearly defined crystallographic structure. The grains are predominantly equiaxed, indicating that their dimensions are approximately equal in all directions. The microstructure mainly consists of ferrite, which is essentially iron containing a low concentration of carbon and minor alloying elements. Such a ferritic structure promotes good ductility and formability. In general, ferritic microstructures are associated with enhanced plastic deformation capability, making the material well suited for forming and fabrication processes. The development of this ferritic structure in WAAM-produced carbon steel is influenced by factors such as cooling conditions during deposition and the carbon content of the alloy. This microstructural configuration plays a key role in determining the overall mechanical response, providing a balanced combination of strength, toughness, and workability.

Figure 2 presents a cross-sectional view of the WAAM carbon steel wall, with an average thickness of approximately 3.92 mm. The surface finish appears reasonably uniform for an additively manufactured component, although some variation in wall thickness can be observed between layers. A particularly important finding of this study is the absence of porosity or other significant manufacturing defects in the WAAM carbon steel.

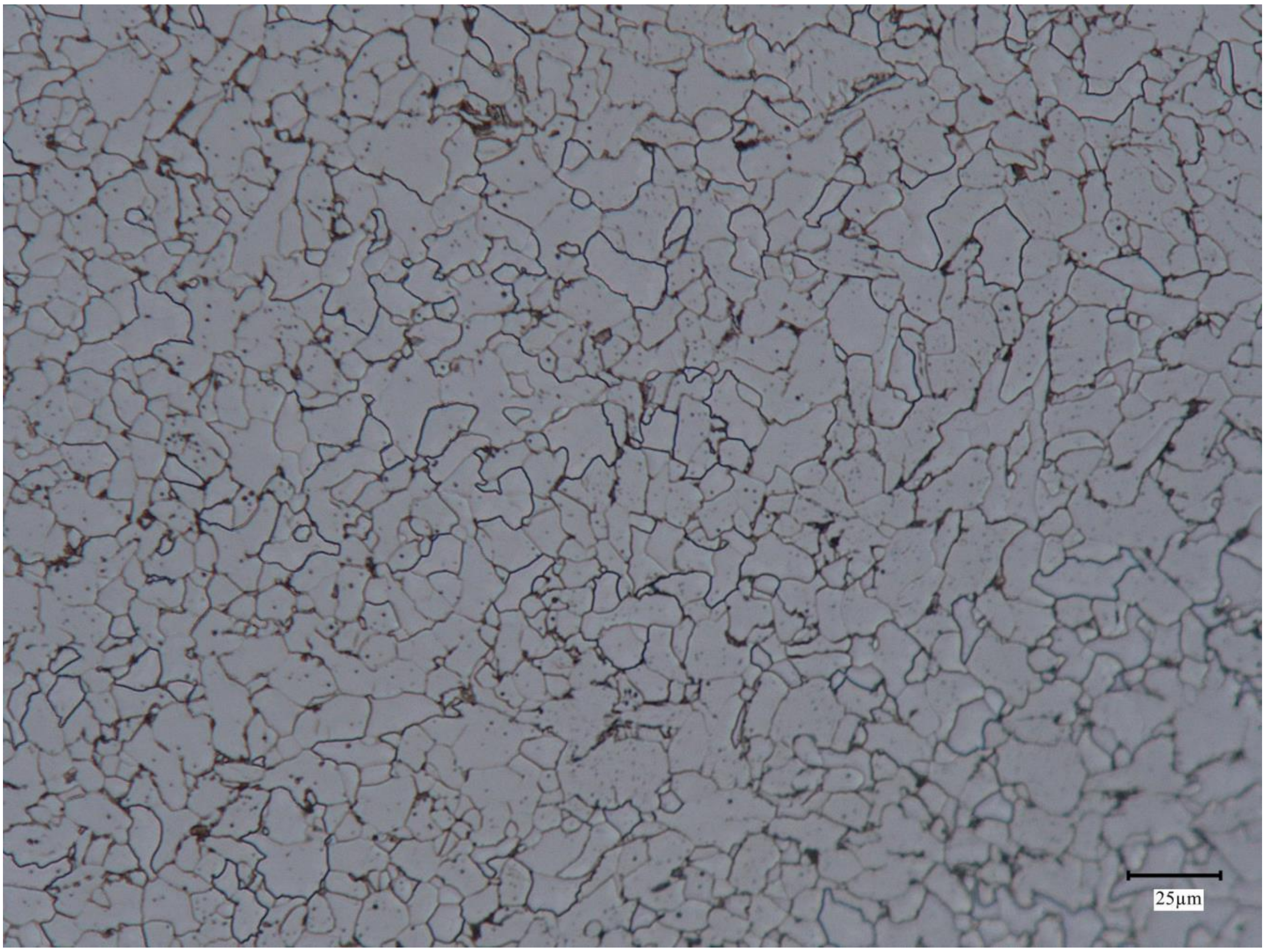

Fig. 1. Microstructure of WAAM carbon steel.

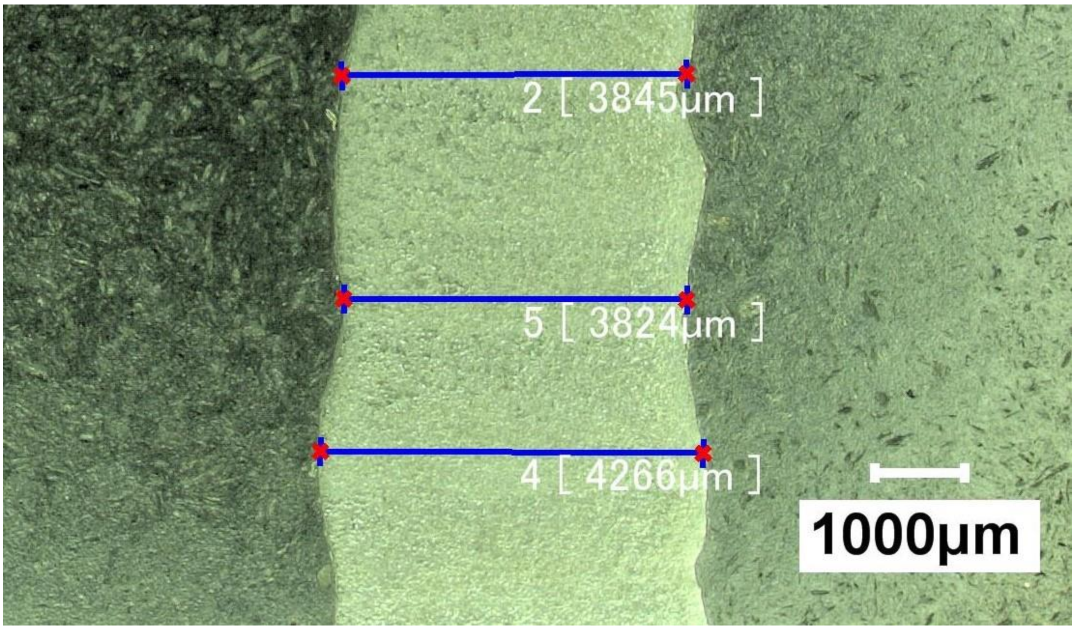

Fig. 2. Cross-section of WAAM carbon steel.

2.6.4 Hardness measurements

Hardness measurements were performed along the deposition direction of the component to evaluate potential variations through the build. The results indicated an average base material hardness of approximately 159 HV.

As shown in Fig. 3, the hardness values are evenly distributed along the measured path, demonstrating a stable and uniform hardness profile. This consistency suggests that the WAAM-produced carbon steel possesses homogeneous mechanical properties. The findings are in good agreement with the uniform microstructure observed in the microscopic examination.

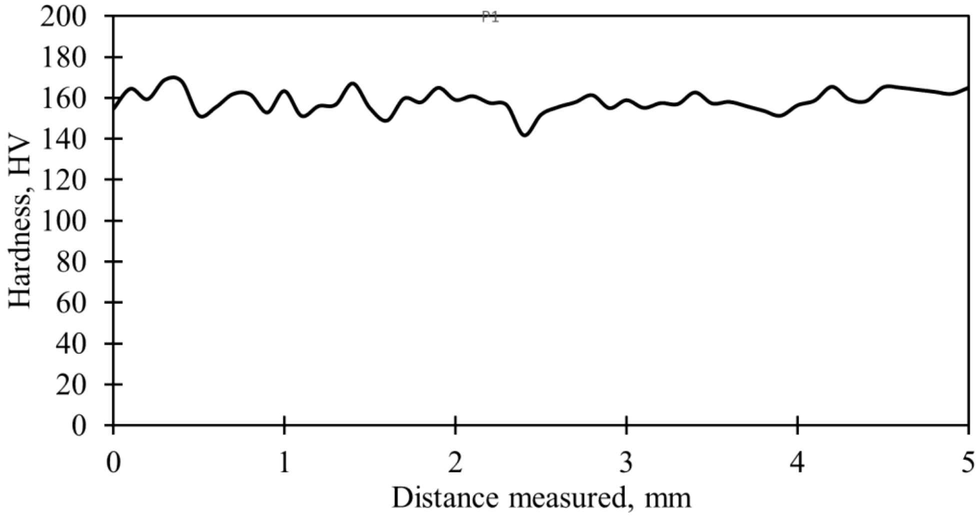

Fig. 3. Hardness of WAAM carbon steel.

2.6.5 Mechanical properties of WAAM carbon steel

Table 3 presents the static mechanical properties of the WAAM-fabricated carbon steel in comparison with the reference material S355MC steel. The results show that the yield strength of the WAAM carbon steel was slightly higher in the vertical direction, reaching a maximum value of 392 MPa, compared to 379 MPa in the horizontal direction. In contrast, the elongation was higher in the horizontal direction (45%) than in the vertical direction (41%), indicating slightly greater ductility when loaded parallel to the deposited layers.

When compared with the reference material, S355MC steel exhibited the highest yield strength, measured at 431 MPa, which is notably higher than that of the WAAM-produced carbon steel. However, the ultimate tensile strengths of all materials were very similar, ranging from 498 MPa to 503 MPa.

A clear difference was observed in ductility. The WAAM carbon steel demonstrated significantly higher elongation values (41–45%) compared to S355MC steel (26%), indicating that the additively manufactured material possesses greater plastic deformation capability before fracture. This difference may be associated with the microstructural characteristics produced during the WAAM deposition process, which can promote enhanced ductility compared to conventionally processed structural steel.

Overall, the results indicate that while S355MC steel provides higher yield strength, the WAAM-fabricated carbon steel exhibits comparable tensile strength and significantly improved ductility.

Table 3. Static properties of the WAAM carbon steel and S355MC.

Material	Printing direction	Yield strength [MPa]	Tensile strength [MPa]	Elongation [%]
WAAM CS	vertical	392	503	41
WAAM CS	horizontal	379	499	45
S355MC		431	498	26

2.6.6 Bending fatigue strength

In the bending fatigue assessment, the fatigue behavior of WAAM-fabricated carbon steel was compared with that of the reference material S355MC structural steel. The fatigue tests were conducted up to a run-out limit of 2×10^6 cycles, which was defined as the fatigue limit. The corresponding S–N curves are shown in Fig. 4.

The results show that the fatigue limit of the WAAM carbon steel was approximately 209 MPa in the vertical direction and 253 MPa in the horizontal direction. In comparison, the fatigue limit of S355MC steel was 161 MPa, which is clearly lower than that of the WAAM-produced material. The S–N curves demonstrate that the WAAM carbon steel exhibits superior fatigue resistance compared to the reference structural steel across the investigated stress range.

Based on these findings, WAAM-fabricated carbon steel shows strong potential for structural applications where cyclic loading is present, such as lattice structures or lightweight load-bearing components. The results indicate that the fatigue performance of WAAM carbon steel is at least comparable—and in this case superior—to that of conventional S355MC structural steel sheet, supporting the feasibility of using WAAM-produced materials in fatigue-critical engineering applications.

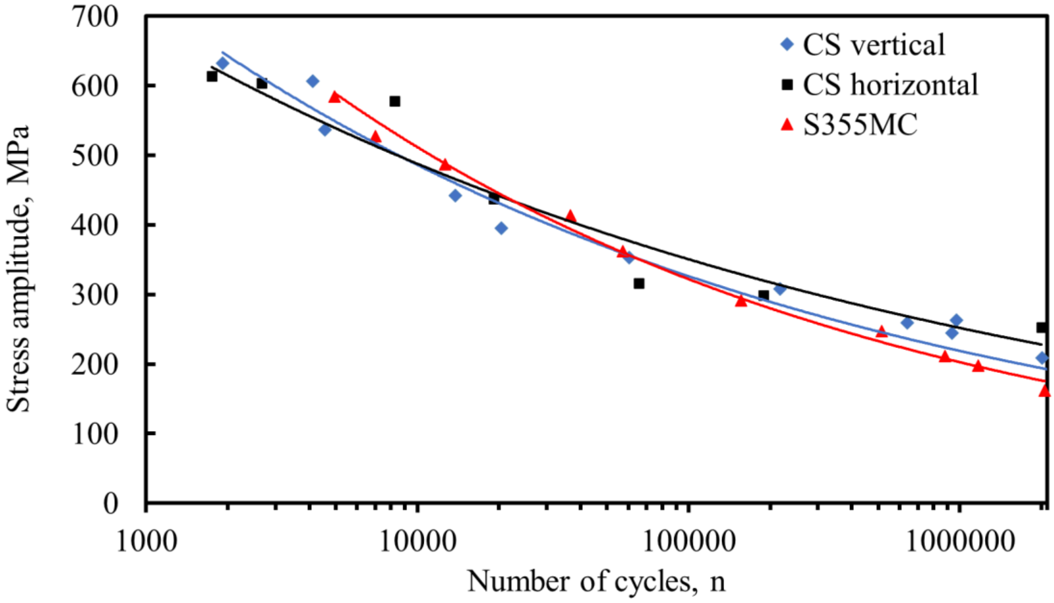

Fig. 4. Fatigue strength of WAAM CS and S355MC.

2.7 Evaluation of the Effect of Severe Shot Peening on the Fatigue Performance of WAAM Carbon Steel

2.7.1 WAAM printing equipment

The WAAM experiments were carried out using a Fronius TransPuls Synergic 2700 system with Cold Metal Transfer (CMT) technology. The deposition speed was kept constant at 0.64 m/min, and a vertical increment of 1.6 mm was applied between successive layers. The welding parameters were set to 163 A current, 11.6 V voltage, and a wire feed speed of 3.5 m/min. A 60-second idle time was introduced between layers to support thermal control during the build. Shielding was provided by a gas mixture of 82% argon and 18% carbon dioxide at a flow rate of 12 l/min, ensuring stable arc conditions and consistent print quality.

The filler material used in the study was carbon steel wire Esab OK Aristorod 12.50, compliant with EN ISO 14341-A (G 38 3 C1 3Si1). The wire diameter was 1.2 mm. Its mechanical properties are presented in Table 1, and the corresponding chemical composition is summarized in Table 2.

Table 1. The static properties of the carbon steel wire.

Yield strength [MPa]	Tensile strength [MPa]	Elongation [%]
470	560	26

Table 2. The chemical composition % of the carbon steel welding wire.

C	S	Mn	Si	P	Cu
0.1	0.012	1.11	0.72	0.0013	0.07

2.7.2 Mechanical characterization

Tensile specimens were extracted from the WAAM-fabricated component after machining approximately 0.8–1.2 mm from both surfaces to remove irregular outer layers. This procedure produced a uniform plate with a final thickness of 2 mm. Standardized tensile samples were subsequently laser-cut and machined to the required dimensions.

Tensile testing was carried out using an Instron 8802 universal testing machine in accordance with SFS-EN ISO 68921:2016. All tests were performed at a constant crosshead speed of 1.0 mm/min to ensure consistency. Vickers microhardness measurements were obtained with an Innovatest Falcon 500 hardness tester using a 0.2 kg load, with indentations spaced at 0.1 mm intervals.

Fatigue performance was evaluated using a custom-designed bending fatigue machine developed by the FMT research group at the University of Oulu. The tests were conducted under fully reversed loading conditions ($R = -1$), with stress amplitudes ranging from 190 MPa to 640 MPa. Each specimen was individually calibrated using a dedicated force sensor to guarantee accurate load application and reliable fatigue data.

Electron backscatter diffraction (EBSD) analysis was performed with a JEOL JSM-7900F scanning electron microscope equipped with an Oxford Instruments Symmetry EBSD detector. The EBSD measurements were conducted at an accelerating voltage of 20 kV and a working distance of 17 mm. Energy-dispersive spectroscopy (EDS) analysis was performed at 10 kV with a working distance of 8 mm.

The severe shot peening (SSP) treatment was conducted in a closed blasting cabinet using an ABB industrial robot to ensure process control and repeatability. A custom fixture was designed to enable consistent treatment of both specimen surfaces. Each sample was subjected to up to 22 passes per side, with 180° rotation after each pass to achieve uniform coverage. Spherical martensitic chromium steel shots (STELUX C40) with a diameter range of 0.30–0.85 mm and a hardness of 36 HRC were used as the peening media. The blasting pressure was set to 7.4 bar, and the nozzle distance was maintained at 70 mm. After 22 passes, the Almen intensity measured with type A strips was approximately 300 A.

2.7.3 Microstructure analysis

As shown in Fig. 1, the material is characterized by relatively coarse grains with a well-defined crystallographic structure. The grains are predominantly equiaxed, indicating that their dimensions are approximately uniform in all directions. Overall, the bulk grain size is comparatively large. Fig. 1 demonstrates that the grain size at the surface is significantly refined as a result of the SSP treatment. This grain refinement at the surface contributes to increased hardness and strength in the treated layer. However, the localized nature of this modification produces a gradient in the microstructure, resulting in a non-uniform structural condition within the WAAM carbon steel component after SSP processing.

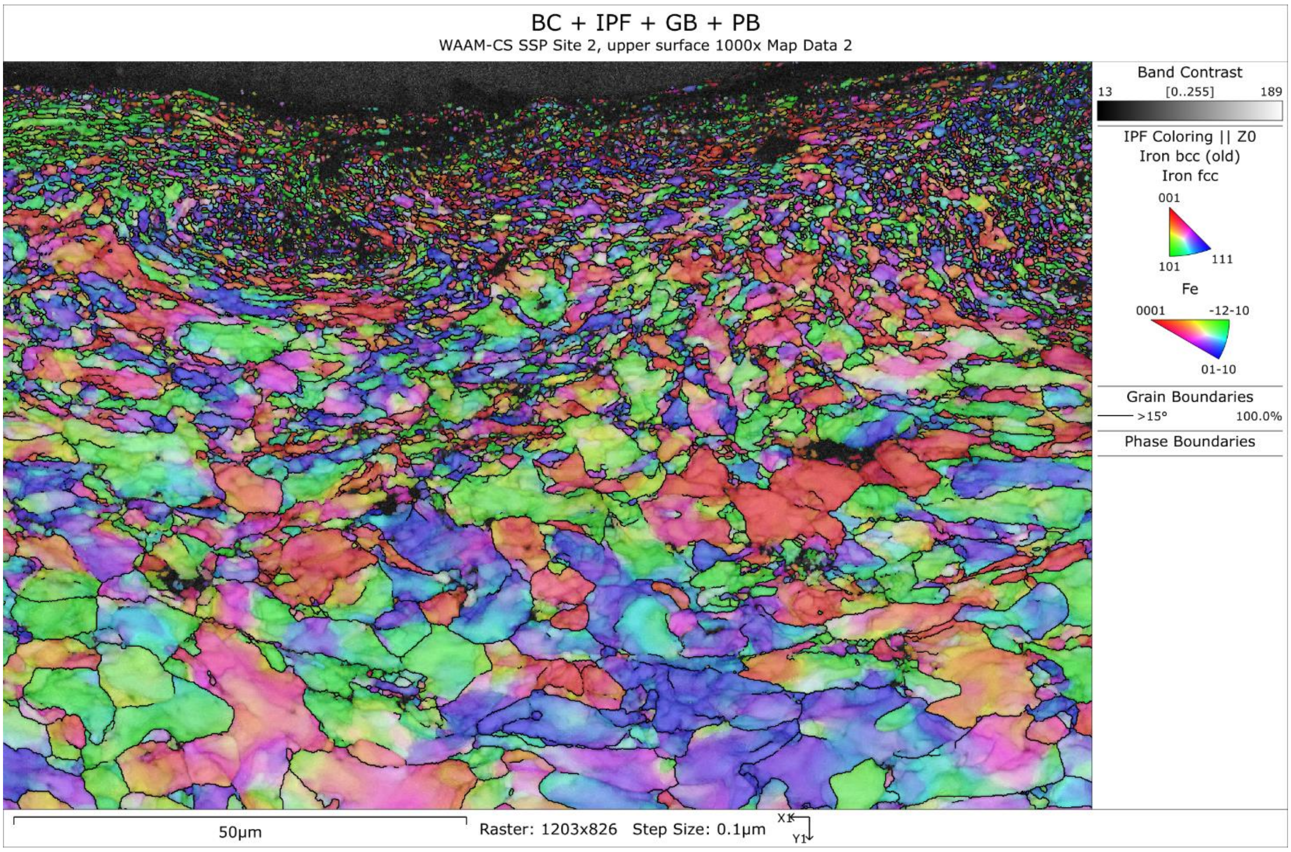

Fig. 1. Band contrast map from the surface of the WAAM CS SSP.

2.7.4 Hardness measurements

The cross-sectional hardness distribution of the WAAM carbon steel specimen treated with severe shot peening is presented in Fig. 2. The results clearly show that the SSP treatment significantly modified the near-surface properties, with the hardened layer extending to a depth of approximately 0.4 mm.

The average hardness of the untreated base material was about 165 HV. In contrast, the maximum hardness value, measured near the treated surface, reached 270 HV. This corresponds to an increase of approximately 64% in surface hardness as a result of the SSP process.

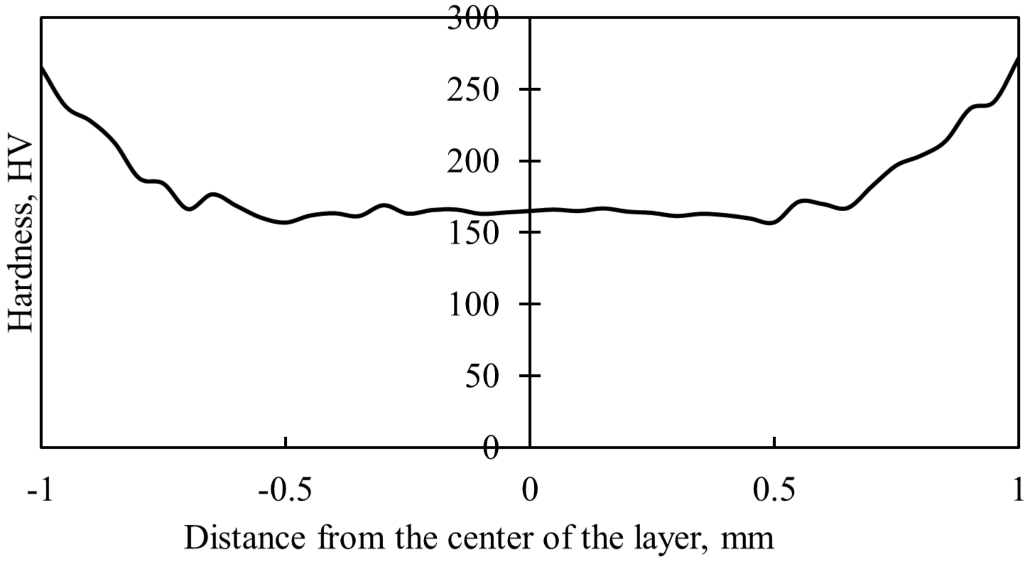

Fig. 2. Hardness of the severe shot peened WAAM carbon steel.

2.7.5 Mechanical properties

Table 3 shows the tensile test results for the as-built WAAM carbon steel and the specimens treated with severe shot peening (SSP). All specimens were manufactured and tested in the vertical build direction. The evaluated mechanical properties included yield strength, ultimate tensile strength, and elongation at fracture.

The results indicate that SSP treatment slightly improved the strength of the WAAM carbon steel. The yield strength increased from 392 MPa to 399 MPa, corresponding to an increase of approximately 7 MPa (about 1.8%). Similarly, the ultimate tensile strength increased from 503 MPa to 513 MPa, representing an improvement of about 10 MPa (approximately 2%). The highest tensile strength measured for the WAAM CS SSP specimens was 513 MPa.

Despite the increase in strength, the ductility decreased after SSP treatment. The elongation at fracture was reduced from 41% for the untreated WAAM carbon steel to 35% for the shot-peened material. This behavior reflects the typical strength–ductility trade-off associated with surface strengthening treatments, where the introduction of compressive residual stresses and surface hardening improves strength but reduces the material’s capacity for plastic deformation.

Table 3. Static properties of the WAAM CS and WAAM CS SSP.

Material	Yield strength [MPa]	Tensile strength [MPa]	Elongation [%]
WAAM CS	392	503	41
WAAM CS SSP	399	513	35

2.7.6 Bending fatigue strength

Bending fatigue tests were performed on WAAM-fabricated carbon steel specimens in two different conditions: as-built WAAM CS and WAAM CS treated with SSP. All specimens were extracted in the horizontal direction. The tests were conducted up to a run-out limit of 2×10^6 cycles, which was defined as the fatigue limit, and the corresponding S–N curves are presented in Fig. 3.

The results show that the fatigue limit remained approximately the same for both conditions, with a value of about 252 MPa for both the untreated WAAM CS and the SSP-treated material. However, the SSP-treated specimens exhibited slightly better fatigue performance overall, particularly in parts of the low- and medium-cycle fatigue regions, where they were able to sustain somewhat higher stress amplitudes at comparable cycle counts.

The improved fatigue behavior after SSP can be attributed to the modified surface condition produced by the shot peening treatment. In bending fatigue, crack initiation typically occurs at or near the surface of the material, making surface integrity a critical factor. Severe shot peening introduces compressive residual stresses and increases surface hardness, both of which help delay crack initiation and slow crack propagation, thereby contributing to the observed improvement in fatigue performance.

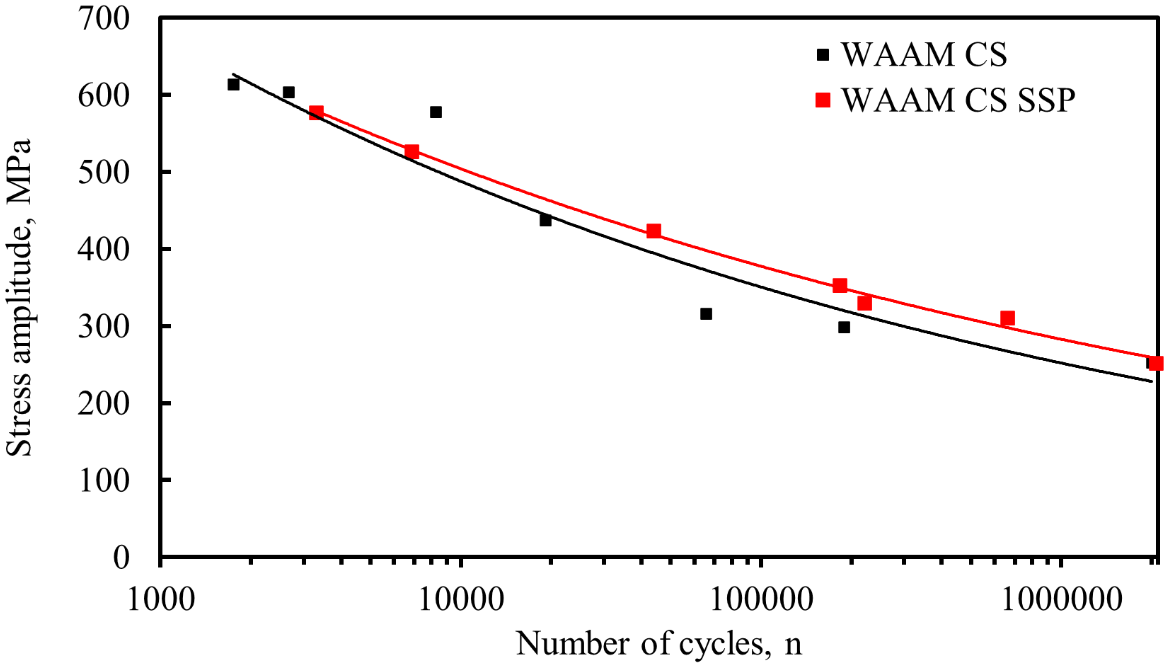

Fig. 3. Bending fatigue strength of WAAM CS and WAAM CS SSP.

2.8 Investigation of the Influence of Surface Condition on the Bending Fatigue Performance of WAAM Carbon Steel

2.8.1 Printing equipment

The WAAM experiments were conducted using a Fronius TransPuls Synergic 2700 welding system operating with Cold Metal Transfer (CMT) technology. The deposition speed was maintained at 0.64 m/min, and a vertical increment of 1.5 mm was applied between successive layers. The welding parameters were set to 163 A current and 11.6 V voltage, with a wire feed rate of 3.5 m/min. An idle time of 60 seconds was introduced between layers to allow controlled cooling. Shielding was provided by a gas mixture of 82% argon and 18% carbon dioxide at a flow rate of 12 l/min.

The filler material used was carbon steel wire Esab OK Aristorod 12.50, compliant with EN ISO 14341-A (G 38 3 C1 3Si1). The wire diameter was 1.2 mm. Its mechanical properties are presented in Table 1.

Table 1. Mechanical properties of the carbon steel wire.

Yield strength [MPa]	Tensile strength [MPa]	Elongation [%]
470	560	26

2.8.2 Mechanical characterization

Fatigue performance was assessed using a custom-designed bending fatigue machine developed by the FMT research group at the University of Oulu. The tests were conducted under fully reversed loading conditions ($R = -1$), with stress amplitudes ranging from 125 MPa to 640 MPa. Each specimen was individually calibrated using a dedicated force sensor to ensure accurate load application and reliable fatigue results.

2.8.3 Surface roughness

Surface roughness was evaluated using laser scanning on specimens with three different surface conditions: machined, polished, and as-built (Fig. 1 a–c). The measured average roughness (Ra) and maximum peak-to-valley height (Rz) values are summarized in Table 2, and representative surface profiles are shown in Fig. 1.

The polished specimen exhibited the best surface quality, with an Ra value of 0.32 μm and an Rz value of 3.79 μm. The machined surface showed moderately higher roughness, with Ra and Rz values of 1.71 μm and 11.51 μm, respectively. In contrast, the as-built surface displayed significantly higher roughness, with Ra reaching 20.67 μm and Rz increasing to 83.95 μm.

These results clearly demonstrate that the as-built condition has the poorest surface quality among the tested states. Given the strong influence of surface condition on crack initiation, it is reasonable to expect reduced fatigue performance for the as-built specimens compared to the machined and polished samples.

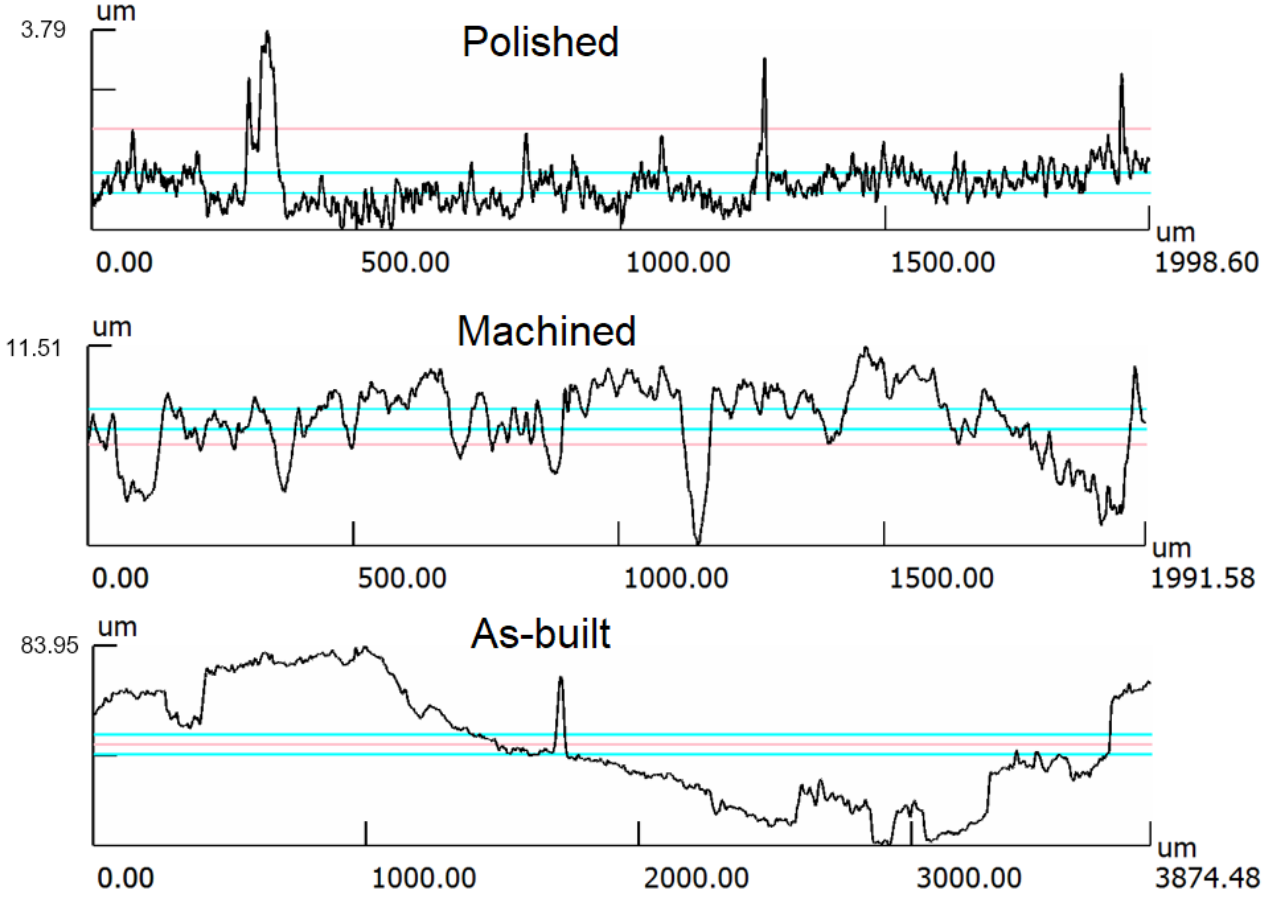

Fig. 1. Surface profiles of WAAM CS with different surface quality.

Table 2. Surface quality of WAAM carbon steel.

Surface	Rz [µm]	Ra [µm]
Polished	3.79	0.32
Machined	11.51	1.71
As-built	83.95	20.67

2.8.4 Fatigue strength

Bending fatigue experiments were conducted on WAAM carbon steel specimens with three different surface conditions: machined, polished, and as-built. All specimens were prepared in the deposition direction to ensure consistent comparison. The tests were carried out up to 2 × 10^6 cycles, which was defined as the fatigue limit and used as the criterion for evaluating fatigue performance.

Clear differences were observed between the surface conditions. The machined specimens exhibited the highest fatigue limit, reaching 250 MPa. Despite having the smoothest surface, the polished specimens showed a lower fatigue limit of 200 MPa. Further analysis indicated that the dry electropolishing process introduced tensile residual stresses into the surface layer. These tensile stresses are detrimental under cyclic loading and contributed to the reduced fatigue strength of the polished samples.

The as-built condition demonstrated the lowest fatigue resistance, with a fatigue limit of approximately 130 MPa. As previously shown in Table 3, the as-built surface had the highest roughness, which promotes crack initiation under cyclic loading. The combined effects of surface roughness and residual stress state highlight the complex relationship between surface condition and fatigue performance in WAAM carbon steel.

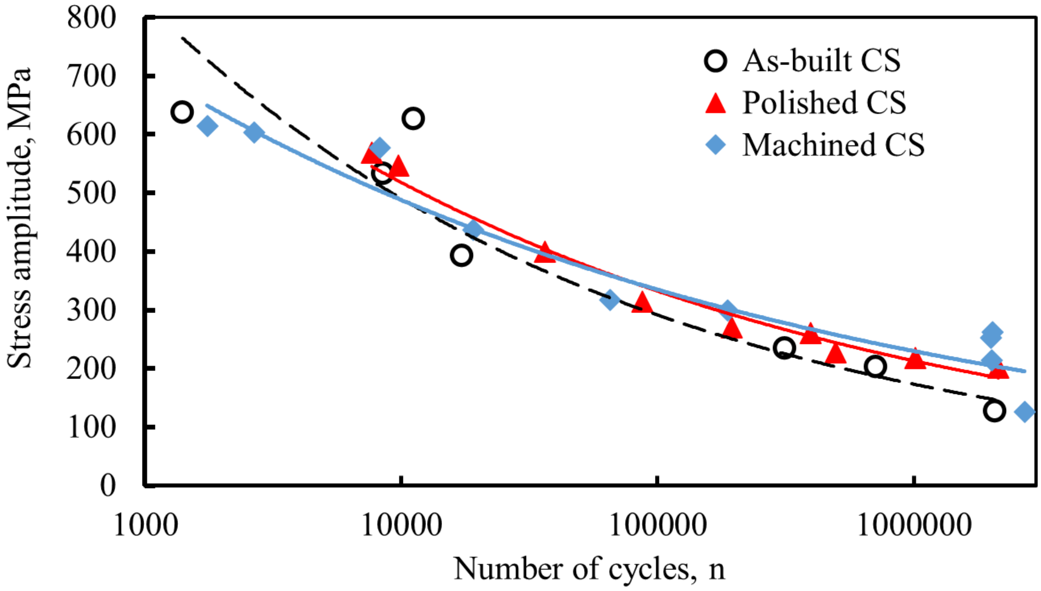

Fig. 2. Fatigue strength of WAAM carbon steel with different surface quality.

2.9 Fatigue Strength of WAAM Ultra-High-Strength Steel

2.9.1 Printing equipment

In the WAAM trials, a Fronius TransPuls Synergic 2700 system operating with Cold Metal Transfer (CMT) technology. The printing speed was set to 0.35 m/min, and a vertical increment of 1.8 mm was applied between consecutive layers. The welding parameters included a current of 131 A, a voltage of 11 V, and a wire feed rate of 2.9 m/min. Between each deposited layer, the component was allowed to cool naturally to 110 °C to maintain controlled thermal conditions. Shielding was provided by a gas mixture of 82% argon and 18% carbon dioxide at a flow rate of 12 l/min.

The welding wire used in the WAAM process was an ultra-high-strength (UHS) (Esab OK Aristorod 89) wire conforming to EN ISO 16834-A: G89 4 M Mn4Ni2CrMo. The wire diameter was 1.2 mm. Its mechanical properties are presented in Table 1, and the chemical composition is listed in Table 2.

Table 1. Static properties of the UHS wire.

Yield strength MPa	Tensile strength MPa	Elongation %
920	940	18

Table 2. Chemical composition (%) of the UHS wire.

C	Si	Mn	Ni	Cr	Mo
0.081	0.8	1.75	2.22	0.41	0.533

2.9.2 Mechanical testing setup

Tensile specimens were prepared from the WAAM-fabricated component by machining approximately 1 mm from both surfaces to remove the uneven outer layers. This procedure produced a uniform plate with a thickness of 2 mm. Standardized tensile samples were then cut from the plate and machined to precise dimensions to ensure reliable and repeatable testing.

Tensile testing was performed using an Instron 8802 universal testing machine in accordance with SFS-EN ISO 68921:2016. A constant crosshead speed of 1.0 mm/min was maintained throughout the experiments. Vickers hardness measurements were carried out using an Innovatest Falcon 500 hardness tester with a 0.2 kg load, and indentations were placed at 0.1 mm intervals.

Fatigue performance was assessed using a custom-designed bending fatigue machine developed by the FMT research group at the University of Oulu. The tests were conducted under fully reversed loading conditions (R = −1), with stress amplitudes ranging from 185 MPa to 860 MPa. Each specimen was individually calibrated using a dedicated force sensor to ensure accurate load application and dependable fatigue results.

For microstructural characterization, samples were first polished and then etched with a 68% nitric acid solution to reveal structural features. The microstructure was subsequently examined using a Keyence VK-X200 laser microscope, enabling high-resolution imaging and detailed analysis of the material’s internal structure.

2.9.3 Hardness measurement and macrostructure analysis

Hardness measurements were carried out on a specimen extracted from the WAAM-fabricated ultra-high-strength (UHS) steel component. The measurements were performed in the vertical direction at a location 3 mm from the reference point, as shown in Fig. 1. The specimen was taken from the central region of the deposited structure to ensure representative results. The hardness profile demonstrated a consistent distribution throughout the component, with an average value of approximately 292 HV. In addition, measurements taken across the deposited layers showed no significant variation in hardness within the interlayer regions, confirming uniform mechanical properties.

As illustrated in Fig. 2a and 2b, the material exhibits relatively fine, equiaxed grains with a well-defined crystallographic structure. The grains are nearly equal in size in all directions, and this refined microstructure contributes significantly to the overall mechanical performance of the material.

Although detailed microstructural analysis was not the primary focus of this study, a macroscopic examination was conducted to identify any porosity or major manufacturing defects that could affect fatigue performance. As seen in Fig. 2, no visible pores or significant defects were detected, indicating good structural integrity of the WAAM-produced UHS steel.

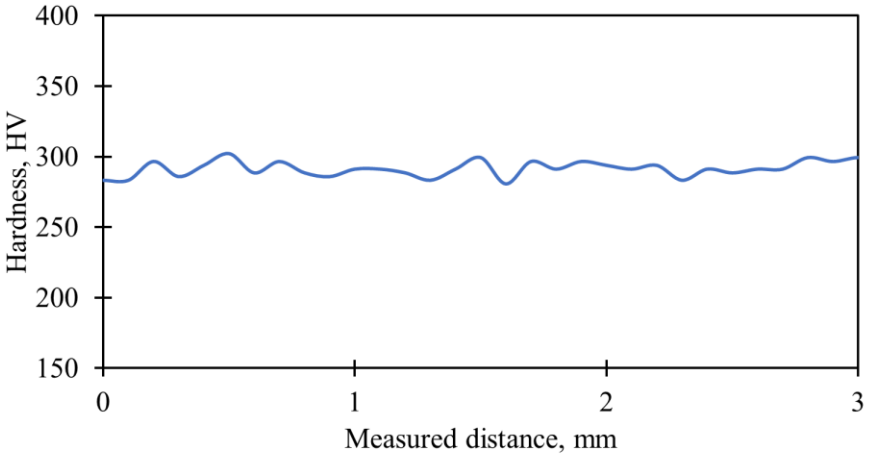

Fig. 1. Microhardness of WAAM ultra-high-strength steel.

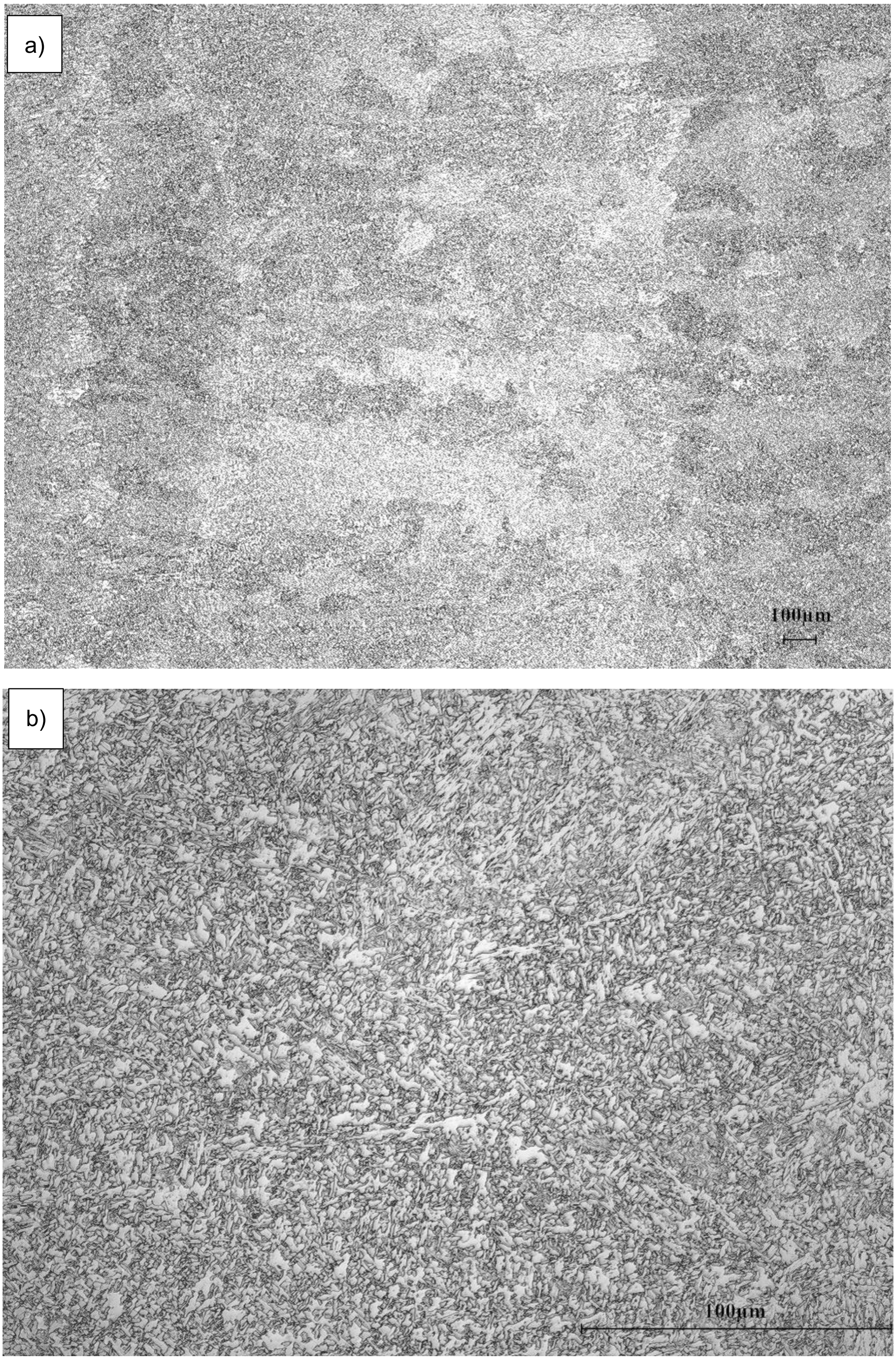

Fig. 2. Macrostructure of WAAM ultra-high-strength steel: (a) 5x magnification; (b) 50x magnification.

2.9.4 Mechanical properties

Tensile tests were performed on specimens extracted from the WAAM-fabricated UHS steel, and the results are summarized in Table 3. The results indicate a moderate anisotropy in mechanical properties depending on the build orientation. The yield strength measured in the vertical direction was 836 MPa, which is approximately 4 MPa higher than that measured in the horizontal (deposition) direction.

A more pronounced difference was observed in the ultimate tensile strength (UTS). The vertical specimens exhibited a tensile strength of 977 MPa, whereas the horizontal specimens reached 933 MPa, representing a difference of about 34 MPa. In contrast, ductility followed the opposite trend. The elongation in the horizontal direction was 27.55%, which is approximately 20% higher than the 23.03% measured in the vertical direction.

When compared with the mechanical properties specified for the filler wire (Table 1), the yield strength of the WAAM-produced UHS steel was slightly lower, which is likely related to the repeated thermal cycling inherent to the WAAM process, leading to microstructural modifications compared to the original wire material. However, the ultimate tensile strength of the WAAM material exceeded the manufacturer’s reported values for the filler wire, indicating that the deposition process produced a material with very high load-bearing capability while maintaining reasonable ductility.

Table 3. Static properties of the WAAM UHS steel.

Printing direction	Yield strength [MPa]	Tensile strength [MPa]	Elongation [%]
Vertical	836	977	23.03
Horizontal	832	933	27.55

2.9.5 Bending fatigue strength

Bending fatigue tests were conducted on WAAM-fabricated UHS steel specimens to evaluate their cyclic performance. All specimens were extracted in the build direction to ensure consistent comparison between orientations. The tests were performed up to a run-out limit of 2×10^6 cycles, which was defined as the fatigue limit and used as the primary criterion for assessing fatigue resistance.

The results showed that the fatigue limit of the WAAM UHS steel was 370 MPa in the horizontal direction and 419 MPa in the vertical direction. Thus, the specimens tested in the vertical orientation exhibited better fatigue performance compared to those tested in the horizontal direction.

In addition to the higher fatigue limit, the vertical specimens also demonstrated slightly better fatigue strength in the low- and medium-cycle fatigue regimes, sustaining higher stress amplitudes at comparable cycle counts. Overall, the results indicate a moderate anisotropy in fatigue behavior, with the vertical orientation providing somewhat improved resistance to cyclic loading. This difference may be related to the microstructural characteristics and solidification patterns associated with the WAAM deposition process.

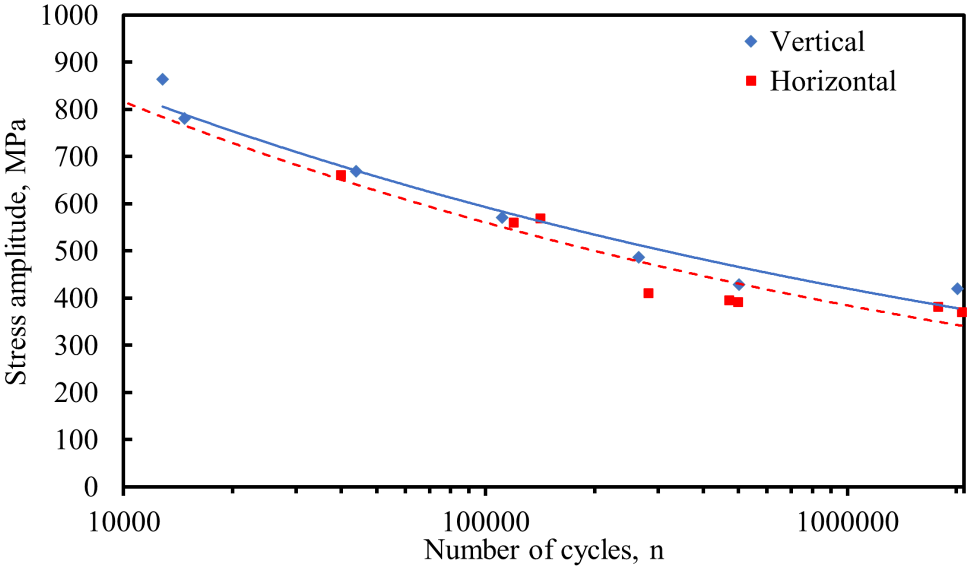

Fig 3. Bending fatigue strength of WAAM UHS steel.

2.9.6 Axial fatigue strength

Axial fatigue tests were performed on WAAM-fabricated UHS steel specimens in the vertical build direction to evaluate their resistance to cyclic loading under fully reversed conditions. The tests were conducted until a run-out limit of 2 × 10^6 cycles, which was defined as the fatigue limit.

The results showed that the fatigue limit of the WAAM UHS steel in the vertical direction was approximately 400 MPa. This relatively high endurance limit indicates that the WAAM-produced UHS steel possesses good resistance to cyclic loading, which is consistent with its high static strength and refined microstructure produced during the additive manufacturing process. The obtained fatigue performance suggests that WAAM-fabricated UHS steel can be suitable for applications subjected to repeated mechanical loading.

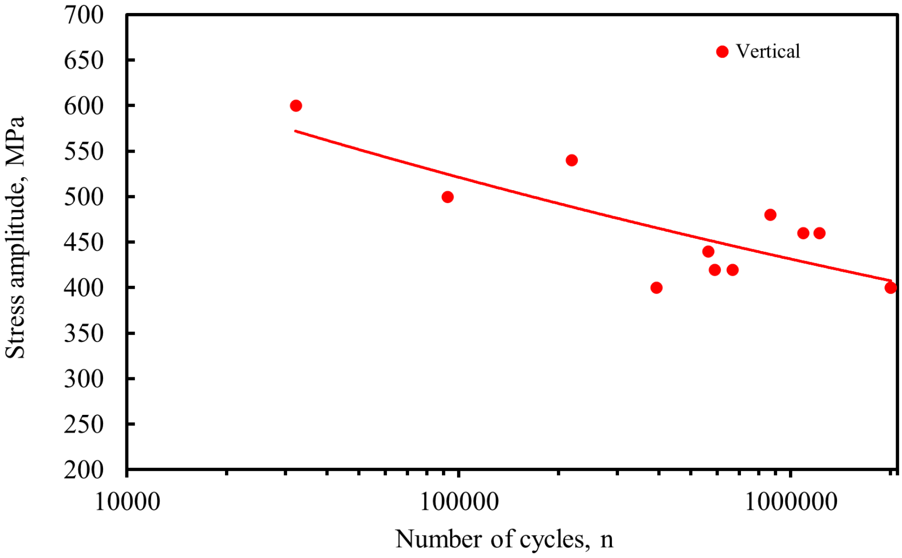

Fig. 4. Fatigue strength of WAAM UHS steel in vertical direction.

2.10 Investigation of the Influence of Severe Shot Peening on the Fatigue Performance of WAAM-Produced Ultra-High-Strength Steel

2.10.1 Printing equipment

The WAAM experiments were performed using a Fronius TransPuls Synergic 2700 system operating with Cold Metal Transfer (CMT) technology. The deposition speed was maintained at 0.35 m/min, and a vertical increment of 1.8 mm was applied between consecutive layers. The welding parameters were set to 131 A current, 11 V voltage, and a wire feed rate of 2.9 m/min. An interpass temperature of 110 °C was controlled between layers using an Optris CT IR pyrometer to ensure stable thermal conditions during the build. Shielding was provided by a gas mixture of 82% argon and 18% carbon dioxide at a flow rate of 12 l/min.

The ultra-high-strength (UHS) steel filler wire (Esab OK Aristorod 89) used in the process complied with EN ISO 16834-A: G89 4 M Mn4Ni2CrMo and had a diameter of 1.2 mm. Its chemical composition is presented in Table 1, while the corresponding mechanical properties are summarized in Table 2.

Table 1. The chemical composition % of the UHS steel wire.

C	Cr	Mn	Ni	Si	Mo
0.08	0.41	1.11	2.22	0.80	0.53

Table 2. The mechanical properties of the UHS steel wire.

Yield strength [MPa]	Tensile strength [MPa]	Elongation [%]
920	940	18

2.10.2 Mechanical test setup

Tensile specimens were prepared from the WAAM-fabricated component by machining approximately 1.7 mm from both surfaces to remove irregular outer layers. This process produced a uniform plate with a final thickness of 2 mm. Standardized tensile and fatigue specimens were subsequently laser-cut and finish-machined to precise dimensions.

Tensile testing was performed using an Instron 8802 universal testing machine in accordance with SFS-EN ISO 6892-1:2019. A constant crosshead speed of 1.0 mm/min was maintained throughout the tests. Vickers hardness measurements were carried out with an Innovatest Falcon 500 hardness tester using a 0.1 kg load, with indentations spaced at 0.05 mm intervals. Surface roughness was evaluated using a Keyence VK-X200 laser microscope with non-contact laser scanning technology, offering a measurement resolution of 0.5 nm.

Fatigue performance was assessed using a custom-designed bending fatigue machine developed by the FMT research group at the University of Oulu. The tests were conducted under fully reversed loading conditions (R = −1), with stress amplitudes ranging from 390 MPa to 850 MPa. Each specimen was individually calibrated using a dedicated force sensor to ensure accurate load application and reliable fatigue data.

Electron backscatter diffraction (EBSD) analysis was conducted using a JEOL JSM-7900F scanning electron microscope equipped with an Oxford Instruments Symmetry EBSD detector, operating at 20 kV with a working distance of 17 mm.

Severe shot peening (SSP) was performed on the machined surfaces of the WAAM specimens in a closed blasting cabinet using an ABB industrial robot. A custom fixture was designed to ensure repeatable treatment of both sides. Each specimen underwent up to 22 passes per side, with a 180° rotation between passes to achieve uniform coverage. Spherical martensitic chromium steel shots (STELUX C40), with a size range of 0.30–0.85 mm and a hardness of 36 HRC, were used as the peening media. Blasting was conducted at a pressure of 7.4 bar with a nozzle distance of 70 mm. After 22 passes, the Almen intensity measured using type A strips was approximately 300 A.

2.10.3 Microstructure analysis

The microstructure of the WAAM-produced UHS steel following severe shot peening is shown in Fig. 1a. Near the surface, clear signs of plastic deformation are visible as a result of the SSP treatment. The original martensitic/bainitic structure is noticeably distorted compared to the underlying base material.

The kernel average misorientation (KAM) map in Fig. 1b highlights the contrast between the surface layer and the interior microstructure. A distinct deformed surface layer is evident, characterized by increased local misorientation, indicating a higher density of lattice strain.

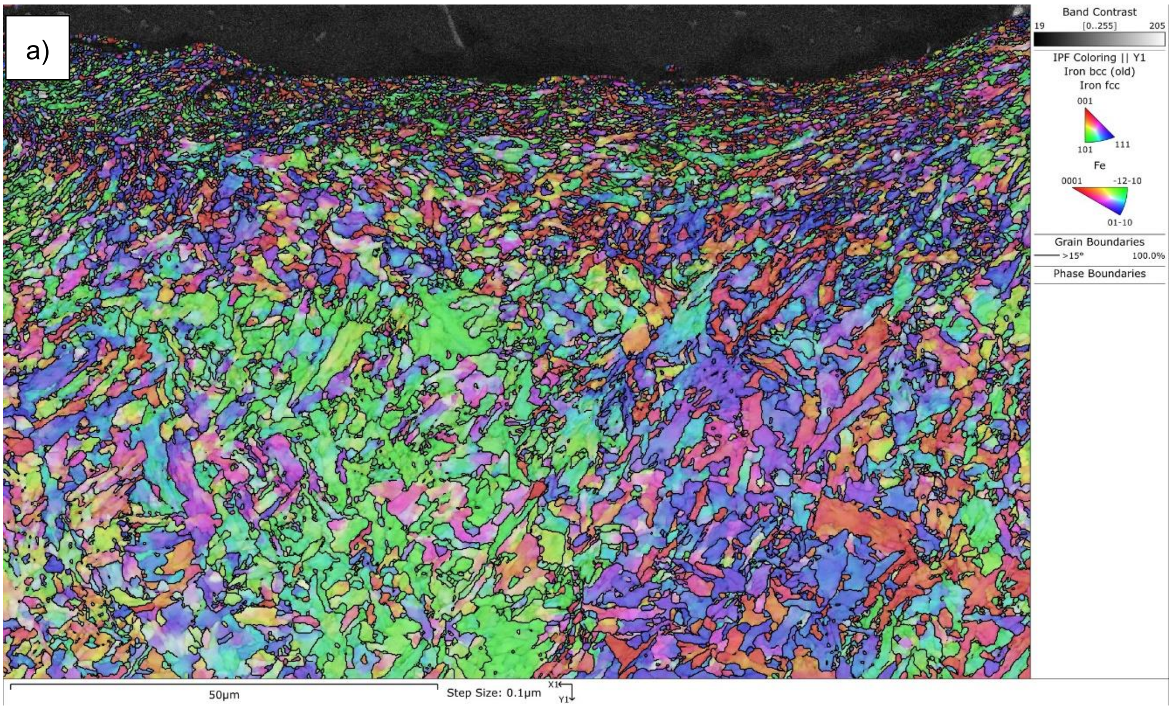

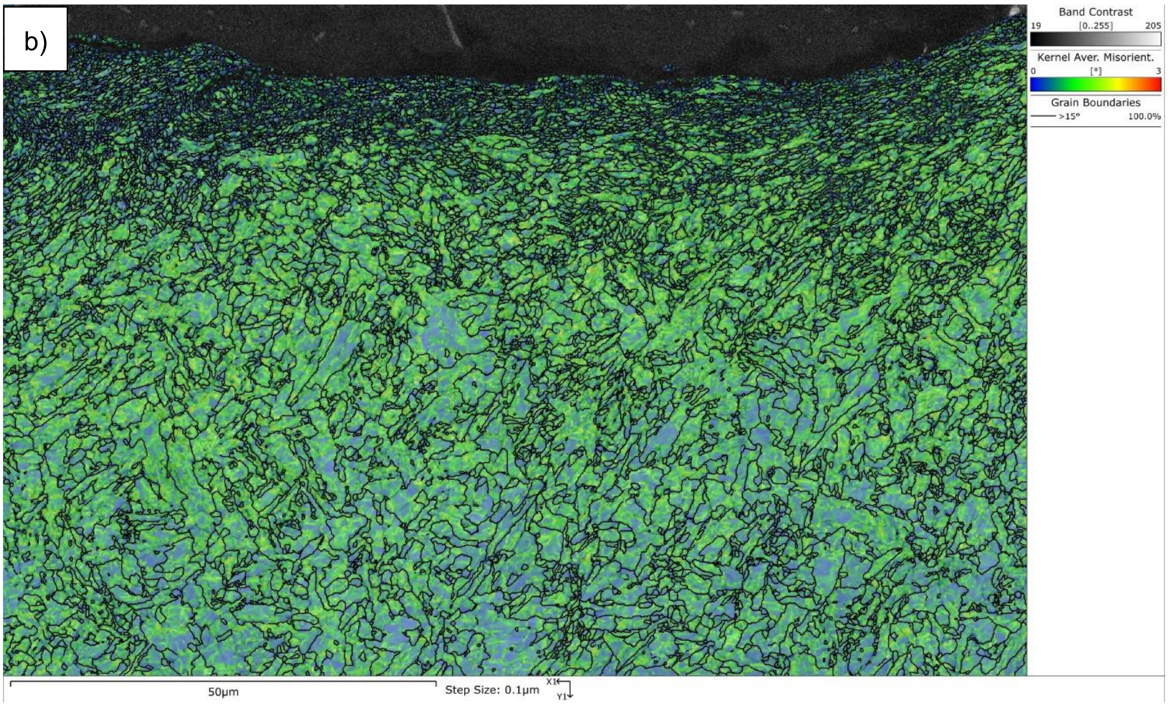

Fig. 1. (a) IPF map of the shot-peened surface; (b) KAM map from the same area illustrating the gradient in local misorientation.

2.10.4 Hardness measurements

Figure 2 illustrates the cross-sectional hardness profile of the WAAM UHS steel specimen after severe shot peening. The results demonstrate that the SSP treatment significantly modified the near-surface region, with the hardened layer extending to a depth of approximately 0.1 mm.

The average hardness of the untreated base material was about 329 HV. In contrast, the maximum hardness value, measured close to the treated surface, reached 395 HV. These results indicate that the SSP process increased the surface hardness by roughly 20%.

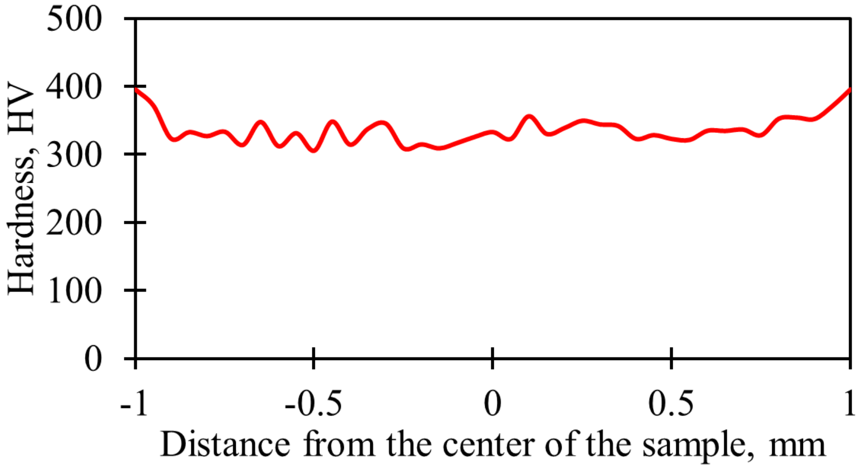

Fig. 2 Hardness of the SSP WAAM UHS steel.

2.10.5 Surface roughness measurement

Surface roughness measurements were performed using laser scanning on both machined and severely shot-peened surfaces. The average roughness (Ra) and maximum peak-to-valley height (Rz) values are summarized in Table 3, while the corresponding surface profiles are presented in Fig. 3.

The machined specimen exhibited the smoothest surface finish, with an Ra value of 0.37 µm. In comparison, the shot-peened surface showed significantly higher roughness, with an Ra value of 4.62 µm. A similar trend was observed in the Rz values, which were 2.23 µm for the machined sample and 30.42 µm for the severely shot-peened specimen.

These results indicate that applying severe shot peening to the machined surface substantially increases surface roughness.

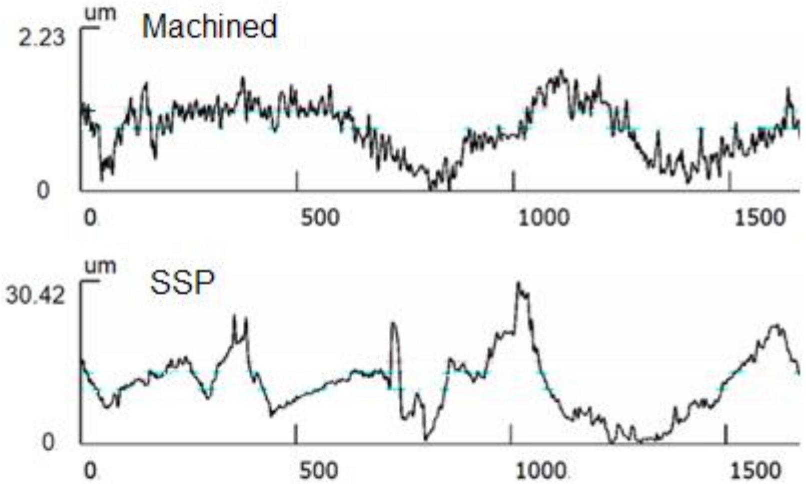

Fig. 3. Surface profile of machined WAAM UHS steel and SSP WAAM UHS steel.

Table 3. Surface quality of the WAAM UHS steel.

	Ra [µm]	Rz [µm]
Machined	0.37	2.23
SSP	4.62	30.42

2.10.6 Mechanical properties

The results demonstrate that severe shot peening had a clear effect on the mechanical properties of the material. On average, the yield strength decreased by approximately 49 MPa after SSP treatment. In contrast, the ultimate tensile strength showed a slight increase of about 5 MPa, with the maximum value reaching 904 MPa for the WAAM UHS steel after SSP, as reported in Table 4.

Ductility was reduced following SSP, as elongation at fracture decreased from 26.3% for the untreated WAAM UHS steel to 22.3% after shot peening (Fig. 5). Since SSP mainly modifies the near-surface region, any strengthening effect is confined to a shallow layer. In the case of WAAM UHS steel, the affected depth was only about 0.1 mm (Fig. 3), which explains the limited influence on overall tensile strength. However, the surface deformation introduced by SSP alters the material's plastic response, contributing to the observed reduction in yield strength.

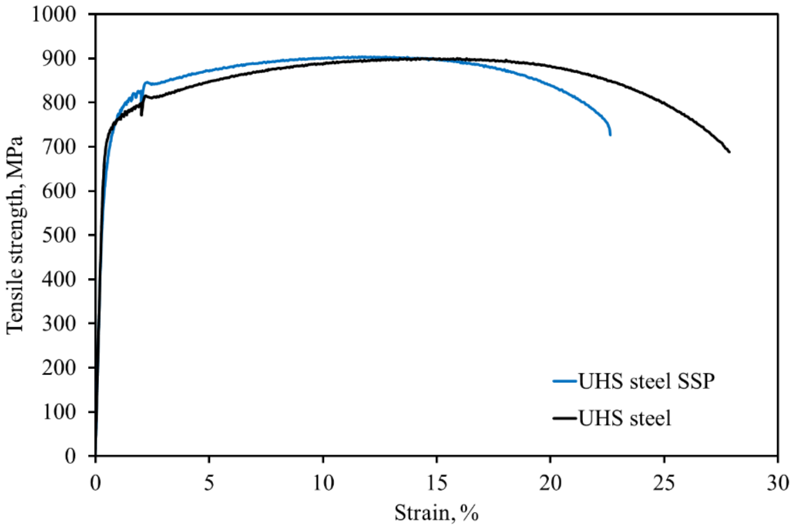

Fig. 4. Mechanical properties of WAAM UHS steel and WAAM UHS steel SSP.

Table 4. Mechanical properties of WAAM UHS steel and WAAM UHS steel SSP

	Yield strength [MPa]	Tensile strength [MPa]	Elongation [%]
UHS steel	739	899	26.3
UHS steel SSP	690	904	22.3

2.10.7 Bending fatigue strength

Bending fatigue tests were conducted on WAAM-produced UHS steel specimens in both untreated and severe shot-peened conditions. All samples were prepared in the horizontal direction to ensure consistent evaluation. The experiments were carried out up to 2×10^6 cycles, which was defined as the fatigue limit. The corresponding results are presented in Fig. 5.

The results indicate that SSP enhanced the fatigue performance of WAAM UHS steel, particularly in the high-cycle fatigue region. The fatigue limit increased from 370 MPa for the untreated material to 392 MPa after SSP treatment, representing an improvement of 22 MPa (approximately 6%).

Although severe shot peening did not significantly improve the overall static mechanical properties, it resulted in enhanced fatigue performance. At the same time, SSP increased surface roughness, which would generally be expected to reduce fatigue strength.

However, the treatment also produced higher hardness in the near-surface layer, leading to improved surface strength compared to the untreated base material. This localized strengthening contributed positively to fatigue resistance. In addition, SSP is known to alter residual stress states, which are critical factors in fatigue behavior. It should be noted, however, that residual stresses were not examined in the present study.

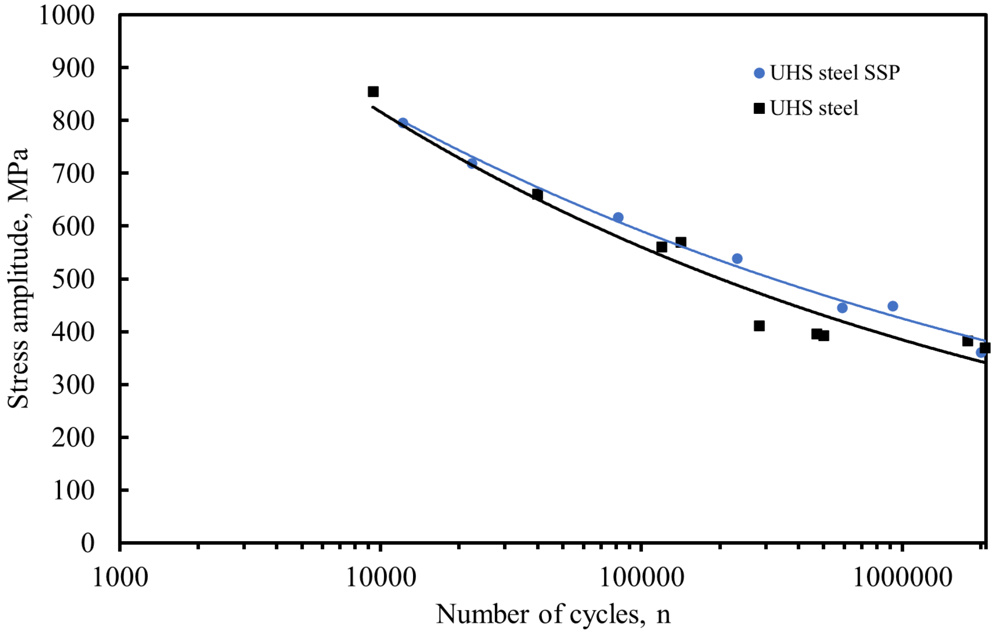

Fig. 5. Fatigue strength of WAAM UHS steel.

2.11 Evaluation of the Effect of Surface Condition on the Bending Fatigue Performance of WAAM Ultra-High-Strength Steel

2.11.1 Printing equipment

In the WAAM trials, a Fronius TransPuls Synergic 2700 CMT welding system was employed. The deposition process was carried out at a travel speed of 0.35 m/min, with a layer height increment of 1.8 mm applied after each pass. The process parameters were defined by a welding current of 131 A, an arc voltage of 11 V, and a wire feed speed of 2.9 m/min. To ensure adequate cooling between layers, the component was permitted to cool naturally to an interpass temperature of 110 °C prior to subsequent deposition. Throughout the fabrication process, a shielding gas composed of 82% argon and 18% carbon dioxide was supplied at a constant flow rate of 12 l/min.

The ultra-high-strength (UHS) steel wire (Esab OK Aristorod 89) used in the WAAM process conformed to the EN ISO 16834-A: G89 4 M Mn4Ni2CrMo classification and had a diameter of 1.2 mm. The mechanical properties of the wire are summarized in Table 1, and its chemical composition is listed in Table 2.

Table 1. Static properties of the UHS wire.

Yield strength [MPa]	Tensile strength [MPa]	Elongation [%]
920	940	18

Table 2. Chemical composition (%) of the UHS wire.

C	Mn	Si	Ni	Mo	Cr
0.08	1.75	0.80	2.22	0.53	0.41

2.11.2 Mechanical characterization

After fabrication, the WAAM-produced component was machined by removing material from both sides of the deposited wall. This operation was necessary to produce a plate with a final thickness of 2 mm and a smooth, uniform surface suitable for subsequent tensile and fatigue testing. Test specimens were then accurately laser-cut from the 2 mm thick plate to ensure dimensional precision. Following laser cutting, the specimens underwent additional machining to meet the exact geometrical requirements of the experiments.

Tensile testing was carried out using an Instron 8802 universal testing machine in accordance with the SFS-EN ISO 6892-1:2019 standard [16]. All tests were performed at a constant crosshead speed of 1.0 mm/min to maintain consistency and reliability. Hardness measurements were obtained with an Innovatest Falcon 500 hardness tester, applying a load of 0.2 kg and recording indentations at 0.1 mm intervals. Surface roughness was evaluated using a Keyence VK-X200 laser microscope operating with non-contact laser scanning technology.

The bending fatigue performance of the WAAM-fabricated specimens was assessed using a custom-built reversed flexural bending device (Fig. 1b), derived from the WEBI machine originally developed by Carl Schenck. Fatigue experiments were conducted under fully reversed loading conditions with a stress ratio (R) of −1, where R is defined as the ratio of minimum to maximum stress within a loading cycle. Stress amplitudes between 230 MPa and 470 MPa were systematically applied during testing.

To ensure high measurement accuracy, each specimen was individually calibrated using a force sensor prior to testing. The fatigue machine operates with eccentric lifts of varying magnitudes, and calibration was performed separately for each lift configuration. During calibration, the applied force was recorded via the force sensor while the specimen dimensions were carefully measured, allowing precise calculation of the stress amplitude. Each specimen was rotated three times into different orientations during calibration, and the average of these measurements was used to determine the effective force. This procedure improved the reliability and validity of the results by compensating for potential material or geometrical variations and ensuring accurate force determination throughout the fatigue tests.

2.11.3 Geometry evaluation

Figure 1 illustrates a cross-sectional view of the WAAM-fabricated UHS steel wall. The wall thickness shows a minor variation, ranging from 5.3 mm to 5.6 mm, with an average value of approximately 5.5 mm. Notably, no visible porosity or significant printing defects were detected under the selected processing parameters. This observation confirms the robustness and effectiveness of the applied WAAM process, demonstrating its ability to produce components of high structural integrity.

From a fatigue performance perspective, the absence of pores and other defects is particularly critical, as such imperfections can act as crack initiation sites and significantly reduce fatigue life.

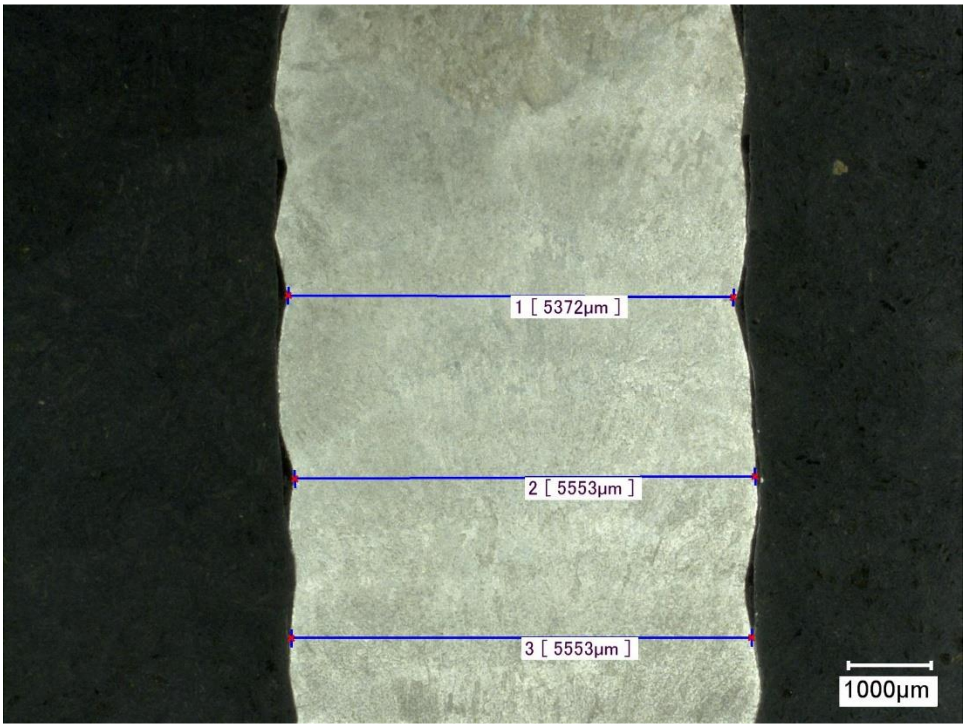

Fig. 1. Geometry of WAAM UHS steel.

2.11.4 Surface roughness measurements

Surface roughness was evaluated by means of laser scanning on three different surface conditions: machined, electro-polished, and as-built. The mean roughness values (Ra) and the average maximum peak-to-valley heights (Rz) are summarized in Table 3, while the corresponding surface profiles are shown in Fig. 2.

Of the examined specimens, the electro-polished surface demonstrated the highest surface quality, with an Ra value of 0.28 μm. The machined specimen exhibited slightly greater roughness, with an Ra of 0.37 μm. In comparison, the as-built surface showed significantly higher roughness, reaching an Ra value of 9.8 μm.

The measured Rz values were 2.03 μm for the polished sample, 2.23 μm for the machined sample, and 74.1 μm for the as-built sample. Based on these findings, it can be concluded that the polished specimen is expected to possess the greatest fatigue strength, whereas the as-built specimen is likely to exhibit the lowest fatigue performance due to its substantially higher surface roughness.

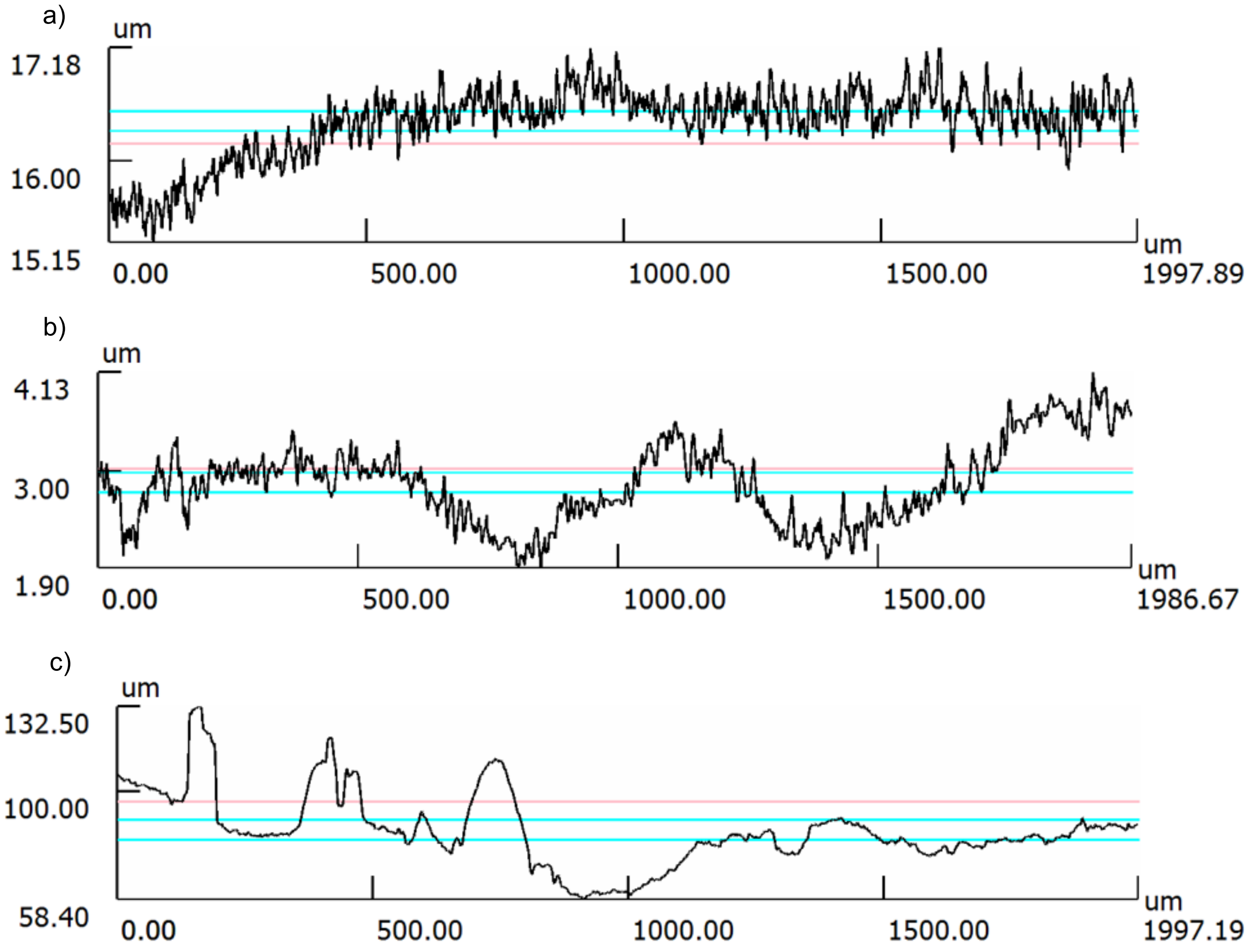

Fig. 2. Surface roughness of the WAAM UHS steel for (a) polished surface, (b) machined surface and (c) as-built surface.

Table 3. Surface quality of the WAAM UHS steel.

	Rz [µm]	Ra [µm]
Polished	2.03	0.28
Machined	2.23	0.37
As-built	74.10	9.80

2.11.5 Bending fatigue strength

Bending fatigue experiments were carried out on WAAM-fabricated UHS steel specimens with polished, machined, and as-built surface conditions. All samples were produced in the deposition direction. The maximum test duration was set to 2 × 10^6 cycles, which was defined as the fatigue limit.

The results show that the polished specimens achieved slightly superior bending fatigue performance compared to the machined ones, with a fatigue limit of 381 MPa (Fig. 3). The machined samples exhibited a slightly lower fatigue limit of 370 MPa. In contrast, the as-built specimens demonstrated the poorest fatigue behavior, reaching a fatigue limit of approximately 254 MPa.

As indicated earlier in Table 3, the as-built condition had the highest surface roughness, which negatively affected fatigue performance by increasing susceptibility to crack initiation. This influence is especially significant in ultra-high-strength steels, as these materials are particularly sensitive to notches and surface irregularities.

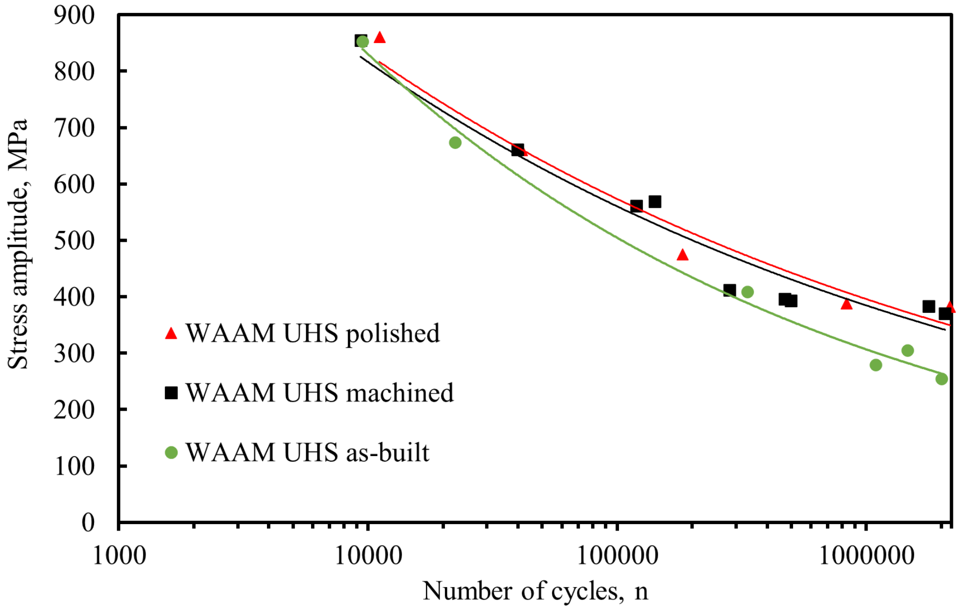

Fig. 3. Fatigue strength of WAAM UHS steel with different surface quality.

2.12 Analysis of Microstructure, Mechanical Performance, and Fatigue Behavior of a WAAM-Fabricated Multi-Material Structure Combining AISI 316L Stainless Steel and Carbon Steel

2.12.1 Printing equipment

The WAAM trials were performed using a Fronius TransPuls Synergic 2700 CMT welding system. Process parameters were individually adjusted for each material to achieve optimal deposition performance, and the selected parameters are summarized in Table 1. The travel speed was maintained at 0.64 m/min throughout fabrication. A layer height increment of 1.25 mm was applied for WAAM 316L, while a 1.6 mm lift was used for WAAM carbon steel (CS).

Different shielding gas mixtures were selected according to the material: 98% Ar with 2% O_2 for WAAM 316L, and 82% Ar with 18% CO_2 for WAAM CS. In both cases, the shielding gas flow rate was kept constant at 12 l/min. To promote controlled cooling between successive layers, deposition was paused to allow the workpiece temperature to decrease naturally to approximately 100 °C before continuing the build.

Table 1. WAAM parameters.

Material	Voltage V	Current A	Wire feed m/min
316L	13.5	107	3.2
Carbon steel	11.6	163	3.5

The welding wires used in this study consisted of a 1.2 mm diameter INEFIL INOX AISI 316L stainless steel wire and an ESAB AristoRod 12.50 carbon steel wire. The carbon steel wire complies with the EN ISO 14341-A standard and is classified as G 38 3 C1 3Si1. The chemical compositions of both the 316L and carbon steel (CS) wires are presented in Table 2, while their manufacturer-reported mechanical properties are summarized in Table 3.

Table 2. Chemical composition (%) of the welding wire.

Material	Cr	Ni	Mo	Mn	Si	C	Cu
316L	18.50	12.20	2.50	1.70	0.80	0.02	0
Carbon steel	0	0	0	1.11	0.72	0.10	0.07

Table 3. Static properties of the welding wire.

Material	Yield strength MPa	Tensile strength MPa	Elongation %
316L	440	560	40
Carbon steel	470	560	26

2.12.2 Printing setup

The specimens were fabricated using the WAAM process to produce oval-shaped structures. The deposition strategy was deliberately designed so that each new layer began from the opposite side of the component compared to the previous one. In addition, the travel direction was alternated between successive layers to create a symmetrical build pattern.

The resulting oval component measured 240 mm in length and 40 mm in width, with a curved section radius of 20 mm. Fabrication was carried out on a 20 mm thick substrate plate. Deposition started at a height of 75 mm using 316L stainless steel, after which the material was gradually transitioned to carbon steel (CS), continuing up to a final height of 150 mm.

2.12.3 Test setup

After fabrication, the WAAM-produced component was subjected to precision machining, during which approximately 1 mm of material was removed from both sides of the deposited wall. This step was necessary to obtain a 2 mm thick plate with a smooth and defect-free surface to ensure consistency in subsequent testing. Test specimens for tensile and fatigue experiments were then prepared from this finished plate. The blanks were first cut by laser and subsequently machined to achieve the final required dimensions. All specimens were oriented in the build direction.

Tensile testing was performed using an Instron 8802 universal testing machine. The specimens were prepared in accordance with SFS-EN ISO 6892-1:2016, with a width of 2 mm, a parallel length of 6 mm, and a gauge length of 25 mm. The tests were carried out at a constant crosshead speed of 1.0 mm/min until failure. Microhardness measurements were obtained using an Innovatest Falcon 500 hardness tester with a 0.3 kg load, with indentations made at intervals of 0.2 mm.

Bending fatigue behavior was evaluated using a custom-built reversed flexural bending device derived from the WEBI machine originally manufactured by Carl Schenck. Fatigue tests were conducted under fully reversed loading conditions ($R = -1$), where R represents the ratio of minimum to maximum stress within a single loading cycle. Stress amplitudes between 215 MPa and 630 MPa were applied, and each specimen was individually calibrated using a force sensor prior to testing.

Microstructural characterization by electron backscatter diffraction (EBSD) was performed using a JEOL JSM-7900F field emission scanning electron microscope equipped with an Oxford Instruments Symmetry S2 EBSD detector. The analysis was conducted at an accelerating voltage of 20 kV and a working distance of 15 mm.

2.12.4 Microstructure analysis

Figure 1 presents the Inverse Pole Figure (IPF) maps illustrating the microstructures of WAAM-fabricated carbon steel (CS) and 316L stainless steel. In the case of CS, the microstructure is primarily composed of equiaxed ferrite grains with an average grain size of approximately 10 μm (Fig. 1a). The formation of this ferritic structure is influenced by the thermal conditions inherent to the WAAM process, particularly the cooling rates, as well as the carbon content of the welding wire. These factors promote the development of a relatively soft and ductile ferritic matrix.

In contrast, the 316L stainless steel exhibits a coarse columnar grain structure (Fig. 1b), resulting from the high heat input associated with the WAAM process. The repeated remelting of previously deposited layers facilitates pronounced epitaxial grain growth. The columnar grains can reach widths of several millimeters, and a dendritic substructure is also visible within them. Detailed examination further revealed the presence of a body-centered cubic (BCC) phase, most likely δ-ferrite, which appears as a red phase in Fig. 1b. This phase formed along the dendrite arm boundaries during solidification.

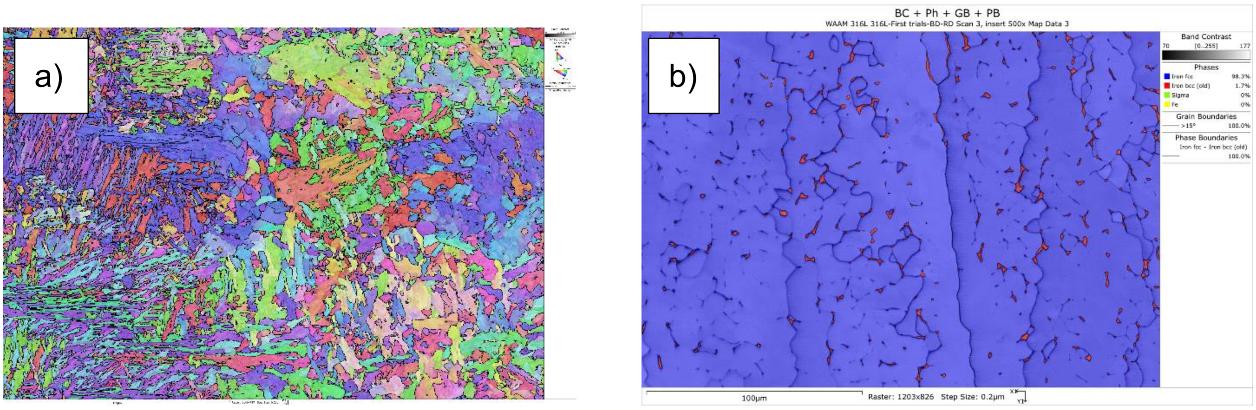

Fig. 1. (a) IPF-map of the CS and (b) phase map of WAAM 316L.

Figure 2 presents the macroscopic phase distribution of the WAAM-fabricated specimen. It can be observed that the region close to the material interface—indicated by yellow arrows in Fig. 2—consists predominantly of a body-centered cubic (BCC) phase. This suggests that the high heat input during deposition promotes elemental diffusion across the interface between carbon steel (CS) and 316L stainless steel.

As the concentration of austenite-stabilizing elements, particularly nickel, decreases in the vicinity of the interface, the 316L matrix loses its austenitic stability and transforms into martensite upon cooling. This instability appears to extend several millimeters away from the interface, after which the composition becomes sufficiently balanced for the structure to remain austenitic during solidification and cooling.

A higher magnification image of the interfacial region (Fig. 3) further highlights the microstructural differences between the two materials. The CS side exhibits a comparatively coarser grain structure, and based on its morphology, it is likely that the interfacial region on the CS side is at least partially martensitic. In contrast, the 316L side displays a finer martensitic microstructure in the transformed region.

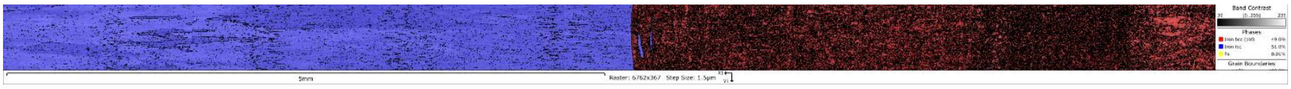

Fig. 2. (a) Macroscopic EBSD scan from the WAAM sample, showing the transition from the Body-centered cubic (BCC, red) to Face-centered cubic (FCC, blue) phase.

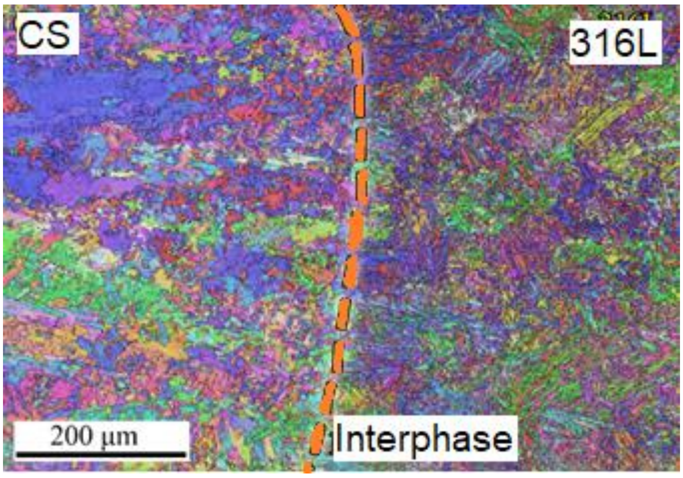

Fig. 3. IPF-map of the interphase between the WAAM CS and 316L.

2.12.5 Hardness measurement

Hardness measurements of the WAAM-fabricated dissimilar material specimen were performed along the build direction at a location 12 mm from the reference point, as illustrated in Fig. 4. The highest hardness value, 407 HV, was measured near the center of the interfacial region on the 316L side. The interphase on the 316L side showed a hardness of approximately 385 HV, which is associated with its refined grain structure. A pronounced hardness gradient was observed between the interphase and the 316L base material, indicating a sharp transition in microstructure.

In contrast, the interfacial region on the carbon steel (CS) side exhibited an average hardness of around 316 HV, considerably lower than that measured on the 316L side. This difference is likely related to the coarser grain structure present in the CS region. The distinct hardness distributions on either side of the interface highlight the complex interaction between material composition, microstructural evolution, and thermal conditions in the WAAM-processed dissimilar material system.

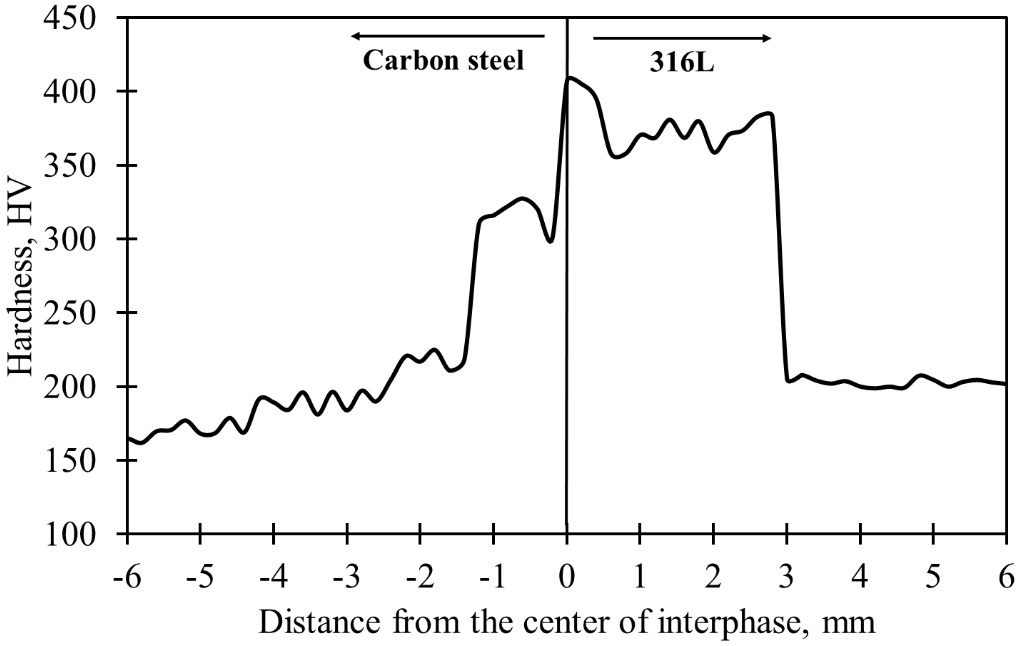

Fig. 4. Hardness profile of WAAM CS and 316L.

2.12.6 Mechanical properties

The measured yield strengths indicate that both WAAM carbon steel (CS) and the dissimilar WAAM material possess higher yield strength than WAAM 316L, as presented in Table 4 and Fig. 5. The yield strength of the dissimilar material is very close to that of WAAM CS, suggesting that the carbon steel portion plays a dominant role in determining the overall yield behavior of the hybrid structure.

A comparable trend is observed in ultimate tensile strength. WAAM 316L exhibits the highest tensile strength, followed by the dissimilar material and then WAAM CS. The lower tensile strength of WAAM CS relative to WAAM 316L implies that incorporating carbon steel into the dissimilar structure reduces the overall tensile strength compared to pure 316L.

Elongation results show a clear decrease in ductility for the dissimilar material when compared with both WAAM 316L and WAAM CS. This reduced ductility likely stems from the challenges associated with achieving homogeneous mechanical performance across a dissimilar material interface. Experimental observations support this interpretation: noticeable plastic deformation occurred predominantly on the CS side of the specimen, whereas the 316L side exhibited more limited elongation. In all tensile tests, fracture consistently initiated and propagated on the CS side, as illustrated in Fig. 6.

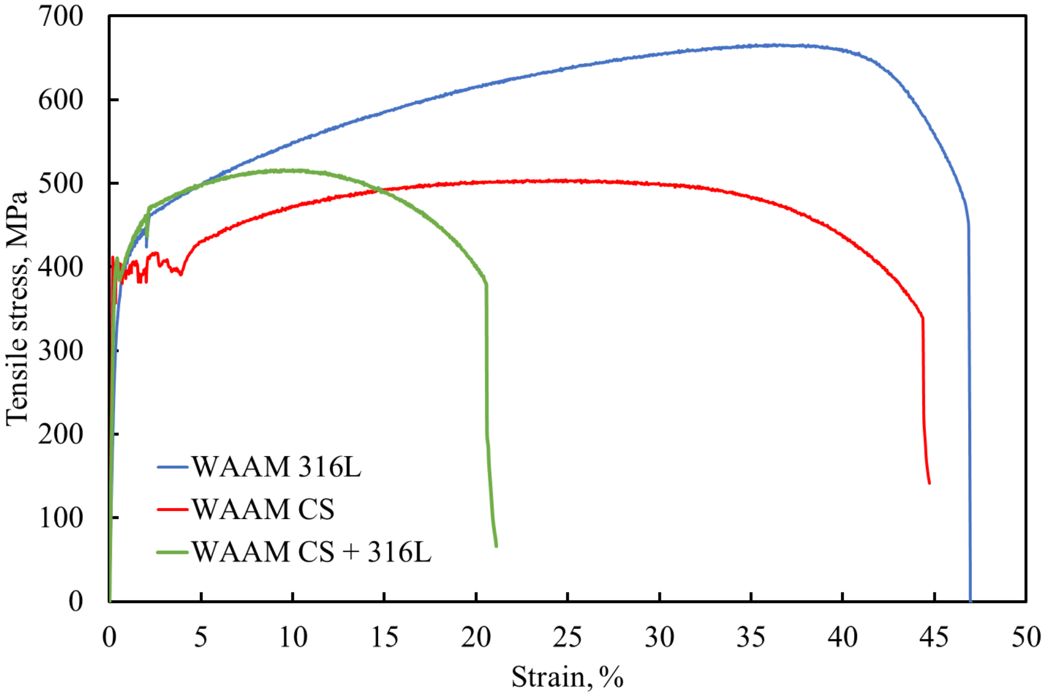

Fig. 5. Tensile strength of tested materials.

Table 4. Tensile strength of WAAM 316L, CS and dissimilar samples.

Material	Yield strength [MPa]	Tensile strength [MPa]	Elongation [%]
WAAM 316L	359	656	49.6
WAAM CS	391	503	44.9
WAAM dissimilar	391	520	20.4

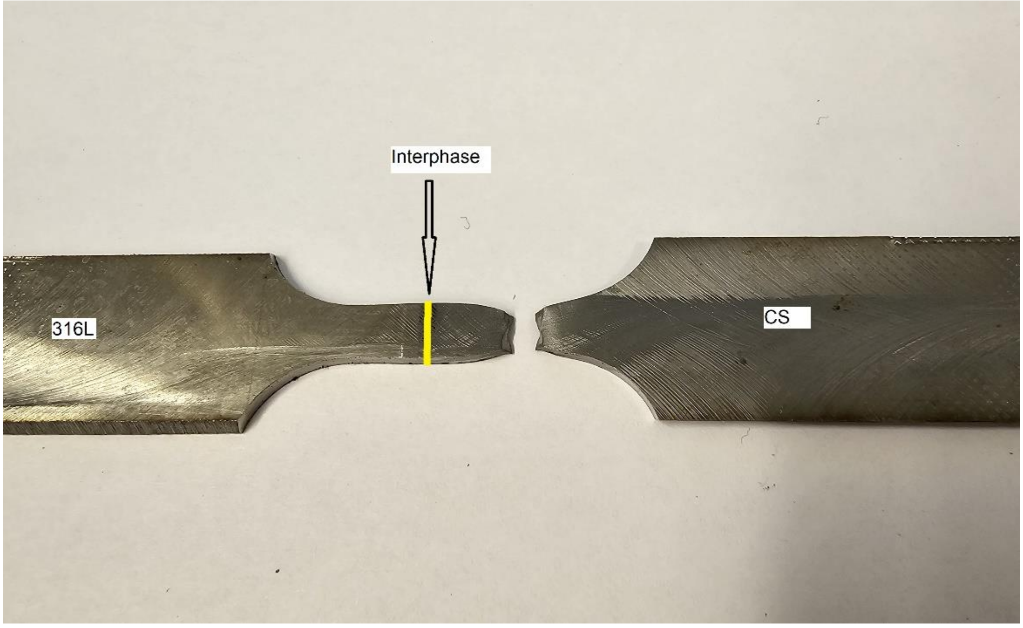

Fig. 6. Fracture of the tensile test sample.

2.12.7 Bending fatigue strength

Bending fatigue experiments were performed on WAAM 316L, WAAM carbon steel (CS), and the hybrid dissimilar material produced from their combination. Particular attention was given to the interfacial region located transversely at the center of the specimen. All fatigue specimens were prepared in the build direction, which had previously demonstrated the most favorable static mechanical properties.

The tests were conducted up to a maximum of 2×10^6 cycles to determine the fatigue limit. The fatigue limit of WAAM 316L was approximately 225 MPa, while WAAM CS exhibited a slightly lower value of 210 MPa. The dissimilar WAAM material showed a fatigue limit lower than that of 316L but essentially equal to that of WAAM CS, at about 210 MPa (Fig. 7).

In the low- and medium-cycle fatigue regions, the dissimilar material demonstrated marginally better fatigue performance than WAAM CS, likely due to its somewhat higher static strength. This subtle difference highlights the complex interaction of mechanical properties within the hybrid structure and provides insight into its fatigue response under varying loading conditions. Throughout the fatigue testing, fracture consistently occurred on the CS side of the specimen, as illustrated in Fig. 8.

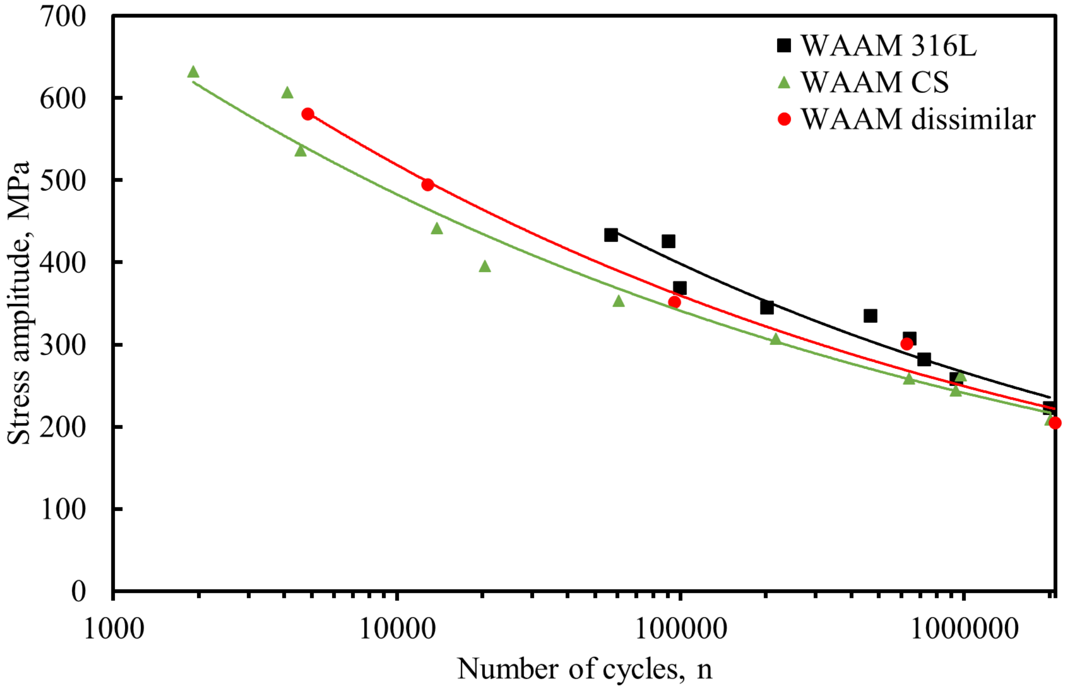

Fig. 7. Fatigue strength of WAAM 316L, WAAM CS, and WAAM dissimilar material.

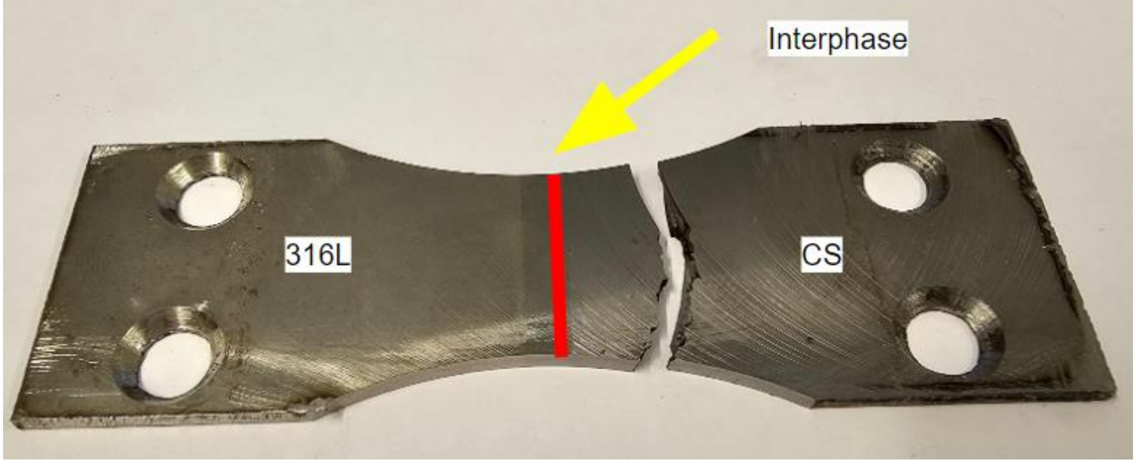

Fig. 8. Fracture of the bending fatigue test sample.

2.13 Analysis of Microstructure, Mechanical Properties, and Bending Fatigue Performance of WAAM-Produced Super Duplex Stainless Steel

2.13.1 Printing equipment

The experiments were carried out using a Fronius TransPuls Synergic 2700 CMT welding system. A travel speed of 0.37 m/min was applied during deposition, with a layer height increment of 1.55 mm between successive passes. The selected process parameters included a welding current of 100 A, an arc voltage of 11.8 V, and a wire feed rate of 3.3 m/min. An interpass temperature of 150 °C was maintained and carefully monitored using an Optris CT infrared pyrometer to ensure accurate thermal control. Shielding was provided with pure argon (100%) at a constant flow rate of 12 l/min.

The super duplex stainless steel (SDSS) wire (Esab Exaton 29.8.2.L) used in the process conformed to the EN ISO 14343-A: G/W/P Z 29 8 2 L classification and had a diameter of 1.2 mm. The detailed chemical composition of the SDSS wire is presented in Table 1, while its mechanical properties are summarized in Table 2.

Table 1. The chemical composition of the SDSS wire.

C	Cr	Ni	Mo	Mn	Si
0.017	29.0	6.7	2.2	0.9	0.3

Table 2. Mechanical properties of the SDSS wire.

Yield strength [MPa]	Tensile strength [MPa]	Elongation [%]
730	850	25

2.13.2 Test setup

Tensile and fatigue specimens were prepared from the printed component by machining away approximately 1.7–2.0 mm of material from both sides. This step was necessary to eliminate surface irregularities and obtain a uniform plate with a final thickness of 2 mm. The test specimens were then accurately produced to their final dimensions using a combination of laser cutting and precision machining.

Mechanical characterization was performed with an Instron 8802 testing machine in accordance with the SFS-EN ISO 6892-1:2019 standard. A constant crosshead speed of 1.0 mm/min was applied during tensile testing. Vickers hardness measurements were carried out using an Innovatest Falcon 500 system with a load of 300 g, and indentations were made at intervals of 0.1 mm.

Bending fatigue performance was evaluated using a custom-designed reversed flexural bending device based on the WEBI machine originally developed by Carl Schenck. The tests were conducted under fully reversed loading conditions (R = −1), with stress amplitudes ranging from 300 MPa to 700 MPa. Each specimen was individually calibrated using a force sensor prior to fatigue testing.

Microstructural analysis by EBSD was conducted using a JEOL JSM-7900F field emission scanning electron microscope equipped with an Oxford Instruments Symmetry EBSD detector. The analysis was performed at an accelerating voltage of 20 kV and a working distance of 15 mm. Prior to examination, metallographic samples were sectioned, mounted in thermosetting resin, mechanically ground, and polished to a mirror finish. A final polishing step with 0.1 µm colloidal silica was applied to remove any surface deformation introduced during preparation.

Temperature monitoring during the process was performed using an Optris CT 3MH2 pyrometer, which operates within a temperature range of 200–1500 °C and a spectral wavelength of 2.3 µm. Measurements were recorded at intervals of 0.1 seconds.

2.13.3 Microstructure analysis

Figure 1 presents the microstructure of the super duplex stainless steel (SDSS) produced by the WAAM process. The structure consists of a combination of phases, primarily an almost equiaxed body-centered cubic (BCC) matrix accompanied by finer, elongated grains of face-centered cubic (FCC) austenite. The austenitic phase is distributed both within the BCC matrix and along its grain boundaries.

The WAAM process resulted in an FCC phase fraction of approximately 40%, highlighting its significant role in shaping the alloy's microstructural development. Grain size measurements show a clear difference between the two phases: the average grain size of the BCC phase is about 125 µm, whereas the FCC phase exhibits a much finer average grain size of 10.5 µm.

Additionally, the austenite displays varied morphologies, appearing both as intragranular formations and along grain boundaries. This morphology resembles the characteristic Widmanstätten structure frequently reported in WAAM-fabricated duplex stainless steels, consistent with earlier findings by Hosseini et al. [1] and Kannan et al. [2].

It is important to recognize that the microstructure may also contain various intermetallic phases and precipitates, reflecting the inherent complexity of alloy solidification and phase transformation processes. To fully identify and understand the range of phases present, more detailed investigations are required. These should include thorough chemical composition analysis and studies of elemental segregation to clarify how these phases influence the mechanical performance and thermal behavior of the alloy.

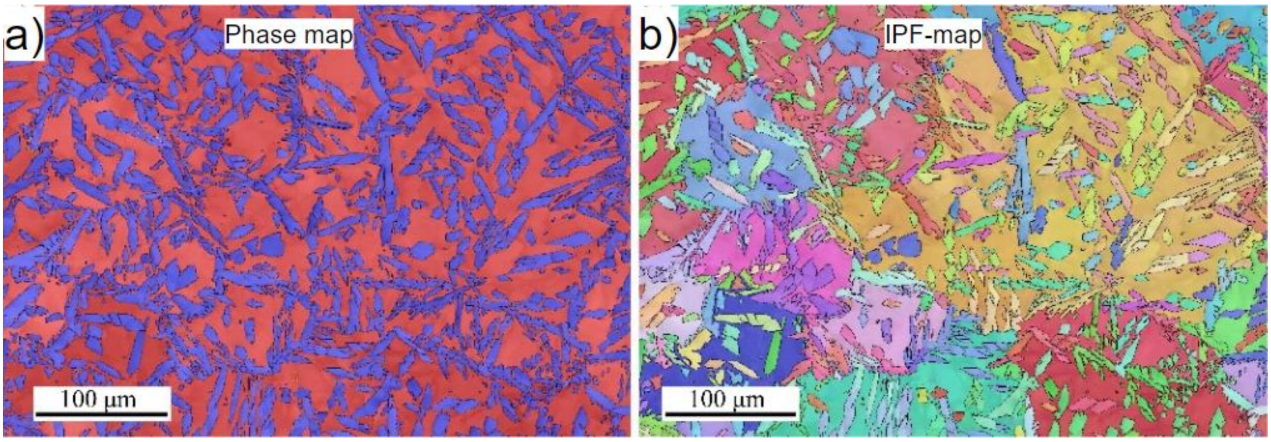

Fig. 1. (a) Phase map of the SDSS, BCC and FCC colored in red and blue; (b) IPF-map of the same area showing coarse BCC matrix.

2.13.4 Hardness and geometry measurements

Hardness measurements of the WAAM-produced SDSS were carried out along the build direction at a position 10 mm from the reference point, as shown in Fig. 2. The indentations were made in the central region of the deposited wall to ensure representative results. The measurements revealed a uniform hardness distribution throughout the entire structure, with an average value of approximately 302 HV. Furthermore, hardness profiles taken across individual layers showed no notable differences in the interlayer regions, confirming the homogeneity of the material.

Figure 3 illustrates a cross-sectional view of the printed SDSS component. The wall thickness varied slightly between 5.5 mm and 6.0 mm, with an average thickness of about 5.75 mm. No visible porosity or significant defects were detected, demonstrating the stability and effectiveness of the WAAM process in producing high-quality components.

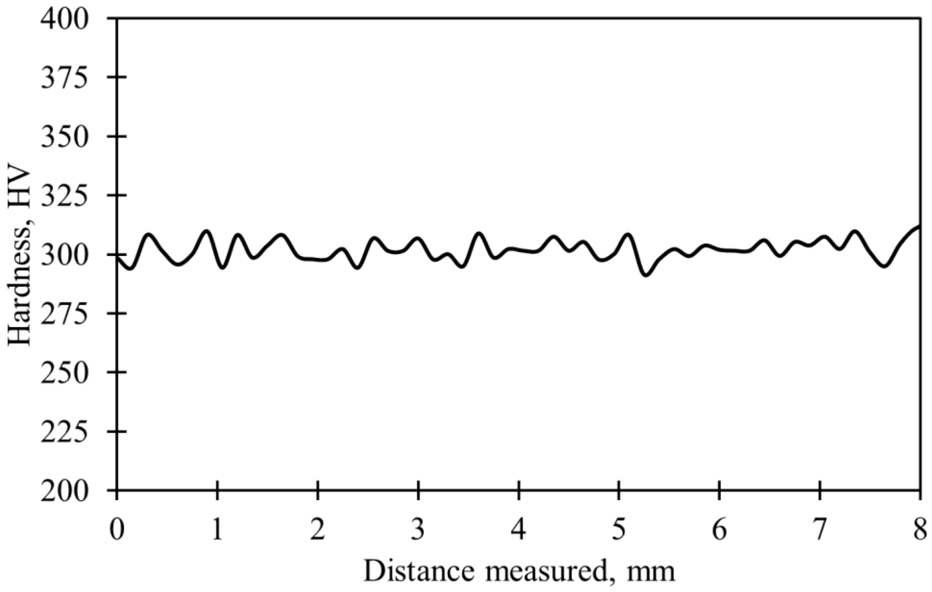

Fig. 2. Hardness of the WAAM SDSS.

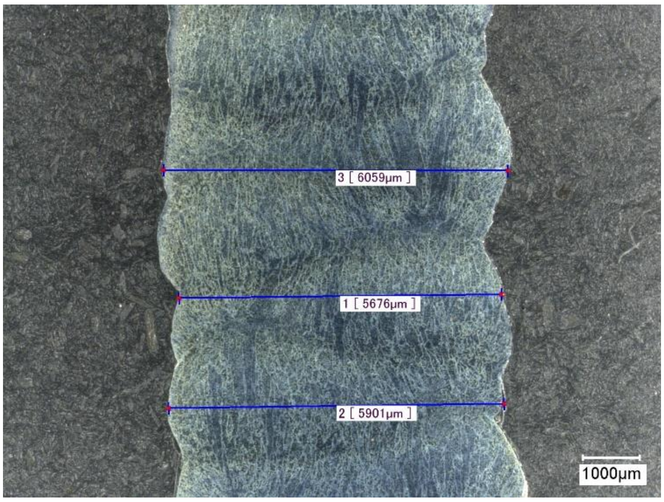

Fig 3. Cross-section of the WAAM SDSS.

2.13.5 Temperature analysis

The interpass temperature between consecutive layers was regulated at 150 °C and monitored using a pyrometer. It should be noted that the pyrometer employed in this study had a lower measurement limit of 200 °C; therefore, temperatures below this value are not shown in Fig. 4.

Temperature monitoring was performed from the surface of the deposited structure, with the pyrometer fixed in a constant position. As a result, the measurement location remained unchanged during the entire printing process and was not influenced by the progression of material deposition. The peak temperature measured during the printing process was approximately 1100 °C. The overall thermal cycle recorded throughout fabrication is presented in Fig. 4. The time interval between successive layers was about 460 seconds, corresponding to the cooling period required for the component to reach the specified interpass temperature of 150 °C.

It can be observed that the maximum recorded temperature gradually decreased as the deposition height moved further away from the fixed measurement location. The t8/5 cooling time measured at the surface layer was 14.9 seconds. In addition, the third layer beneath the surface represented the final instance where the temperature exceeded 800 °C. For this layer, the t8/5 cooling time was determined to be 16.1 seconds.

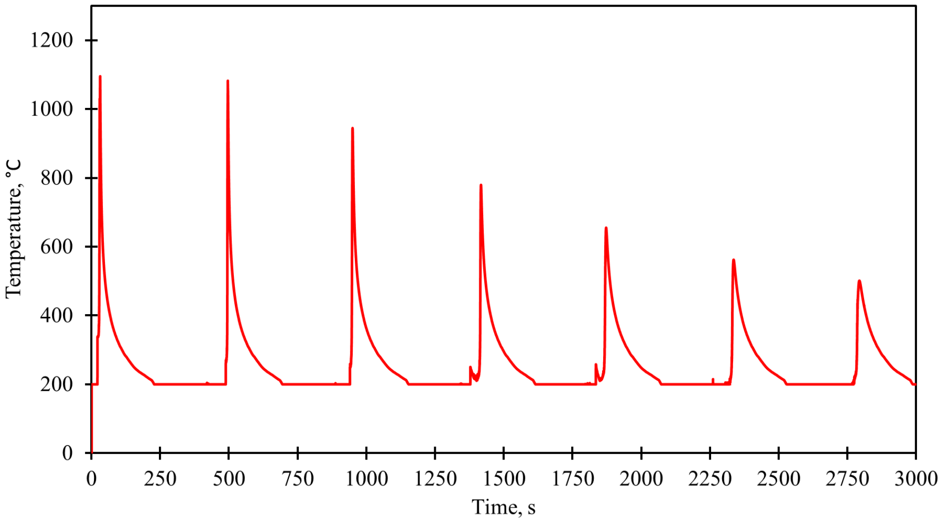

Fig. 4. Temperature of the WAAM SDSS for 7 layers.

2.13.6 Mechanical properties

The purpose of the tensile testing program was to determine the static mechanical properties of the WAAM-fabricated SDSS. The results are presented in Table 3. The measured yield strength was 630 MPa in the vertical (build) direction and 688 MPa in the horizontal direction, demonstrating clearly higher yield strength in the horizontal orientation. It should be noted that the yield strength values of the WAAM SDSS were lower than those reported by the wire manufacturer (Table 1), which can likely be attributed to thermal accumulation and cyclic reheating effects inherent to the WAAM process.

The ultimate tensile strength was 820 MPa in the vertical direction and 867 MPa in the horizontal direction. Interestingly, the horizontal tensile strength slightly exceeded the manufacturer’s specified value. The elongation at fracture was 34.7% in the vertical direction and 38.6% in the horizontal direction, both of which were considerably higher than the value provided by the manufacturer.

Overall, the results indicate that the WAAM-produced SDSS exhibits anisotropic mechanical behavior, which is consistent with findings reported by Huang et al. [3].

Table 3. Mechanical properties of the SDSS.

	Yield strength [MPa]	Tensile strength [MPa]	Elongation [%]
Vertical	630	820	37.4
Horizontal	688	867	38.6

2.13.7 Bending fatigue strength

The fatigue tests were performed up to 2×10^6 cycles, which was defined as the criterion for determining the fatigue limit. The obtained results are presented in Fig. 5. The data indicate that the fatigue limit of the WAAM-produced SDSS was 377 MPa in the vertical (build) direction and 303 MPa in the horizontal direction.

The S–N curves show that, in the low-cycle fatigue regime, the horizontally oriented specimens demonstrated slightly higher fatigue strength, consistent with the tensile test results. In contrast, within the high-cycle fatigue region, the vertically oriented specimens exhibited superior fatigue performance.

The underlying cause of this directional difference is not yet fully clarified and warrants further investigation. One possible explanation could be the influence of residual stress distributions associated with the printing orientation.

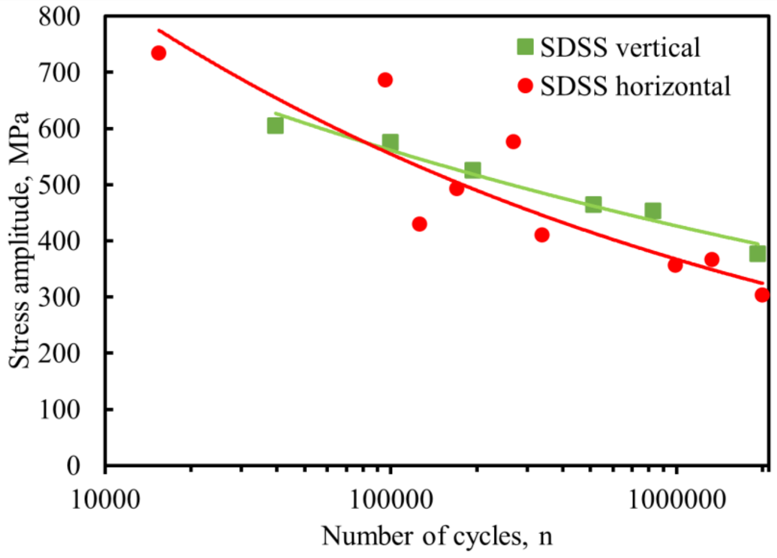

Fig. 5. Fatigue strength of the SDSS.

2.13.8 References

[1] Hosseini, V.A., Karlsson, L.: Physical and kinetic simulation of nitrogen loss in high temperature heat affected zone of duplex stainless steels. Materialia 6, 100325 (2019).

[2] Kannan, A.R., Shanmugam, N.S., Ramkumar, K.D.: Studies on super duplex stainless steel manufactured by wire arc additive manufacturing. Transactions of the Indian Institute of Metals 74, 1673–1681 (2021)

[3] Huang, X., Kwok, C. T., Niu, B., Luo, J., Zou, X., Cao, Y., Yi, J., Pan, L., Qiu, W., Zhang, X.: Anisotropic behavior of super duplex stainless steel fabricated by wire arc additive manufacturing. Journal of Materials Research and Technology 27, 1651–1664 (2023).

2.14 Influence of Porosity on the Bending Fatigue Performance of WAAM-Produced Super Duplex Stainless Steel

2.14.1 Printing equipment

WAAM fabrication was carried out using a Fronius TransPuls Synergic 2700 CMT welding system. The applied process parameters are summarized in Table 1. Two different parameter sets and shielding gas compositions were employed during printing. The produced materials are designated as follows: sound super duplex stainless steel is referred to as SDSS, while the intentionally porous material is labeled SDSS P.

Porosity in SDSS P was deliberately introduced by selecting an inappropriate shielding gas during deposition, which resulted in the formation of numerous pores within the structure. Because the change in shielding gas also influenced the welding characteristics, identical processing parameters could not be maintained for both material conditions. An interpass temperature of 150 °C was controlled throughout the process using an Optris CT infrared pyrometer. For SDSS, pure argon (100%) was used as the shielding gas at a flow rate of 10 l/min. In contrast, SDSS P was produced using a shielding gas mixture of 98% argon and 2% oxygen, supplied at 12 l/min.

The super duplex stainless steel wire (Esab Exaton 29.8.2.L) utilized in the WAAM process met the requirements of EN ISO 14343-A: G/W/P Z 29 8 2 L and had a diameter of 1.2 mm. The wire contained approximately 50 FN ferrite. The manufacturer-reported mechanical properties are listed in Table 2, and the detailed chemical composition is provided in Table 3.

Table 1. WAAM parameters

	Printing speed [m/min]	Voltage [V]	Current [A]	Wire feed [m/min]	Lift between layers [mm]
SSDS	0.37	11.7	100	3.3	1.55
SDSS P	0.42	12.2	110	3.4	1.65

Table 2. Mechanical properties of the SDSS wire.

Yield strength [MPa]	Tensile strength [MPa]	Elongation [%]
730	850	25

Table 3. Chemical composition of the SDSS wire.

C	Cr	Ni	Si	Mo
0.017	29.0	6.7	0.3	2.2

2.14.2 Test setup

Specimens were prepared from the WAAM-fabricated component through machining, during which approximately 1.5–2.0 mm of material was removed from all surfaces. This procedure was carried out to eliminate surface imperfections and achieve a uniform final thickness of 2 mm. Afterward, tensile and fatigue specimens were accurately produced using a combination of laser cutting and precision machining to meet the required dimensions.

Tensile testing was performed on an Instron 8802 universal testing machine in accordance with the SFS-EN ISO 6892-1:2019 standard. A constant crosshead speed of 1.0 mm/min was applied during testing. Vickers hardness measurements were obtained using an Innovatest Falcon 500 hardness tester with a 0.2 kg load, with indentations spaced at 0.1 mm intervals. The geometry of the printed components was examined using optical microscopy (Keyence VHX-200).

Fatigue performance was evaluated using a custom-designed bending fatigue system developed by the FMT research group at the University of Oulu. The apparatus was configured for fully reversed loading conditions ($R = -1$), and stress amplitudes between 150 MPa and 630 MPa were applied. Prior to testing, each specimen was individually calibrated using a dedicated force sensor to ensure accurate determination of fatigue strength.

2.14.3 Cross-sections and X-ray images

Figure 2 presents cross-sectional images of the fabricated specimens. The average wall width of the SDSS sample is approximately 5.8 mm. As shown in Fig. 2a, the SDSS wall is roughly 1 mm wider than the SDSS P wall depicted in Fig. 2b. This difference can be attributed to the lower travel speed used for SDSS as well as the influence of the different shielding gas on weld pool behavior. In Fig. 2b, a pore with an approximate diameter of 0.45 mm is clearly visible in the SDSS P cross section.

Figures 2c and 2d display X-ray images of the as-built (non-machined) components. The X-ray image of SDSS (Fig. 2c) confirms the absence of porosity. Although some indications in the image might suggest incomplete fusion, no such defects were observed after machining. The darker regions visible in the image are associated with variations in wall thickness. As demonstrated in Fig. 2c, it is feasible to produce SDSS without porosity using appropriate processing conditions.

In contrast, the X-ray image of SDSS P (Fig. 2d) reveals a significant presence of pores distributed fairly uniformly throughout the cross section. While porosity could be successfully introduced into the material, precise control over pore size and location was not achievable. The pores are predominantly spherical in shape, with diameters ranging from 0.4 mm to 1.1 mm. These pore sizes correspond to approximately 8.1–22.5% of the total wall width.

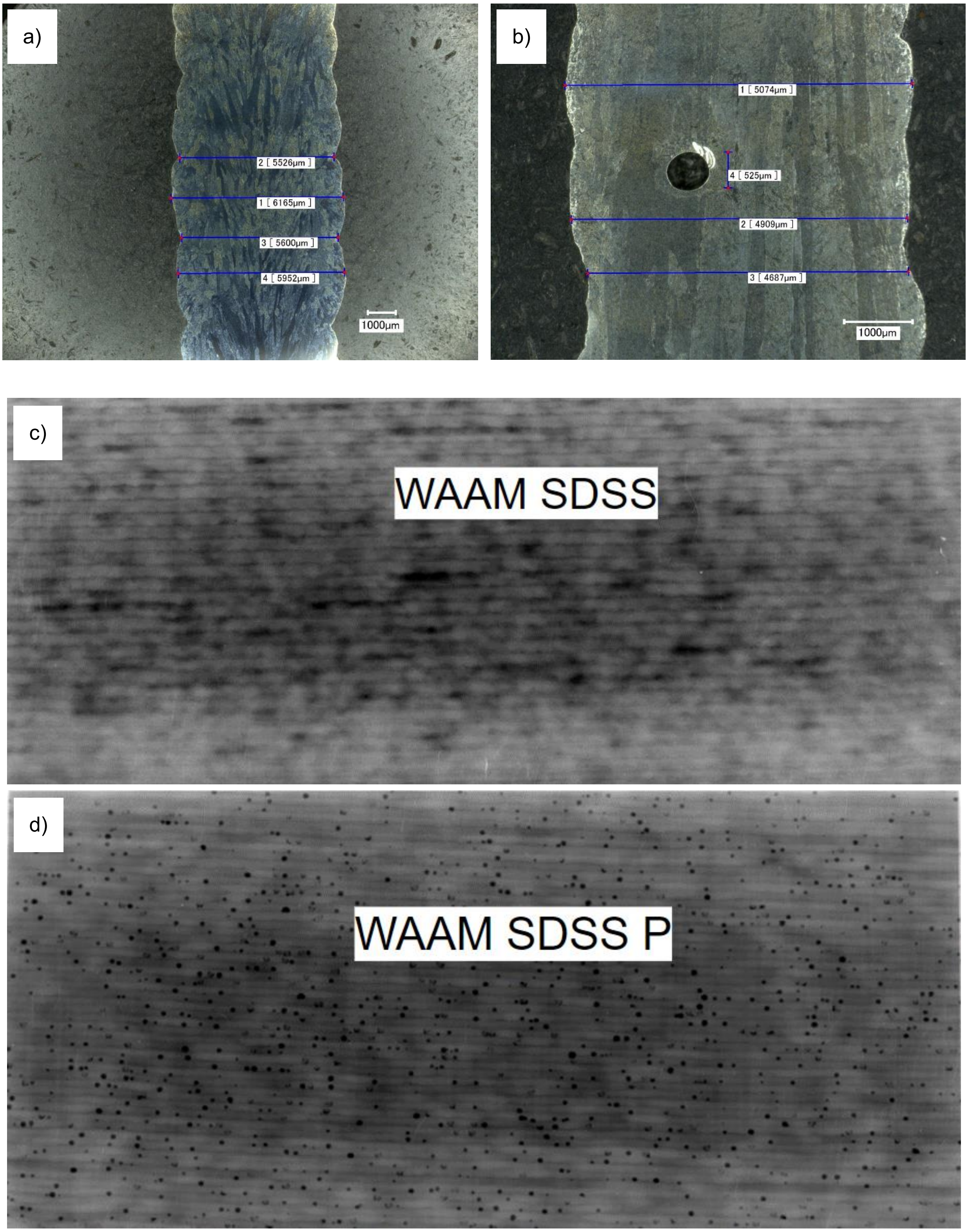

Fig. 2. (a) Cross-section of WAAM SDSS, (b) Cross-section of WAAM SDSS P, (c) X-ray image of WAAM SDSS and (d) X-ray image of WAAM SDSS P.

2.14.4 Microhardness

Hardness testing was performed along the build (vertical) direction. For the SDSS P specimens, special care was taken to ensure that indentations were not placed over pores. The results, shown in Fig. 3, demonstrate a uniform hardness distribution throughout the base material for both SDSS and SDSS P. The average hardness of the SDSS material was approximately 312 HV, while SDSS P exhibited a slightly lower average value of 301 HV.

Overall, the measurements indicate that the hardness levels of SDSS and SDSS P are very similar. The hardness profiles remained consistent across the examined regions (Fig. 4), confirming uniform mechanical properties throughout the WAAM-produced structures. These findings suggest that, excluding the influence of porosity, both materials possess comparable intrinsic strength characteristics.

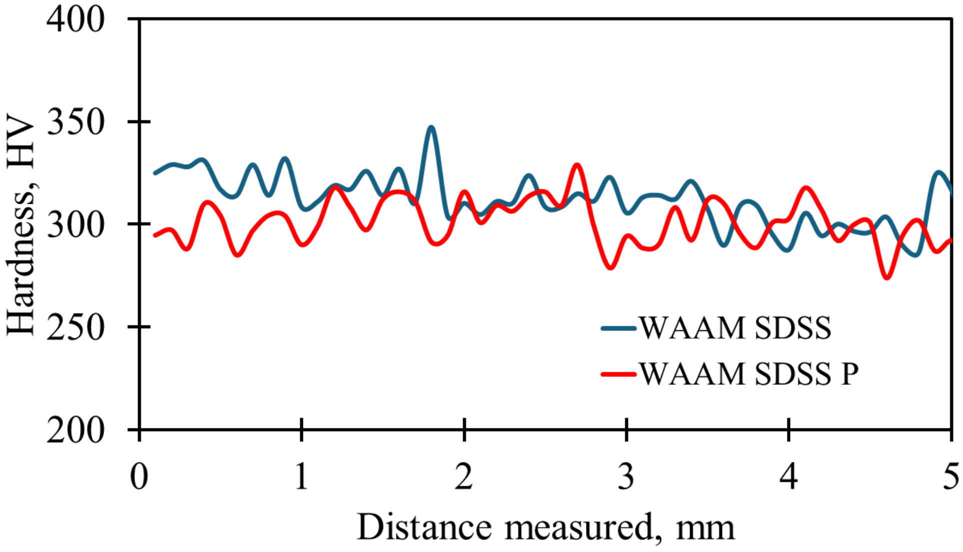

Fig. 3. Hardness profiles of WAAM SDSS and SDSS P.

2.14.5 Mechanical properties

Table 4 summarizes the tensile properties of WAAM SDSS and the porous variant, SDSS P, with all tests performed in the vertical direction. The yield strength of SDSS was clearly higher than that of SDSS P, showing an increase of 15.4%. Similarly, the ultimate tensile strength (UTS) was greater for SDSS (819 MPa) compared to SDSS P (697 MPa), confirming the superior strength of the non-porous material.

The most pronounced difference was observed in ductility. The elongation of SDSS was approximately 118.7% higher than that measured for SDSS P. This substantial reduction in elongation for SDSS P is consistent with the detrimental effect of porosity on mechanical behavior. In addition, the elongation values for SDSS P exhibited a relatively large standard deviation, as indicated in Table 4, reflecting variability caused by pore distribution and size.

Although hardness measurements initially suggested that both materials would exhibit comparable strength levels, tensile testing revealed that porosity significantly impairs the mechanical performance of SDSS P. Overall, the presence of pores markedly reduces both strength and ductility, limiting the suitability of the material for demanding structural applications.

The measured yield and ultimate tensile strengths of the WAAM-produced SDSS were lower than the values reported by the wire manufacturer (Table 2). In contrast, the elongation at fracture surpassed the manufacturer's specified value. This increased ductility is likely a consequence of thermal accumulation and repeated reheating cycles inherent to the WAAM process.

Table 4. Mechanical properties of WAAM SDSS and WAAM SDSS P.

	Yield strength MPa	Tensile strength MPa	Elongation %
SDSS	630	819	37.4
SDSS P	546	697	17.1

2.14.6 Bending fatigue strength

The fatigue tests were performed up to 2 × 10^6 cycles, which was used as the criterion for defining the fatigue limit. The bending fatigue results are illustrated in Fig. 4. The fatigue limit of WAAM SDSS in the vertical direction was determined to be 377 MPa, whereas the porous variant, WAAM SDSS P, exhibited a substantially lower fatigue limit of 152 MPa. This means that the fatigue limit of SDSS is approximately 148% higher than that of SDSS P.

Overall, the results clearly show that SDSS possesses markedly better fatigue resistance than SDSS P across both low-cycle and high-cycle fatigue regimes. The introduction of porosity significantly degrades fatigue performance, an effect that is especially severe in high-strength materials such as super duplex stainless steel.

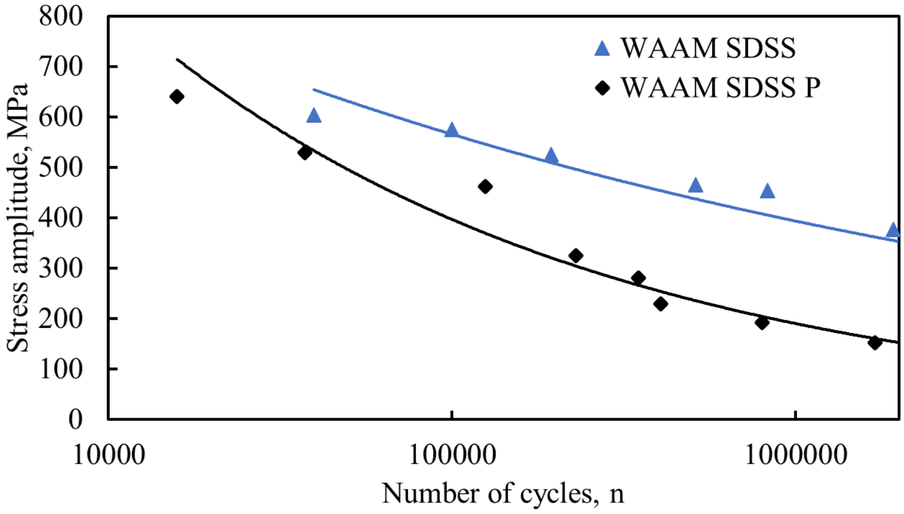

Fig. 4. Fatigue strength of WAAM SDSS and WAAM SDSS P.

Figure 5a shows a representative specimen highlighting the influence of porosity on the fatigue performance of SDSS P. In addition to the primary fracture location, crack propagation was also observed from the region indicated in Fig. 5b, where the crack clearly initiated at a pore.

The fracture surface of a specimen that failed during fatigue testing is presented in Fig. 5c. The image reveals several pores within the fracture area, the largest of which has a diameter of approximately 1 mm. Considering that this pore size corresponds to roughly half of the specimen thickness, it has severely reduced the fatigue resistance of the sample.

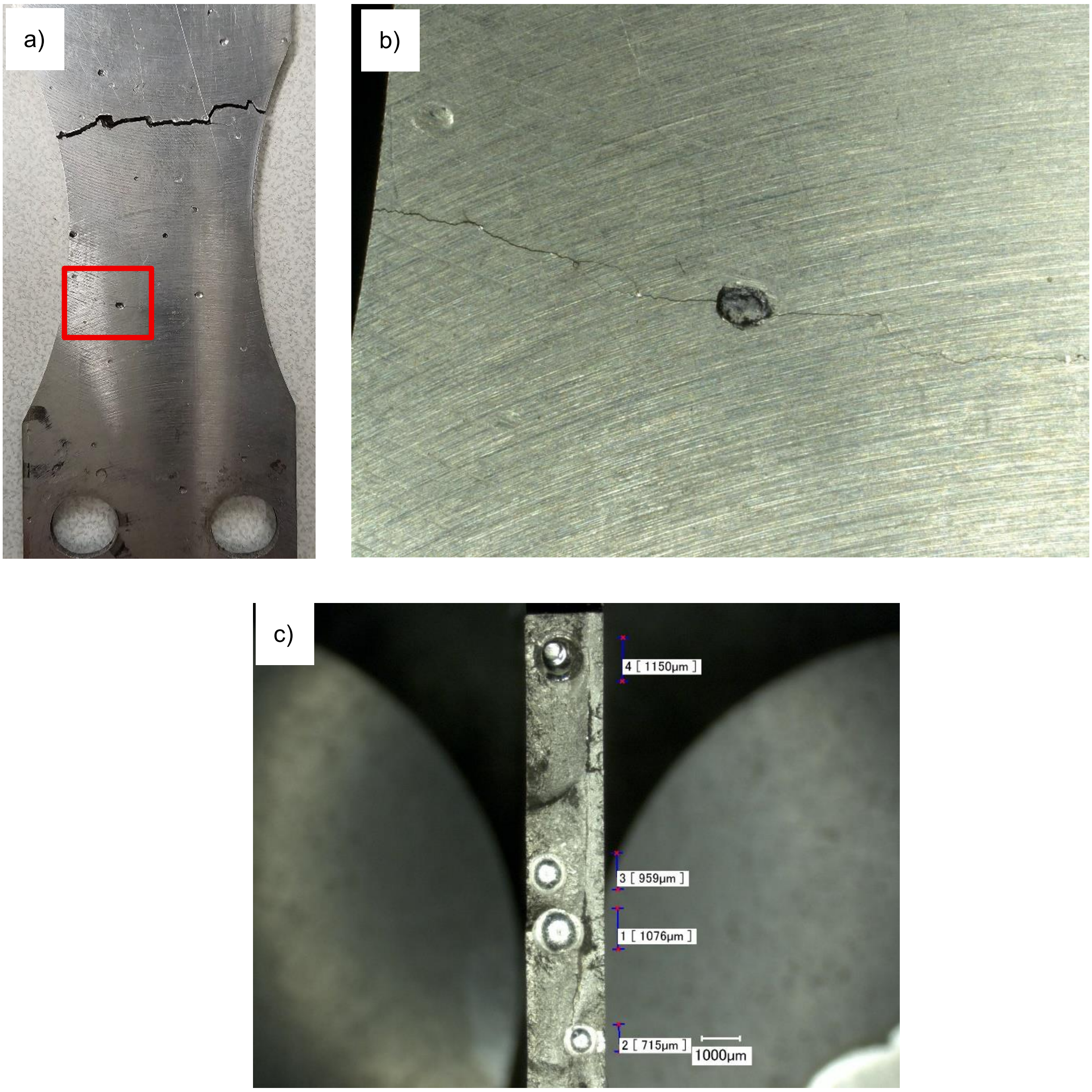

Fig. 5. (a) Specimen fractured during a bending fatigue test, (b) Magnified view of the area enclosed by the rectangle in Fig. 5a, and (c) Fracture surface of the WAAM SDSS P.

2.15 Bending Fatigue Performance of WAAM AISI 316L with Severe Shot Peening Treatment on the As-Built Surface

2.15.1 Printing equipment

The components were fabricated using a Cold Metal Transfer (CMT) welding system (Fronius TransPuls Synergic 2700). The welding torch was integrated with a CNC platform to ensure accurate motion control. The initial layer was deposited at a travel speed of 0.35 m/min using a current of 110 A, a voltage of 13.5 V, and a wire feed rate of 3.2 m/min. For the subsequent layers, the same travel speed of 0.35 m/min was maintained, with a layer increment of 1.4 mm between passes. The parameters for these layers were adjusted to 50 A current, 10.8 V voltage, and a wire feed speed of 2.6 m/min. Between layers, the component was allowed to cool naturally to 150 °C before deposition resumed. Shielding was provided by a gas mixture of 98% argon and 2% oxygen at a flow rate of 12 l/min.

The feedstock material was 1.2 mm diameter AISI 316L stainless steel wire, with nominal mechanical properties of 440 MPa yield strength, 560 MPa ultimate tensile strength, and 40% elongation.

2.15.2 Test setup

Fatigue specimens with machined surfaces were prepared by removing approximately 0.5 mm of material from each side of the printed wall to eliminate surface irregularities and produce a uniform plate. Final specimen dimensions were achieved through laser cutting followed by precision machining. Hardness measurements were performed using an Innovatest Falcon 500 Vickers hardness tester with a 100 g load, with indentations spaced at 0.05 mm intervals. Surface roughness was evaluated using a Keyence VK-X200 laser microscope operating with non-contact laser scanning at a resolution of 0.5 nm.

Bending fatigue performance was assessed using a custom-built fatigue testing machine developed by the FMT research group at the University of Oulu. The device operates under fully reversed loading conditions ($R = -1$), with stress amplitudes ranging from 75 MPa to 580 MPa. Each specimen was individually calibrated using a force sensor prior to testing to ensure measurement accuracy.

Severe shot peening (SSP) treatment was performed inside an enclosed chamber using an ABB industrial robot. The process was applied to the machined surfaces of the WAAM samples, with a specially designed fixture ensuring consistent treatment on both sides. Each specimen underwent up to 22 treatment cycles per side, with a 180° rotation between cycles to maintain uniform peening intensity. Spherical chromium steel shots (STELUX C40) with diameters between 0.30 and 0.85 mm and a hardness of 36 HRC were used. Peening was carried out at a pressure of 7.4 bar with a nozzle distance of 70 mm. The resulting Almen intensity, measured using type A strips, reached 300 A after completion of the full 22-cycle treatment.

2.15.3 Geometry of the printed part and surface roughness

Figure 1 presents a cross-sectional optical micrograph of a WAAM-fabricated AISI 316L wall. The image reveals a characteristic multi-layered structure, with clearly distinguishable interfaces between successive deposited layers. This layered appearance is inherent to the WAAM process, where material is deposited sequentially, each pass building upon the previous one. Slight undulations at the layer boundaries can be observed, which are commonly associated with thermal cycling and melt pool dynamics during deposition.

Some variation in wall width is visible along the build height, suggesting minor non-uniformity in material deposition. Such variations are likely related to factors such as heat distribution and cooling conditions during fabrication. The average wall width was approximately 2.4 mm. The layer height remained relatively consistent within the expected range for WAAM, reflecting stable process control, with an average layer thickness of about 1.45 mm. Although not quantitatively evaluated in this figure, WAAM-produced surfaces are generally known to exhibit moderate to relatively high surface roughness.

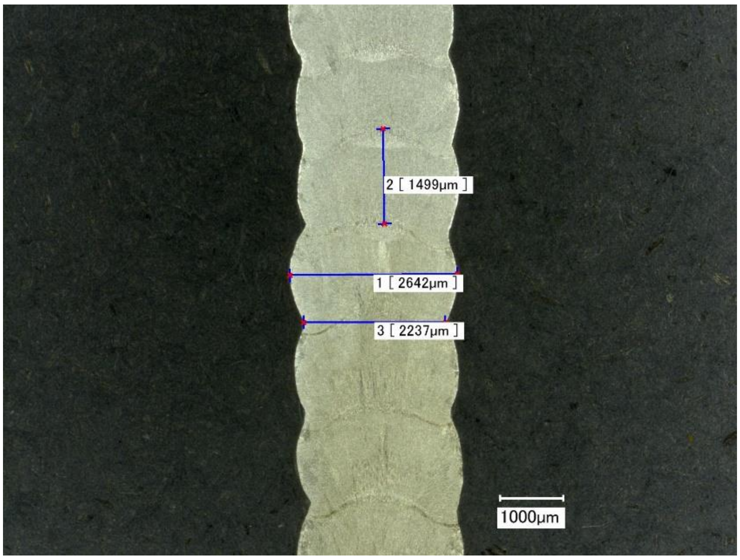

Fig. 1. Cross-section of WAAM 316L part.

The surface roughness profiles shown in Fig. 2a and 2b represent measurements obtained from WAAM-produced as-built and severe shot peened (SSP) as-built walls, respectively. The corresponding roughness parameters are summarized in Table 1, which also includes values for a machined surface condition.

These results highlight key features of the surface morphology generated by the layer-by-layer WAAM process, as well as the influence of SSP treatment. As expected, the machined surface exhibits substantially lower roughness values. The Ra value of 0.43 μm indicates a very smooth finish, and the Rz value of 3.21 μm confirms minimal peak-to-valley variation.

For the WAAM as-built wall (Fig. 2a), the maximum peak-to-valley height (Rz) reaches approximately 134.4 μm, reflecting pronounced surface irregularities typical of additive deposition. The surface displays noticeable waviness caused by successive weld passes, resulting in moderate overall roughness.

In the WAAM SSP-treated as-built wall (Fig. 2b), the Rz value is slightly higher, around 159.4 μm, suggesting somewhat more pronounced peak-to-valley variation compared to the untreated as-built condition. It should be noted that the specimens originated from different printing batches, which may introduce natural variability in surface texture. Nevertheless, the results indicate that SSP does not significantly reduce the Rz value. Interestingly, the Ra value for the SSP-treated surface (34.67 μm) is slightly lower than that of the as-built surface, suggesting a minor improvement in average surface smoothness.

Overall, the machined surface clearly provides the best surface quality, with Ra and Rz values far below those of the as-built and SSP-treated conditions. This emphasizes the importance of machining or similar post-processing techniques in applications requiring high surface quality. While the as-built surface roughness is typical for WAAM and may necessitate finishing for structural applications, SSP offers only limited improvement in average roughness and does not fully eliminate surface irregularities.

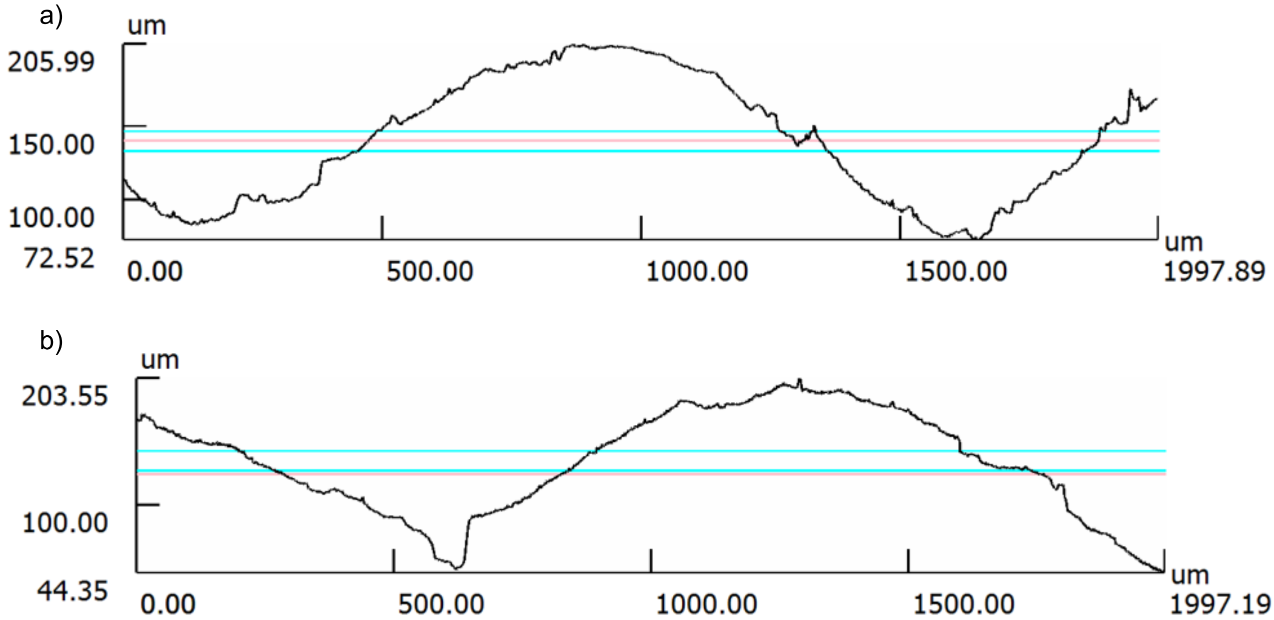

Fig. 2. Surface roughness of (a) as-built and (b) as-built SSP.

Table 1. Surface quality of the WAAM samples.

Surface	Rz [µm]	Ra [µm]
Machined	3.21	0.43
As-built	134.4	37.56
As-built SSP	159.4	34.67

2.15.4 Hardness measurements

Hardness was evaluated as a function of distance from the centerline of the printed wall, as illustrated in Fig. 3. In the as-built condition, the hardness values remained relatively stable across the width of the specimen, varying between 200 HV and 220 HV. The minimal fluctuation in hardness indicates a fairly uniform microstructure throughout the component. Such consistency is characteristic of WAAM-produced structures, where moderate cooling rates and stable thermal gradients promote homogeneous mechanical properties.

In contrast, the surface treated by severe shot peening (SSP) exhibited markedly higher hardness values compared to the as-built material. Across the width, hardness ranged approximately from 250

HV to 450 HV. A pronounced increase in hardness was observed near the edges, reaching peak values of about 450 HV at distances of ±1.4 mm from the center. At the center of the SSP-treated surface, hardness values remained similar to the as-built condition (around 200–220 HV).

This sharp rise in hardness near the surface edges is attributed to the SSP process, which induces significant plastic deformation and work hardening. Severe shot peening enhances surface hardness by refining the microstructure and generating compressive residual stresses, particularly in the near-surface region. The hardness distribution indicates that the strengthening effect of SSP is concentrated close to the treated surfaces, while deeper regions remain largely unaffected. Such surface hardening is advantageous in applications where improved wear resistance and enhanced fatigue performance are required, as the increased near-surface hardness can delay crack initiation and reduce surface damage.

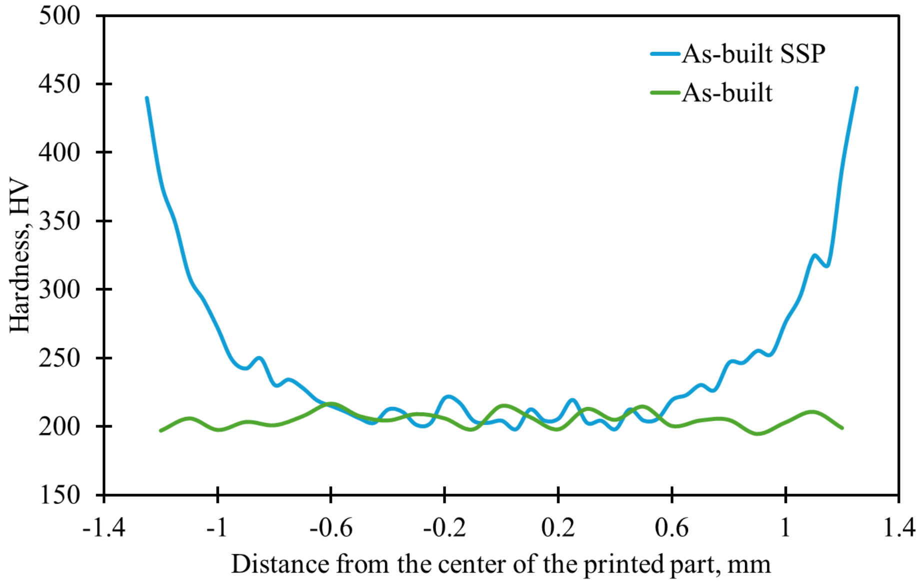

Fig. 3. Hardness profiles of the WAAM 316L as-built and as-built SSP.

2.15.5 Bending fatigue strength

Figure 4 presents the S–N curves comparing the bending fatigue behavior of WAAM 316L in three different surface conditions: machined, as-built, and SSP-treated as-built.

The machined specimens demonstrate the highest fatigue resistance, primarily due to their smooth surface finish, which minimizes surface defects and stress concentration sites that could trigger crack initiation. The fatigue limit for the machined condition was 223 MPa. In both low-cycle and high-cycle fatigue regions, the machined samples exhibited the longest fatigue life.

The SSP-treated as-built specimens showed intermediate fatigue performance, with a fatigue limit of 198 MPa. Severe shot peening introduces compressive residual stresses at the surface, which counterbalance applied tensile stresses and thereby enhance fatigue resistance. Although SSP significantly improves performance compared to the untreated as-built condition, it does not fully reach the level achieved by machining, as the surface remains relatively rough despite the beneficial residual stress state.

The as-built condition displayed the lowest fatigue resistance, with a fatigue limit of only 75 MPa. This reduced performance is mainly attributed to the high surface roughness and residual tensile stresses generated during the WAAM process, both of which promote early crack initiation. Consequently, the as-built specimens exhibited the shortest fatigue life, particularly at lower stress amplitudes.

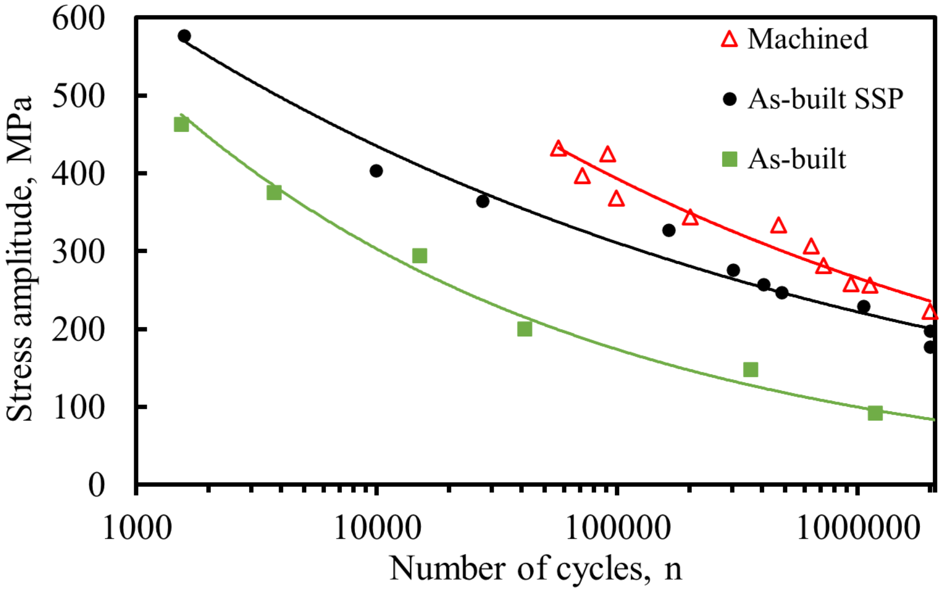

Fig. 4. Fatigue strength of WAAM 316L with machined, as-built and as-built SSP surfaces.

2.16 Fatigue Performance of WAAM-Fabricated Carbon Steel: Comparison Between As-Built and Severe Shot Peened Surface Conditions

2.16.1 Printing equipment

WAAM specimens were produced using a Fronius TransPuls Synergic 2700 welding system. The initial layer was deposited at a travel speed of 0.36 m/min with a current of 105 A, a voltage of 12.5 V, and a wire feed rate of 3.0 m/min. For the subsequent layers, the same deposition speed was maintained, with a layer increment of 1.18 mm between passes. The process parameters for these layers were modified to 45 A current, 10.5 V voltage, and a wire feed rate of 1.0 m/min.

An interpass temperature of 150 °C was applied to control heat accumulation during fabrication. Shielding was provided by a gas mixture of 92% argon and 8% carbon dioxide at a flow rate of 12 l/min. The feedstock material was ESAB Purus 46 carbon steel wire with a diameter of 1.2 mm. According to the manufacturer, the wire has a yield strength of 500 MPa, an ultimate tensile strength of 600 MPa, and an elongation at fracture of 25%.

2.16.2 Mechanical testing setup

Microhardness measurements were performed using an Innovatest Falcon 500 hardness tester in Vickers mode with a 5 g load. Indentations were made at 0.05 mm intervals to obtain a detailed hardness profile and accurately capture potential gradients. EBSD characterization was conducted using a JEOL JSM-7900F scanning electron microscope equipped with an Oxford Instruments Symmetry EBSD detector. The analysis was carried out at an accelerating voltage of 20 kV and a working distance of 17 mm.

Fatigue behavior was evaluated using a dedicated bending fatigue testing system designed for fully reversed loading conditions ($R = -1$). The applied stress amplitudes ranged from 105 MPa to 610 MPa. Before testing, each specimen (Fig. 1b) was individually calibrated using a built-in force sensor to ensure accurate stress determination.

Severe shot peening (SSP) treatment was conducted with a Motoman robotic system. Each side of the specimen was treated with up to 22 peening passes, rotating the sample 180° between passes to ensure uniform coverage. The peening media consisted of spherical chromium steel shots (STELUX C40) with diameters between 0.30 mm and 0.85 mm and a hardness of 36 HRC. The process was performed at an air pressure of 7.4 bar, with a nozzle stand-off distance of 70 mm. Almen intensity testing using type A strips yielded a cumulative intensity of 300 A after completion of all treatment cycles.

2.16.3 Microstructure analysis

Microstructural examination of the surface layer shows pronounced plastic deformation and substantial grain refinement. The EBSD image (Fig. 1) illustrates the near-surface region of the SSP-treated specimen. Close to the surface, the structure consists of densely packed, fine equiaxed grains, clearly indicating significant refinement. This transformation results from the severe plastic deformation induced by the shot peening process. Repeated impacts from the spherical media create localized strain, which promotes dynamic recovery and progressive grain subdivision.

The Kernel Average Misorientation (KAM) map reveals areas with varying degrees of local lattice misorientation. Regions exhibiting elevated internal strain energy point to high dislocation densities and pronounced work hardening. These characteristics are typical of SSP treatment, which not only refines grains but also enhances strain hardening through the accumulation of geometrically necessary dislocations.

The observation of numerous low-angle grain boundaries and substructural features further confirms the formation of dislocation cells or subgrains. With continued peening, these structures evolve into finer grains. The resulting ultrafine-grained layer remains confined to the near-surface region, consistent with the limited penetration depth associated with SSP treatment.

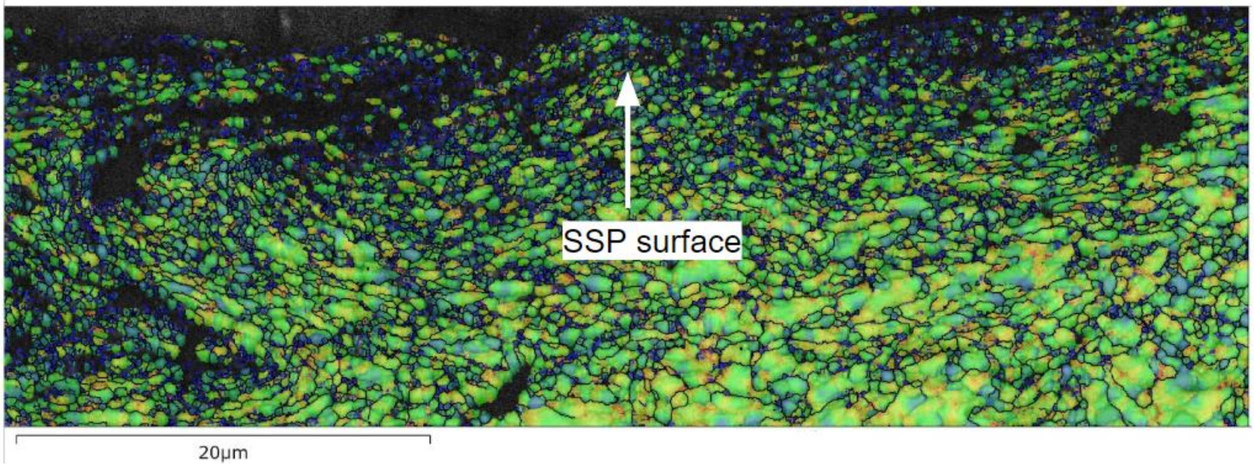

Fig. 1. Microstructure of WAAM carbon steel as-built SSP surface.

2.16.4 Hardness measurement

The untreated base material showed a fairly consistent hardness distribution across the cross-section, with values ranging from 190 HV to 205 HV (Fig. 2). A minor decrease in hardness was detected near the outer surface, where values dropped to approximately 160–170 HV. This reduction may be associated with thermal gradients or localized microstructural variations occurring during the deposition process.

Following SSP treatment, a substantial increase in surface hardness was observed, reaching peak values of about 290 HV. In contrast, the central region maintained hardness levels between 195 HV and 210 HV, comparable to the as-built condition. The increase in surface hardness is attributed to plastic deformation and strain hardening induced by the SSP process, which produced a hardened layer extending roughly 0.3 mm below the surface. This treatment refines the near-surface microstructure and introduces compressive residual stresses, thereby enhancing mechanical performance at the surface. The observed hardness profile clearly indicates that the effect of SSP is most pronounced at the surface and gradually diminishes with depth.

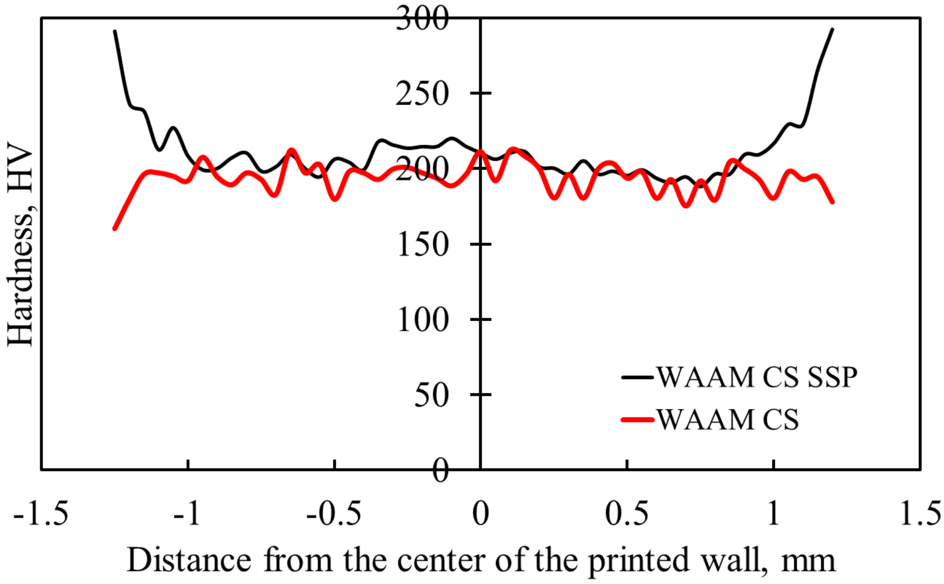

Fig. 2. Hardness profile of WAAM CS and WAAM CP SSP.

2.16.1 Mechanical properties

WAAM carbon steel specimens were evaluated in the as-built state and after severe shot peening (SSP). The SSP treatment led to an average increase of about 13 MPa in yield strength, with the treated specimens reaching 434 MPa. A slight improvement was also recorded in ultimate tensile strength, which increased by approximately 11 MPa to a maximum value of 523 MPa following SSP. However, this gain in strength was accompanied by a reduction in ductility: elongation at fracture decreased from 26.4% in the as-built condition to 18.0% after SSP.

The effect of SSP is primarily confined to the near-surface region, as the treatment mainly alters surface properties. Consequently, the enhancement in yield strength is largely limited to the outer layer of the material. Since the hardened zone extends only about 0.3 mm in depth, the overall influence of SSP on bulk tensile properties remains relatively modest.

2.16.2 Bending fatigue strength

The fatigue experiments were performed up to 2 × 10^6 cycles, which was defined as the fatigue limit. Figure 3 illustrates the bending fatigue behavior of WAAM carbon steel in three surface conditions: machined, as-built, and SSP-treated as-built.

The machined specimens achieved the highest fatigue resistance, with a fatigue limit of 220 MPa. This superior performance is mainly due to the smooth surface finish obtained through machining, which minimizes stress concentrations and reduces the likelihood of crack initiation.

The SSP-treated as-built specimens displayed intermediate fatigue performance, reaching a fatigue limit of 170 MPa. The improvement compared to the untreated as-built condition can be attributed to the compressive residual stresses introduced by the SSP process. These stresses counterbalance tensile stresses during cyclic loading and delay crack initiation. Nevertheless, because the SSP-treated surface still retains noticeable roughness relative to the machined condition, its fatigue life remains lower than that of the machined specimens.

The as-built condition showed the lowest fatigue resistance, with a fatigue limit of 110 MPa. This reduced performance is primarily linked to the inherent surface roughness and residual tensile stresses associated with the WAAM process. Fractographic examination of failed specimens indicated that, in both the as-built and SSP-treated states, cracks propagated parallel to the deposited layers. This fracture orientation corresponds to the characteristic layer morphology of WAAM and suggests that interlayer boundaries serve as preferred crack propagation paths under cyclic loading.

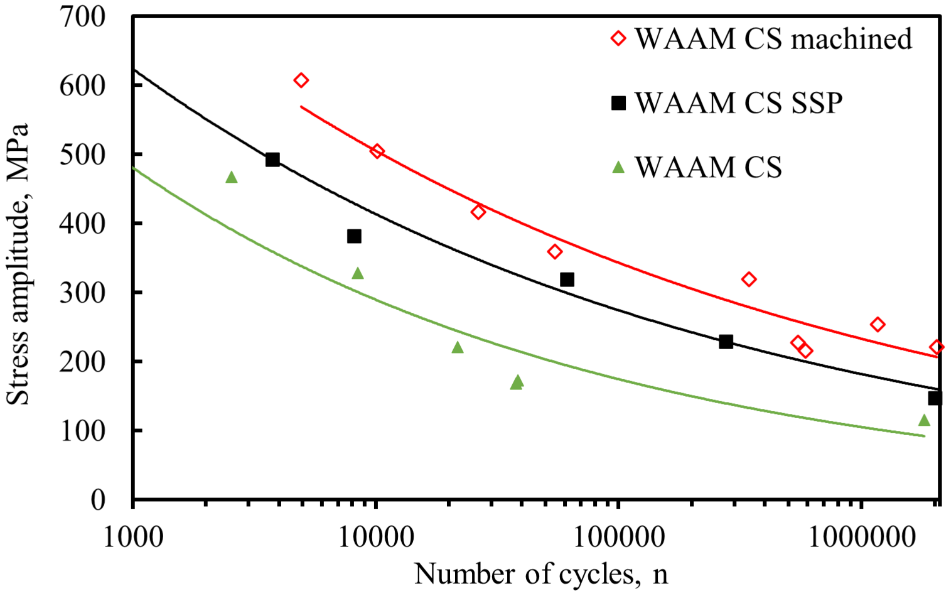

Fig. 3. Fatigue strength of WAAM CS machined, WAAM CS SSP and WAAM CS.

2.17 Comparison of Machined and As-Built Surface Conditions on the Bending Fatigue Performance of WAAM-Fabricated Duplex Steel

2.17.1 Printing equipment

WAAM tests were performed using a Fronius TransPuls Synergic 2700 CMT system. Duplex stainless steel (DSS) walls were produced at a travel speed of 0.37 m/min, with a welding current of 100 A and an arc voltage of 11.7 V. The wire feed rate was maintained at 3.3 m/min, and a vertical layer increment of 1.55 mm was applied between successive passes. The interpass temperature was controlled at 150 °C using an Optris CT infrared pyrometer, and shielding was provided by argon at a flow rate of 10 l/min.

The DSS filler wire (Esab Exaton 29.8.2.L) used in the process complied with EN ISO 14343-A: G/W/P Z 29 8 2 L and had a diameter of 1.2 mm. The wire contained approximately 50 FN ferrite. According to manufacturer specifications, the material exhibits a yield strength of 730 MPa, an ultimate tensile strength of 850 MPa, and an elongation of 25%.

2.17.2 Test setup

Specimens were extracted from the WAAM-fabricated structure through machining, during which approximately 1.5–2.0 mm of material was removed from all surfaces of the machined samples. Milling was performed using a Ø50 mm indexable end mill with a cutting speed of 120 m/min and a feed rate of 367 mm/min. This process eliminated surface irregularities and ensured a consistent final thickness of 2 mm.

For the as-built condition, components were initially produced at a thickness of 2 mm, and machining was applied to only one side. As a result, these specimens had one original as-built surface and one machined surface. Final tensile and fatigue specimens were then precisely prepared using a combination of laser cutting and precision machining to meet strict dimensional requirements.

For each surface condition (as-built and fully machined), five tensile specimens, three hardness profiles, and twenty bending fatigue specimens were evaluated. Tensile tests were conducted using an Instron 8802 universal testing machine in accordance with SFS-EN ISO 6892-1:2019, employing a constant crosshead speed of 1.0 mm/min. Hardness measurements were performed with an Innovatest Falcon 500 Vickers hardness tester using a 0.3 kg load and 0.05 mm spacing between indentations. The geometry of the fabricated components was examined using a Keyence VHX-200 optical microscope. Surface roughness was measured with a Keyence VK-X200 laser microscope using non-contact laser scanning, offering a resolution of 0.5 nm.

Fatigue performance was assessed using a custom-designed bending fatigue testing system developed by the FMT research group at the University of Oulu. The device operates under fully reversed loading conditions (R = −1), with applied stress amplitudes ranging from 90 MPa to 630 MPa. Prior to testing, each specimen was individually calibrated using a dedicated force sensor to ensure precise and reliable fatigue measurements. At least two specimens per condition were tested to construct S–N curves, following common practice in exploratory fatigue studies. Although not based on a full statistical design, this level of replication ensured consistent trends and reproducibility of results.

2.17.3 Cross-section and surface roughness measurements

Figure 1 presents the cross-sectional profile of a duplex stainless steel (DSS) wall produced by WAAM. The image illustrates the typical structural features of an additively manufactured wall, with both external surfaces preserved in the as-built state.

The wall shows a distinct layered structure with clearly visible bead boundaries and slight waviness along the side surfaces. These undulations arise from the layer-by-layer deposition process characteristic of WAAM. The wall width exhibits minor variation along the vertical direction, with measurements at three different locations ranging from approximately 5.72 mm to 5.97 mm. This indicates generally stable deposition, although small localized geometric variations are present.

The as-built surfaces exhibit noticeable irregular contours, which are common in WAAM components due to factors such as wire feed rate, torch movement, thermal gradients, and gravity-driven effects during solidification. If left untreated, these surface features can serve as stress concentration sites and significantly impair fatigue performance, especially under bending loads where maximum tensile stresses occur at the surface.

In the context of this study, the observed geometry highlights the importance of post-processing methods such as machining or polishing to enhance surface quality and mechanical performance. The rough and wavy nature of the as-built surface correlates with the reduced bending fatigue strength measured in untreated specimens. Machining removes this irregular surface layer, smooths the profile, and eliminates potential near-surface defects or microstructural inconsistencies.

Additionally, the consistent stacking of weld beads without visible separation suggests strong metallurgical bonding between layers, which is critical for maintaining bulk mechanical strength. Nevertheless, surface-connected defects or lack-of-fusion imperfections—potentially undetectable in polished cross sections—may still promote early fatigue crack initiation if not removed through post-processing.

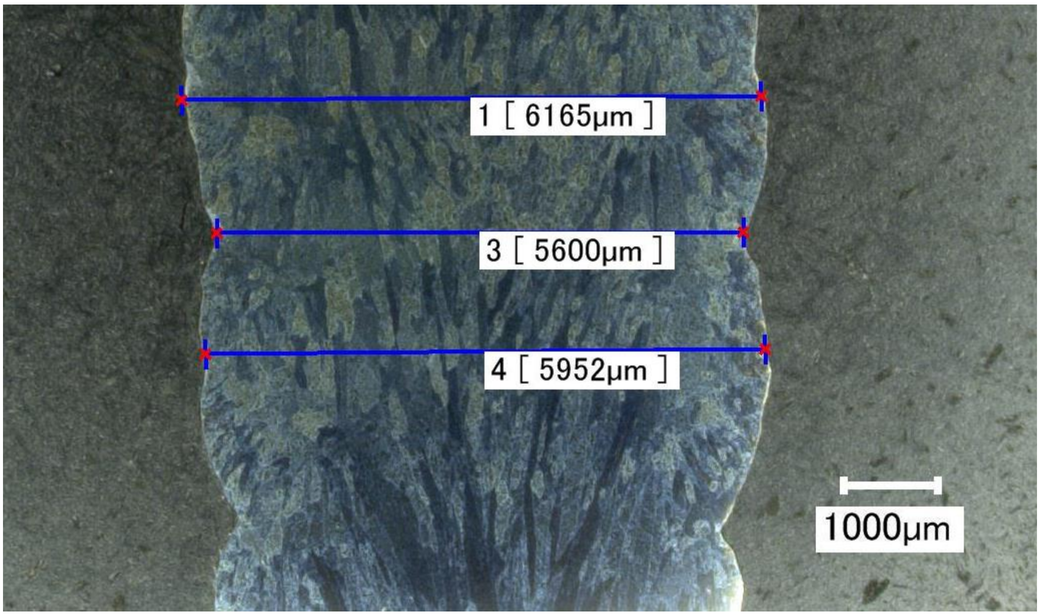

Fig. 1. WAAM DSS geometry.

Table 1 summarizes the surface roughness values measured for both machined and as-built WAAM-produced DSS specimens. The corresponding surface profiles are illustrated in Fig. 2a (machined) and Fig. 2b (as-built).

The as-built surface exhibits exceptionally high roughness, with an average roughness (Ra) of 89.82 µm and a maximum peak-to-valley height (Rz) of 473.99 µm. These elevated values are characteristic of WAAM-fabricated surfaces, where large melt pools, sequential layer solidification, and limited surface finishing control result in pronounced surface irregularities. Such severe roughness introduces significant stress concentration sites under cyclic loading conditions, leading to reduced fatigue resistance—particularly in bending applications, where maximum tensile stresses occur at the surface.

In comparison, the machined surface exhibits a markedly smoother finish, with an Ra value of 0.49 µm and an Rz value of 10.13 µm. This corresponds to a reduction of more than 99% in Ra and 98% in Rz relative to the as-built condition. Such significant improvements in surface quality are essential for increasing fatigue performance, as they substantially reduce stress concentration effects and postpone the initiation of fatigue cracks.

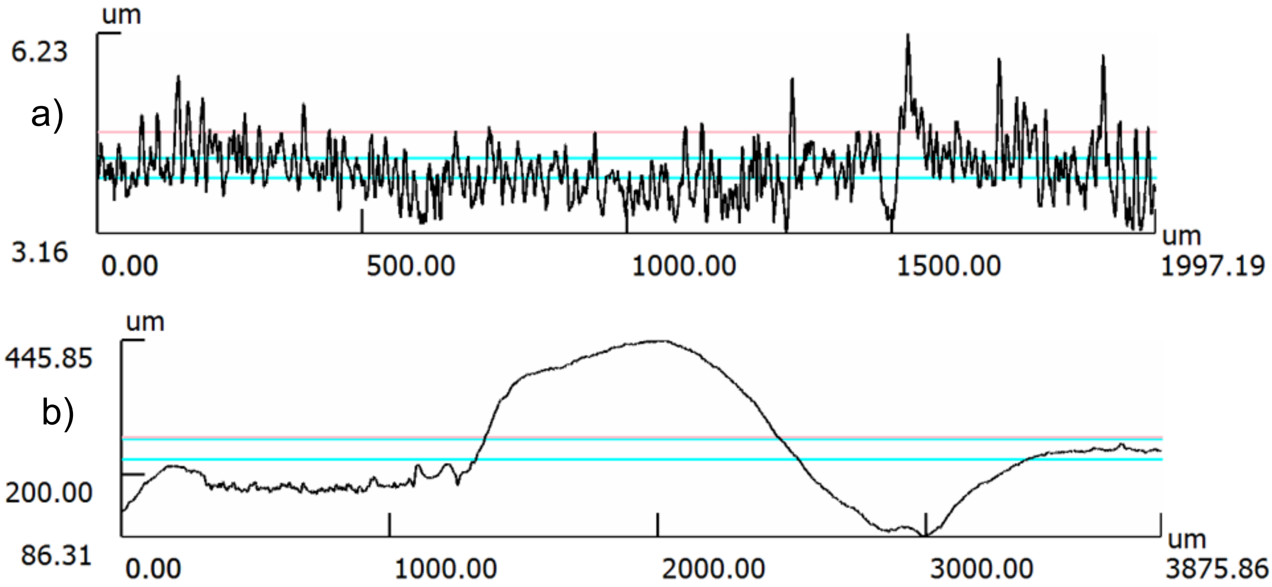

Fig. 2. Surface profiles of WAAM DSS surfaces: (a) machined sample, (b) as-built sample.

Table 1. Surface roughness.

Surface	Rz [µm]	Ra [µm]
Machined	10.13	0.49
As-built	473.99	89.82

2.17.4 Hardness measurements

Figure 3 illustrates the microhardness distribution measured across a 2 mm path in a WAAM-fabricated DSS specimen, extending from the external as-built surface (left side) toward the region corresponding to the machined surface (right side).

The results indicate that the as-built surface shows slightly lower hardness values, approximately 285 HV, whereas the region near the machined surface exhibits higher and more stable hardness values in the range of 295–310 HV. This localized increase in hardness near the machined side suggests strain hardening introduced during the machining operation.

Duplex stainless steels, owing to their dual-phase microstructure, are especially susceptible to work hardening when exposed to plastic deformation. Machining processes—particularly cutting and finishing operations—can induce plastic deformation in the near-surface layers, increasing dislocation density and consequently forming a hardened surface layer.

This localized surface hardening has significant implications for fatigue performance. The increased hardness near the machined surface likely enhances fatigue resistance by locally raising the yield strength and improving resistance to microcrack initiation. Moreover, machining may introduce compressive residual stresses, which help counteract tensile stresses during cyclic bending and thereby delay crack formation.

By contrast, the as-built surface exhibits lower hardness, which may be associated with surface-connected imperfections originating from the WAAM process. These features are consistent with the reduced fatigue strength observed in as-built specimens, as they promote early crack initiation under cyclic loading.

Overall, the hardness distribution supports the conclusion that machining improves fatigue behavior not only by smoothing the surface and removing defects, but also by modifying the near-surface mechanical state through strain hardening and potentially beneficial residual stress development. Additional microstructural investigations—such as EBSD or high-resolution optical microscopy—could further clarify the extent of machining-induced grain refinement, phase changes, or deformation structures near the surface. Such analyses would complement the hardness findings and provide a more comprehensive understanding of the observed fatigue improvements.

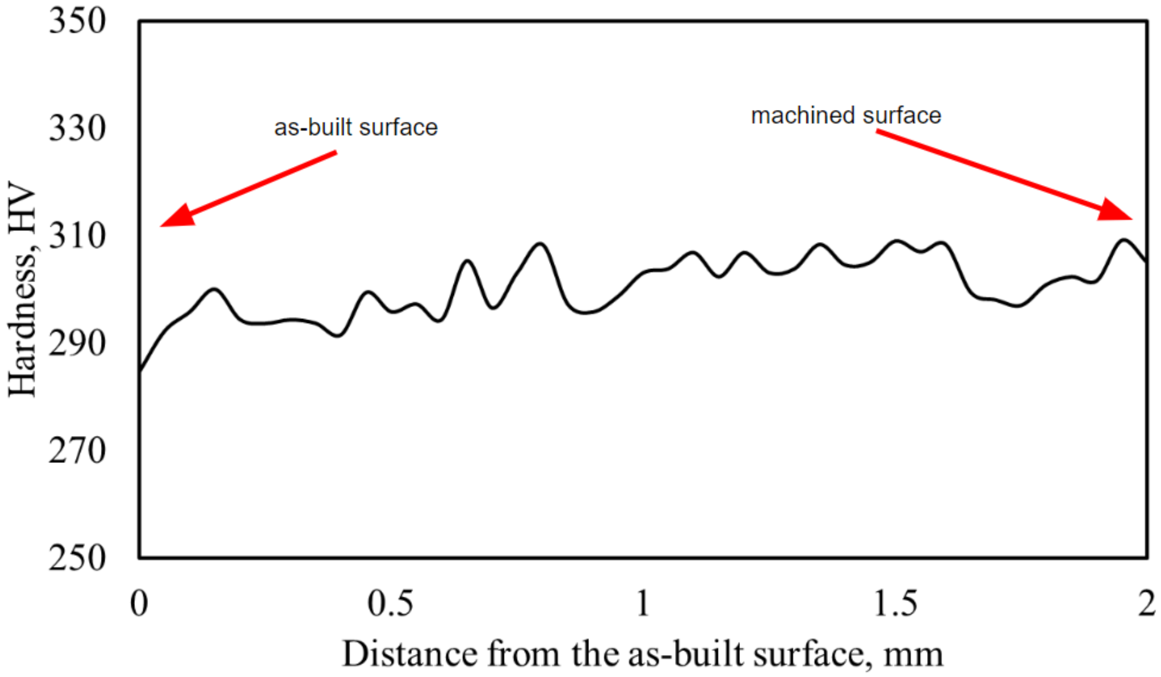

Fig. 3. Hardness profile of WAAM DSS.

2.17.5 Mechanical properties

To evaluate the intrinsic mechanical properties of the WAAM-produced duplex stainless steel (DSS), tensile tests were performed on specimens taken from the deposited material. The average ultimate tensile strength (UTS) was 820 MPa, the 0.2% proof yield strength was 625 MPa, and the total elongation at fracture reached 36.2%. These results demonstrate a favorable balance between strength and ductility, consistent with properly processed duplex stainless steels.

While tensile properties are generally not strongly affected by surface condition, they provide essential background information for this study. Under tensile loading, the entire cross-section carries the load uniformly, making the test less sensitive to surface roughness or localized surface defects. Therefore, tensile results primarily reflect the bulk material response, independent of whether the surface is in the as-built or machined state. In contrast, bending fatigue performance is highly dependent on surface quality, since cyclic tensile stresses are concentrated at the outer surface, where imperfections have the greatest impact.

It is important to recognize that as-built surfaces may reduce the reliability of tensile test outcomes. Surface-connected defects can lead to premature fracture that does not accurately represent the true bulk material capacity, particularly in geometries or loading scenarios sensitive to crack-like discontinuities. As a result, tensile data from as-built specimens should be interpreted carefully.

Within the scope of this study, the tensile results confirm that the WAAM DSS possesses a strong and ductile material base. However, the pronounced differences observed in bending fatigue strength between machined and as-built conditions are not attributable to changes in tensile properties. Instead, they highlight the critical influence of surface condition in fatigue-dominated applications.

2.17.6 Bending fatigue strength

A comparison between as-built and machined specimens was performed to evaluate how surface condition influences the bending fatigue performance of WAAM-produced DSS. The results presented in Fig. 4 clearly show that specimens retaining the as-built surface exhibit substantially lower fatigue resistance than those subjected to machining.

Fatigue testing was carried out under fully reversed loading conditions, and S–N curves were generated for both surface states. Using 2×10^6 cycles as the fatigue limit criterion, the as-built specimens achieved a fatigue limit of 94 MPa, whereas the machined specimens reached 377 MPa. This significant difference confirms that surface machining markedly enhances fatigue strength.

The inferior fatigue performance of the as-built specimens is primarily attributed to the pronounced surface roughness and geometric irregularities characteristic of the WAAM process. These surface features act as stress concentration sites, facilitating early crack initiation under cyclic bending loads, particularly in regions subjected to tensile stress.

In contrast, machining improves fatigue resistance by smoothing the surface and eliminating major notches and surface-connected defects. Additionally, machining may induce beneficial compressive residual stresses and cause localized strain hardening in the near-surface region. Duplex stainless steels, due to their ferritic–austenitic microstructure, are especially susceptible to strain hardening during plastic deformation such as cutting or grinding. This hardened surface layer can increase the local yield strength, thereby delaying crack initiation and slowing early crack propagation.

Overall, the improvement in bending fatigue performance observed in machined specimens can be attributed to a combination of surface smoothing and microstructural strengthening effects. These findings emphasize the critical role of appropriate surface finishing treatments when employing WAAM-fabricated duplex stainless steel components in fatigue-critical applications.

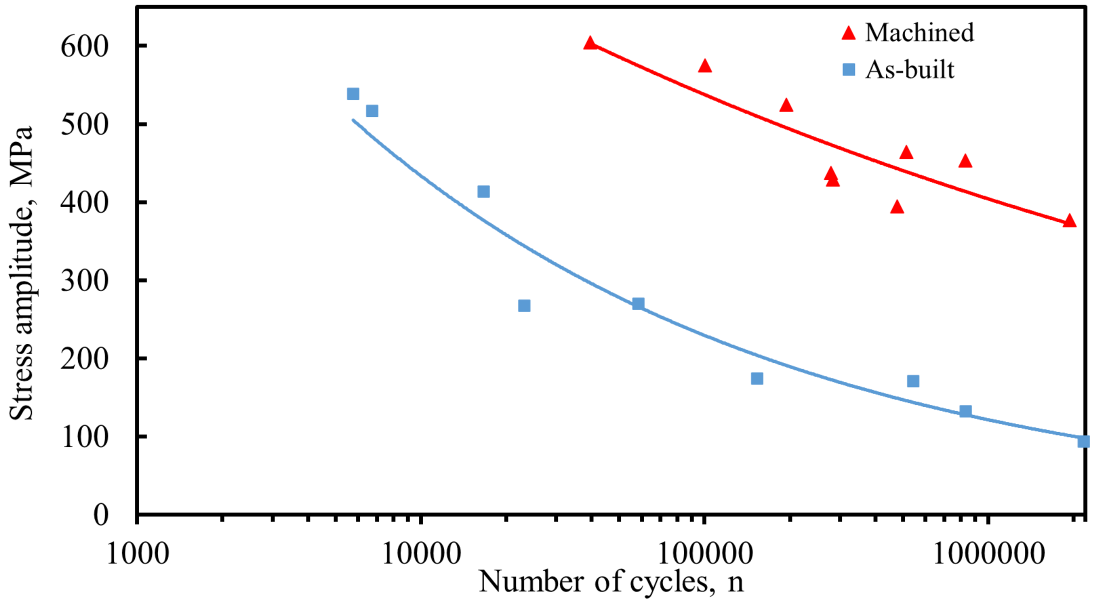

Fig. 4. Fatigue strength of WAAM DSS with machined and as-built conditions.

The linear fracture observed in the as-built specimen (Fig.6) reflects the inherent anisotropy of WAAM-produced structures. Surface waviness and other irregularities typical of the as-built condition intensify this behavior by creating stress concentrations at layer interfaces, which promote crack growth along these planes.

The straight crack path indicates minimal crack deflection, implying lower energy absorption during fracture. This response is consistent with the expected performance of as-built WAAM components, where high surface roughness (elevated Ra and Rz values) and possible internal imperfections contribute to relatively brittle fatigue failure under bending loads. The combination of layer boundaries and surface irregularities provides a preferential route for crack propagation, resulting in reduced fatigue life compared to machined specimens.

In contrast, the machined specimen shown in Fig. 5 displays a more irregular and tortuous fracture path, without clear alignment to the original WAAM layer structure. This suggests that machining diminishes the influence of layer interfaces on crack propagation. By removing the rough as-built surface, machining reduces stress concentrations associated with the deposition process. Additionally, machining may introduce a strain-hardened surface layer and beneficial compressive residual stresses, both of which can delay crack initiation and encourage crack deflection.

The non-linear fracture path in the machined sample indicates a more ductile failure mechanism, with crack growth occurring through the bulk material rather than along predefined weak planes. This behavior likely results from the more uniform surface and subsurface conditions achieved after machining, which reduce the anisotropic effects of the WAAM process. As the crack encounters various microstructural features—such as grain boundaries and phase interfaces—it follows a more complex trajectory, increasing energy dissipation during propagation. This greater energy absorption contributes to the superior bending fatigue strength observed in machined specimens.

These results are particularly significant for the adoption of WAAM in industries such as aerospace, marine, and oil and gas, where duplex stainless steels are frequently subjected to cyclic loading. The findings clearly demonstrate that post-process machining is a critical step in ensuring that WAAM-produced DSS components meet the fatigue performance requirements of such demanding applications.

Fig. 5. The machined specimen fractured in fatigue test.

Fig. 6. As-built specimen fractured in fatigue test.

2.18 Influence of Interpass Temperature on the Mechanical Performance and Fatigue Behavior of Wire Arc Additively Manufactured Carbon Steel

2.18.1 Printing setup

The WAAM specimens were manufactured using a Fronius TransPuls Synergic 2700 welding system. The selected process parameters included a wire feed rate of 8.1 m/min, a welding current of 234 A, and an arc voltage of 16.1 V. Deposition was carried out at a constant travel speed of 0.9 m/min, and the build was executed with a layer height increment of 1.65 mm.

Fabrication was performed using three different interpass temperatures: 200°C, 400°C, and 600°C. Shielding was provided by a gas mixture containing 82% argon and 18% carbon dioxide, supplied at a flow rate of 12 l/min. The consumable material was a carbon steel wire, ESAB OK Aristorod 12.50, with a diameter of 1.2 mm. According to the manufacturer's specifications, the wire exhibits a yield strength of 470 MPa, an ultimate tensile strength of 560 MPa, and an elongation at break of 26%.

2.18.2 Test setup

Uniaxial tensile tests were performed using an Instron 8802 universal testing system in accordance with the SFS-EN ISO 6892-1:2016 standard. The experiments were carried out at a constant crosshead speed of 1.0 mm/min to ensure consistent and accurate measurement of mechanical properties. Microhardness measurements were obtained using an Innovatest Falcon 500 hardness tester with a load of 0.3 kg, and indentations were placed at intervals of 0.2 mm. The microstructure of the specimens was analyzed with a Keyence VK-X200 laser scanning microscope.

The bending fatigue performance of the WAAM-fabricated specimens was evaluated using a custom-built reversed bending fatigue device based on the original WEBI machine developed by Carl Schenck. Fatigue experiments were conducted under fully reversed loading conditions with a stress ratio (R) of −1, where R represents the ratio of minimum to maximum stress within a loading cycle. Stress amplitudes between 230 MPa and 610 MPa were applied in a controlled manner. For each interpass temperature condition, 15 specimens were tested. To ensure accuracy and repeatability, every sample was individually calibrated using a force sensor prior to testing, allowing compensation for material variations and enabling precise force control throughout the fatigue experiments.

2.18.3 Hardness measurements

Figure 1 illustrates the variation in hardness with changing interpass temperature. At an interpass temperature of 200 °C, the measured hardness values fall roughly between 155 and 170 HV, with clear fluctuations observed along the measurement line. When the interpass temperature is raised to 400 °C, the hardness decreases to approximately 145–155 HV, and the scatter becomes less pronounced, indicating moderate material softening. At 600 °C, hardness declines further to about 130–140 HV and displays the most uniform distribution, suggesting that the material reaches its lowest hardness and highest structural homogeneity at this temperature.

The progressive reduction in hardness with increasing interpass temperature is mainly attributed to tempering phenomena occurring between successive deposition passes. At 200 °C, tempering is limited, allowing harder microstructural constituents, such as martensite, to remain largely intact. In contrast, interpass temperatures of 400–600 °C enhance tempering reactions, which reduce dislocation density and promote the formation of softer phases such as ferrite and pearlite. This transformation leads to an overall decrease in hardness. Additionally, higher interpass temperatures result in more consistent hardness values along the build direction, reflecting a more uniform thermal exposure and microstructural evolution throughout the component.

The significant hardness variations observed at 200 °C can be linked to the layer-wise deposition process and localized thermal cycling, which generate microstructural inhomogeneities. At 600 °C, these variations are minimal, indicating that elevated interpass temperatures contribute to a more stabilized and homogeneous microstructure.

From a microstructural perspective, the hardness trend corresponds closely to the thermal conditions experienced during fabrication. Lower interpass temperatures promote rapid cooling, encouraging martensitic or bainitic transformations that increase hardness but also produce structural heterogeneity. As the interpass temperature rises, accumulated heat input facilitates tempering and grain growth, yielding a softer yet more uniform microstructure. This softening effect is also associated with carbide precipitation and recovery processes within the lath martensite, both of which reduce the density of strengthening defects.

The relationship between hardness and interpass temperature highlights the importance of precise thermal management in WAAM processing. Lower interpass temperatures may enhance hardness and strength but can also introduce residual stresses and microstructural gradients that may adversely affect fatigue behavior. Conversely, higher interpass temperatures promote structural uniformity and stability, potentially improving toughness and dimensional accuracy, albeit at the cost of reduced hardness. These results emphasize the need to tailor interpass temperature to achieve an optimal balance between strength, ductility, and fatigue performance in WAAM-fabricated components.

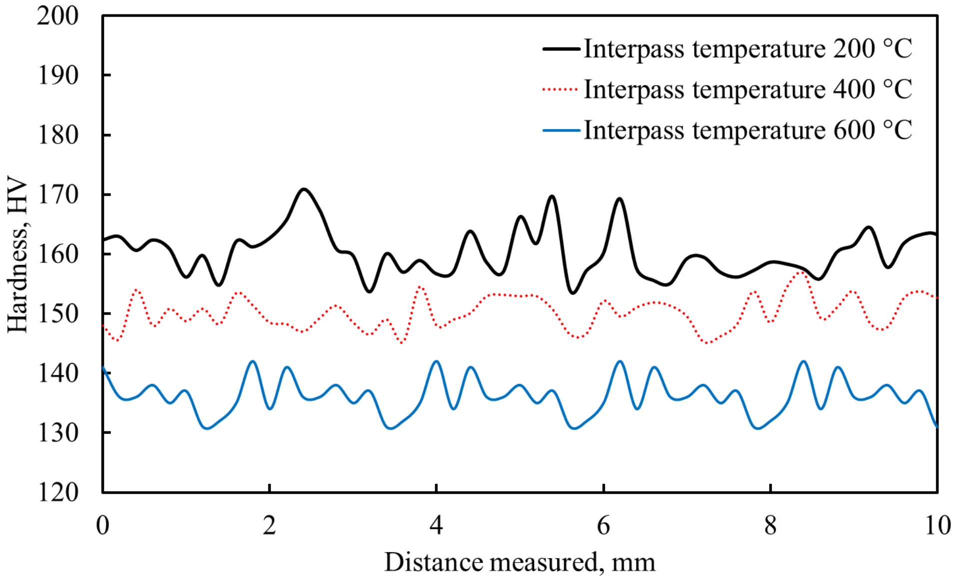

Fig. 1. Hardness profiles of WAAM carbon steel at different interpass temperature.

2.18.4 Mechanical properties

Figure 2 illustrates how interpass temperature affects the tensile behavior of WAAM-fabricated carbon steel specimens. A clear downward trend in both yield strength and ultimate tensile strength is observed as the interpass temperature increases. When the interpass temperature rises from 200 °C to 600 °C, the ultimate tensile strength decreases by approximately 8%, from 510 MPa to 470 MPa. Over the same temperature range, the yield strength shows a more pronounced reduction of about 23%, declining from 390 MPa to 300 MPa. These results indicate that elevated interpass temperatures lead to a softer material condition, primarily due to reduced cooling rates during layer deposition. Slower cooling favors the formation of coarser ferritic–pearlitic microstructures while limiting the development of harder constituents such as martensite or bainite, which are more likely to form under rapid cooling conditions at lower interpass temperatures.

The greater decrease in yield strength compared to tensile strength suggests that mechanisms associated with rapid solidification—such as high dislocation density and fine microstructural features—are diminished at higher interpass temperatures. Increased thermal exposure between passes promotes recovery and possibly partial recrystallization, which reduce internal stresses and dislocation density. As a result, the material exhibits lower resistance to the onset of plastic deformation and a reduced strain-hardening capability. Although both yield and tensile strengths decline, this softening is accompanied by improved plastic deformation behavior.

Elongation increases markedly as interpass temperature rises, improving by approximately 38%, from 32% at 200 °C to 44% at 600 °C. This inverse relationship between strength and ductility reflects the typical behavior of thermally softened steels. Higher interpass temperatures facilitate dislocation rearrangement and grain boundary relaxation, enabling the material to undergo greater uniform plastic deformation prior to fracture. Consequently, the steel becomes more ductile and better suited to applications requiring toughness or formability, though at the expense of load-bearing capacity.

Overall, the results demonstrate that interpass temperature plays a crucial role in determining the balance between strength and ductility in WAAM carbon steel. Lower interpass temperatures, around 200 °C, encourage the development of finer microstructures with higher dislocation densities and possible martensitic or bainitic features, resulting in higher strength but reduced ductility. In contrast, higher interpass temperatures, near 600 °C, promote ferrite–pearlite formation and grain coarsening, leading to decreased strength but enhanced ductility and toughness.

These observations highlight the importance of tailoring interpass temperature to meet specific service requirements. For structural components where high strength and load-carrying capacity are critical, lower interpass temperatures may be preferable. Conversely, for applications involving impact loading or requiring significant deformation capability, higher interpass temperatures can provide improved toughness and formability through the development of a more stable and homogeneous ferritic–pearlitic microstructure.

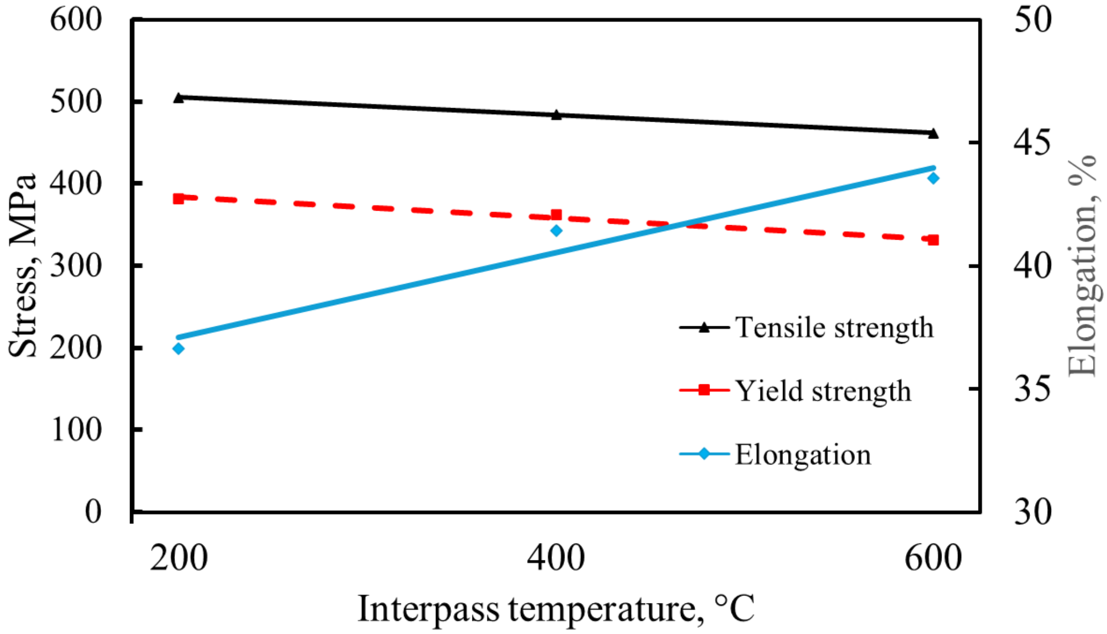

Fig. 2. Mechanical properties of WAAM carbon steel at different interpass temperature.

2.18.5 Bending fatigue strength

In the bending fatigue experiments, WAAM carbon steel specimens fabricated at three interpass temperatures—200 °C, 400 °C, and 600 °C—were tested up to 2 × 10^6 loading cycles, which was taken as the fatigue limit criterion. As shown in Fig. 3, the fatigue limit is approximately 220 MPa for all temperature conditions, indicating minimal variation between the different interpass settings.

Notably, the bending fatigue performance appears largely unaffected by interpass temperature. Although increasing interpass temperature leads to reductions in yield and tensile strength due to tempering effects and microstructural coarsening, these changes do not significantly alter the fatigue limit. This behavior suggests that fatigue performance in WAAM carbon steel is primarily controlled by crack initiation mechanisms rather than bulk mechanical strength. Factors such as surface condition, microcrack formation, inclusions, and residual stress distribution in the near-surface region play a dominant role under cyclic bending loads.

At elevated interpass temperatures (400–600 °C), repeated thermal exposure during deposition facilitates partial relaxation of residual stresses and improves ductility. Both effects can contribute positively to fatigue resistance. Additionally, the softer microstructure formed at higher temperatures may reduce localized stress concentrations around microstructural heterogeneities, thereby delaying the onset of crack initiation. These beneficial effects appear to counterbalance the reduction in static strength, resulting in a nearly unchanged fatigue limit across the tested temperature range.

The similar fatigue limits observed for all interpass temperatures indicate that, once surface imperfections or geometric irregularities are present, fatigue behavior is governed mainly by local stress intensification at these sites. In WAAM-fabricated components, surface roughness and process-induced features frequently serve as preferential locations for crack initiation. Consequently, improving surface quality through post-processing techniques such as machining, polishing, or shot peening is likely to have a more significant impact on fatigue performance than moderate adjustments in interpass temperature.

From a microstructural standpoint, the findings indicate that variations in interpass temperature do not substantially modify the near-surface microstructure in a way that would markedly influence crack propagation. Under bending fatigue loading, cracks are likely to advance through ferritic–pearlitic regions that exhibit comparable fracture resistance throughout the investigated temperature range. In addition, the relaxation of residual stresses at higher interpass temperatures may compensate for the reductions in hardness and yield strength, leading to similar fatigue limit values despite differences in static properties.

In summary, the results demonstrate that the bending fatigue behavior of WAAM carbon steel is influenced more strongly by surface integrity and residual stress distribution than by changes in bulk microstructure or tensile properties. Therefore, enhancing surface quality and reducing manufacturing-related defects are essential measures for improving the fatigue performance and long-term reliability of WAAM-produced structural components.

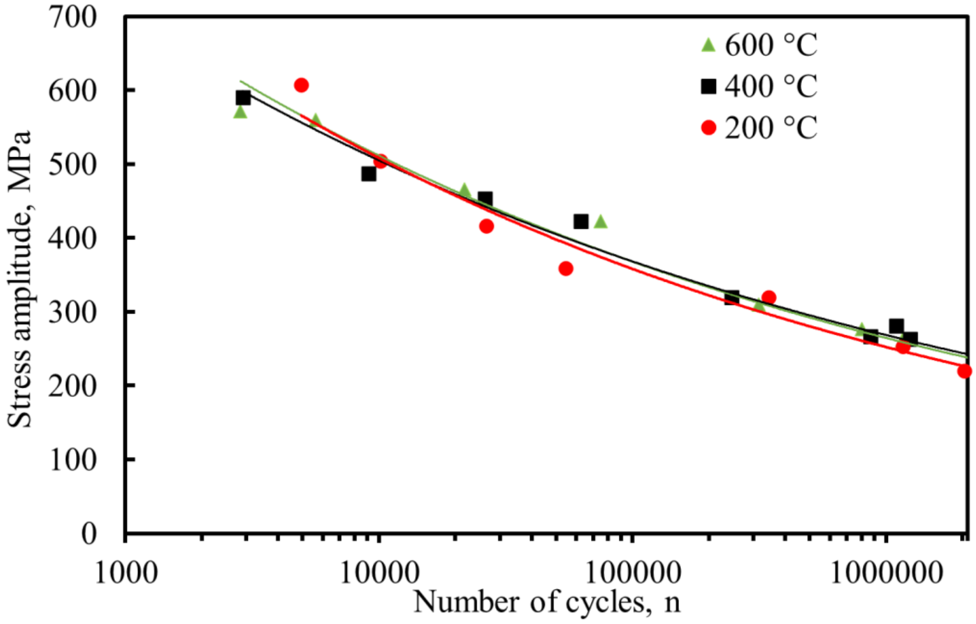

Fig. 3. Influence of interpass temperature on the fatigue strength of WAAM carbon steel.

2.18.6 Comparative Testing of Different Carbon Steel Welding Wires Using Interpass Temperature Control

2.18.6.1 Printing equipment and welding wires

The WAAM parts were printed using Fronius TransPuls Synergic 2700 CMT welding equipment. The printing speed was 0.50 m/min, current 113 A, voltage 14.1 V, wire feed 3,2 m/min and lift between layers was 1.4 mm. An interpass temperature of 200 °C was controlled using an Optris CT infrared pyrometer. The flow rate of shielding gas was 12 l/min, and the composition of the gas was 92% Argon + 8% CO2.

The welding wires used in the WAAM experiments were Esab Purus 46 and Esab OK Aristorod 12.50. The thickness of the wire was 1.2 mm. Mechanical properties of the wires are shown in Table 1.

Table 1. Mechanical properties of the carbon steel wires.

	Yield strength MPa	Tensile strength MPa	Elongation %
Aristorod 12.50	470	560	26
Purus 46	500	600	25

2.18.6.2 Mechanical properties

WAAM experiments were conducted using two different carbon steel filler wires, and the resulting mechanical properties of the deposited materials in both vertical and horizontal directions are summarized in Table 2.

For the material produced using OK Aristorod 12.50, the yield strength was 382 MPa in the vertical direction and 387 MPa in the horizontal direction. The corresponding ultimate tensile strengths were 505 MPa (vertical) and 497 MPa (horizontal), while the elongation increased from 36.64% in the vertical direction to 43.52% in the horizontal direction. This indicates slightly improved ductility in the horizontal orientation, accompanied by a minor reduction in tensile strength.

For the material deposited using Purus 46, the yield strength was 407 MPa in the vertical direction and 392 MPa in the horizontal direction. The ultimate tensile strengths were 518 MPa (vertical) and 516 MPa (horizontal), showing only a small variation between orientations. The elongation values were 41.99% in the vertical direction and 42.47% in the horizontal direction, indicating relatively consistent ductility.

Overall, the Purus 46 wire produced higher strength levels compared to Aristorod 12.50 in both orientations, while maintaining comparable ductility. The results also suggest that anisotropy is more pronounced in the Aristorod 12.50 material, particularly in terms of elongation, whereas the Purus 46 material exhibits more uniform mechanical properties between the vertical and horizontal directions.

Table 2. Mechanical properties of WAAM carbon steel.

Wire	Printing direction	Yield strength	Tensile strength	Elongation

		MPa	MPa	%
OK Aristorod 12.50	vertical	382	505	36.64
OK Aristorod 12.50	horizontal	387	497	43.52
Purus 46	vertical	407	518	41.99
Purus 46	horizontal	392	516	42.47

A comparison between the mechanical properties of the feedstock wires (Table 1) and the corresponding WAAM-fabricated materials (Table 2) reveals a noticeable reduction in strength after deposition.

For OK Aristorod 12.50, the wire exhibited a yield strength of 470 MPa and a tensile strength of 560 MPa, whereas the WAAM-deposited material showed lower values in both orientations. The yield strength decreased to 382 MPa in the vertical direction and 387 MPa in the horizontal direction, while the tensile strength decreased to 505 MPa (vertical) and 497 MPa (horizontal).

Similarly, for Purus 46, the wire properties were 500 MPa yield strength and 600 MPa tensile strength, while the WAAM-fabricated material exhibited reduced values. The yield strength was 407 MPa in the vertical direction and 392 MPa in the horizontal direction, and the tensile strength was 518 MPa (vertical) and 516 MPa (horizontal).

Despite the reduction in strength, elongation increased significantly in the WAAM-fabricated materials. For Aristorod 12.50, elongation increased from 26% (wire) to 36.64% (vertical) and 43.52% (horizontal). For Purus 46, elongation increased from 25% (wire) to 41.99% (vertical) and 42.47% (horizontal). This indicates a transition toward a more ductile microstructure after deposition.

Overall, the results suggest that the WAAM process leads to a reduction in strength but a significant increase in ductility, likely due to microstructural changes associated with thermal cycling during layer-by-layer deposition.

2.18.6.3 Bending fatigue strength

Bending fatigue tests were carried out to evaluate the fatigue performance of WAAM carbon steel produced using Purus 46 and Aristorod 12.50 welding wires. The Purus 46 specimens were tested in both vertical and horizontal build directions, while the Aristorod 12.50 specimens were tested in the vertical direction.

The results showed that the fatigue limit of the Purus 46 material was 251 MPa in the vertical direction and 255 MPa in the horizontal direction, indicating very similar endurance performance in both orientations. Despite the nearly identical fatigue limits, the vertical specimens exhibited slightly better fatigue strength in the low- and medium-cycle fatigue regimes, sustaining somewhat higher stress amplitudes at comparable cycle counts.

The Aristorod 12.50 material exhibited a fatigue limit of 216 MPa, which is lower than that of the Purus 46 material. However, in the low- and medium-cycle fatigue regions, the fatigue strength of Aristorod 12.50 was very similar to that of the Purus 46 material tested in the vertical direction. In addition, Aristorod 12.50 showed slightly better fatigue strength than Purus 46 in the horizontal direction within the low- and medium-cycle regimes.

Overall, the results indicate that Purus 46 provides higher fatigue resistance in the high-cycle fatigue region, as reflected by the higher fatigue limit, while Aristorod 12.50 demonstrates comparable fatigue strength under higher stress amplitudes in the finite-life fatigue regime.

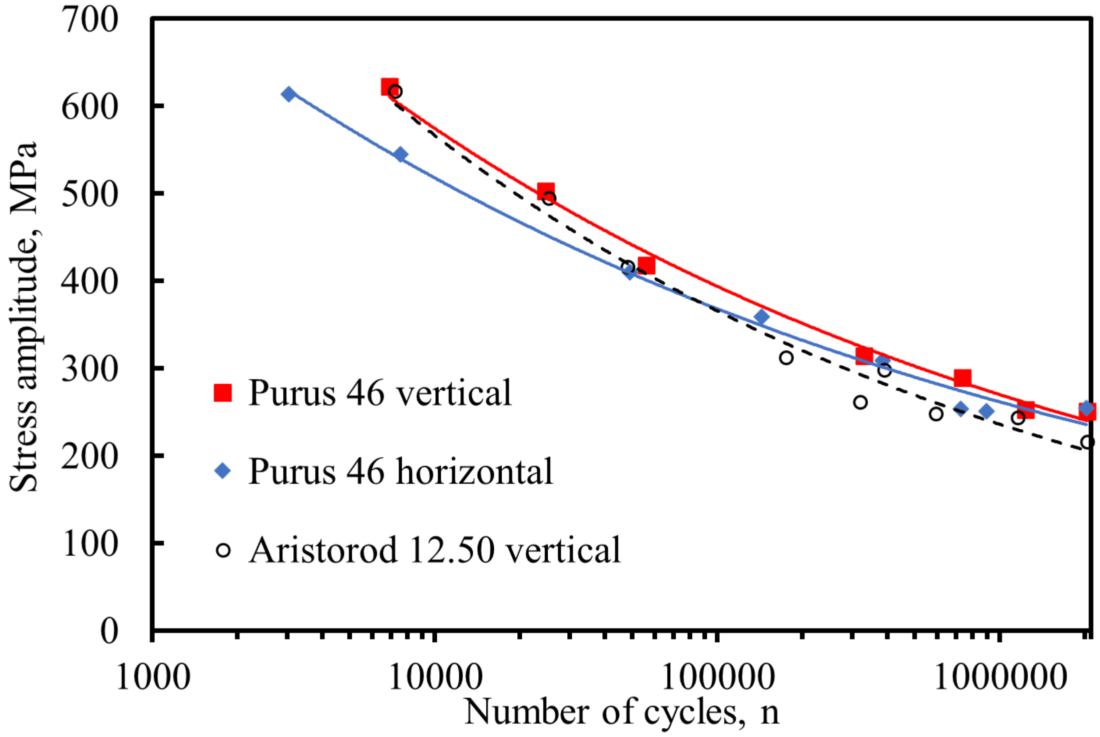

Fig. 1. Bending fatigue strength of the WAAM carbon steel with different welding wire.

2.18.7 Axial fatigue strength with machined surface

Axial fatigue tests were conducted on WAAM-fabricated carbon steel produced using Purus 46 wire in order to evaluate directional dependence under uniaxial cyclic loading (Fig. 2). The fatigue limit in the vertical build direction was 260 MPa, whereas the horizontal direction exhibited a significantly higher fatigue limit of 310 MPa. In addition to the higher endurance limit, specimens tested in the horizontal orientation also demonstrated superior fatigue strength in the low- and medium-cycle fatigue regimes.

The improved fatigue performance in the horizontal direction can be attributed primarily to microstructural anisotropy and the layer-wise nature of the WAAM process. In WAAM fabrication, material is deposited bead by bead and layer by layer, resulting in distinct interlayer boundaries and fusion zones aligned parallel to the build plane. When specimens are loaded in the vertical direction, cyclic stresses act perpendicular to these interlayer interfaces. These regions may contain microstructural heterogeneities, such as coarser grains, localized residual stresses, or minor lack-of-fusion imperfections, which can serve as preferential crack initiation sites. Consequently, fatigue cracks can nucleate and propagate more readily across layer boundaries, reducing fatigue strength.

In contrast, when specimens are loaded in the horizontal direction, the principal cyclic stress is applied parallel to the deposited layers. In this orientation, interlayer boundaries are less critically stressed, and crack propagation must proceed across multiple solidified beads rather than along potentially weaker fusion interfaces. Additionally, residual stress distributions may be more favorable in the horizontal direction, further contributing to improved fatigue resistance.

The results therefore indicate that axial fatigue performance in WAAM-fabricated Purus 46 material is strongly influenced by build orientation, with the horizontal direction providing enhanced resistance to crack initiation and propagation under cyclic loading.

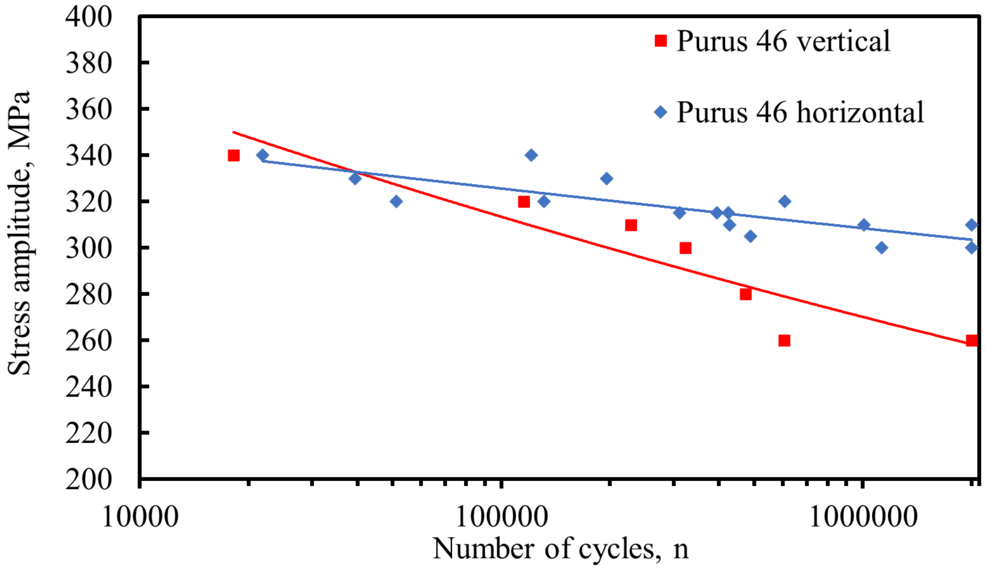

Fig. 2. Fatigue strength of WAAM carbon steel with machined surface.

2.18.8 Axial fatigue strength with as-built surface

Axial fatigue tests were performed on WAAM carbon steel produced using Purus 46 and Aristorod 12.50 welding wires (Fig. 3). The specimens were tested in the vertical build direction, and the surfaces were kept in the as-built condition to evaluate the influence of surface quality on fatigue performance.

The results showed that the fatigue limit for both materials was approximately 80 MPa, indicating similar endurance performance in the high-cycle fatigue region when the as-built surface condition is retained. However, differences were observed in the low- and medium-cycle fatigue regimes. In these regions, the Purus 46 specimens exhibited slightly better fatigue strength, sustaining higher stress amplitudes at comparable cycle counts than the Aristorod 12.50 specimens.

When compared with the previous axial fatigue tests performed on specimens with machined surfaces, a significant reduction in fatigue performance is evident. The machined specimens showed considerably higher fatigue limits, indicating that surface finish plays a critical role in fatigue behavior. The lower fatigue limits observed in the as-built specimens can be attributed to the higher surface roughness and the presence of surface irregularities, which act as stress concentration sites and promote earlier crack initiation under cyclic loading.

These results clearly demonstrate that surface condition strongly influences the fatigue performance of WAAM-fabricated components, and post-processing operations such as machining can substantially improve fatigue resistance.

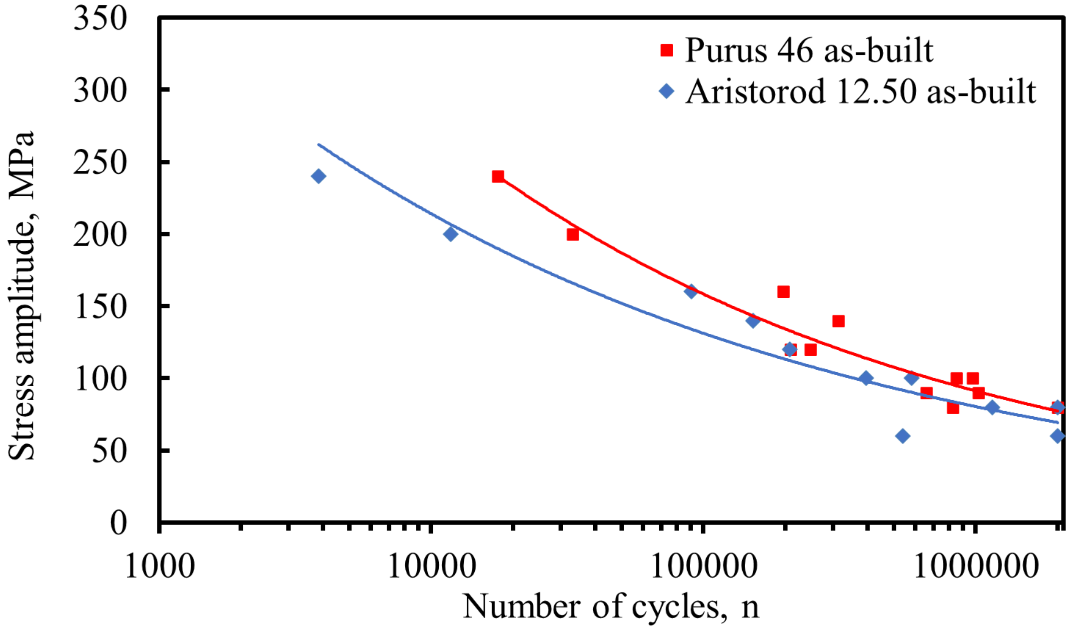

Fig. 3. Fatigue strength of WAAM carbon steel with as-built surface and different welding wire.

2.19 Mechanical Properties and Fatigue Strength of WAAM Carbon Steel with CO2 Shielding Gas

2.19.1 Printing equipment

The WAAM parts were printed using Fronius TransPuls Synergic 2700 CMT welding equipment.

For the samples produced using a shielding gas mixture of 92% Ar + 8% CO_2, the WAAM process was carried out with the following parameters: a printing speed of 0.50 m/min, current of 113 A, voltage of 14.1 V, and a wire feed rate of 3.2 m/min. The layer height (lift between layers) was maintained at 1.4 mm. The interpass temperature was controlled at 200 °C using an Optris CT infrared pyrometer. The shielding gas was supplied at a flow rate of 12 L/min.

For the samples manufactured using 100% CO_2 shielding gas, slightly different parameters were applied. The printing speed was 0.44 m/min, the current was 183 A, and the voltage was 14.5 V. The wire feed rate was increased to 4.7 m/min, and the layer height between successive passes was 2.0 mm. As in the previous case, the interpass temperature was maintained at 200 °C and monitored using an Optris CT infrared pyrometer. The shielding gas flow rate was 15 L/min.

The welding wire used in the WAAM experiments was Esab Purus 46. The thickness of the wire was 1.2 mm. Mechanical properties of the wires are shown in Table 1.

Table 1. Mechanical properties of the carbon steel wire.

Yield strength MPa	Tensile strength MPa	Elongation %
500	600	25

2.19.2 Hardness measurement

Hardness measurements were carried out to evaluate the effect of shielding gas composition on the hardness of WAAM-fabricated carbon steel. The results show a clear difference in hardness between the two shielding gas conditions.

For the material produced using a shielding gas mixture of 92% Ar + 8% CO_2, the average hardness was approximately 169 HV. In contrast, the samples manufactured using 100% CO_2 shielding gas exhibited a lower average hardness of about 151 HV.

The higher hardness observed in the material produced with the argon-based shielding gas mixture may be related to differences in heat input, cooling rate, and resulting microstructure during deposition. The results suggest that the choice of shielding gas can influence the mechanical properties of WAAM carbon steel, with the Ar–CO_2 mixture producing a slightly harder material compared to pure CO_2 shielding gas.

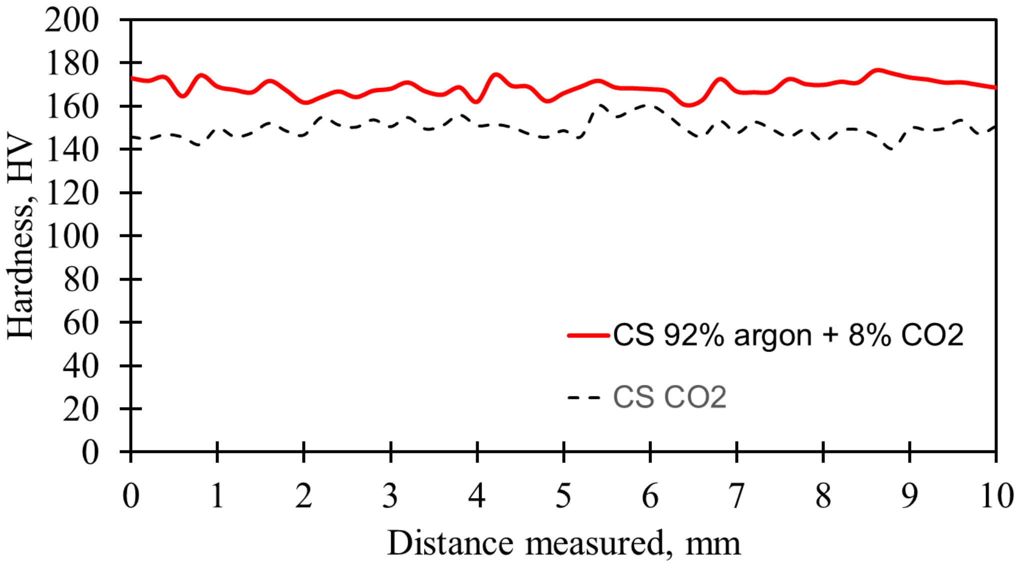

Fig. 1. Hardness profiles for WAAM CS with different shielding gas.

2.19.3 Mechanical properties

Mechanical properties of WAAM-fabricated carbon steel were evaluated using two different shielding gases in order to assess their influence on tensile performance. The results are summarized in Table 2.

As shown in Table 2, the material deposited using a shielding gas mixture of 98% Ar + 8% CO_2 exhibited a yield strength of 407 MPa and a tensile strength of 518 MPa, with an elongation of 41.99%. In contrast, the use of pure CO_2 as the shielding gas resulted in lower strength values, with a yield strength of 371 MPa and a tensile strength of 489 MPa. However, the elongation was slightly higher at 43.43%.

The results indicate that the Ar–CO_2 gas mixture promotes higher strength, whereas pure CO_2 produces marginally improved ductility. The reduction in strength observed with pure CO_2 shielding may be attributed to increased oxidation and higher heat input associated with a more reactive arc atmosphere, which can influence microstructural evolution during solidification. The Ar- CO_2 mixture likely provides a more stable arc and reduced oxygen pickup, contributing to improved strength while maintaining good ductility.

Overall, the choice of shielding gas has a measurable effect on the mechanical performance of WAAM-fabricated carbon steel, particularly in terms of strength.

Table 2. Mechanical properties of carbon steel with different shielding gas.

Shielding gas	Yield strength MPa	Tensile strength MPa	Elongation %
98% Ar + 8% CO2	407	518	41.99
CO2	371	489	43.43

2.19.4 Bending fatigue strength

Bending fatigue tests were performed on WAAM-fabricated carbon steel produced using two different shielding gases in order to evaluate their influence on fatigue performance (Fig. 2).

The material deposited with pure CO_2 shielding gas exhibited a fatigue limit of 230 MPa. In comparison, the use of a 92% Ar + 8% CO_2 shielding gas mixture resulted in a higher fatigue limit of 251 MPa. This represents a clear improvement in endurance performance when an argon-rich shielding atmosphere was employed.

In addition to the higher fatigue limit, specimens produced with the argon–CO_2 mixture demonstrated slightly better fatigue strength in both the low- and medium-cycle fatigue regimes. Across the finite-life region, the argon-mixed shielding gas consistently sustained higher stress amplitudes at equivalent cycle counts compared to pure CO_2 shielding.

The improved fatigue performance associated with the argon-rich shielding gas may be attributed to enhanced arc stability, reduced oxidation, and more favorable microstructural characteristics, which collectively contribute to improved resistance to crack initiation and propagation under cyclic bending loading.

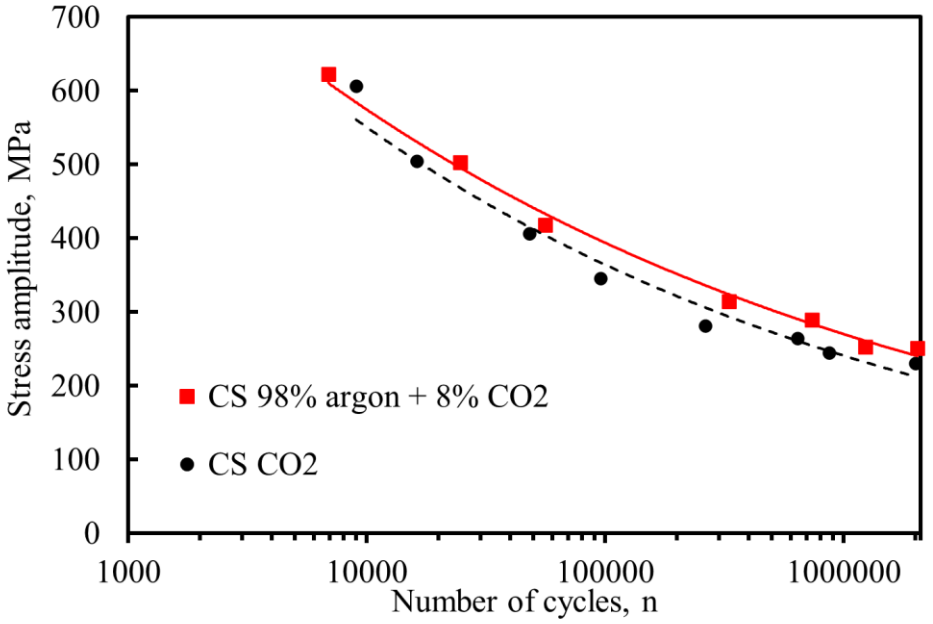

Fig. 2. Bending fatigue strength of carbon steel (CS) with different shielding gas.

2.19.5 Axial fatigue strength

Axial fatigue tests were performed on WAAM-fabricated carbon steel produced using two different shielding gases: pure CO_2 and a shielding gas mixture of 92% Ar + 8% CO_2. The tests were conducted in the vertical build direction in order to evaluate the influence of shielding gas on fatigue performance (Fig. 3).

The material deposited with pure CO_2 shielding gas exhibited a fatigue limit of 270 MPa, while the material produced using the argon–CO_2 mixture showed a slightly lower fatigue limit of 260 MPa. Despite this small difference in fatigue limit, the fatigue behavior differed in the finite-life regime.

In the low- and medium-cycle fatigue regimes, the material produced with the 92% Ar + 8% CO_2 shielding gas demonstrated better fatigue strength compared to the material deposited with pure CO_2 shielding. At equivalent stress amplitudes within the finite-life region, specimens fabricated using the argon-rich shielding gas sustained a higher number of cycles before failure.

These results indicate that although pure CO_2 shielding gas produced a marginally higher fatigue limit, the argon–CO_2 mixture provided improved fatigue performance under higher stress amplitudes. This behavior may be related to differences in arc stability, oxidation level, and resulting microstructural characteristics associated with the shielding gas composition.

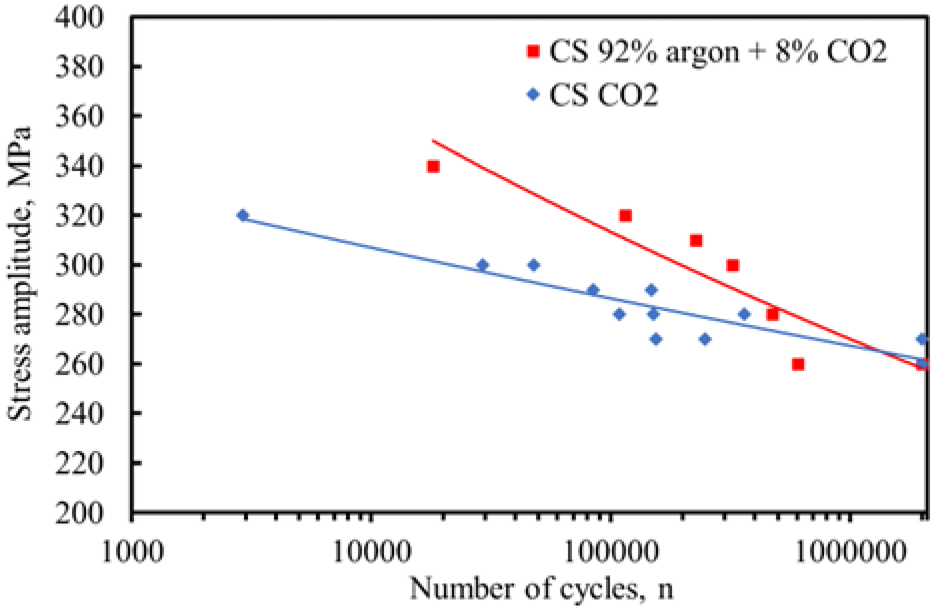

Fig. 3. Fatigue strength of WAAM carbon steel with different shielding gas.

2.20 WAAM Aluminum 6061

2.20.1 Test information

We obtained WAAM-printed 6061 aluminum samples that were ready for testing. Since the printing parameters were not available, this section focuses solely on evaluating the mechanical properties and fatigue performance of the material. The purpose of this section is to provide general insight into the mechanical behavior and fatigue resistance of WAAM-fabricated 6061 aluminum.

2.20.2 Mechanical properties

Table 1 presents the tensile properties of WAAM-fabricated aluminum 6061 tested in the vertical build direction. The results show a yield strength of 284 MPa, an ultimate tensile strength of 316 MPa, and an elongation of 5.2%.

The relatively high strength values indicate that the WAAM 6061 aluminum maintains good load-bearing capacity. However, the elongation is comparatively low, suggesting limited ductility. This reduced ductility is attributed to process-related defects such as porosity, microcracks, and microstructural inhomogeneity, which are commonly observed in additively manufactured aluminum alloys. These defects can act as stress concentration points, reducing the material's ability to undergo plastic deformation before fracture.

Overall, the tensile test results indicate that WAAM 6061 aluminum exhibits adequate strength but limited ductility, which should be considered when evaluating its suitability for structural applications, particularly those involving cyclic loading or high deformation requirements.

Table 1. Mechanical properties of WAAM aluminum 6061 in vertical direction.

Yield strength MPa	Tensile strength MPa	Elongation %
284	316	5.2

2.20.3 Bending fatigue strength

Bending fatigue tests were also performed on WAAM-fabricated aluminum 6061 to evaluate its fatigue performance under cyclic bending loading. The specimens were tested in the vertical build direction, and the results indicated a fatigue limit of approximately 59 MPa (Fig. 1).

A relatively large scatter was observed in the fatigue results. The variation in fatigue life is likely related to material defects such as porosity and microcracks, which are commonly present in WAAM-processed aluminum alloys. These defects can act as stress concentration sites, leading to premature crack initiation and contributing to the significant deviation observed between individual test results.

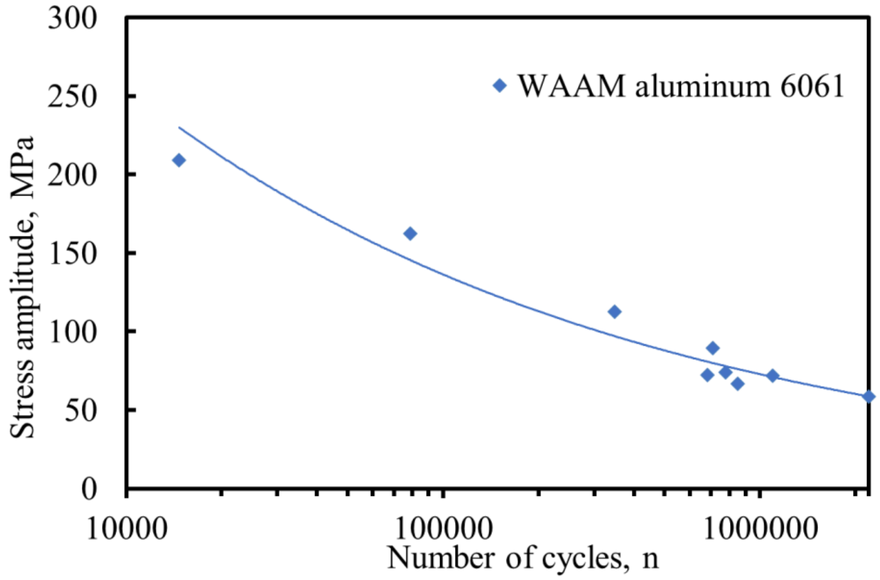

Fig. 1. Bending fatigue strength of WAAM aluminum 6061.

2.20.4 Axial fatigue strength

Axial fatigue tests were conducted to evaluate the fatigue performance of WAAM-fabricated aluminum 6061. The specimens were tested in the vertical build direction, and the results showed a fatigue limit of approximately 50 MPa (Fig. 2).

A relatively large scatter in the fatigue results was observed among the tested specimens (Fig. 3). This variability is likely associated with internal defects present in the material, such as porosity and microcracks, which are commonly found in additively manufactured aluminum alloys. These defects can act as stress concentration sites, promoting early crack initiation under cyclic loading and significantly influencing fatigue life. As a result, the presence and distribution of such imperfections contribute to the observed deviation in fatigue performance between individual specimens.

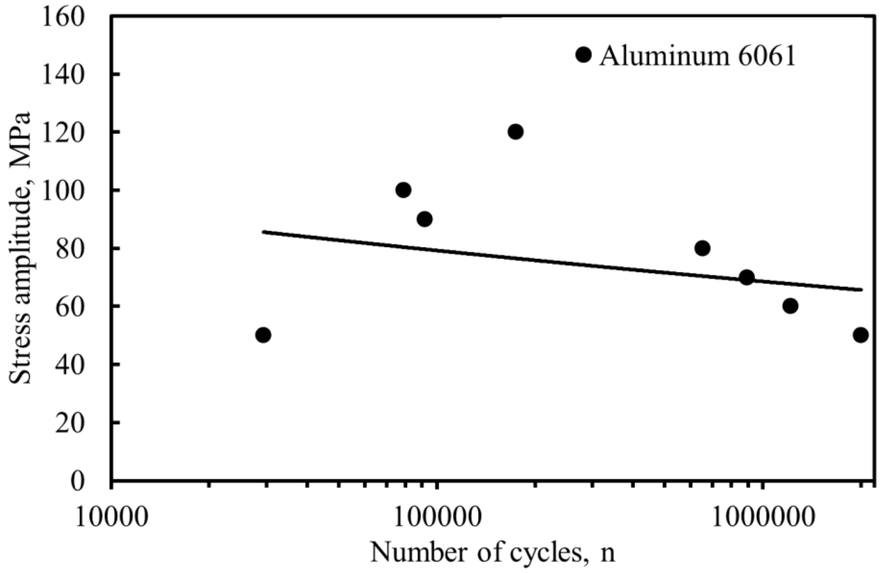

Fig. 2. Axial fatigue strength of WAAM aluminum 6061.

Fig. 3. Discarded fatigue sample.

2.21 Comparative Analysis of CMT and GMAW Processes in WAAM of Carbon Steel

2.21.1 Printing equipment

We used a Fronius TransPuls Synergic 2700 CMT welding machine, while the other set was fabricated using a Kemppi AX500 Pulse+ machine (GMAW). In both cases, the feedstock material was ESAB OK AristoRod 12.50 carbon steel wire with a diameter of 1.2 mm.

The deposition speed differed between the two processes. The samples produced with the Fronius system were printed at a travel speed of 0.64 m/min, whereas the samples fabricated with the Kemppi system were deposited at 0.48 m/min. The lift between layers was 1.6 mm for the samples produced with the Fronius and 1.5 mm for those produced with the Kemppi.

For the Fronius, the main operating parameters consisted of a welding current of 163 A, voltage of 11.6 V, and a wire feed rate of 3.5 m/min. In comparison, the Kemppi system operated at a current of 145 A, voltage of 15 V, and a wire feed rate of 3.0 m/min. Both processes employed a shielding gas mixture of 82% argon and 18% CO_2, supplied at a flow rate of 12 L/min.

Different thermal control strategies were used during the deposition. For the samples produced with the Fronius system, a fixed cooling period of 60 seconds was applied after each deposited layer. In contrast, the samples fabricated with the Kemppi system used temperature-controlled interpass conditions, where the build was allowed to cool to 150 °C before the next layer was deposited.

2.21.2 Microstructure analysis

The microstructures observed in both materials were typical for carbon steel and consisted mainly of ferrite and pearlite phases. The etched specimens were examined using a laser microscope, and the results are presented in Figure 1. In both cases, the microstructure exhibited an equiaxed grain morphology, where ferrite grains were clearly visible and darker regions corresponded to pearlite colonies.

The material produced using the Fronius CMT process showed a relatively fine ferrite–pearlite microstructure with smaller ferrite grains and a more uniform distribution of pearlite colonies. This refined microstructure is likely related to the lower heat input characteristic of the CMT process, which promotes faster cooling of the deposited material. Reduced heat input limits grain growth during solidification and the subsequent thermal cycles, resulting in a finer microstructure.

In contrast, the material fabricated using the Kemppi GMAW system displayed a slightly coarser ferrite–pearlite structure, characterized by larger ferrite grains and more widely spaced pearlite colonies. The pulsed GMAW process used by the Kemppi system generally involves higher heat input compared to the CMT process, which can lead to slower cooling rates and increased grain growth during the deposition process. The higher thermal input therefore likely contributed to the development of the coarser microstructure observed in this material.

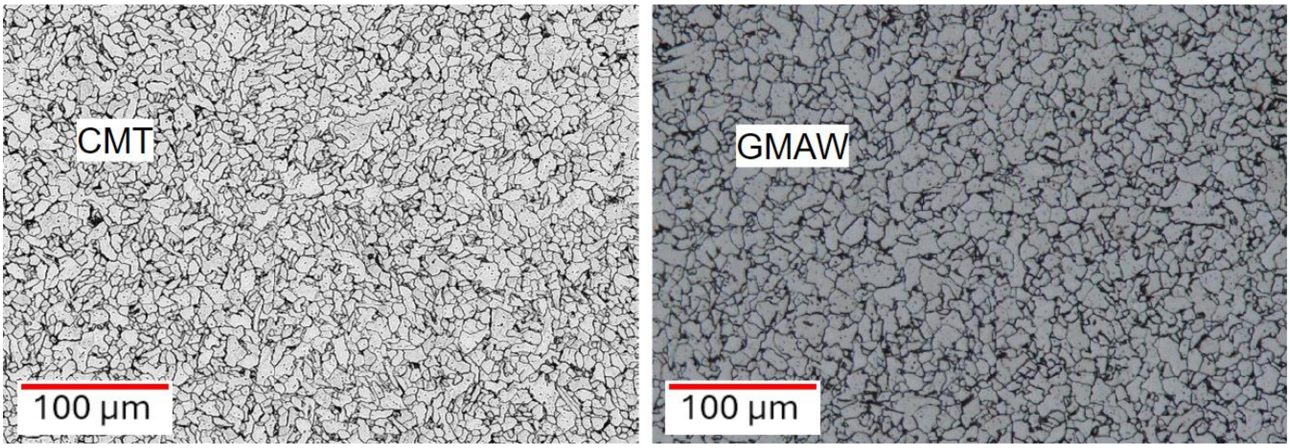

Fig. 1. Microstructure of (a) CMT carbon steel, (b) GMAW carbon steel.

2.21.3 Mechanical properties

Table 1 summarizes the tensile properties of the WAAM-fabricated carbon steel produced using the CMT and GMAW processes. The results show that both manufacturing methods produced materials with very similar mechanical performance.

The material fabricated using the CMT process exhibited a yield strength of 377 MPa, an ultimate tensile strength of 498 MPa, and an elongation of 39%. In comparison, the material produced using the GMAW process showed a yield strength of 369 MPa, an ultimate tensile strength of 499 MPa, and a slightly higher elongation of 39.7%.

Overall, the differences between the two materials are relatively small. The CMT-produced material demonstrated a slightly higher yield strength, while the GMAW-produced material showed marginally higher ductility. The tensile strengths of the two materials were nearly identical. These results indicate that both WAAM processes produce comparable mechanical properties, despite the differences in heat input and microstructural characteristics observed between the CMT and GMAW processes.

The similarity in mechanical performance suggests that the ferrite–pearlite microstructures formed during both processes provide a balanced combination of strength and ductility, typical for low-carbon structural steels. Consequently, both CMT and GMAW WAAM processes appear suitable for producing carbon steel components with reliable mechanical properties.

Table 1. Mechanical properties of CMT carbon steel and GMAW carbon steel.

	Yield strength MPa	Tensile strength MPa	Elongation %
CMT	377	498	39
GMAW	369	499	39.7

2.21.4 Bending fatigue strength

Bending fatigue tests were conducted to evaluate the fatigue performance of WAAM-fabricated carbon steel produced using the CMT and GMAW processes. The specimens were tested in the vertical build direction in order to compare the influence of the deposition method on fatigue behavior.

The results showed that the material produced using the CMT process exhibited a fatigue limit of 209 MPa, while the material manufactured with the GMAW process showed a slightly lower fatigue limit of 180 MPa. This indicates that the CMT-produced material has somewhat better endurance performance under cyclic bending loading.

In the low- and medium-cycle fatigue regimes, however, the difference between the two materials was relatively small. The fatigue strength of the CMT and GMAW materials followed a similar trend, with both materials sustaining comparable stress amplitudes at equivalent cycle counts. Overall, the results suggest that although the CMT process provides a higher fatigue limit, both WAAM processes produce carbon steel with similar fatigue behavior in the finite-life region.

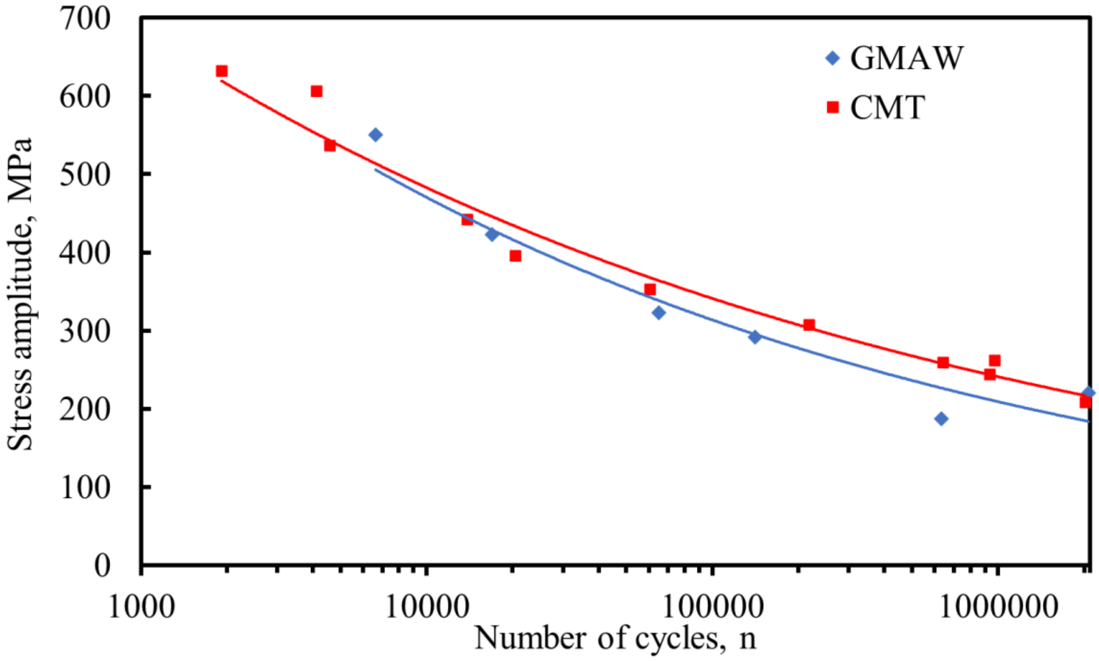

Fig. 2. Bending fatigue strength of CMT and GMAW carbon steel.

2.22 Comparative Analysis of CMT and GMAW Processes in WAAM of AISI 316L Stainless Steel

2.23 Printing equipment

The WAAM experiments were carried out using two different welding systems. One set of samples was produced using a Fronius TransPuls Synergic 2700 CMT system, while the other set was fabricated with a Kemppi AX500 Pulse+ system (GMAW).

In the CMT based process, the deposition was performed at a travel speed of 0.64 m/min, with a welding current of 107 A and a voltage of 12.5 V. The wire feed rate was 3.2 m/min, and each deposited layer had a height of approximately 1.25 mm.

For the GMAW-based process, the deposition was carried out at a lower travel speed of 0.35 m/min. The process used a layer height of approximately 2.05 mm and a wire feed rate of 2.7 m/min. The welding current was 100 A, while the arc voltage was 14.0 V.

To control the thermal conditions during deposition, the interpass temperature was maintained at 150 °C. The interpass temperature was monitored using an Optris CT infrared pyrometer. A shielding gas mixture consisting of 98% argon and 2% oxygen was supplied at a flow rate of 12 l/min.

The welding wire used in the WAAM experiments was Wurth AISI 316LSI. The thickness of the wire was 1.2 mm.

2.24 Microstructure analysis

The microstructural analysis of the WAAM specimens revealed noticeable differences between the samples produced using the CMT system and those manufactured with the GMAW system. These variations can largely be attributed to the different processing parameters applied during deposition.

Figure 1a illustrates the microstructure of the sample fabricated using the CMT process. The grains are predominantly columnar and oriented along the vertical direction, extending vertically through the deposited layers. This grain alignment is typical for WAAM processes and reflects directional solidification during layer-by-layer deposition. The relatively fine and uniform microstructure observed in the material produced by the CMT process is likely related to the lower effective heat input characteristic of CMT, together with the higher travel speed used during deposition. These conditions promote reduced thermal accumulation and relatively rapid solidification, which can limit grain coarsening and contribute to a more refined microstructure.

The grain structure appears relatively uniform and well-defined, with limited evidence of secondary phase formation or defects along the grain boundaries. This suggests that the selected deposition parameters enabled stable thermal conditions during printing. The controlled heat input and solidification behavior likely helped maintain consistent grain growth while reducing the likelihood of excessive thermal gradients that could otherwise lead to microstructural irregularities or internal stresses.

In contrast, Figure 1b shows the microstructure of the material produced using the GMAW process, which exhibits clear differences compared to the CMT-deposited material. The microstructure is characterized by coarser grains and a less uniform morphology, with more irregular grain boundaries. This coarser structure is consistent with the higher heat input typically associated with pulsed GMAW-based WAAM processes, which promotes slower cooling and increased grain growth during solidification.

A notable feature of the GMAW-produced material is the presence of delta ferrite, visible as lighter regions located along grain boundaries and within the matrix. The formation of delta ferrite is associated with the thermal conditions during solidification, particularly the slower cooling rates and higher thermal input experienced during deposition.

The presence of delta ferrite can influence the mechanical performance of the material. While this phase can be beneficial during welding by reducing susceptibility to solidification cracking, it may also affect the strength and fatigue performance of the deposited structure depending on its distribution and volume fraction.

Both WAAM processes were conducted using the same interpass temperature of 150 °C and identical shielding gas composition, ensuring comparable environmental conditions during deposition. However, differences in heat input, travel speed, wire feed rate, and free wire length resulted in distinct thermal histories during the build process. These differences strongly influenced the resulting microstructures, highlighting the sensitivity of WAAM-fabricated materials to process parameter selection.

The finer and more uniform microstructure observed in the CMT-produced material suggests a potentially more favorable combination of strength and fatigue resistance. In contrast, the coarser grain structure and presence of delta ferrite in the GMAW-produced material may lead to slightly reduced mechanical performance in certain applications.

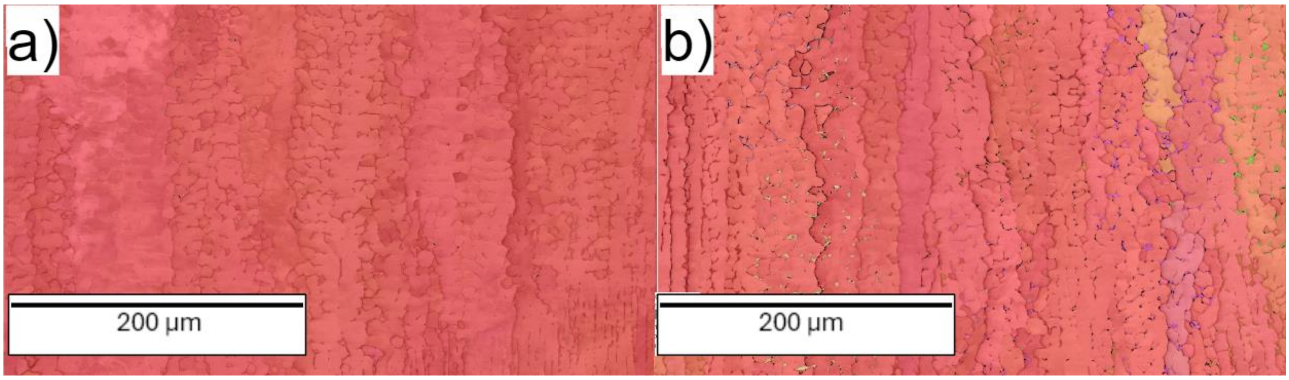

Fig. 1. Microstructure (a) CMT WAAM 316L, (b) GMAW WAAM 316L.

2.25 Geometry

The geometries of the WAAM components produced using the two different welding systems are presented in Figure 2 and 3, and clear differences can be observed due to the distinct process parameters used during fabrication.

The component manufactured with the CMT system (Fig. 2) shows a regular and well-defined cross-sectional shape, which is close to rectangular and maintains a consistent thickness throughout the structure. The deposited layers appear uniform and tightly stacked, indicating a stable deposition process. Each layer has an approximate height of 1.25 mm, resulting in a smooth layered structure without visible defects such as porosity or lack of fusion. This geometry suggests that the process parameters allowed good control of arc stability and thermal conditions, enabling the production of parts with accurate dimensions and minimal distortion.

In comparison, the component produced using the GMAW system (Fig.3) exhibits a less uniform cross-sectional profile. The deposited layers show noticeable variations in thickness, and some regions appear to contain either excessive or insufficient material deposition. These irregularities may be related to the lower printing speed and longer free wire length, which can influence heat input and melt pool behavior during the process. The larger layer height of approximately 2.05 mm is also clearly visible in the cross-section.

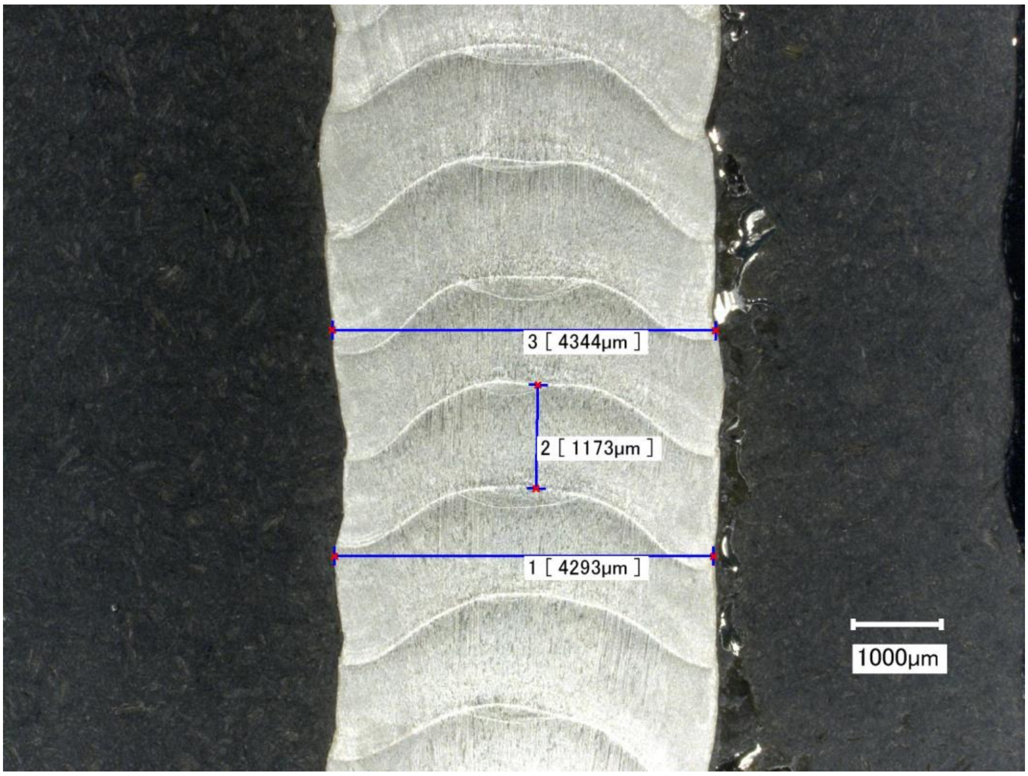

Fig. 2. Cross-section of CMT WAAM 316L.

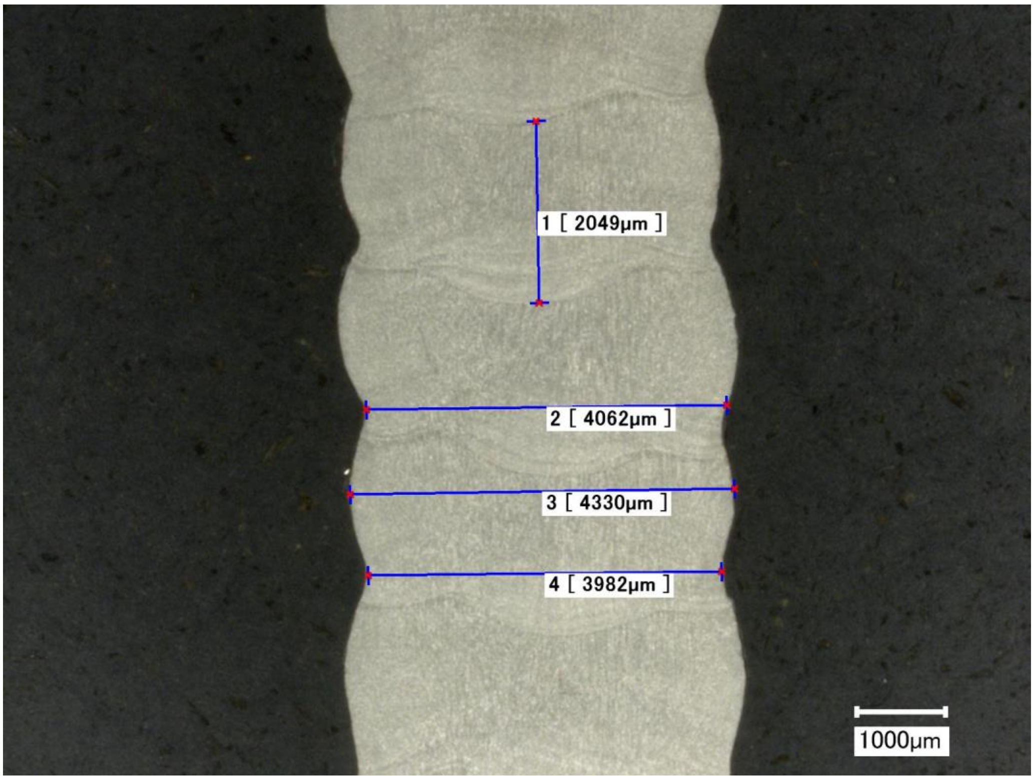

Fig. 3. Cross-section of GMAW WAAM 316L.

2.25.1 Mechanical properties

The mechanical properties of the WAAM-fabricated 316L stainless steel were assessed in both the vertical and horizontal build orientations. The measured mechanical properties are presented in Table 1.

The highest yield strength was measured for the vertical specimen produced using the CMT process (375 MPa). In contrast, the GMAW-produced vertical specimen exhibited a slightly lower yield strength (355 MPa). For both processes, a reduction in yield strength was observed in the horizontal direction, with values of 333 MPa for CMT and 332 MPa for GMAW, indicating the presence of anisotropy in the material.

A similar trend was observed for the tensile strength. The highest tensile strength was achieved by the GMAW vertical specimen (645 MPa), followed closely by the CMT vertical specimen (635 MPa). In the horizontal direction, both processes showed a noticeable decrease in tensile strength, with values of 543 MPa for CMT and 547 MPa for GMAW. These differences can be attributed to variations in microstructure and thermal history between the build orientations.

Regarding ductility, the GMAW specimens exhibited higher elongation values, reaching 54.5% in the vertical orientation and 50.5% in the horizontal orientation. The CMT specimens showed lower elongation in the vertical direction (37.2%) but higher elongation in the horizontal direction (44.8%). This variation suggests differences in microstructural characteristics and deformation behavior between the two processes and build orientations.

These results demonstrate the strong influence of WAAM process parameters on tensile behavior. The GMAW process produced higher ductility and slightly higher tensile strength, while the CMT process resulted in higher yield strength in the vertical direction. Both processes exhibited anisotropy, with generally higher strength observed in the vertical direction compared to the horizontal direction.

Table 1. Mechanical properties of CMT 316L and GMAW 316L.

	Yield strength MPa	Tensile strength MPa	Elongation %
CMT vertical	375	635	37.2
CMT horizontal	333	543	44.8
GMAW vertical	355	645	54.5
GMAW horizontal	332	547	50.5

2.25.2 Bending fatigue strength

Bending fatigue tests were carried out to evaluate the fatigue performance of WAAM-fabricated 316L stainless steel produced using the CMT and GMAW processes. All specimens were tested in the vertical build direction in order to compare the influence of the deposition method on fatigue behavior.

The results showed a clear difference in fatigue limit between the two processes (Fig. 4). The material produced using the CMT process exhibited a fatigue limit of approximately 308 MPa, whereas the material fabricated using the GMAW process showed a significantly lower fatigue limit of about 180 MPa.

In the low- and medium-cycle fatigue regimes, however, the fatigue strength of the two materials was relatively similar, and both materials sustained comparable stress amplitudes at equivalent cycle counts. A more pronounced difference appeared in the high-cycle fatigue region. When the number of cycles exceeded 1×10^6 cycles, the CMT-produced material demonstrated significantly better fatigue resistance compared to the GMAW-produced material.

This behavior suggests that although both materials perform similarly under higher stress levels and shorter fatigue lives, the CMT process provides superior long-term fatigue performance, which may be related to its lower heat input, finer microstructure, and reduced defect formation compared to the GMAW process.

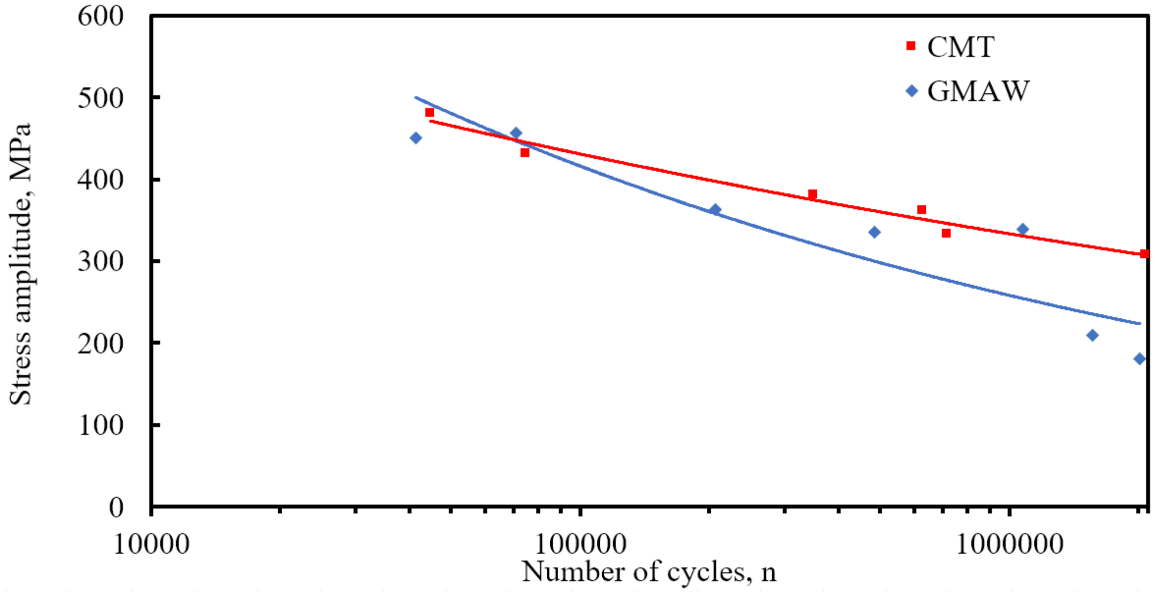

Fig. 4. Bending fatigue strength of CMT and GMAW 316L.

2.26 Comparison of Lab-Scale and Industrial-Scale WAAM-Fabricated AISI 316L Stainless Steel

2.26.1 Printing equipment

Laboratory-scale WAAM deposition was carried out using a Fronius TransPuls Synergic 2700 CMT system. The process was performed at a travel speed of 0.64 m/min, with a welding current of 107 A and a voltage of 12.5 V. The wire feed rate was 3.2 m/min, and each deposited layer had a height of approximately 1.25 mm. A 1.2 mm diameter Wurth 316LSi wire was used as the feedstock material. To ensure stable thermal conditions during deposition, the interpass temperature was maintained at 150 °C, and it was continuously monitored using an Optris CT infrared pyrometer. Shielding was provided by a gas mixture of 98% Ar and 2% O_2 (Woikoski SO_2) at a flow rate of 12 L/min.

Industrial-scale WAAM deposition was performed using a Fronius TPS 500i CMT system. The process employed a travel speed of 0.60 m/min, and each deposited layer had a height of approximately 2.0 mm. The feedstock material was a 1.0 mm diameter Wurth 316LSi wire. The idle time between layers ranged from 30 to 60 seconds, allowing partial cooling between successive passes. Shielding gas consisted of a mixture of 68% Ar, 30% He, 2% CO_2, and 0.03% NO (Linde Mison 2He), supplied at a flow rate of 18 L/min.

2.26.2 Geometry

Geometrical measurements were performed on WAAM-fabricated 316L stainless steel specimens produced under both industrial-scale and laboratory-scale conditions. The measured geometries are presented in Fig. 1 (industrial) and Fig. 2 (laboratory).

The results reveal clear differences in bead geometry and dimensional consistency between the two manufacturing conditions. The industrial-scale specimen exhibits larger bead widths, with measured values of approximately 7.3 mm, and layer heights in the range of 1.5–2.5 mm. In contrast, the laboratory-scale specimen shows significantly smaller and more uniform bead widths, approximately 4.3 mm, with more consistent layer heights around 1.25 mm.

These observations indicate that the laboratory-scale WAAM process provides better control over bead geometry and layer consistency. The industrial specimen, while producing wider deposits, shows greater variation in both width and layer height, which may be attributed to higher heat input, differences in process parameters, or reduced control of the melt pool.

The results demonstrate that process conditions have a significant influence on the geometric accuracy and stability of WAAM-fabricated structures, with the laboratory-scale process yielding more uniform and controlled geometries.

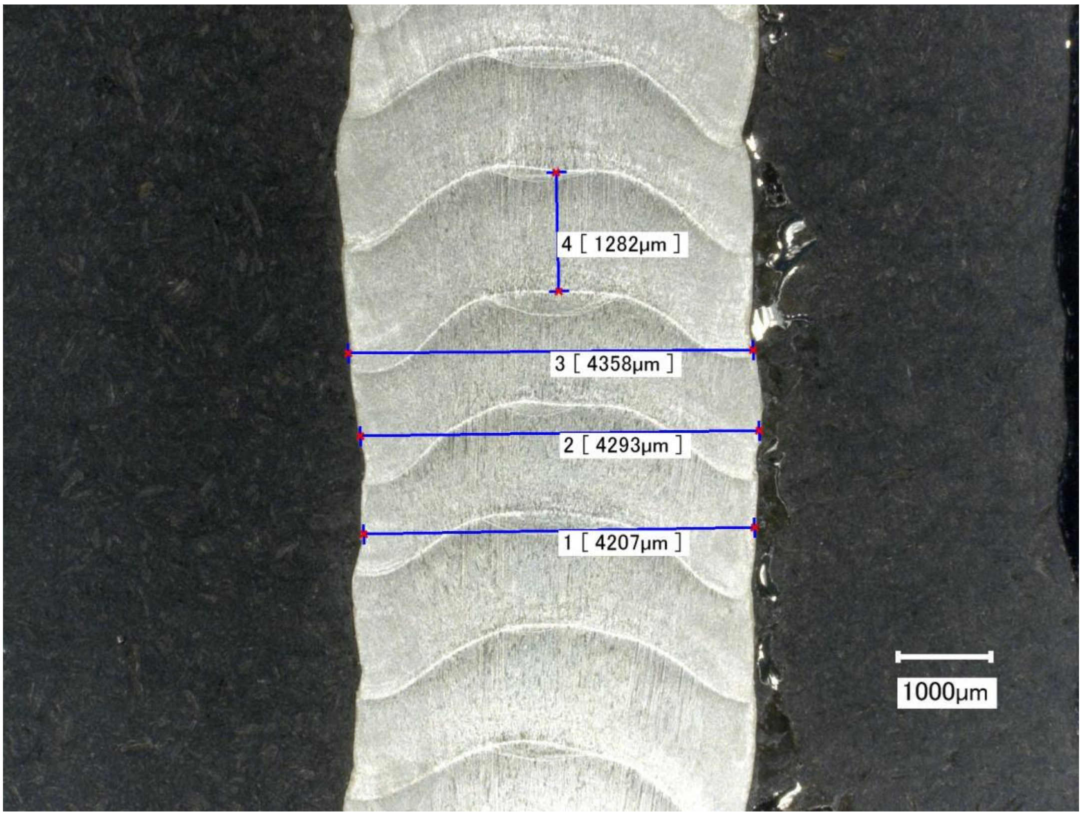

Fig. 1. Laboratory WAAM 316L.

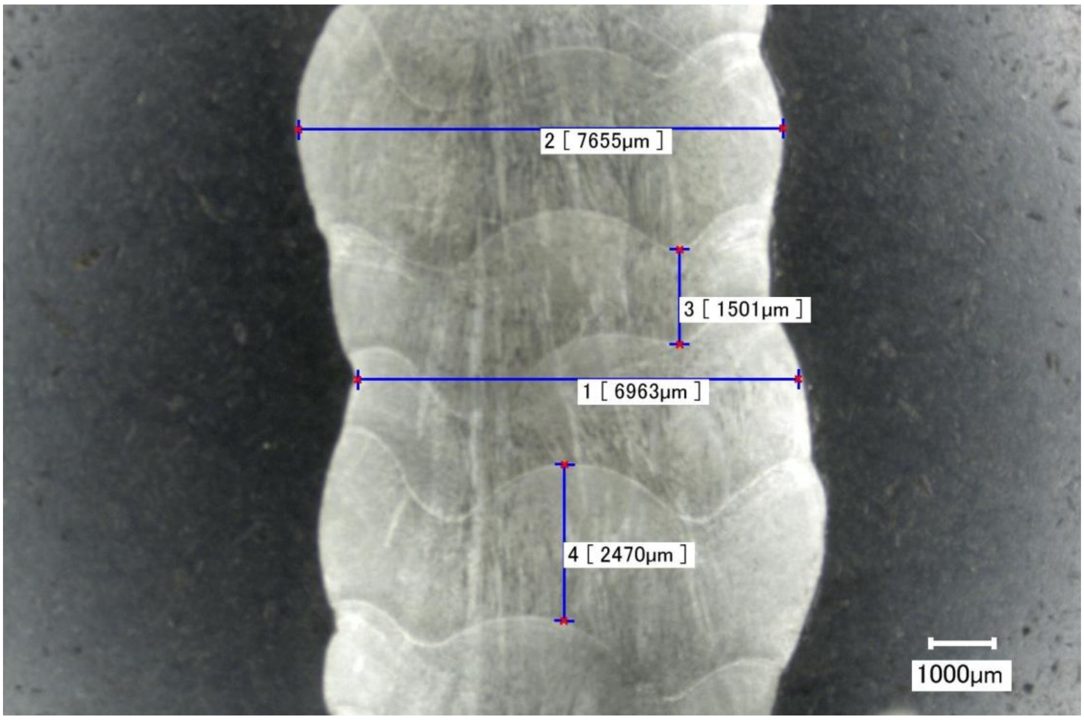

Fig. 2. Industrial WAAM 316L

2.26.3 Hardness measurements

Hardness measurements were performed on WAAM-fabricated 316L stainless steel specimens produced under both laboratory-scale and industrial-scale conditions in the vertical (build) direction. The hardness profiles are presented in Fig. 3.

The results indicate that both materials exhibit relatively similar hardness levels across the measured distance. The average hardness of the laboratory-scale WAAM 316L was approximately 194 HV, while the industrial-scale material showed a slightly higher average hardness of 199 HV.

Although the overall hardness levels are comparable, the industrial material exhibits greater local variation, with occasional peaks along the measurement line. In contrast, the laboratory-scale material shows a more uniform hardness distribution. These differences may be attributed to variations in thermal history, process stability, or microstructural heterogeneity between the two manufacturing conditions.

The hardness results suggest that both WAAM processes produce similar baseline mechanical properties, while the laboratory-scale process provides a more consistent hardness profile.

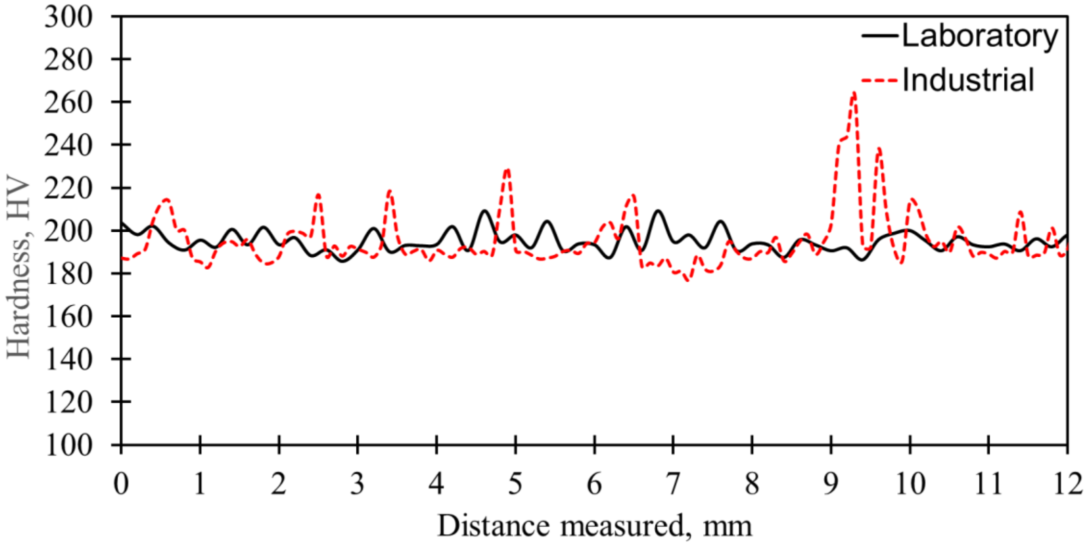

Fig. 3. Hardness profile of laboratory and industrial WAAM 316L in vertical direction.

2.26.4 Mechanical properties

Tensile tests were conducted on WAAM-fabricated 316L stainless steel specimens produced under both laboratory-scale and industrial-scale conditions. All specimens were extracted in the vertical (build) direction. The measured mechanical properties are summarized in Table 1.

The results show that the laboratory-scale WAAM 316L exhibited higher strength compared to the industrial-scale material. The yield strength of the laboratory-produced specimens was 375 MPa, whereas the industrial specimens showed a lower value of 324 MPa. A similar trend was observed for the ultimate tensile strength, with values of 635 MPa for the laboratory material and 603 MPa for the industrial material.

The industrial-scale WAAM specimens demonstrated higher ductility, with an elongation of 45.9% compared to 37.2% for the laboratory specimens. This indicates a trade-off between strength and ductility, where the laboratory process resulted in higher strength, while the industrial process produced a more ductile material.

The results highlight the influence of processing conditions on the mechanical performance of WAAM-fabricated 316L stainless steel, with noticeable differences between laboratory-scale and industrial-scale production.

Table 1. Mechanical properties of laboratory and industrial WAAM 316L in vertical direction.

	Yield strength MPa	Tensile strength MPa	Elongation %
Laboratory	375	635	37.2
Industrial	324	603	45.9

2.26.5 Bending fatigue strength

Bending fatigue tests were conducted on WAAM-fabricated 316L stainless steel specimens produced in both industrial and laboratory environments. The specimens were extracted in both vertical (build) and horizontal directions. For clarity, the samples were designated as follows: Industrial vertical, Industrial horizontal, Laboratory vertical, and Laboratory horizontal.

The results revealed clear differences between the two manufacturing conditions. The fatigue limit of the industrially produced specimens was 218 MPa in the vertical direction and 215 MPa in the horizontal direction, indicating nearly isotropic fatigue behavior. In contrast, the laboratory-fabricated specimens exhibited significantly higher fatigue performance, with fatigue limits of 317 MPa in the vertical direction and 246 MPa in the horizontal direction.

The laboratory-produced WAAM 316L demonstrated better fatigue strength compared to the industrial material, particularly in the vertical direction. Additionally, a more pronounced anisotropy was observed in the laboratory samples, where the vertical direction outperformed the horizontal direction more clearly than in the industrial counterparts.

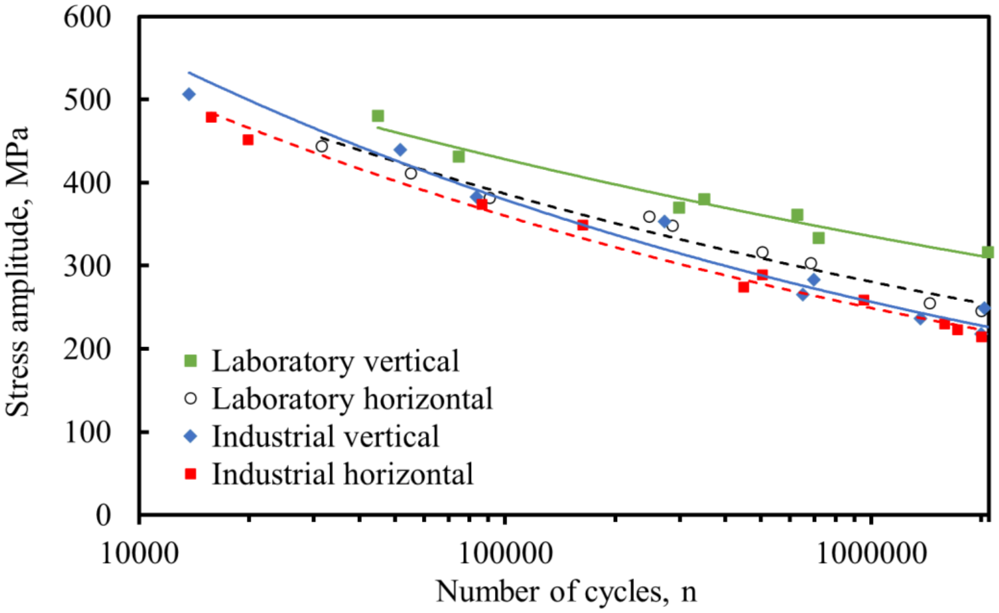

Fig. 4. Bending fatigue strength of laboratory-scale and industrial-scale WAAM 316L.

2.27 WAAM Sandwich Panels

2.27.1 WAAM Printed Sandwich Panel

A fully WAAM-fabricated carbon steel sandwich panel was also manufactured in order to investigate the feasibility of producing complete sandwich structures using a single additive manufacturing process. In this configuration, both the inner core structure and the outer face plates were produced directly by WAAM without the use of separately manufactured components or additional joining processes.

The sandwich panel was fabricated layer-by-layer, where the whole geometry was deposited using WAAM. This manufacturing approach enables the production of complex internal core geometries while maintaining continuous metallurgical bonding between the core and the face plates.

Producing the entire sandwich panel using WAAM offers several advantages, including reduced manufacturing steps, elimination of mechanical joining processes, and improved structural integration between the core and face sheets. Additionally, the additive manufacturing approach allows the design of optimized internal lattice or cellular structures that can enhance stiffness-to-weight ratio and energy absorption capabilities. However, process control is essential to ensure dimensional accuracy, uniform layer bonding, and consistent mechanical properties throughout the structure.

The fully WAAM-fabricated sandwich panel therefore represents a promising approach for manufacturing lightweight yet mechanically robust structural components, particularly for applications where customized geometry and efficient material utilization are required.

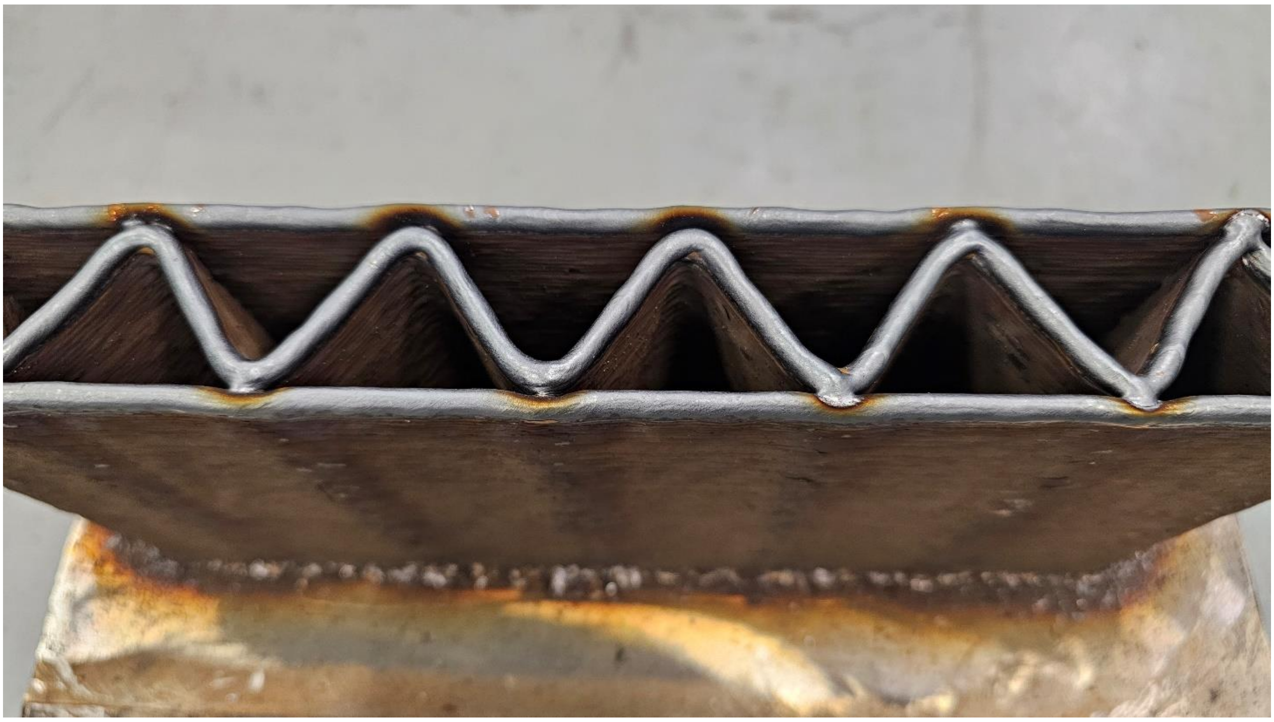

Fig. 1. Sandwich panel after printing.

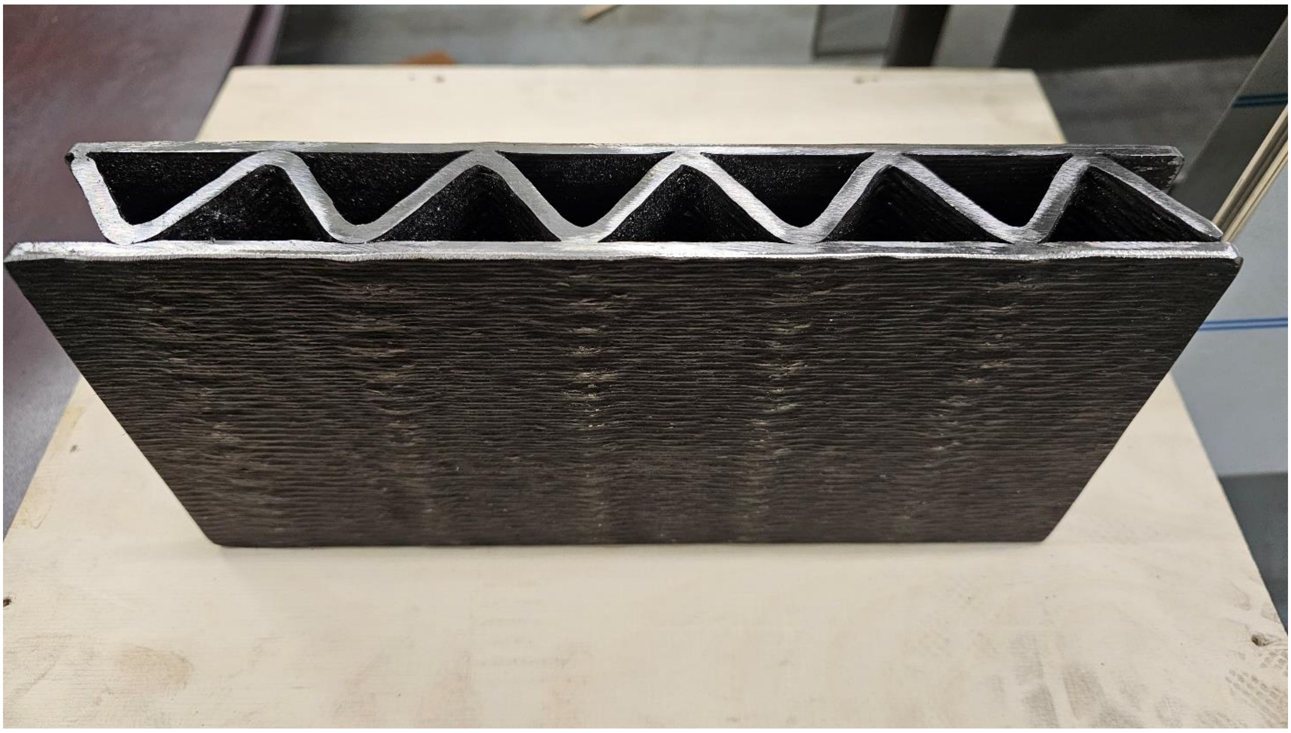

Fig. 2. Sandwich panel after removing from substrate and cutting.

2.27.2 Sandwich Panel Structure Consisting of a WAAM-Manufactured Inner Core and Laser Welded Sheet Metal Face Plates

A sandwich panel structure was manufactured using a WAAM-fabricated carbon steel inner core combined with sheet metal face plates. The inner core was produced by WAAM (Fig. 1), allowing the creation of a tailored internal geometry designed to provide structural support and energy absorption while maintaining relatively low weight.

After fabrication of the core structure, sheet metal face plates were attached to both sides of the core using laser welding. Before welding the core was machined as shown in Fig. 2. The laser welding process enabled precise and localized joining with minimal heat input, thereby reducing distortion and preserving the mechanical integrity of the WAAM-produced core. The resulting sandwich panel combines the advantages of additively manufactured internal structures with the stiffness and load-bearing capacity provided by the metallic face sheets.

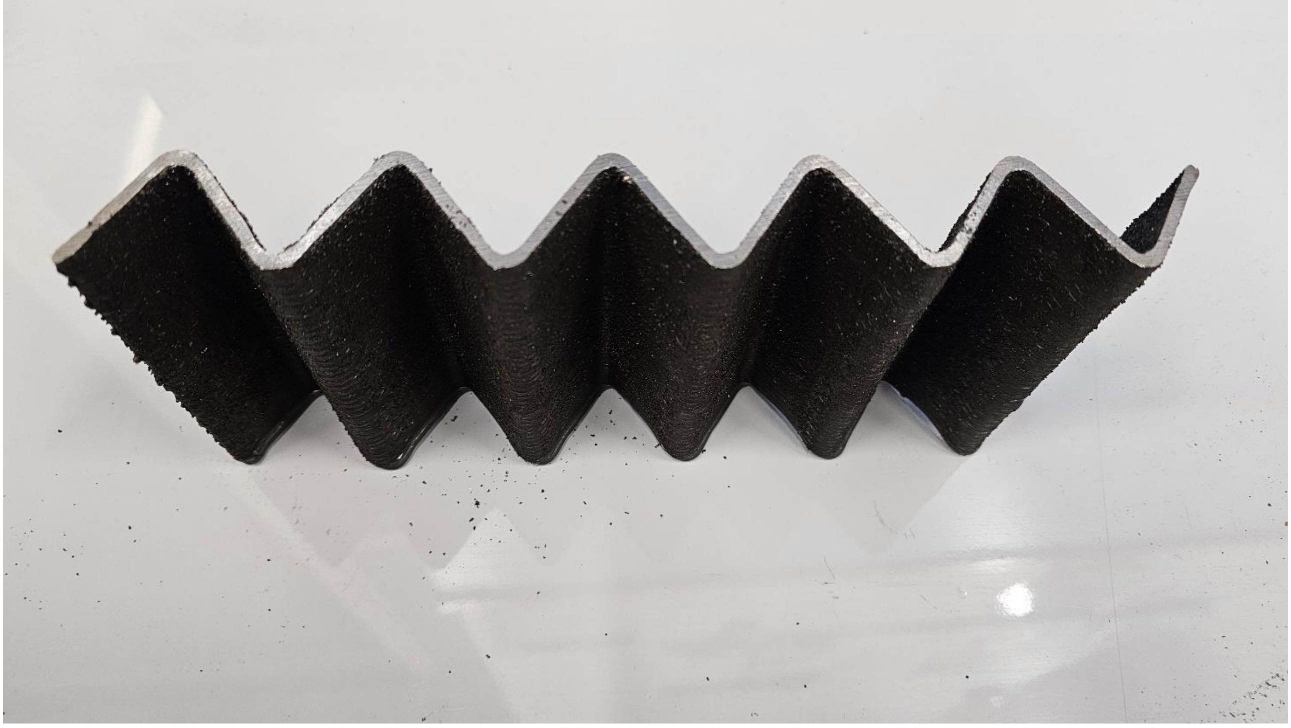

Fig. 1. WAAM-fabricated core.

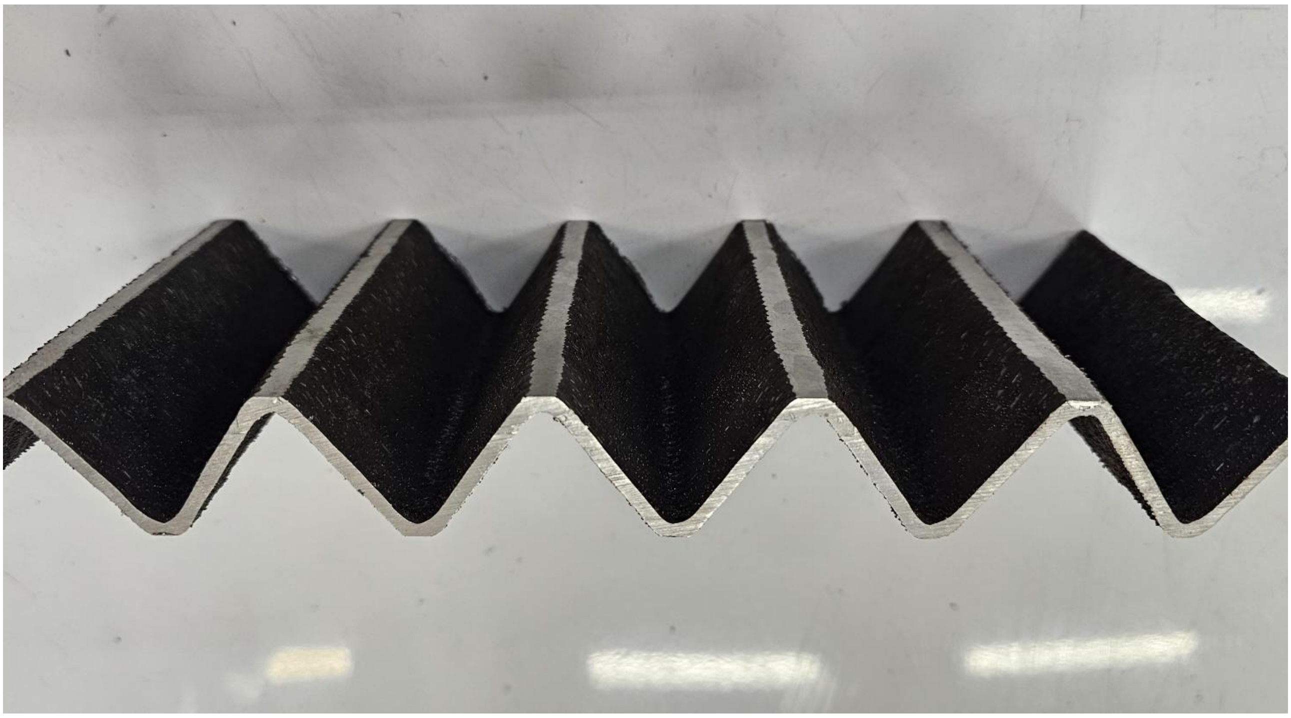
Fig. 2. Machined core.

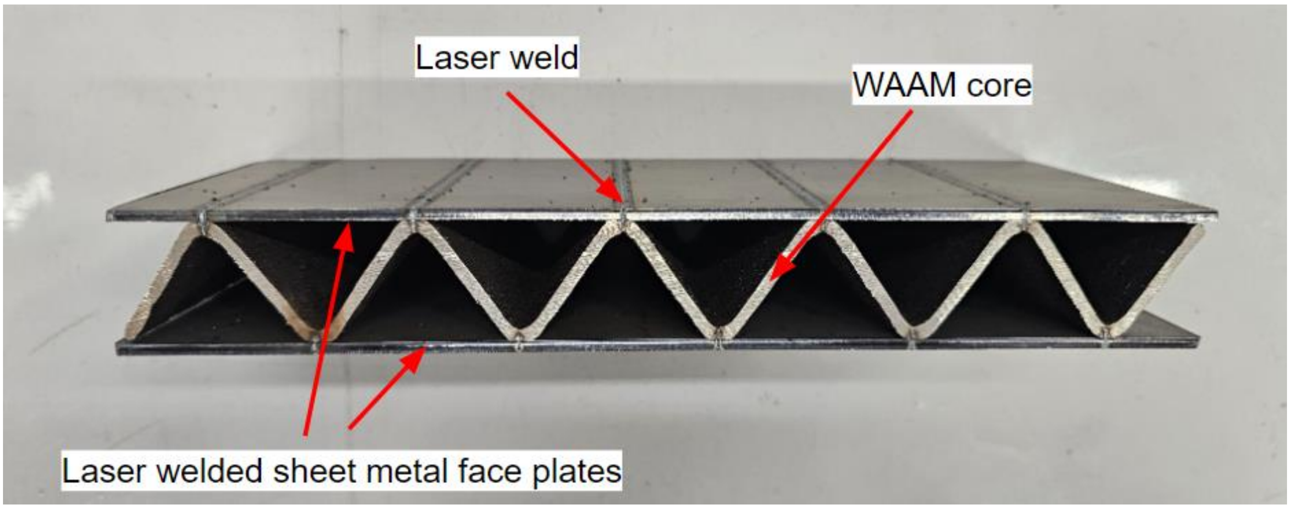

Fig. 3. Laser welded sandwich panel.

2.27.3 Fabrication of Complex Geometries Using WAAM

A complex geometry component, namely an impeller, was manufactured using the WAAM process. The WAAM system was integrated into a robotic manufacturing cell, enabling precise control of the deposition path and process parameters during fabrication. The robotic setup allowed multi-axis movement of the welding torch, which is essential for producing geometrically complex components such as impellers with curved blades and varying wall thicknesses.

The impeller was fabricated layer-by-layer directly from carbon steel wire feedstock using an arc welding process. The robotic WAAM cell enabled accurate toolpath execution and stable deposition conditions throughout the build. This approach demonstrates the capability of WAAM to manufacture complex three-dimensional geometries that would be difficult or costly to produce using conventional manufacturing methods.

The successful fabrication of the impeller highlights the potential of robot-assisted WAAM systems for producing customized components with intricate geometries, particularly for applications in energy, marine, and industrial machinery sectors.

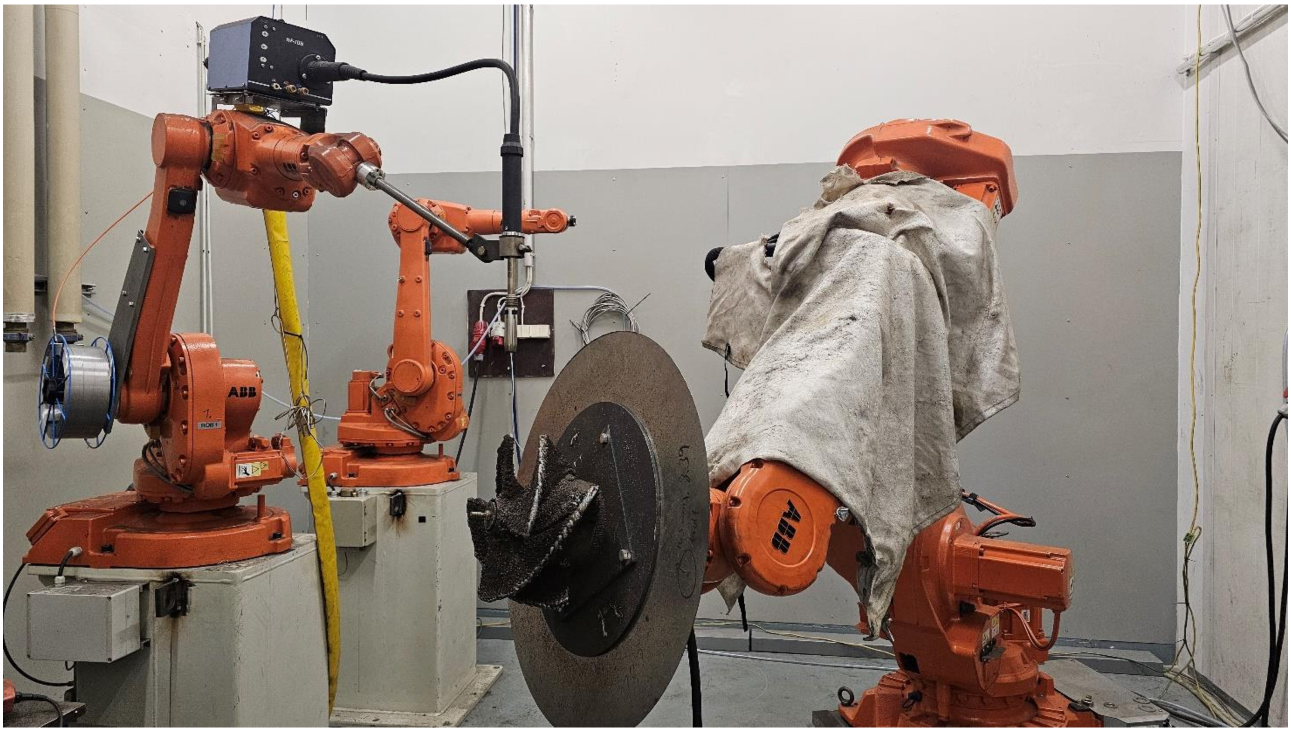

Fig. 1. WAAM printing of complex geometry with robot.

Fig. 2. WAAM fabricated complex geometry.

3 WP 4 Laser DED experiments

3.1 Laser wire DED 316L

3.1.1.1 Test part

The specimens were provided for testing by Meltio. They were manufactured from 316L stainless steel using Meltio’s laser wire DED system. The printed components are shown in Figure 1.

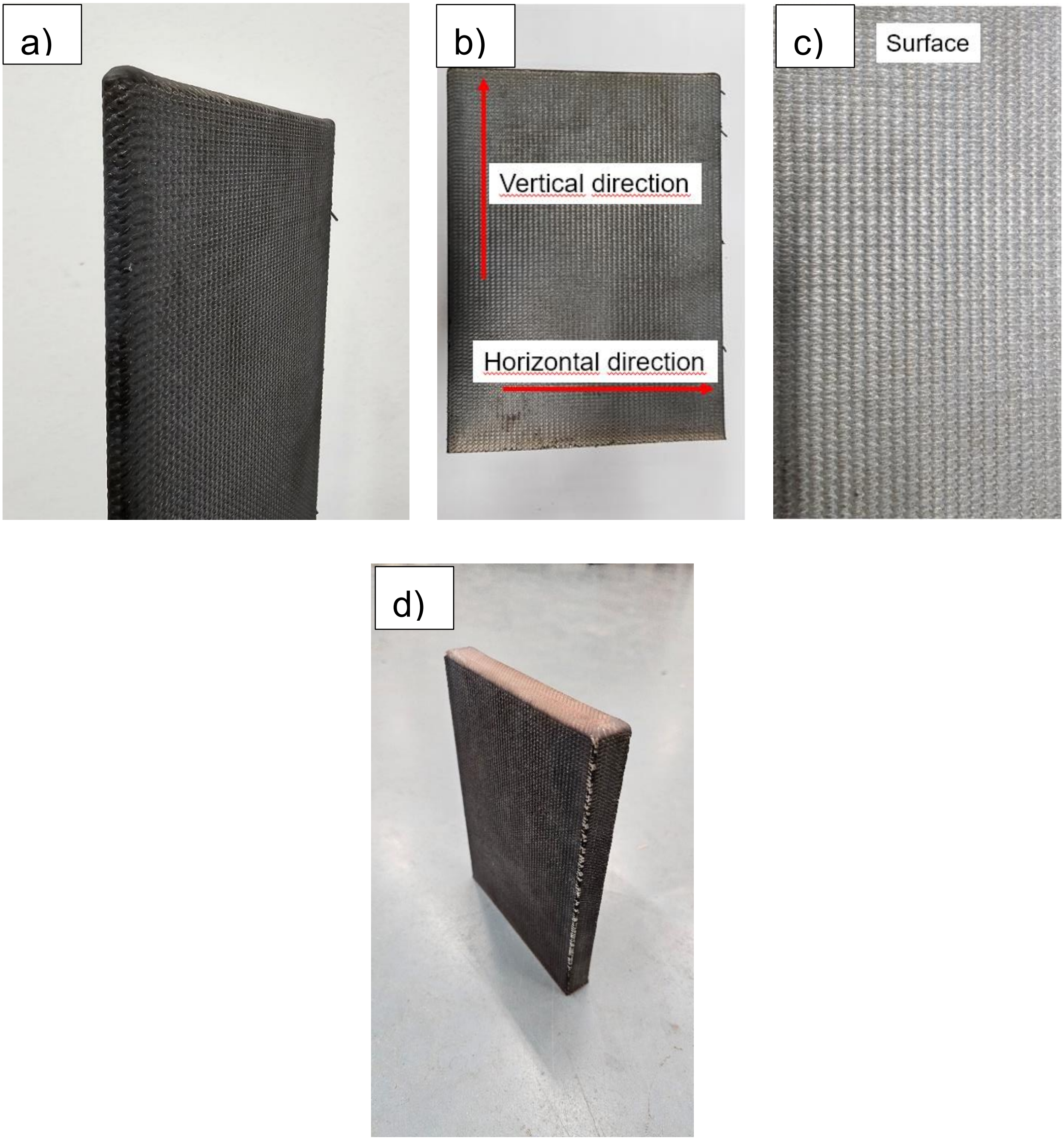

Fig. 1. (a) Thin part; (b) Printing directions of the thin part; (c) Surface of the thin part and (d) Thick part.

3.1.2 X-Ray examination for thin laser wire DED part

X-ray examination was performed on the laser wire DED–fabricated 316L stainless steel part to evaluate the internal quality of the deposited material (Fig. 2). The inspection was carried out to detect potential defects such as porosity, cracks, or lack-of-fusion regions that could affect the mechanical performance of the part.

The radiographic analysis revealed no detectable internal defects or porosity within the part. The deposited material appeared uniform and free of discontinuities, indicating a high-quality deposition process and good metallurgical integrity of the laser wire DED–produced part. These results suggest that the selected process parameters enabled stable material deposition and effective fusion between layers, resulting in a defect-free structure.

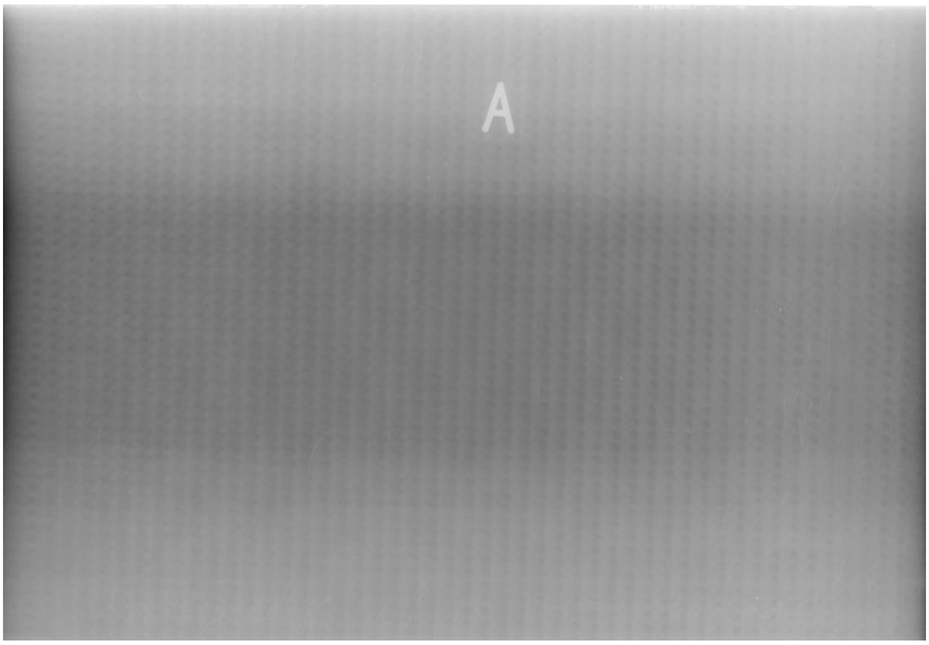

Fig. 2. X-ray image of the thin part.

3.1.3 Microstructure analysis of thin laser wire DED part

The EBSD phase map of the laser wire DED–fabricated 316L stainless steel reveals a microstructure dominated by austenite (γ-Fe, FCC) with a small fraction of retained δ-ferrite. The analysis indicates that the material consists of approximately 95.8% austenite and 4.2% δ-ferrite, with the ferrite phase mainly located along interdendritic regions and grain boundaries. The grain structure appears equiaxed with high-angle grain boundaries, which is typical for additively manufactured 316L stainless steel subjected to repeated thermal cycles during layer-by-layer deposition. The presence of a small amount of δ-ferrite is characteristic of the ferritic–austenitic solidification mode (FA) commonly observed in welding and wire-based additive manufacturing of austenitic stainless steels. This phase distribution is beneficial, as limited δ-ferrite content can reduce susceptibility to solidification cracking while maintaining good ductility and mechanical performance.

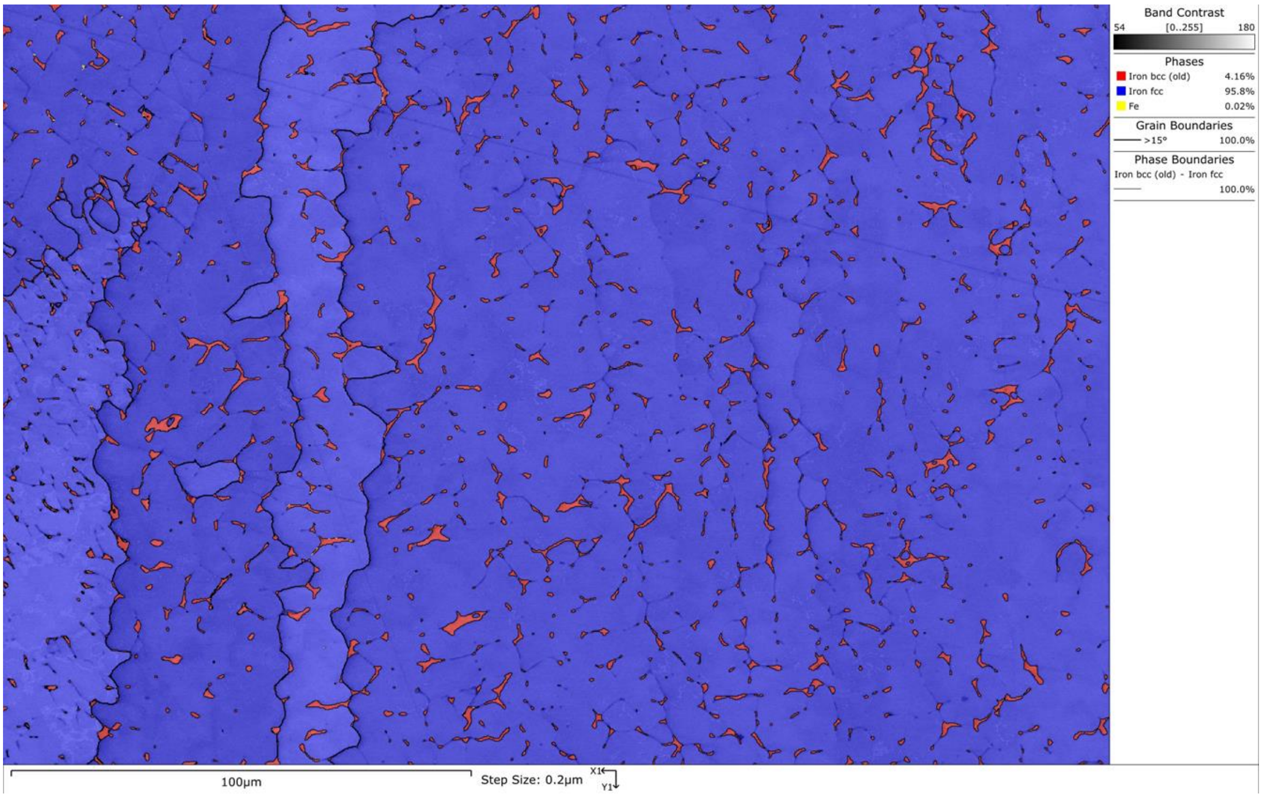

Fig. 3. Microstructure of laser wire DED 316L.

3.1.4 Comparison of microstructures of laser wire DED 316L and WAAM 316L

A comparison of the microstructures of laser wire DED–fabricated 316L stainless steel and WAAM-produced 316L stainless steel reveals clear differences in grain morphology and phase distribution, which are mainly related to the distinct thermal conditions and solidification behavior of the two additive manufacturing processes.

The laser wire DED 316L microstructure is predominantly composed of equiaxed austenitic grains, with a small fraction of retained δ-ferrite distributed mainly along grain boundaries and interdendritic regions. EBSD phase analysis indicated that the material consisted of approximately 95–96% austenite and about 4% δ-ferrite. The grains appear relatively uniform and equiaxed, which suggests that the thermal gradients during deposition were moderate and that partial grain refinement occurred due to repeated thermal cycling during the layer-by-layer deposition process. The δ-ferrite phase appears as discontinuous networks and small islands, which is typical for austenitic stainless steels solidified through a ferritic–austenitic (FA) solidification mode.

In contrast, the WAAM 316L microstructure is characterized by large columnar austenitic grains that extend along the build direction. EBSD phase analysis showed a higher fraction of austenite, approximately 98–99%, with a smaller amount of δ-ferrite (~1–2%) present mainly in thin interdendritic stringers. The strong columnar grain morphology observed in the WAAM material is typical for wire arc additive manufacturing processes and results from directional solidification under steep thermal gradients and high heat input. The grains grow epitaxially across multiple deposited layers, producing elongated grain structures aligned with the thermal gradient during solidification.

The differences in grain morphology between the two materials can largely be explained by the different heat sources and thermal histories associated with the processes. Laser wire DED generally produces lower melt pool volumes and higher cooling rates, which promote grain refinement and the formation of more equiaxed microstructures. In contrast, WAAM processes involve higher heat input and larger melt pools, leading to slower cooling rates and directional solidification, which favors columnar grain growth.

Despite these differences, both materials exhibit a predominantly austenitic microstructure with small amounts of retained δ-ferrite, which is beneficial for preventing solidification cracking during processing. However, the more pronounced columnar grain structure in WAAM 316L may contribute to greater microstructural anisotropy, potentially influencing mechanical properties such as fatigue strength and tensile behavior. In comparison, the more equiaxed grain structure observed in the laser wire DED material may lead to more isotropic mechanical performance.

Overall, the comparison demonstrates that while both additive manufacturing processes produce high-quality austenitic stainless steel microstructures, the laser wire DED process tends to promote finer and more equiaxed grain structures, whereas WAAM processing results in larger columnar grains aligned with the build direction, reflecting the different thermal characteristics of the two deposition techniques.

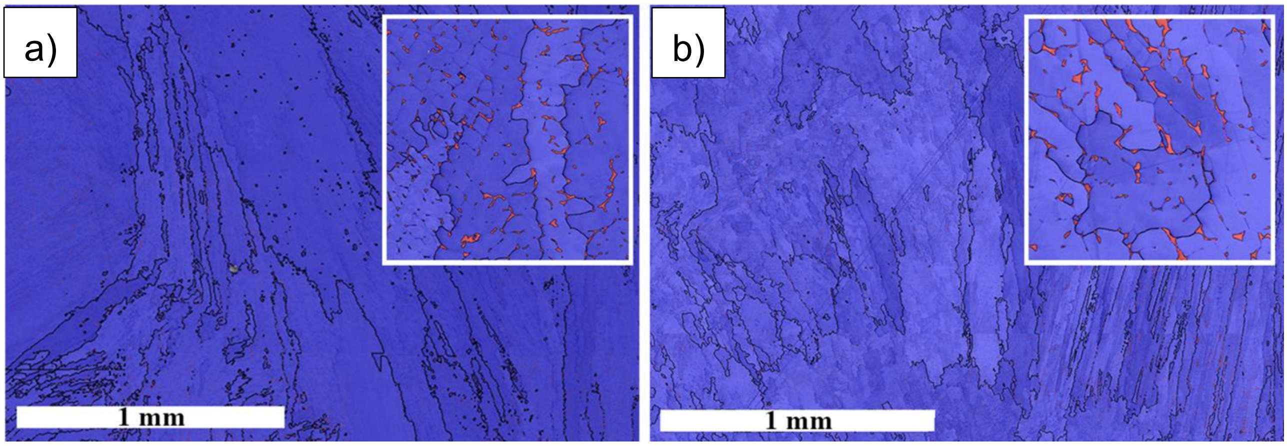

Fig. 4. Microstructure of (a) laser wire DED 316L and (b) WAAM 316L.

3.1.5 Surface quality of thin laser wire DED part

Surface roughness measurements were conducted to evaluate the surface quality of the laser wire DED–fabricated 316L stainless steel. The results are presented in Table 1. The surface profile is presented in Fig 5 and 6.

The measurements show that the as-built surface condition of the laser wire DED 316L material exhibited an average roughness (Ra) of 40.67 μm and a maximum height roughness (Rz) of 202.28 μm. These relatively high roughness values are typical for DED manufactured components produced by wire-based deposition processes, where the layer-by-layer build strategy and melt pool dynamics create a pronounced surface topology.

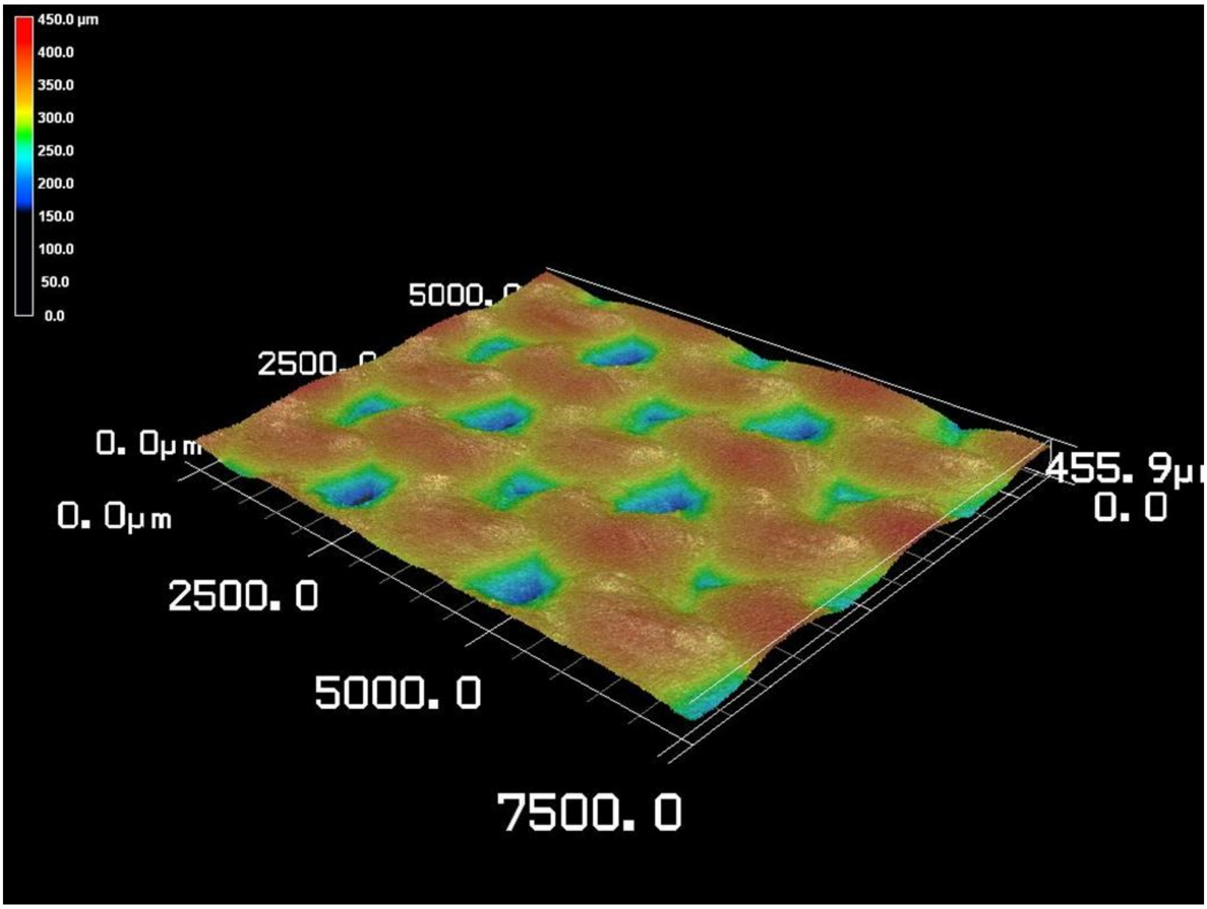

Fig. 5. Surface profile of laser wire DED 316L.

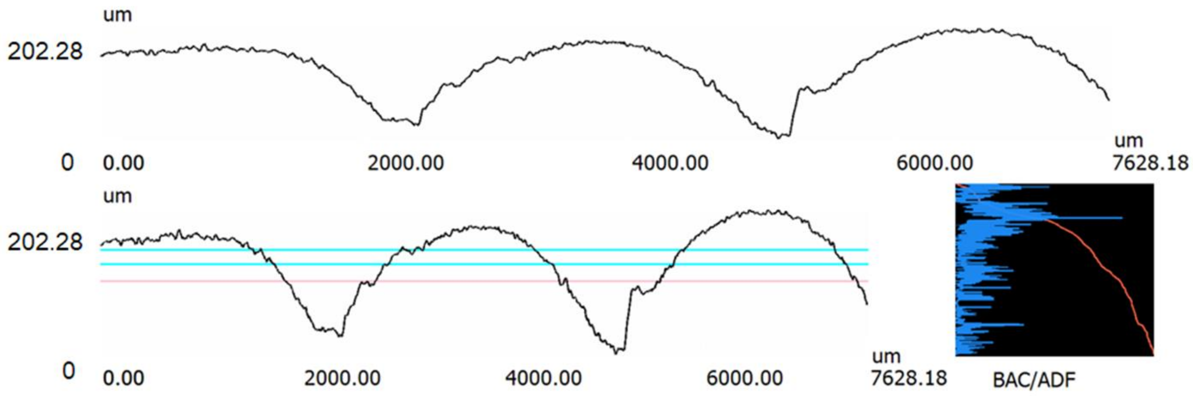

Fig. 6. Surface profile of laser wire DED 316L in as-built condition.

Table 1. Surface roughness of laser wire DED 316L.

Surface of the sample	Ra [µm]	Rz [µm]
As-built	40.67	202.28

3.1.6 Tensile strength of thin laser wire DED part.

Tensile tests were conducted to evaluate the mechanical properties of laser wire DED–fabricated 316L stainless steel in both the vertical and horizontal build orientations. The results of the tests are summarized in Table 2.

The specimens tested in the vertical direction exhibited a yield strength of 306.8 MPa, an ultimate tensile strength of 563.2 MPa, and an elongation of 53.81%. In comparison, the specimens tested in the horizontal direction showed a yield strength of 302 MPa, a tensile strength of 552.5 MPa, and a slightly higher elongation of 55.2%.

The results indicate that the mechanical properties of the laser wire DED 316L material are relatively similar in both build orientations, suggesting limited anisotropy in tensile performance. The vertical specimens exhibited slightly higher strength values, whereas the horizontal specimens showed marginally greater ductility. The high elongation values observed in both orientations demonstrate excellent ductility of the material, which is characteristic of austenitic stainless steels such as 316L.

Table 2. Tensile strength of laser wire DED 316L

	Yield strength [MPa]	Tensile strength [MPa]	Elongation [%]
Vertical	306.8	563.2	53.81
Horizontal	302	552.5	55.2

3.1.7 Bending fatigue strength thin laser wire DED part

In the bending fatigue tests, the fatigue limit of the laser wire DED 316L was 227 MPa in the vertical build orientation and 219 MPa in the horizontal orientation. The vertically fabricated specimens exhibited slightly superior fatigue performance, a trend that was consistently observed also in the low- and medium-cycle fatigue regimes.

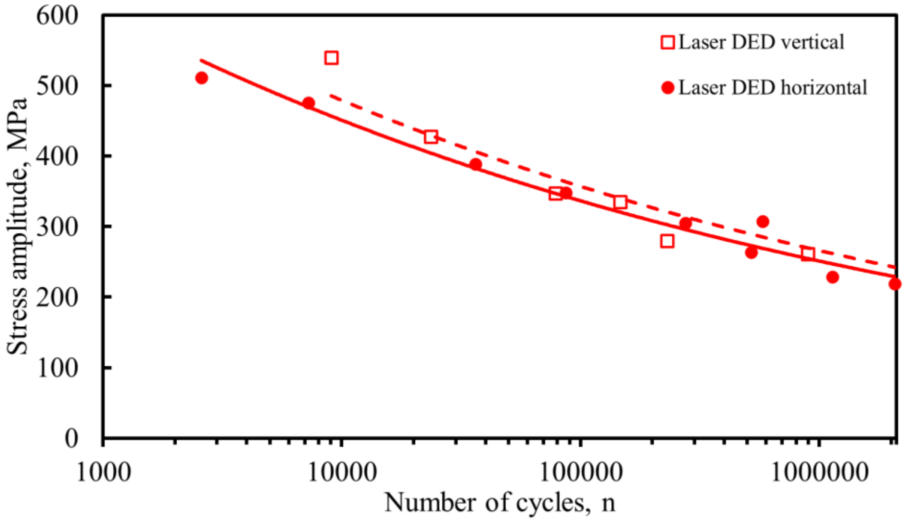

Fig. 7. Bending fatigue strength of laser wire DED 316L.

3.1.7.1 Comparison between laser wire DED 316L and WAAM 316L

When compared to laser wire DED 316L, the WAAM 316L specimens exhibited better bending fatigue performance (Fig. x). A pronounced anisotropy between the two build orientations was observed across the entire fatigue life regime. Specimens loaded in the vertical direction consistently sustained higher stress amplitudes at equivalent cycle counts than those fabricated in the horizontal direction. The fatigue limit, defined as the stress amplitude corresponding to long-life performance, was determined to be 317 MPa in the vertical orientation and 246 MPa in the horizontal orientation.

In contrast, the laser wire DED material demonstrated lower bending fatigue limits (227 MPa in the vertical direction and 219 MPa in the horizontal direction) and exhibited only minor anisotropy between build orientations. Overall, WAAM 316L showed clearly better bending fatigue strength compared to laser wire DED, particularly in the vertical build orientation.

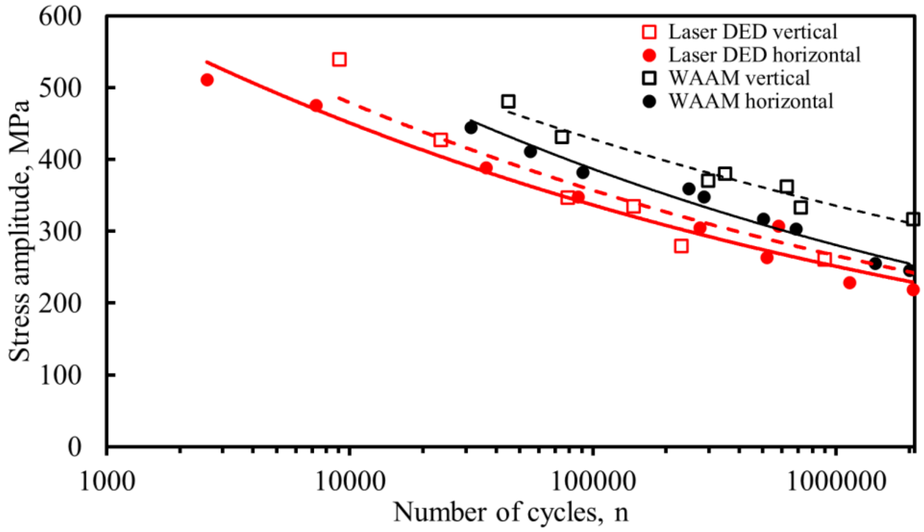

Fig. 8. Bending fatigue strength of laser wire DED 316L and WAAM 316L.

3.1.8 Fatigue strength thin laser wire DED part

Axial fatigue tests were conducted to evaluate the fatigue performance of laser wire DED–fabricated 316L stainless steel. The specimens were tested in the vertical build direction under cyclic loading conditions.

The results showed that the fatigue limit of the laser wire DED 316L material was approximately 230 MPa in the vertical direction. This value represents the stress amplitude at which the material can withstand a high number of load cycles without failure.

The observed fatigue performance indicates that the laser wire DED process produced material with good resistance to cyclic loading. The relatively high fatigue limit suggests that the deposited material contains minimal internal defects and a dense microstructure, which is consistent with the X-ray examination results that showed no detectable porosity or internal discontinuities.

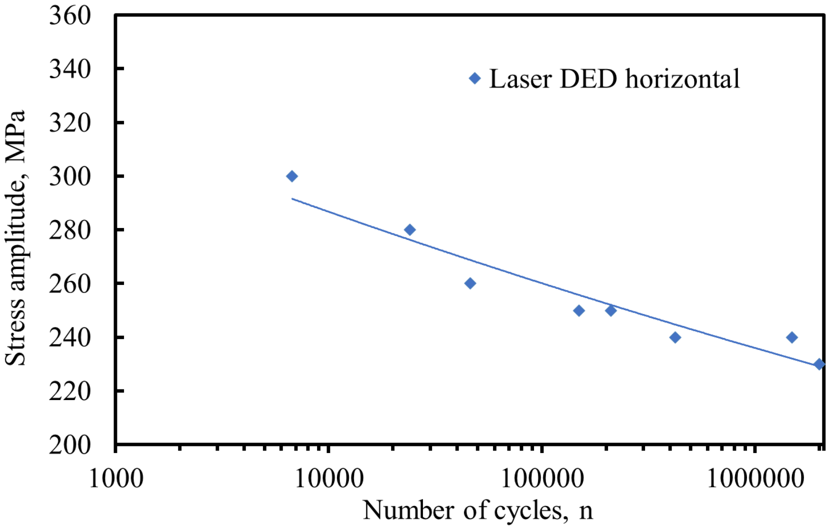

Fig. 9. Axial fatigue strength of laser wire DED 316L.

Axial fatigue tests were carried out to compare the fatigue performance of laser wire DED–fabricated 316L stainless steel and WAAM-produced 316L stainless steel in different build orientations.

The laser wire DED 316L specimens tested in the horizontal direction exhibited a fatigue limit of 230 MPa. For the WAAM 316L material, the vertical specimens showed the highest fatigue limit of 280 MPa, while the horizontal specimens had a fatigue limit of 255 MPa.

The fatigue behavior in the low- and medium-cycle fatigue regimes followed the same order as the fatigue limits. The WAAM 316L material tested in the vertical direction consistently demonstrated the highest fatigue strength, followed by the WAAM horizontal specimens, while the laser wire DED specimens showed the lowest fatigue strength.

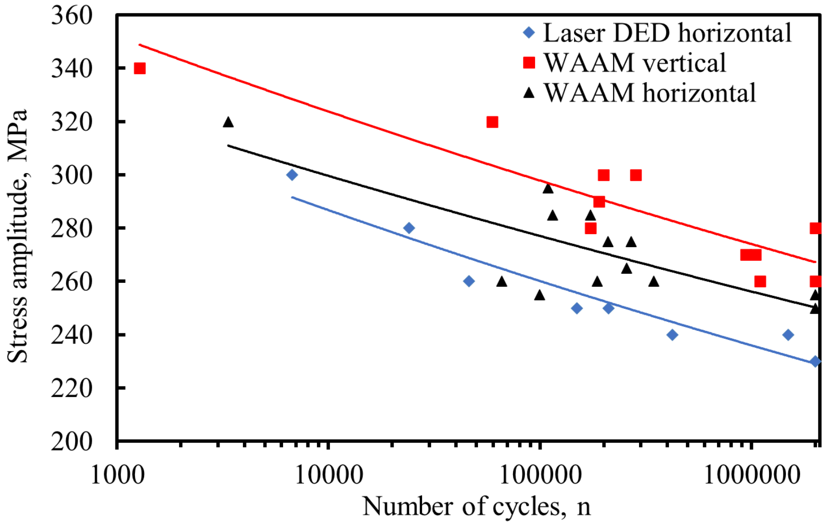

Fig. 10. Axial fatigue strength of laser wire DED 316L and WAAM 316L.

3.1.9 Fatigue strength thick laser wire DED part

The fatigue limit of the laser wire DED material was approximately 250 MPa in both the vertical and horizontal build orientations, indicating no significant anisotropy at the fatigue limit. However, in the low- and medium-cycle fatigue regimes, specimens fabricated in the horizontal orientation demonstrated better fatigue strength compared to those built in the vertical orientation. When compared with WAAM 316L stainless steel, the laser wire DED material exhibited comparable fatigue performance, with both materials showing an equivalent fatigue limit.

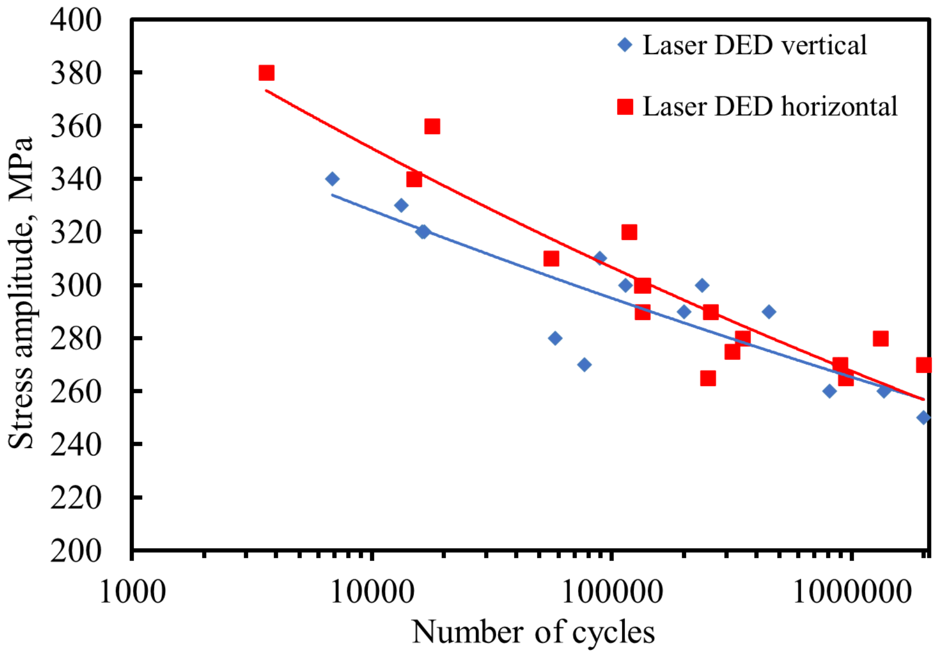

Fig. 11. Axial fatigue strength of laser wire DED 316L.

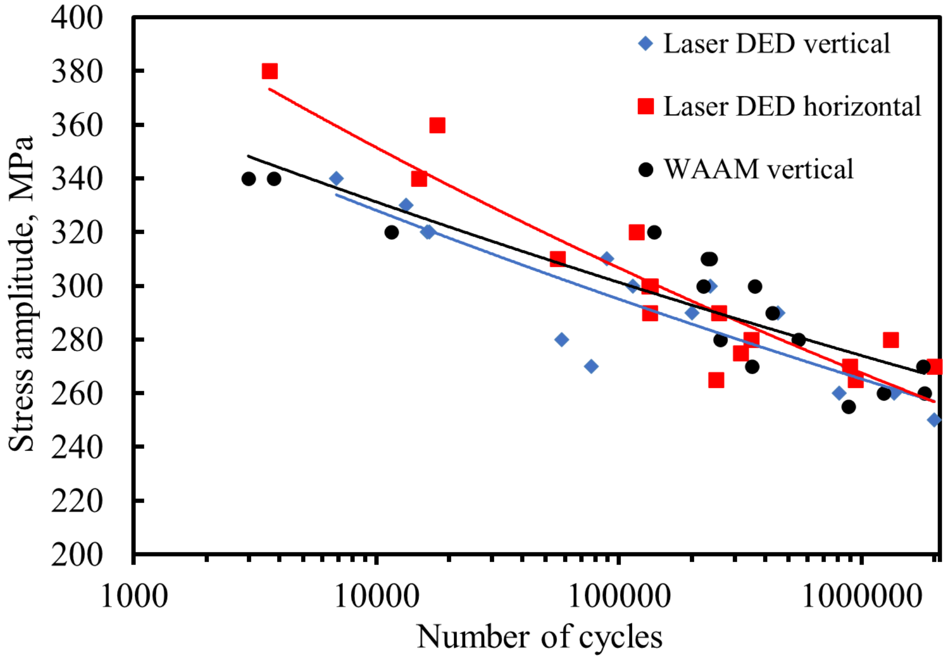

Fig. 12. Axial fatigue strength of laser wire DED 316L and WAAM 316L.

3.1.10 Charpy impact test for thick laser wire DED part

Charpy impact testing was conducted on laser wire DED 316L specimens in both vertical and horizontal printing directions at temperatures of 0 °C and −40 °C. The results are summarized in Table 3. At 0 °C, the absorbed impact energy was 202 J in the vertical direction and 191 J in the horizontal direction. When the temperature was reduced to −40 °C, the impact energy decreased slightly to 190 J and 178 J for the vertical and horizontal directions, respectively.

The vertical direction consistently exhibited higher impact toughness compared to the horizontal direction. As expected, a reduction in temperature led to a decrease in absorbed energy; however, the material maintained relatively high toughness even at −40 °C. These results indicate good low-temperature impact performance of laser wire DED 316L, with only moderate anisotropy between the printing directions.

Table 3. Charpy impact test results in different printing directions.

Printing direction	Temperature °C	Energy absorbed J
Vertical	0	202
Horizontal	0	191
Vertical	-40	190
Horizontal	-40	178

4 WP5 Repair of Broken Steel Products and Replacement of Casting in Manufacturing of Iron-Based Components

4.1 Steel Product Repair by WAAM

4.1.1 Circularity and flatness measurement results

Measurements were performed using a Zeiss Carmet C6 CNC 3D coordinate measuring machine. Circularity and diameter were measured using six measurement points, and flatness was measured using eight measurement points. Circularity was measured from the inner circumference of the mold.

The inner diameter of the mold was measured after printing at two different heights relative to the mold surface (Figure 1). Flatness was measured 10 mm inward from the outer circularity of the mold (Figure 1) from the bottom surface. Flatness was measured from this surface because the coating on the upper surface of the mold did not allow accurate measurements to be taken from that surface.

Table 1 presents the measurement results before and after printing. As shown in Table 1, the deviation in circularity of the mold increased during printing and was 0.0277 mm after printing.

Before printing, the flatness of the mold was 0.017 mm. The flatness changed significantly during the printing process and was 1.888 mm after printing. In this case, flatness refers to the maximum deviation between two measured points from the set of points measured on the plane.

Table 1. Results of the coordinate measurements of the mold. Measurement points are shown in Fig. 1.

	Before printing (mm)	After printing (mm)
Circularity	0.0097	0.0277
Flatness	0.017	1.888

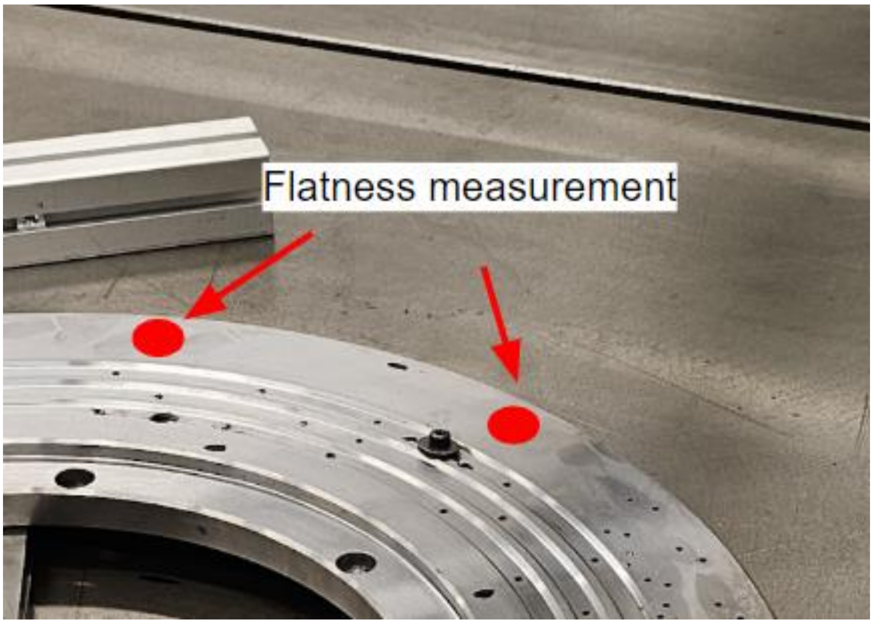

Fig. 1. Measurement points. The red points indicate the flatness measurement points (8 points).

4.1.2 WAAM equipment and parameters

The printing was performed using a Motoman UP-50 robot equipped with a welding torch. A Fronius TransPuls Synergic 2700 CMT power source was used for the welding process. The printing speed was 0.9 m/min. The wire feed rate was approximately 8.5 m/min, with a welding current of 245 A and a voltage of 19.3 V. The stick-out length was approximately 10 mm.

A shielding gas mixture consisting of 82% argon and 18% CO_2 was used, with a gas flow rate of 15 l/min. The filler material was ESAB OK Aristorod 12.50 carbon steel wire with a diameter of 1.2 mm. The overlap between the weld beads was 3.5 mm.

The height of the deposited coating obtained through printing was approximately 2.5 mm, measured using a caliper. A more precise coating thickness could be determined by preparing metallographic cross-sections; however, this was not carried out at this stage of the study.

Prior to printing, the specimen was cleaned twice with ethanol to remove contaminants from the surface.

4.1.3 Finalization of the WAAM-Based Repair

The repair was carried out using the WAAM process, in which new material was deposited onto the worn or damaged surface in order to restore the original geometry of the component. Prior to deposition, the surface of the component was thoroughly cleaned to remove contaminants such as grease, oxides, and debris that could negatively affect weld quality and bonding. The surface preparation ensured proper metallurgical bonding between the deposited material and the substrate.

During the repair process, carbon steel filler wire was deposited layer by layer onto the repair area using a robotic WAAM system. The welding torch followed a predefined toolpath, allowing controlled material deposition over the targeted region. Adjacent weld beads were deposited with a controlled overlap to ensure complete coverage and a uniform build-up of material. Process parameters such as wire feed rate, travel speed, welding current, and shielding gas composition were carefully selected to achieve stable arc conditions and consistent deposition quality.

The deposited layers gradually rebuilt the damaged region until the required repair width was achieved. This deposition allowed precise control of the repaired geometry while maintaining good bonding with the base material. After completion of the WAAM deposition, the repaired surface could be further processed by machining or grinding if tighter dimensional tolerances or improved surface finish were required.

The WAAM repair approach offers several advantages compared to conventional repair techniques. It allows efficient restoration of worn components with minimal material waste, reduced downtime, and the possibility of repairing complex geometries that would be difficult to restore using traditional welding or machining methods.


[redacted]

Fig. 2. WAAM repair of the mold.

Fig. 3. Completed repair.

Fig. 4. Completed repair (large view).

4.2 Mechanical Properties and Fatigue Behavior of the WAAM 316L–Wrought 316L Interphase

4.2.1 Printing equipment

WAAM deposition was performed using a Fronius TransPuls Synergic 2700 CMT welding system. The feedstock material consisted of 1.2 mm diameter 316LSi stainless steel wire, compliant with the AWS A5.9 ER316LSi classification. The material was deposited onto a wrought 316L stainless steel.

The deposition was carried out at a constant travel speed of 0.32 m/min, while maintaining a layer height of approximately 1.25 mm between consecutive layers. Process parameters were selected to achieve stable arc conditions and consistent material deposition. The welding current was 111 A, the voltage 12.7 V, and the wire feed rate was set to 3.1 m/min.

The interpass temperature was maintained at 150 °C, monitored using an Optris CT infrared pyrometer to ensure controlled thermal conditions during the build process. Throughout the deposition, shielding gas was continuously supplied using a mixture of 98% argon and 2% oxygen, with a flow rate of 12 l/min.

4.2.2 Testing setup

The 316L stainless steel wrought plate was positioned vertically and secured between two aluminum supports. A wall structure was then produced along one side of the plate using the WAAM process (Fig. 1). Deposition followed a linear toolpath, where successive layers were deposited using a bidirectional strategy. Each subsequent layer began from the opposite end of the plate, thereby alternating the deposition direction to ensure uniform heat distribution during the build. The resulting printed wall had a length of 270 mm and a height of 70 mm. The base plate dimensions were 270 mm in length, 80 mm in height, and 8 mm in thickness.

Rectangular specimens intended for microstructural characterization were extracted from the WAAM–wrought 316L interface region. Sample preparation involved sequential grinding with silicon carbide abrasive papers, followed by mechanical polishing to achieve a mirror-like surface finish. Final surface treatment was performed by electropolishing in a 50% aqueous nitric acid solution at 1.3 V, which minimized surface deformation and improved phase contrast for microstructural observation. The microstructure was examined using a Keyence VK-X200 laser microscope.

Specimens for tensile and fatigue testing were machined from the WAAM-fabricated section. A face milling operation was first carried out to remove approximately 1.5 mm of material from both sides of the WAAM wall, eliminating surface irregularities and producing a uniform plate with a final thickness of 5 mm. Test specimens were subsequently laser-cut and machined to the required geometries and dimensions.

During tensile testing, a constant crosshead speed of 1.0 mm/min was applied throughout the experiments. The tensile tests were conducted using an Instron 8802 universal testing machine, following the SFS-EN ISO 6892-1:2019 standard. A total of five specimens were tested to evaluate tensile properties.

Hardness measurements were performed using an Innovatest Falcon 500 Vickers hardness tester, applying a 0.2 kg load, with indentations spaced at 0.1 mm intervals.

Fatigue testing was carried out using a StepLab UD020 electric linear actuator. The tests were performed at a stress ratio (R) of −1 and a frequency of 50 Hz, following the ASTM E466-21 standard. In total, 25 specimens were evaluated in fatigue testing. The fatigue specimens were manufactured according to the standard requirements, with a gauge length of 50 mm and a gauge width of 9 mm.

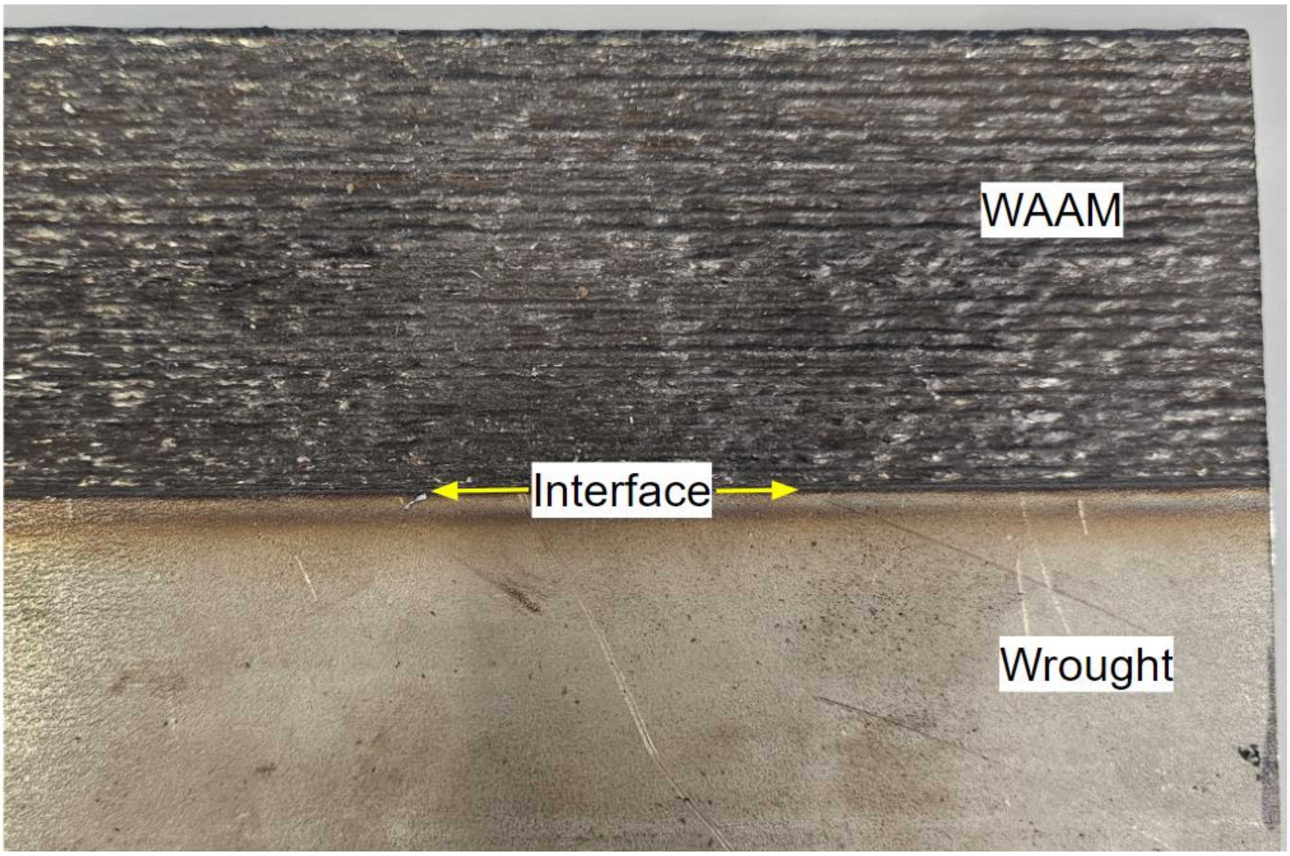

Fig. 1. WAAM-fabricated part.

4.2.3 Microstructure analysis

Figure 2 presents the microstructure at the interface between the WAAM-deposited 316L stainless steel and the wrought 316L stainless steel substrate, observed by optical microscopy at both low and high magnifications. Overall, the interface exhibits a sound metallurgical bond without visible porosity. The absence of interfacial defects, such as lack-of-fusion regions or voids, indicates good wetting behavior and sufficient thermal fusion between the deposited WAAM material and the wrought 316L substrate.

At lower magnification, a clear transition can be observed between the two materials. The WAAM region is characterized by a columnar solidification structure, while the wrought substrate shows a typical equiaxed grain morphology. The WAAM-deposited material consists predominantly of austenite with interdendritic retained δ-ferrite, which forms as a result of rapid and non-equilibrium solidification during the deposition process. In contrast, the wrought substrate exhibits a uniform equiaxed austenitic microstructure. The retained δ-ferrite appears as elongated, darker features within the austenitic matrix and is mainly located along interdendritic regions.

This difference in microstructure across the interface may influence important mechanical properties, including fatigue resistance, strength, toughness, and hardness, which are critical for the performance of hybrid WAAM structures. In addition, a narrow heat-affected zone (HAZ) can be observed adjacent to the interface. Within this region, slight coarsening of the austenitic grains in the wrought 316L substrate is visible, indicating the thermal influence of the WAAM deposition process. The interfacial region is therefore of particular interest, as the distinct contrast in grain morphology between the deposited and wrought materials may lead to variations in mechanical behavior, especially with respect to strength and fatigue performance.

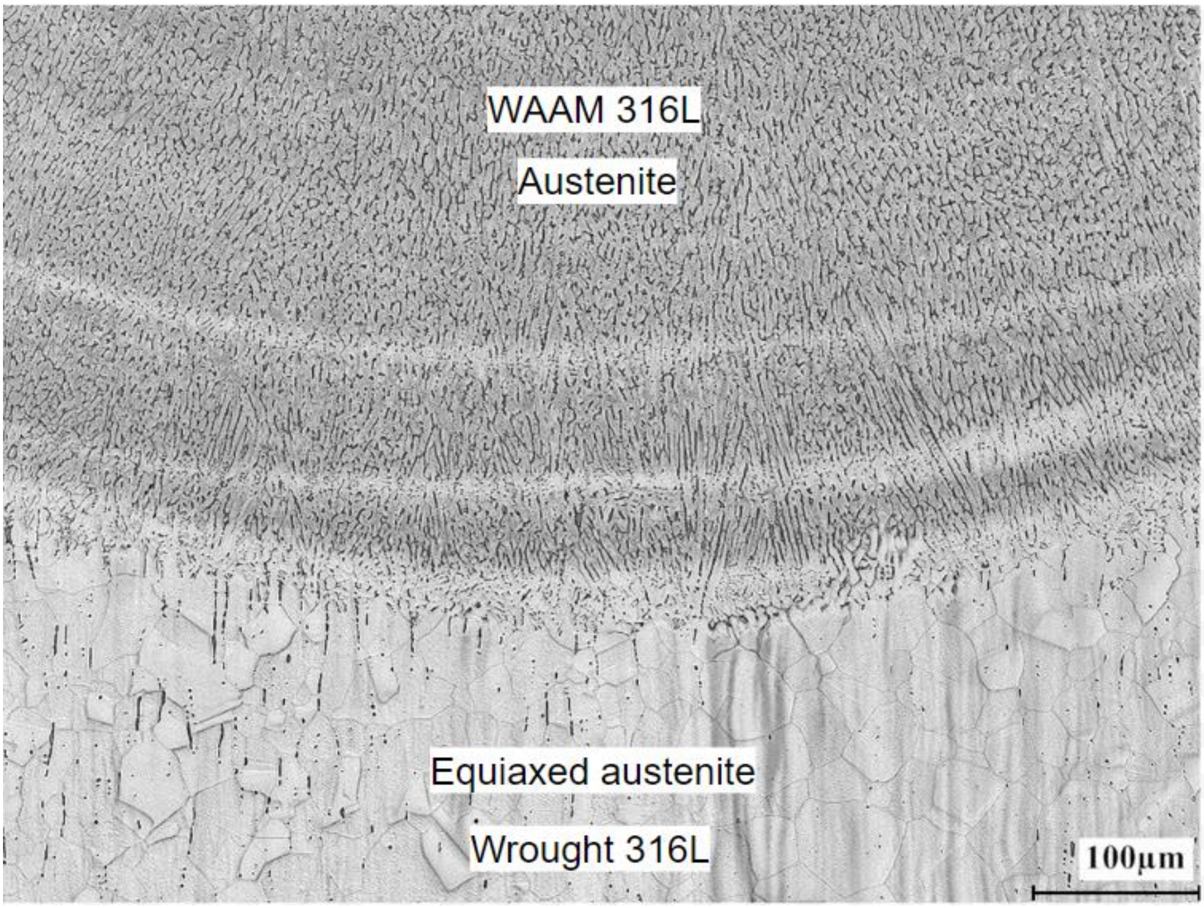

Fig. 2. Microstructure of the interface between WAAM 316L and wrought 316L stainless steel.

4.2.4 Hardness measurement

Vickers hardness measurements were carried out across the interfacial region, as illustrated in Fig. 3. The results show a relatively uniform hardness distribution throughout the measured area, with values generally ranging from 170 to 210 HV. The WAAM-deposited region exhibited a slightly higher average hardness of approximately 195 HV, whereas the wrought stainless steel showed an average hardness of about 177 HV. Greater variability in hardness values was observed within the WAAM region, which can likely be attributed to its layered microstructure and the repeated thermal cycling inherent to the additive manufacturing process. In contrast, the wrought stainless steel displayed a more consistent hardness profile, reflecting its more homogeneous microstructure. Importantly, no significant hardness discontinuity was detected at the fusion boundary. The lack of a pronounced increase or decrease in hardness indicates that the interfacial region is free from extensive heat-affected zone formation or detrimental metallurgical transformations.

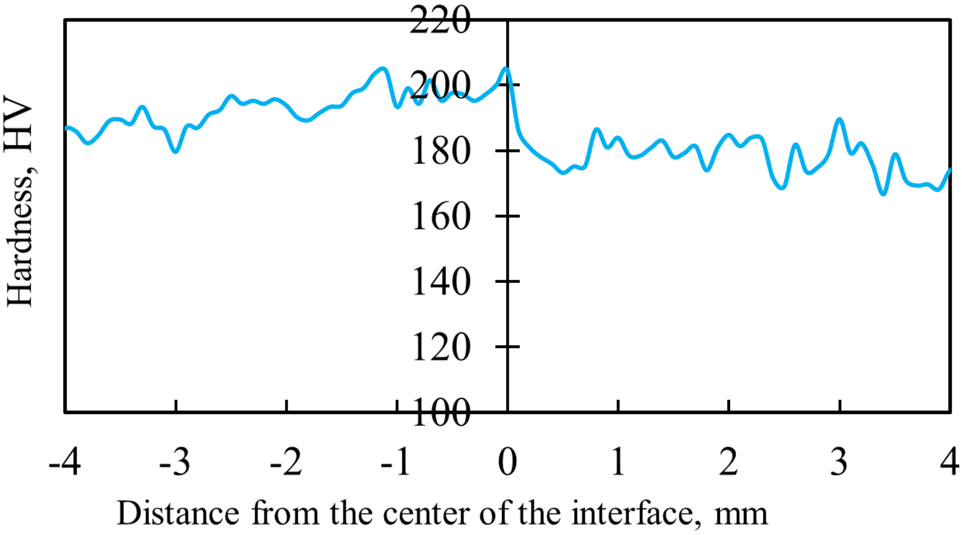

Fig. 3. Hardness of the interface of the WAAM 316L and wrought 316L.

4.2.5 Mechanical properties

The results show a yield strength of 320 MPa, an ultimate tensile strength of 568 MPa, and an elongation at fracture of 56%, indicating excellent ductility of the structure. Despite the presence of dissimilar microstructures across the interface, the specimen exhibited stable deformation behavior without premature strain localization at the interphase. Fracture consistently occurred within the WAAM-deposited region rather than at the interface or within the wrought 316L stainless steel. This observation suggests that the metallurgical bonding between the WAAM material and the wrought substrate was robust and did not represent a weak point under tensile loading. The columnar grain structure typically associated with WAAM materials may have contributed to slightly reduced ductility and damage tolerance compared to the wrought 316L stainless steel.

4.2.6 Bending fatigue strength

The S–N fatigue curves for the WAAM, wrought, and hybrid joint conditions are presented in Fig. 4. The wrought 316L stainless steel demonstrated the highest fatigue resistance, with a fatigue limit of 305 MPa. The WAAM-produced 316L material exhibited moderate fatigue performance, with a fatigue limit of 270 MPa. This behavior is consistent with previous studies showing that microstructural characteristics typical of additive manufacturing, such as columnar grains and layer banding, may reduce fatigue life. Nevertheless, the WAAM material still demonstrated acceptable cyclic performance.

The hybrid WAAM–wrought 316L stainless steel structure showed the lowest fatigue performance, with a fatigue limit of 220 MPa. Fatigue cracks were initiated at the interfacial region, indicating that the fusion boundary acted as a site for stress concentration. This behavior may be associated with microstructural discontinuities, residual stresses, or localized mechanical incompatibilities at the interface. Although hardness measurements indicated a relatively smooth transition across the fusion zone, the fatigue results suggest that the interfacial region remains mechanically vulnerable under cyclic loading conditions. The observed reduction in fatigue strength can therefore be attributed to the combined effects of microstructural heterogeneity, residual stress distribution, and mechanical mismatch across the interface, all of which reduce the ability of the hybrid joint to withstand repeated loading.

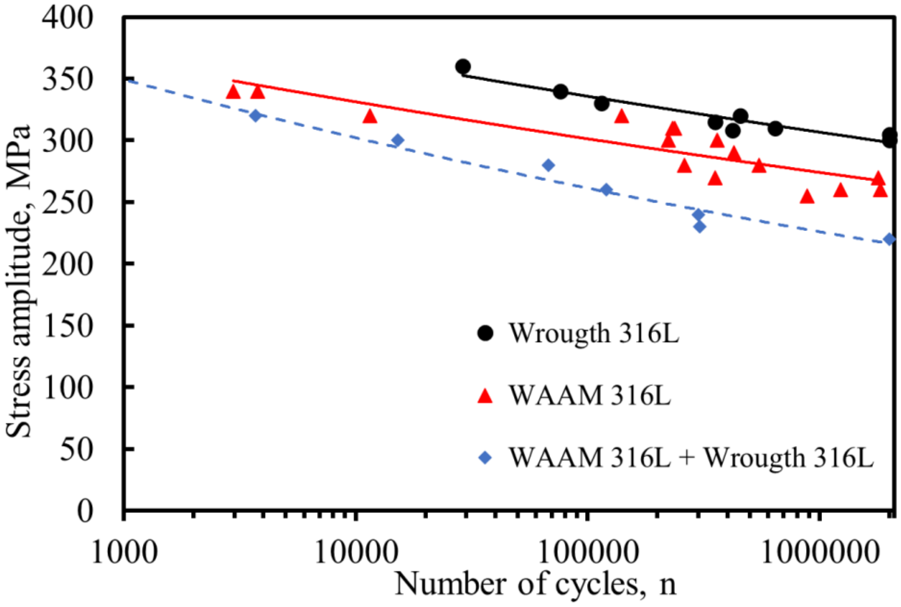

Fig. 4. Bending fatigue strength.

4.2.7 Axial fatigue strength

Axial fatigue tests were conducted to evaluate the fatigue performance of wrought 316L stainless steel, WAAM 316L stainless steel, and the hybrid structure consisting of a WAAM 316L and wrought 316L interphase. The objective of the tests was to investigate the influence of the manufacturing method and the interfacial region on the fatigue behavior of the material under cyclic loading conditions.

The results showed that the wrought 316L stainless steel exhibited the highest fatigue resistance, with a fatigue limit of 305 MPa (Fig. 5). The WAAM 316L material demonstrated a slightly lower fatigue limit of 280 MPa. The hybrid structure containing the WAAM–wrought interphase showed the lowest fatigue performance, with a fatigue limit of 220 MPa.

A similar trend was observed in the finite-life regime. In the low- and medium-cycle fatigue regimes, the fatigue strength of the materials followed the same order as the endurance limits. The wrought 316L stainless steel consistently sustained higher stress amplitudes at equivalent cycle counts, followed by the WAAM material, while the hybrid WAAM–wrought specimens showed the lowest fatigue strength.

These results indicate that the presence of the WAAM–wrought interface significantly influences fatigue performance, acting as a potential site for crack initiation under cyclic loading. In contrast, the homogeneous microstructure of the wrought material provides superior resistance to fatigue crack initiation and propagation.

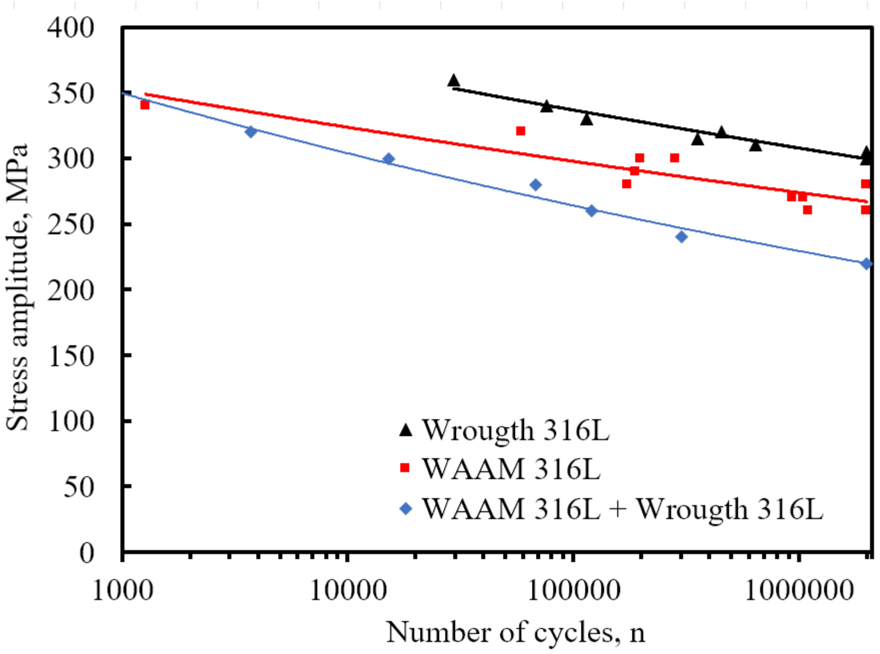

Fig. 5. Axial fatigue strength.

4.3 Mechanical Properties and Fatigue Behavior of the WAAM Carbon Steel–Wrought S355 Interface

4.3.1 Printing equipment

The WAAM experiments were performed using a Fronius TransPuls Synergic 2700 CMT welding system. During the deposition process, a constant travel speed of 0.35 m/min was maintained, while the layer height between successive passes was approximately 1.65 mm. The welding parameters were selected to ensure stable arc behavior and uniform bead formation, with a current of 160 A, voltage of 10.6 V, and a wire feed rate of 3.2 m/min.

The interpass temperature was controlled at 200 °C and monitored using an Optris CT infrared pyrometer to maintain consistent thermal conditions throughout the fabrication process. To protect the molten pool from atmospheric contamination, a shielding gas mixture consisting of 92% argon and 8% CO_2 was continuously supplied at a flow rate of 12 L/min during deposition.

In this work, ESAB Purus 46 carbon steel wire, compliant with the SFA/AWS A5.18 ER70S-6 classification, was used as the feedstock material for the WAAM process. The wire had a diameter of 1.2 mm, and its mechanical properties are presented in Table 1. The substrate material consisted of a 10 mm thick S355 structural steel plate (wrought carbon steel), whose mechanical properties are also listed in Table 1. The chemical compositions of both the carbon steel wire and the wrought S355 steel are provided in Table 2.

Table 1. Mechanical properties of the carbon steel wire and wrought carbon steel.

	Yield strength [MPa]	Tensile strength [MPa]	Elongation [%]
Carbon steel wire	470	560	26
Wrought carbon steel	355	430-550	23

Table 2. Chemical composition (%) of the carbon steel wire and wrought carbon steel.

	C	Mn	Si	P	S
Carbon steel wire	0.1	1.11	0.72	0.013	0.0012
Wrought carbon steel	0.1	1.50	0.03	0.025	0.010

4.3.2 Test setup

The WAAM carbon steel wall was produced on a vertically oriented wrought carbon steel (S355) plate with dimensions of 320 × 75 × 10 mm, which was clamped between two aluminum supports during the deposition process. Material was deposited along the length of the plate following a linear toolpath. Successive layers were printed using a bidirectional deposition strategy, where each pass alternated direction to promote uniform heat distribution and consistent layer formation. Consequently, every new layer began from the opposite end of the previous pass. The final deposited wall had a length of 320 mm and a height of 75 mm.

Following the WAAM process, the deposited wall was machined from both sides to eliminate surface irregularities and produce a smooth and uniform surface suitable for mechanical testing. This machining step ensured improved dimensional accuracy and reduced the influence of surface roughness on the results of the subsequent experimental investigations.

Test specimens were extracted from the machined WAAM carbon steel wall using laser cutting, which allowed accurate specimen geometry while minimizing thermal distortion during sectioning. The tensile and fatigue specimens were subsequently machined to the required dimensions to comply with the tolerance requirements of the respective testing standards. For statistical reliability, five tensile specimens and twelve fatigue specimens were prepared. All specimens were taken from the central region of the WAAM wall, thereby representing the bulk deposited material while avoiding edge regions and potential boundary effects.

Tensile testing was performed using an Instron 8802 universal testing machine in accordance with the SFS-EN ISO 6892-1:2016 standard. The tests were conducted under displacement control, with a constant crosshead speed of 1.0 mm/min to ensure consistent and repeatable measurements. Hardness measurements were carried out using an Innovatest Falcon 500 Vickers hardness tester with a 0.2 kgf load (HV0.2). Indentations were placed at 0.2 mm intervals along the measurement line to capture detailed hardness variations across the analyzed region. Microstructural analysis of the samples was performed using a Keyence VK-X200 laser scanning microscope, which provided high-resolution imaging of the WAAM-deposited carbon steel, the interface region, and the wrought carbon steel substrate.

The bending fatigue behavior of the WAAM-fabricated specimens was evaluated using a custom-built reversed flexural bending fatigue testing machine, developed based on the WEBI system originally manufactured by Carl Schenck. The fatigue tests were conducted under fully reversed loading conditions, corresponding to a stress ratio (R) of –1, where R represents the ratio between the minimum and maximum stress within a loading cycle. Stress amplitudes ranging from 160 MPa to 670 MPa were applied to investigate fatigue performance over a wide range of cyclic loading conditions. Prior to testing, each specimen was individually calibrated using a force sensor to ensure accurate stress application. This calibration procedure reduced potential variability between samples and improved the accuracy, repeatability, and reliability of the fatigue test results.

4.3.3 Microstructure analysis

Figure 1 presents the microstructure across the interface between the WAAM-deposited carbon steel and the wrought carbon steel substrate. The microstructure on the left side of the image represents the WAAM-deposited carbon steel. This region exhibits a comparatively coarse ferrite–pearlite microstructure with partially elongated grains. Such a morphology is typical for material exposed to repeated thermal cycles during the layer-by-layer WAAM deposition process, as well as relatively slower cooling rates within the deposited region.

Moving toward the right side of the image, the microstructure gradually transitions into that of the wrought carbon steel substrate. This area is characterized by a finer and more equiaxed ferrite–pearlite microstructure, which is typical of rolled and normalized structural steels. The progressive refinement in grain size from the WAAM region toward the wrought material indicates the presence of a heat-affected zone (HAZ) at the interface. In this region, the thermal input from the WAAM deposition process has caused partial austenitization and subsequent recrystallization of the base material.

Importantly, no visible defects, such as cracks, pores, or lack-of-fusion regions, were observed at the interface. This indicates that a metallurgically sound bond was formed between the WAAM-deposited material and the wrought carbon steel substrate, confirming effective fusion and good compatibility between the two materials.

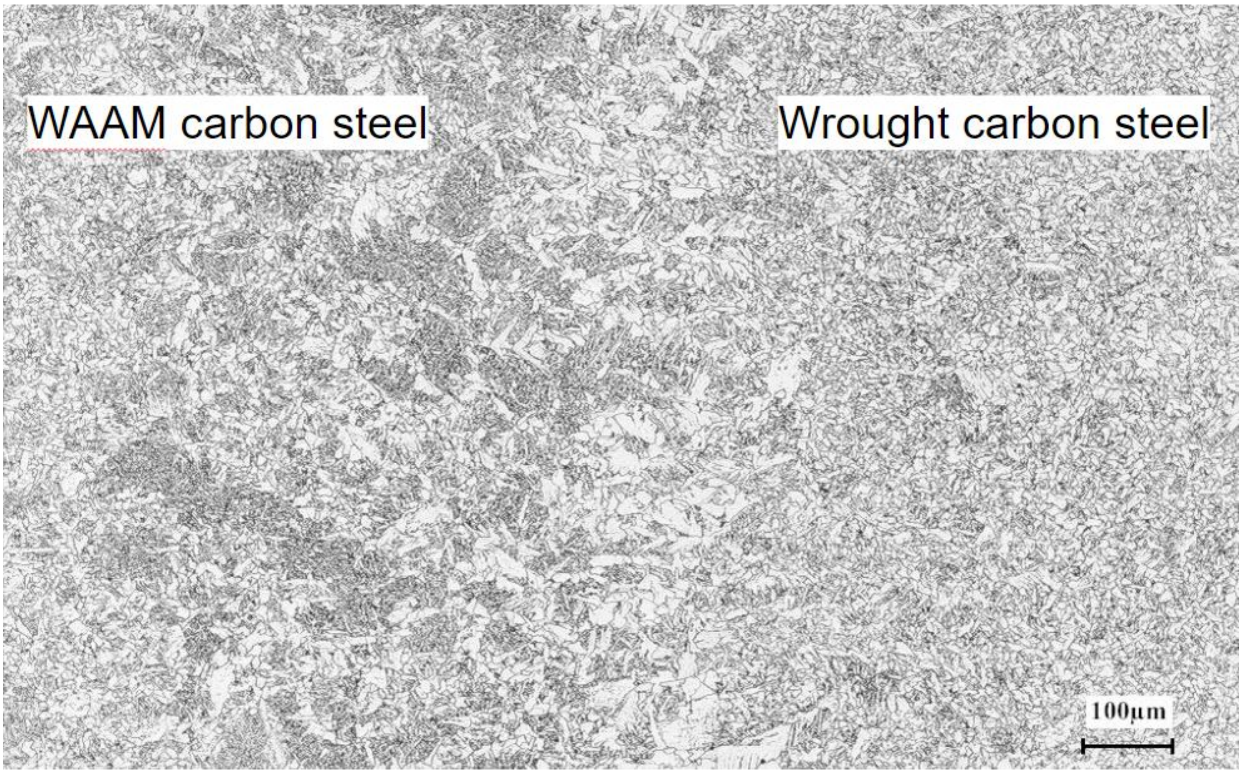

Fig. 1. Microstructure from the interface.

4.3.4 Hardness measurement

Figure 2 illustrates the hardness profile measured across the interface between the WAAM-deposited carbon steel (left side) and the wrought carbon steel substrate (right side). The WAAM-deposited region shows relatively stable hardness values ranging from approximately 190 to 210 HV, which correspond to the ferrite–pearlite microstructure typically formed under the repeated thermal cycles characteristic of the WAAM process. Small variations in hardness within this region may result from localized differences in cooling rates and minor microstructural heterogeneities caused by overlapping deposition passes.

At the interfacial region, a slight increase in hardness is observed, reaching values of approximately 200–210 HV. This localized hardness peak is associated with the formation of a fine-grained heat-affected zone (HAZ), where the thermal input from the WAAM process caused partial grain refinement during rapid cooling. The refined microstructure in this region may also contain a slightly increased fraction of pearlite, contributing to the observed hardness increase. Although the present study focused primarily on hardness measurements, it should be noted that elemental diffusion across the interface may also influence local microstructural characteristics and hardness variations. The repeated thermal cycles during the WAAM process could promote limited diffusion of carbon or alloying elements between the deposited material and the wrought substrate, potentially affecting phase distribution within the HAZ. While compositional analysis was not performed in this work, such effects should be investigated in future studies to better understand interfacial phenomena.

Further away from the interface, within the wrought carbon steel region, the hardness gradually decreases to approximately 150–170 HV, which is consistent with the ferrite–pearlite microstructure typical of normalized structural steels. Overall, the hardness transition across the interface is gradual and continuous, with no abrupt changes or soft zones detected. This smooth hardness gradient indicates good metallurgical bonding and thermal compatibility between the WAAM-deposited carbon steel and the wrought substrate. The slightly elevated hardness near the interface further suggests that the WAAM process did not introduce detrimental softening effects within the HAZ, supporting the structural integrity of the joint for potential repair and reinforcement applications.

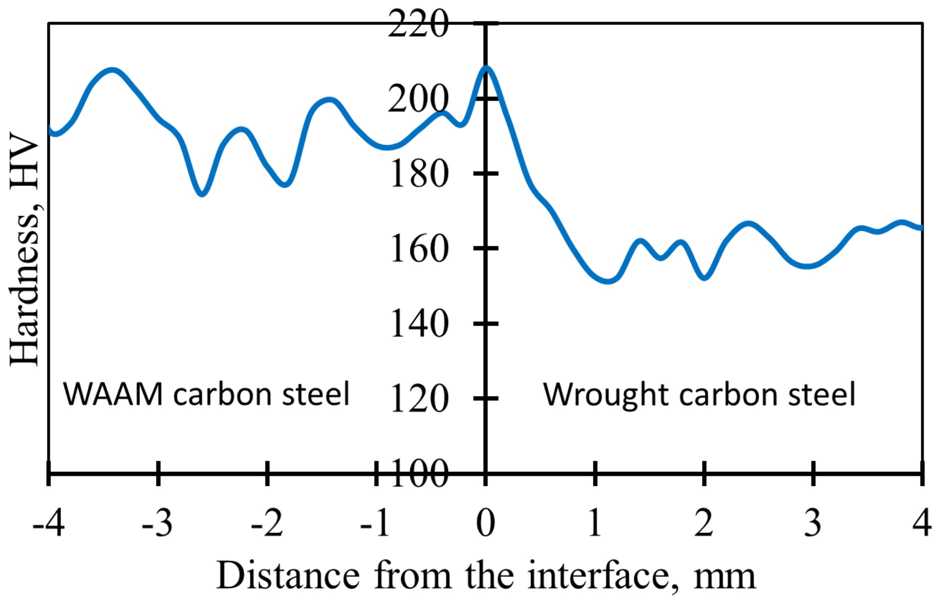

Fig. 2. Hardness profile of WAAM CS and wrought CS.

4.3.5 Mechanical properties

Table 3 summarizes the tensile properties of the WAAM-deposited carbon steel (CS), the wrought carbon steel (CS), and the hybrid specimen composed of WAAM CS deposited onto wrought CS (WAAM CS–Wrought CS). The WAAM-deposited carbon steel exhibited a yield strength of 418 MPa and an ultimate tensile strength of 519 MPa, both of which are slightly higher than those measured for the wrought carbon steel, which showed values of 406 MPa and 481 MPa, respectively. In addition to the higher strength values, the WAAM carbon steel demonstrated a relatively high elongation of 41%, exceeding that of the wrought material. This indicates a favorable combination of strength and ductility, which can be attributed to the refined ferrite–pearlite microstructure and the repeated thermal cycles experienced during the WAAM deposition process.

The hybrid WAAM CS–Wrought CS specimen exhibited intermediate mechanical properties, with a yield strength of 428 MPa and an ultimate tensile strength of 500 MPa, along with an elongation of 36%. These results indicate that the interface between the WAAM-deposited carbon steel and the wrought substrate enables effective load transfer without significant degradation of mechanical strength. The slightly lower elongation compared to the pure WAAM material may be related to the presence of the interfacial region and the microstructural gradient between the two materials.

During the tensile testing of the hybrid WAAM CS–Wrought CS specimens, fracture consistently occurred within the wrought carbon steel region, rather than at the interface. This observation suggests that the metallurgical bond between the WAAM-deposited carbon steel and the wrought substrate was stronger than the base material itself, confirming the structural integrity and reliability of the fusion interface.

Table 3. Tensile strength of the WAAM and wrought materials.

	Yield strength [MPa]	Tensile strength [MPa]	Elongation [%]
WAAM CS	418	519	41
Wrought CS	406	481	25
WAAM CS–Wrought CS	428	500	36

4.3.6 Bending fatigue strength

Figure 3 illustrates the bending fatigue performance of the WAAM-deposited carbon steel (CS), the hybrid specimen consisting of WAAM CS deposited on wrought CS (WAAM CS–Wrought CS), and the wrought carbon steel (CS). The S–N curves show that the WAAM-deposited material exhibits the highest fatigue strength throughout the investigated stress range. The WAAM carbon steel demonstrates a fatigue limit of approximately 250 MPa, which is slightly higher than that of the hybrid specimen (approximately 205 MPa) and clearly higher than that of the wrought carbon steel (approximately 162 MPa).

The hybrid WAAM CS–Wrought CS specimens display fatigue behavior that falls between that of the pure WAAM carbon steel and the wrought carbon steel. This indicates that the interface between the WAAM-deposited material and the wrought substrate does not represent a critical weakness in the structure. The slightly reduced fatigue strength compared to the pure WAAM material may be associated with minor stress concentrations or localized microstructural variations in the interfacial region. Nevertheless, no sudden decrease in fatigue life was observed in the hybrid specimens, suggesting that the WAAM-deposited carbon steel and the wrought substrate deform compatibly under cyclic bending conditions.

During the bending fatigue experiments, all WAAM CS–Wrought CS specimens fractured within the wrought carbon steel region, and no failures were initiated at the interface. This observation further confirms the mechanical integrity and fatigue durability of the metallurgical bond between the WAAM-deposited carbon steel and the wrought substrate.

The superior fatigue performance of the WAAM-deposited carbon steel compared to the wrought material may be attributed to its refined ferrite–pearlite microstructure and potentially favorable residual stress distribution generated during the layer-by-layer deposition process. These results demonstrate that WAAM-deposited carbon steel can retain high fatigue resistance and that the interface formed with wrought carbon steel remains mechanically robust, highlighting the potential of WAAM for repair and reinforcement of structural components subjected to cyclic loading.

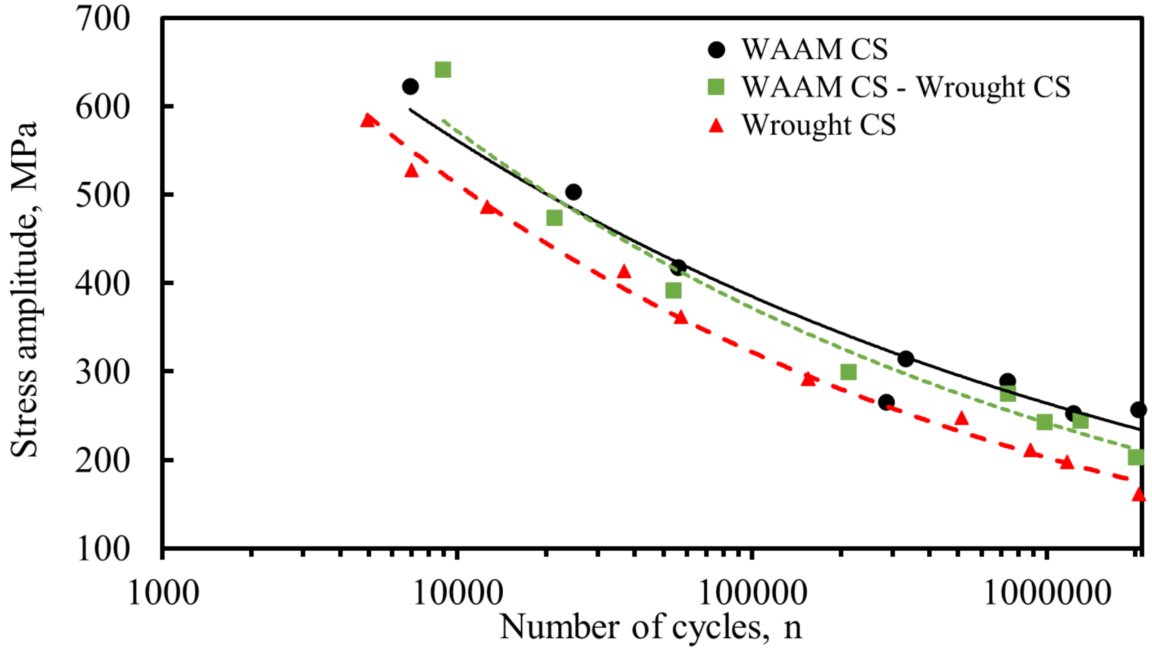

Fig. 3. Bending fatigue strength of the test material.

4.4 Comparison Between WAAM Steels and Cast Steel

4.4.1 Test material

4.4.1.1 Cast steel

Cast steel G24Mn6+QT1, specified in EN 10293, is a quenched and tempered low-alloy manganese steel commonly used in components requiring a combination of high strength, toughness, and good fatigue resistance. The material is widely applied in mechanically loaded structural components, such as machine parts, heavy equipment structures, and load-bearing cast components.

The +QT1 condition refers to the quenched and tempered heat treatment, which significantly improves the mechanical properties of the steel. During quenching, the steel is rapidly cooled from the austenitizing temperature to form a hardened microstructure, typically consisting of martensite or bainite. Subsequent tempering reduces brittleness and adjusts the balance between strength and ductility, producing a tempered martensitic or bainitic microstructure with improved toughness.

According to EN 10293, the typical mechanical properties of G24Mn6+QT1 include a minimum yield strength of approximately 355–420 MPa, depending on section thickness, and an ultimate tensile strength typically in the range of 500–650 MPa. The material also exhibits good ductility, with elongation values generally above 20%, which indicates a good capacity for plastic deformation before fracture. In addition, impact toughness requirements are specified to ensure adequate resistance to brittle fracture, particularly in demanding service conditions.

The relatively high manganese content in G24Mn6 contributes to improved hardenability and strength, while maintaining acceptable weldability and toughness. The quenched and tempered condition ensures that the material achieves a balanced combination of strength, ductility, and impact resistance, making it suitable for dynamically loaded components.

4.4.1.2 WAAM steels

Esab Purus 46 was used as WAAM carbon steel wire (WAAM CS), compliant with the SFA/AWS A5.18 ER70S-6 classification. The wire had a diameter of 1.2 mm, and its mechanical properties are presented in Table 1.

Esab OK Aristorod 89 was used as WAAM ultra-high-strength (UHS) steel filler wire, compliant with EN ISO 16834-A: G89 4 M Mn4Ni2CrMo and had a diameter of 1.2 mm. The mechanical properties of WAAM UHS steel wire are presented in Table 1.

The WAAM parts were printed using Fronius TransPuls Synergic 2700 CMT welding equipment.

For WAAM UHS the printing speed was 0.35 m/min, current 159 A, voltage 10.6 V, wire feed 4.0 m/min and lift between layers was 1.85 mm.

For WAAM CS the printing speed was 0.50 m/min, current 113 A, voltage 14.1 V, wire feed 3.2 m/min and lift between layers was 1.4 mm.

For WAAM UHS and WAAM CS an interpass temperature of 200 °C was controlled using an Optris CT infrared pyrometer. The flow rate of shielding gas was 12 l/min, and the composition of the gas was 92% Argon + 8% CO2.

Table 1. Mechanical properties of the WAAM UHS and WAAM CS wire.

	Yield strength MPa	Tensile strength MPa	Elongation %
WAAM UHS	920	940	18
WAAM CS	500	600	25

4.4.2 Hardness measurements for cast steel

Hardness measurements were performed on the G24Mn6+QT1 cast steel to evaluate the local mechanical properties of the material. The results showed that the average hardness was approximately 253 HV.

Some variation in hardness was observed across the measured locations, with values ranging from 229 HV to 290 HV. Such variation is typical for cast and heat-treated steels, where local differences in cooling rate, microstructure, and section thickness can lead to small hardness fluctuations. Overall, the measured hardness values are consistent with the quenched and tempered condition of G24Mn6+QT1 steel, indicating a microstructure that provides a balanced combination of strength and toughness.

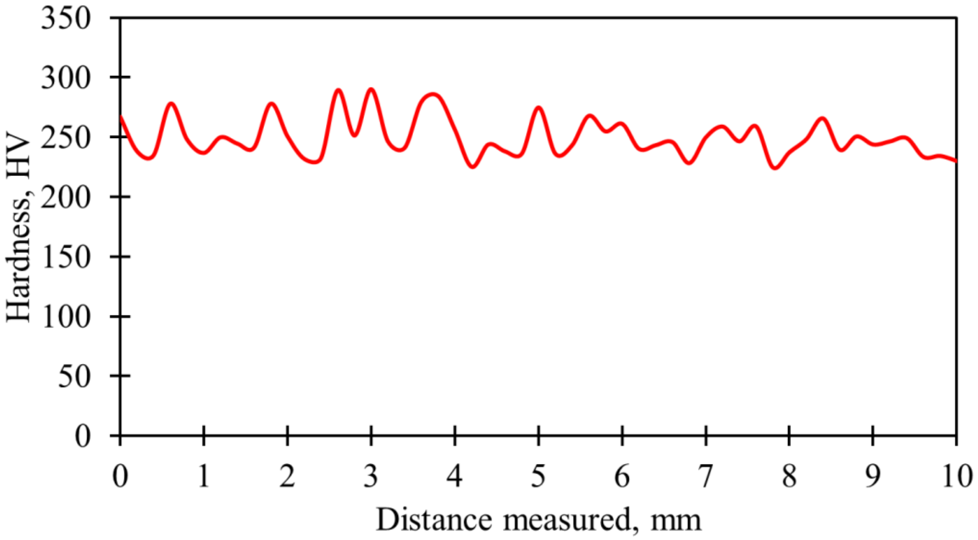

Fig. 1. Hardness profile for G24Mn6+QT1.

4.4.3 Mechanical properties

Tensile tests were conducted to compare the mechanical properties of G24Mn6 cast steel, WAAM CS, and WAAM UHS steel. The WAAM materials were tested in the vertical build direction, and the results are summarized in Table 1.

The G24Mn6 cast steel exhibited a yield strength of 754 MPa and an ultimate tensile strength of 846 MPa, with an elongation of 14.25%. These values indicate high strength but relatively limited ductility compared to the additively manufactured materials.

The WAAM carbon steel showed significantly lower strength values, with a yield strength of 406 MPa and a tensile strength of 518 MPa. However, it demonstrated the highest ductility among the tested materials, with an elongation of 41.99%, indicating excellent plastic deformation capability.

The WAAM ultra-high-strength steel displayed the highest strength levels, with a yield strength of 818 MPa and an ultimate tensile strength of 954 MPa. In addition, it maintained relatively good ductility with an elongation of 25.50%, which is considerably higher than that of the cast G24Mn6 steel.

The results show that WAAM UHS steel provides the highest strength performance, while WAAM carbon steel offers superior ductility. The G24Mn6 cast steel demonstrates intermediate strength but lower elongation, reflecting the typical mechanical behavior of quenched and tempered cast steels. These findings highlight the capability of WAAM processes to produce materials with competitive mechanical properties compared to conventional cast steels.

Table 1. Mechanical properties of the test materials.

Material	Yield strength MPa	Tensile strength MPa	Elongation %
G24Mn6	754	846	14.25
WAAM CS	406	518	41.99
WAAM UHS	818	954	25.50

4.4.4 Bending fatigue strength

Bending fatigue tests were conducted to compare the fatigue performance of WAAM-fabricated ultra-high-strength steel (WAAM UHS), WAAM carbon steel (WAAM CS), and cast steel G24Mn6 (Fig. 2). The WAAM specimens were tested in the vertical build direction to ensure consistent comparison. The fatigue tests were performed up to a run-out limit of 2×10^6 cycles, which was defined as the fatigue limit.

The results showed clear differences in fatigue performance among the materials. The WAAM UHS steel exhibited the highest fatigue resistance, with a fatigue limit of 483 MPa. The WAAM carbon steel reached a fatigue limit of 257 MPa, while the G24Mn6 cast steel showed the lowest fatigue limit, approximately 154 MPa.

In the low-cycle fatigue regime, the G24Mn6 cast steel demonstrated slightly better fatigue strength than WAAM carbon steel, sustaining higher stress amplitudes at lower cycle counts. However, as the number of cycles increased, the fatigue performance of WAAM carbon steel improved relative to the cast steel. At approximately 300,000 cycles, the fatigue strength of WAAM carbon steel surpassed that of G24Mn6, and this trend continued toward the high-cycle fatigue region.

Overall, WAAM UHS steel showed significantly superior fatigue performance across the entire fatigue life range, indicating excellent resistance to cyclic loading. The results also highlight that WAAM carbon steel provides better long-life fatigue resistance than the cast G24Mn6 steel, even though the cast material performs slightly better under very high stress levels in the low-cycle fatigue region.

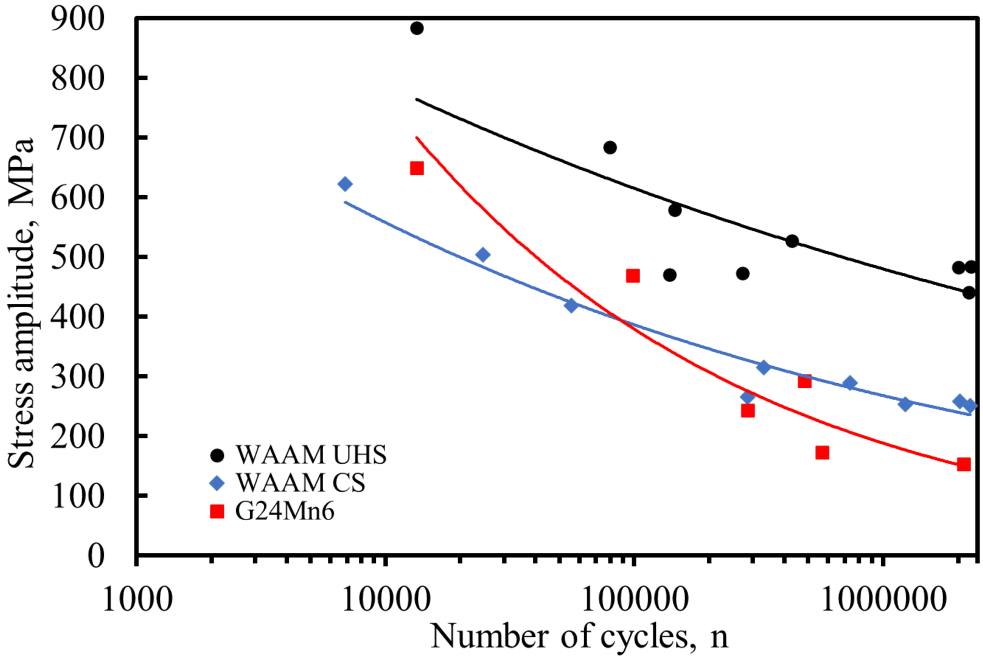

Fig. 2. Bending fatigue strength of WAAM UHS, WAAM CS and G24Mn6.

4.4.5 Axial fatigue strength

Axial fatigue tests were performed to compare the cyclic performance of WAAM UHS, WAAM CS, and cast steel G24Mn6. The tests were conducted up to a run-out limit of 2 × 10^6 cycles, which was defined as the fatigue limit.

The results showed that the WAAM UHS steel exhibited the highest fatigue limit, approximately 400 MPa. The WAAM carbon steel reached a fatigue limit of 260 MPa, while the G24Mn6 cast steel showed a slightly higher fatigue limit of about 280 MPa.

The fatigue behavior in the low- and medium-cycle fatigue regions followed a similar trend to the fatigue limits. Materials with higher endurance limits generally sustained higher stress amplitudes at comparable cycle counts, indicating that the overall fatigue strength across the entire S–N curve was largely proportional to the measured fatigue limits. These results demonstrate that WAAM UHS steel provides the best fatigue resistance among the tested materials, while the fatigue performance of WAAM carbon steel and G24Mn6 cast steel is relatively similar, with the cast steel showing slightly better fatigue strength.

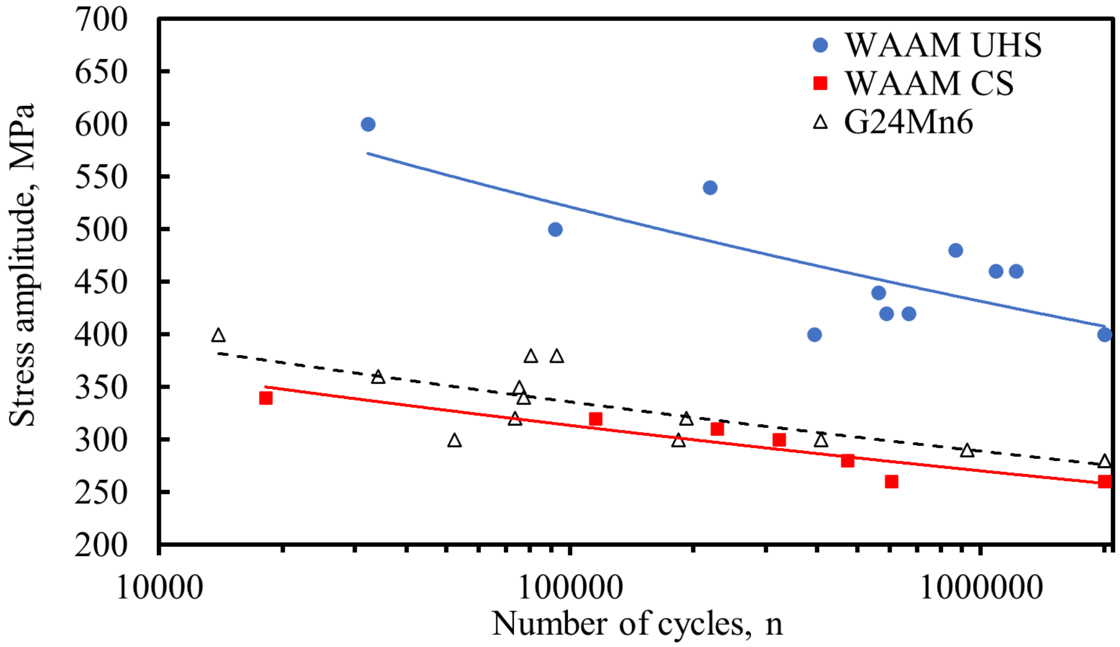

Fig. 3. Fatigue strength of WAAM UHS, WAAM CS and G24Mn6.